DIRECTIONAL PATTERN SYNTHESIS IN CIRCULAR ARRAYS OF DIRECTIONAL ANTENNAS

BY

TEHSEEN RAHIM

A Thesis submitted to the University of London for the Degree of Doctor of Philosophy in Electrical Engineering.

Department of Electronic and Electrical Engineering
University College London

August 1980

MISSING

PRINT

To my parents

Captain and Mrs. A. Rahim

ACKNOWLEDGEMENTS

The author wishes to gratefully acknowledge his supervisor, Professor D.E.N. Davies, for valuable discussions and guidance throughout the course of this work.

The author also wishes to gratefully acknowledge the provision of a 3 year Research Studentship from the Admiralty Surface Weapon Establishment (Funtington) and for the provision of the antenna measurement site.

Thanks are due to Mr. J. Wyatt, Mr. D. Hill and Mr. B. Stemp from the Admiralty Surface Weapons Establishment (Funtington) for their valued assistance during measurements. Thanks are also due to Mr. J. Guy for constructing the Butler Matrix Network.

Finally the author extends his thanks to Julia Mortimer for her expert typing of this thesis.

LIST OF CONTENTS

CHAPTER I· INTRODUCTION

		Page
1.1	The aim of the project	13
1.2	Circular arrays	14
1.3	A review of the previous studies on circular arrays	17
1.4	Null steering in antenna arrays	24
1.5	A review of previous studies on null steering in antenna arrays	28
	Figure 1.1(a) Null pattern	
	(b) Three types of null pattern	32
	Figure 1.2 Davies null steering network	33

CHAPTER II: THEORY OF CIRCULAR ARRAYS OF DIRECTIONAL ANTENNAS

2.1	Introduction	35
2.2	Mode-analysis of continuous circular arrays	35
2.3	Modes in circular arrays of finite number of omnidirectional elements	38
2.4	Modes in circular arrays of infinite number of directional elements	41
2.5	Modes in circular arrays of finite number of directional elements	42
2.6	Comparison of modes in omnidirectional and directional element circular arrays	46
2.7	Effect of directional elements on the vertical radiation pattern of circular arrays	50

2.8	Effect of random amplitude and phase errors in the excitation of circular arrays	52
2.9	Effect of mutual coupling in circular arrays	55
	Figure 2.1 Geometry of circular array	57
	Figure 2.2 Bessel functions	58

CHAPTER III DESIGN OF CIRCULAR ARRAYS

3.1	Introduction	60
3.2	Choice of design parameters for circular array	60
3.3	Design of an experimental circular array	62
3.4	Results of computation	64
3.5	Computation of absolute gain of modes	69
	Figure 3.1 Schematic diagran of the experimental circular array	75
	Figure 3.2 Phase mode patterns	76
	Figure 3.3 Phase mode patterns	77
	Figure 3.4 Phase mode patterns	78
	Figure 3.5 Mode amplitude versus frequency	79
	Figure 3.6 Mode amplitude versus frequency	80
	Figure 3.7 Relative phase shift versus frequency response	81
	Figure 3.8 Vertical patterns of circular array	82
	Figure 3.9 Vertical patterns of circular array	83

Figure 3.10 Absolute gain of modes 84
Figure 3.11 Absolute gain of modes 85

Table 1 74

CHAPTER IV. NEW TECHNIQUES FOR SYNTHESIS OF SHARP NULLS IN OTHERWISE OMNIDIRECTIONAL PATTERN OF CIRCULAR ARRAYS

4.1 Introduction 87
4.2 Synthesis of single sharp null in otherwise omnidirectional pattern 87
4.3 Synthesis of 2n sharp nulls in otherwise omnidirectional pattern 91
4.4 Review of the previous technique for synthesis of n nulls in the directional pattern of circular arrays 93
4.5 Results of computation 94
4.6.1 Synthesis of single sharp null using the concept of imaginary nulls 97
4.6.2 Theory 97
4.6.3 Results of Computation 100

Figure 4.1 Figure 4.10
4.2 4.11
4.3 4.12
4.4 4.13
4.5 4.14
4.6 4.15
4.7 4.16
4.8 4.17
4.9 4.18
106-123

CHAPTER V: EXPERIMENTAL MEASUREMENTS CARRIED OUT AT ASWE (FUNTINGTON) ON THE 16 ELEMENT CIRCULAR ARRAY

5.1	Introduction	125
5.2	Description of circular array and associated system	126
5.3	Description of the antenna measurement site	126
5.4	The wideband Butler matrix network	127
5.5	The wideband elements	129
5.6	Measurement of the phase mode patterns of a 16 element circular array	129
5.7	Measurement of amplitude modes of a 16 element circular array	132
5.8	Measurement of phase shift of a mode in circular array	133
5.9	Measurement of the variation of mode gain with frequency	136
5.10	Formation and steering of a single broad null in the directional pattern of circular array	137
5.11	Formation of a single narrow null in the directional pattern of circular array	138
5.12	Radiation pattern in the vertical plane through the null	140
5.13	Cross-polar patterns in the horizontal plane	141
5.14	Cross-polar patterns in the vertical plane	142
	Table 3-7	143-147
	Figures 5.1 - 5.58	148-206

CHAPTER VI:

6.1 Conclusions 208
6.2 Implications of the work 211

Appendix I 215

Spatial harmonic (amplitude mode) response of circular arrays of directive elements

Appendix II 219

Computation of G_{om}

Appendix III 221

Beam formation in circular arrays

REFERENCES 226

ABSTRACT

This thesis describes a mathematical and experimental study of circular arrays of directional antennas.

For directional pattern synthesis in circular arrays of omnidirectional elements, mode-analysis or Fourier harmonic analysis technique has previously been used. This thesis describes the effect of using any directional element on the mode propoerties - in the horizontal plane, and on the vertical directional pattern of such arrays.

The effect of random amplitude and phase errors in the excitation of circular arrays and of mutual coupling with reference to directional pattern synthesis is also studied.

A procedure is outlined for designing circular arrays of directional elements and a design of an experimental 16-element circular array is then presented. This is an 8 foot diameter array of 16 wideband elements each having a pattern of the form $(1+\cos\phi)$ for operation at 200-400MHz frequency band. Various mode patterns are computed for the array to determine their purity. The theoretical wideband performance of the array is also examined.

New techniques are described for the synthesis of single and 2n sharp nulls in otherwise omnidirectional patterns of circular arrays and the mechanism for independent

steering of these nulls is also described. Patterns are computed to demonstrate and theoretically study the techniques.

Finally, experimental results are presented to complement the theoretical study of circular arrays and null patterns.

LIST OF SYMBOLS

θ	the polar angle of the direction of radiation
ϕ	the azimuth angle of the direction of radiation
$F_m(\phi)$	the normalised far field response in the azimuthal plane for mth sequence excitation
$F(\phi)$	the far field directional pattern
I_m	mth sequence current
λ	wavelength of operation
β	free space propagation constant = $\frac{2\pi}{\lambda}$
r	radius of the array
j	$\sqrt{-1}$
γ_h	horizontal beamwidth of the directional pattern
$J_m(x)$	Bessel function of order m, and argument x
$G(\alpha)$	Element directional pattern in the azimuthal plane
$A_m(\beta r)$	the amplitude of mth phase mode for circular arrays of directional elements
ψ_m	phase of mth phase mode relative to mth sequence excitation
$D_m(\phi)$	distortion in mth phase mode due to the use of finite number of elements
d	interelement spacing = $\frac{2\pi r}{N}$
$C_m(\phi)$	the cosine spatial harmonic response of the array
$S_m(\phi)$	the sine spatial harmonic response of the array
Ω_m	phase of mth mode for array of directional elements relative to the array of omnidirectional elements
L	the highest harmonic of the element directional pattern

$C_{md}(\phi)$ distortion term in the mth cosine spatial harmonic due to the use of finite number of directional elements

$S_{md}(\phi)$ distortion term in the mth sine spatial harmonic due to the use of finite number of directional elements

V_n $\frac{2\pi n}{N}$ is the angular position of the nth element

CHAPTER I

INTRODUCTION

1.1 The aim of the project

The work described in this thesis is part of a study for the Admiralty Surface Weapons Establishment (Ministry of Defence), aimed at a new form of shipborne communications antenna.

In order to avoid mast obscuration the appropriate site to install an antenna would be around the mast. This obviously points to an array solution. The antenna array around a large square structure could take the form of 4 linear arrays or perhaps a circular array. A communication requirement is the production of an omnidirectional pattern in the azimuth and the ability to introduce one or more directional nulls to minimise interference or deliberate jamming. The antenna array may also be required to form a directional beam to enhance communication in a required direction. The overall frequency band of interest covers 200-1800MHz, but the principal communication band treated in this thesis is 200-400MHz. The typical dimensions of a ship mast would be a square structure of approximately 8 foot sides. It is also necessary to maintain the null over a broad elevation angle, to allow for ship movement and also because the interfering signals may arise in the elevation up to 5^{o}.

The obvious disadvantage of 4 linear arrays are that the corners of the array will affect the omnidirectional

pattern, and the steering of the nulls and beams through 360^{o} in the azimuth will require complicated networks for switching from one array to another. Both these disadvantages can be overcome by the use of a circular array. The presence of a metallic mast will inevitably require the use of directional elements. Therefore, the study described in this thesis is primarily directed towards the properties of circular arrays of directional antennas.

The design of such a null steering antenna system can be divided roughly into two parts. First, the synthesis of desired null and beam patterns in the presence of practical constraints and the associated design of a circular array to produce these patterns. Second, the study of networks to electronically steer the beam and nulls into the required directions. The study described in this thesis is generally concerned with the first part.

1.2 Circular Arrays

Historically, antenna arrays have been found useful in applications where it is required to synthesise a given far field radiation pattern. For this purpose a linear or planar antenna array is most commonly used. In this case the desired radiation patterns are synthesised by controlling five basic parameters. Namely, the relative current amplitude of the elements, the relative phase of

the elements, the number of elements, the interelement spacing and the element directional pattern. The same parameters may be used to specify a circular array of equi-spaced elements.

A further attractive feature of antenna arrays is that the radiation pattern can be electronically scanned in space, by appropriate control of the excitation of the array elements. Consequently, linear and planar antenna arrays have found application particularly in radar and direction finding. In these applications, narrow beams with low side-lobes are normally desirable and these can either be continuously scanned or steered in any given direction. This can be achieved electronically in either linear or circular antenna arrays.

Linear arrays can quite conveniently be used when only a sector of the horizontal plane is to be scanned. But when full 360^{o} of the horizontal plane is to be scanned, without appreciable distortion of the radiation pattern, a circular antenna array seems to be the most appropriate choice by virtue of its symmetry. In a circular array the synthesised directional pattern (e.g. a beam pattern) can be steered through 360^{o} in the horizontal plane (the plane of the array) by rotating the current excitation on the array. However, this process requires the change of both the amplitude and phase of all the elements - a process far more complicated than for linear arrays. However, an

attractive feature of circular arrays is the the element mutual coupling effects need not present a significant problem due to symmetry. The basic design parameters for circular arrays are (i) number of elements (ii) array radius in wave lengths or inter-element spacing (iii) amplitude taper around the array (iv) phase taper around the array. In the past three decades circular arrays have been studies by several authors (refs. 1 to 18). A brief review of these studies is given in section 1.3 of this chapter.

For directional pattern synthesis in circular arrays the mode-analysis technique had been used (2), (3),..etc., this analysis is shown for circular arrays of omni-directional elements and the literature has not discussed the effect of using directional elements on the modes. Therefore, in this thesis a general analysis is presented for circular arrays of directional elements in terms of phase and amplitude modes. The analysis shows that the use of directional elements will improve the wideband performance of circular arrays. The omnidirectionality of the vertical radiation pattern can also be improved by the use of directional elements.

A procedure is described for designing circular arrays of directional elements. This involves the choice of number of elements, the array radius and the element directional pattern at the frequency of operation. An experimental

circular array is then designed and theoretically and experimentally studied.

1.3 A Review of the Previous Studies on Circular Arrays

The properties and applications of circular arrays have been studies by various authors (see references) in the last three decades. This section briefly reviews these studies.

It was shown by Longstaff, Chow and Davies (1) that the far field directional pattern of a continuous circular array in the horizontal plane can be analysed in terms of spatial harmonics (amplitude modes). The mth spatial harmonic is defined by equation 1.1.

$$F(\phi) = I_m \cos m\phi \qquad 1.1$$

I_m = harmonic amplitude ϕ = azimuthal angle.

This is justified as the far field function 'F(ϕ)' is periodic with period 2π. The harmonic amplitude being given by the Conventional Fourier analysis techniques. Similarly, the current distribution on the circular aperture can be analysed in terms of Fourier harmonics. A relationship was established (Davies et al (1)) between the current harmonic excited on the aperture and the same harmonic obtained in the far field. In fact, it was shown

that the amplitude of such a far field harmonic is related to the array harmonic by a Bessel coefficient, whose order is the same as the harmonic. It was further shown that a circular array of omnidirectional elements may be regarded as a sampled circular aperture. Therefore when a current harmonic is established on the array the same harmonic is obtained in the far field plus higher order ambiguous harmonics as distortion terms. In general, provided the element spacing is less than $\lambda/2$ the ambiguous harmonics do not cause appreciable distortion of the ideal harmonics. Also as dictated by the sampling theorem harmonics not greater than half the number of elements can be obtained in the far field. In fact for rotating pattern even the harmonic order equal to half the number of elements cannot be utilised, since on rotation, the zeros of the harmonic will periodically coincide with the element position hence the harmonic will not be excited.

An interesting feature of circular arrays outlined in Ref. (1) is that the mutual coupling will alter the element radiation impedence. Due to the symmetrical nature of circular arrays the impedance of all the elements will be modified by the same amount for harmonic excitation. Hence only the amplitude (i.e. Bessel coefficient) of the harmonic will be modified in the far field. Thus the effect of mutual coupling can easily be compensated by measuring the harmonic amplitude in the far field and then adjusting the current harmonic amplitude on the array to obtain the

required far field harmonic. In linear arrays the effects of mutual coupling are affected by, for example, the beam pointing direction due to the end effects. But in circular arrays once the mutual coupling effect is compensated in any one direction, it is retained if the beam is electronically rotated in any other direction.

Some authors (2), (3) have analysed circular arrays of omnidirectional elements in terms of "phase modes". When a circular array is excited such that current amplitude is the same for all the elements but phase varies linearly from 0 to $2n\pi$, the excitation is referred to as "nth sequence excitation", where n is a negative or positive integer or zero. For the nth sequence excitation the far field response is also constant in amplitude (given by a Bessel function) and with phase varying linearly from 0 to $2n\pi$. This far field response is referred to as an "nth phase mode" or "nth order sequence excitation". Such an nth phase mode is represented by equation 1.2

$$F(\phi) = I_n e^{jn\phi} \qquad 1.2$$

Combining two equal order but opposite sign phase modes (see equation 1.3) results in a spatial harmonic (amplitude mode) as described by Longstaff, Chow and Davies (1).

$$F(\phi) = I_n e^{jn\phi} + I_{-n} e^{-jn\phi} \qquad 1.3$$

$$= 2I_n \cos n\phi \qquad (\text{since } I_n = I_{-n})$$

It is clear now that directional patterns can conveniently be synthesised in circular arrays by exciting either spatial harmonics or phase sequence excitations. But there remains the problem of efficiently exciting these harmonics or modes on the array. A solution to this problem was given by Davies (5). It was shown that the nth harmonic or mode can be excited on the array by feeding the appropriate input port of a multiple port beam forming network with the output ports of the network connected to the elements of the circular array. This multiple-port beam forming network may take the form of a Butler Matrix network. It was also shown that the Butler Matrix network provides a transformation between the phasing techniques required for linear and circular antenna arrays. That is, input ports of a Butler Matrix whose output ports feed a circular array are identical to the elements of a linear array. For example, by providing a linear progressive phase shift along the input ports of a Butler Matrix the beam pattern of a circular array can be rotated in angle. This is similar to the case of linear arrays in which the beam is shifted in angle by providing a linear progressive phase shift along the array elements.

Usually Butler Matrix networks are realised using hybrids and fixed phase shifts. The use of fixed phase shifts can adversely affect the wideband operation of those networks since it is difficult to implement a wideband phase shift. Recently work has been completed at UCL on realising a

wideband Butler Matrix network by using a combination of wideband 90^{o} and 180^{o} hybrids. This approach will be taken for designing a Butler Matrix network for the band 200-400MHz. The Butler Matrix network is briefly described in section 5.4.

Shelag (6) has shown that a Butler Matrix fed circular array can be used for forming narrow beams with low side-lobe levels and that the beams can be scanned through 360^{o} in the azimuth. In the first instance the beam was formed by uniformly exciting the modes. The beamwidth could be narrowed by using more modes, hence needing a larger array of greater number of elements. The beam can be scanned through 360^{o} in the azimuth by providing linear progressive phase shift to the modes. It was then shown that sidelobe levels can be reduced by applying cosine and cosine squared amplitude tapers to the modes.

Another method of producing beams is by using "phase-compensated" or "beam cophasal" excitation of circular arrays. Consider a circular array which is excited such that both amplitude and phase are uniform around the array. The contributions due to various elements in any direction in the horizontal plane vary cosinusoidally in phase. The cosinusoidally varying phase in the far field can be corrected by applying a cosinusoidal phase taper around the array. Therefore in the direction where contributions from all the elements are in phase a beam will be formed.

An array with cosinusoidal phase taper is referred to, in various papers, as "phase compensated" and "beam cophasal" circular array.

For phase compensated circular arrays the far field beam pattern is, in fact, of the shape of a zero order Bessel function (equation 1.4). The sidelobe level of the beam pattern is therefore only in the region of -8dB.

$$D(\phi) = J_o(\frac{4\pi r}{\lambda} \sin\phi/2) \qquad 1.4$$

The reduction of sidelobe level in phase compensated circular arrays has been studied in detail by Fenby (7) who has shown that a smooth amplitude taper may lower the sidelobe level but with increased back lobe or vice versa. Similarly directive elements can be used for reducing sidelobes but with increased back lobes or vice versa. This is so because the effect of the amplitude taper on the directional pattern is identical to that of using directional elements of the form similar to the amplitude taper. Thus by the use of both amplitude tapers and directional elements, low sidelobe level beams can be produced. However, since the sidelobe level is not particularly low other techniques have also been studied. Fenby (7) has shown that very low sidelobe beams can be obtained using a semi circular phase compensated array of unidirectional elements or by using a dual ring array of directional elements.

Another type of circular array that has been studied, probably the very first circular array to be studied, is the Wullenweber array for direction finding (8). In this only a small arc of the circular array is used, which might in principle be considered as a bent linear array, with appropriate phasing used to compensate for the physical deformation. Beam pattern can be rotated through 360^{o} in the azimuth by rotating the illuminated arc on the circular array, for example, by using a commutator.

A possible application of circular arrays to radar systems was described by Fenby and Davies (9). The paper describes a 360^{o} electronic beam scanning technique. Consider the beam from a cosinusoidal phase compensated array. Continuous rotation of the beam requires continuous rotation of cosinusoidally varying phase excitation. Hence phase at any element varies cosinusoidally with time. This means sinusoidal frequency modulation. Also since each element is a time delayed version of the one before, feeding the sinusoidal frequency modulated signal via a tapped delay line to the circular array will produce continuous rotation of the beam. The beam rotation rate being equal to the modulating frequency.

1.4 Null Steering in Antenna Arrays

Null steering in the directional pattern of antenna arrays has been a subject of study for about a decade. This subject arose from the requirement of producing directional nulls, in communications or radar antennas, to reject interfering signals from an unwanted source or jammer. Most of the work done has been directed towards null steering in linear arrays (10), (11), (12). But in recent years a new requirement has arisen for the provision of an omnidirectional pattern with one or more independently steerable nulls in the horizontal plane. This has particular application in mobile communication. Omnidirectional patterns with null steering through 360^{o} obviously points to a circular array solution.

Initial work on the synthesis of a single null in an otherwise omnidirectional pattern using a circular array was done by Lim and Davies (13). The characteristics and definition of parameters for null patterns, described in this paper are helpful in making sensible comparisons between performance of various null patterns. Parameters such as null width, null depth and gain ripple in the direction of coverage are defined as analogous to beamwidth and sidelobe level characterising conventional beam patterns.

Consider a null pattern shown in Fig. 1(a). The mean radiation intensity P_m, which is the geometric mean between the peak level P_{pk} and the trough level P_t in the omniregion of the pattern, is assumed to be the reference level. The ratio $\frac{P_{pk}}{P_{pm}}$ equal to $\frac{P_m}{P_t}$ expressed in decibels is defined as the gain ripple in the directions of communications coverage. In practice, fields in the direction of the null may not cancel to zero, hence there may be some radiation in that direction. Therefore, the ratio of the radiation intensity in the direction of the null to the mean radiation intensity in dB is defined as the null depth. Of course, ideally, null depth should be infinite, but changes in operating frequency, array excitation and mutual coupling will significantly affect this parameter. Finally, the null width is defined as the angle between two points, say 10dB, below the level P_m.

The above definitions are only sensible if the gain ripple is less than, for instance, 6dB, and null depth is at least -12dB. In the same way, the conventional definitions of beamwidth and sidelobe level for a beam pattern will lose their significance if the sidelobe level is of the same order of magnitude as the main beam.

Two types of nulls can be synthesised in circular arrays, ref. (13). Namely, tangential null and a zero crossing null. A tangential is one in which the pattern function just touches zero (Fig. 1.1b). Hence there are in fact

two coincident zeros in the direction of the null. The field pattern just before and after the null then has the same sign. For a zero-crossing null, the far field pattern suffers an abrupt phase reversal across the null (fig. 1.1b). For a given physical dimension of the array, zero-crossing null is narrower than the tangential null. If for a tangential null fields in the direction of the null do not cancel exactly to zero, the resulting pattern will be two displaced zero-crossing nulls (Fig. 1.1b).

Various synthesis techniques have been studied (13), (14) (15), for the synthesis of the null patterns described above; these techniques will be briefly described in section 1.5 of this chapter. Steering of these null patterns through 360^{o} in the horizontal plane requires the array excitation to be rotated. This can be achieved electronically by providing a linear progressive phase shift along the input ports of a multiple port beam forming network feeding the circular array (5).

Since there may be more than one interfering source in the coverage region, there may be a need to produce multiple nulls in the directional pattern of circular arrays which are independently steerable. Davies and Rizk (15) have described a method for producing multiple nulls which are independently steerable. The technique for synthesis of multiple nulls is an extension of that described by Schelkunoff (16) for linear arrays. In ref. (15),

experimental results are also presented to demonstrate the practical feasibility of this technique. This employed a 4-element circular array of omnidirectional elements.

The problem with the synthesis techniques, developed to date for single null patterns, is that the null widths are fairly broad. This has the disadvantage that a wanted source nearby an interfering source may also be rejected. With the present techniques, sharpening the null widths results in increased gain ripple in the omniregion. In order to overcome these problems, a new technique is described in Chapter IV, for the synthesis of a single null, only a few degrees wide, in an otherwise omni-directional pattern of circular array with small gain ripple.

Broad nulls may again present a problem in the case of producing multiple nulls. Also, as the nulls are brought closer, gain is reduced considerably between the nulls. To overcome these problems a new technique is described in Chapter IV for the synthesis of 2n very sharp nulls in an otherwise omnidirectional pattern of circular arrays. In this, the gain ripple is small in the omniregion and, provided an adequate number of harmonics is used, gain between nulls is not reduced much even when the null separation is quite small. However, it should be borne in mind that this technique is only applicable to large circular arrays of many elements in which higher order harmonics can be excited.

Steering of nulls can be achieved by manually controlling the amplitude and phase at the input ports of a Butler Matrix feeding the circular array. Also, phase shifter networks can be designed which will adaptively steer nulls in the direction of interference. These systems require a priori knowledge of either the wanted signal or the unwanted signal. Thus, when a signal is received from some direction it is correlated with the known signal, and if required, the null is steered in that direction by electronically controlling the phase shifter network for steering nulls. However, since adaptive null steering is not the subject of study described in this thesis, this topic will not be pursued any further but it is worth mentioning that adaptive null steering techniques can be used for steering nulls by the methods described in this thesis.

1.5 A Review of Previous Studies of Null Steering in Antenna Arrays

Historically, null steering in the directional pattern of linear arrays was studied by Davies (10) in 1967. Schelkunoff (16) had shown that, mathematically, the directional pattern of an n-element linear array can be expressed as a polynomial or order (n-1). Such a polynomial can be expressed as a product of (n-1) factors, and hence (n-1) zeros. The zeros of the polynomial also represent real zeros of the directional pattern. For

independent steering of (n-1) zeros of the directional pattern, amplitude and phase of each element has to be controlled. To simplify the zero steering mechanism, Davies (10) described a phase shifter network feeding the linear array. This network is shown in Fig. 1.2. The row of phase shifters ϕ_r control the angular location of the rth null. The row of phase shifter can also be ganged together and each null steered by a single control unit.

The extension of the zero steering technique to planar arrays for scanning in three dimensional space is described in ref. (12).

Null steering in circular arrays was first studied by Lim and Davies (13) in 1975. It was shown that a single null in an otherwise omnidirectional pattern of circular arrays can be obtained by subtracting an appropriately attenuated cophasal beam from an omnidirectional pattern with constant phase. This gives a broad tangential null. It was then shown that subtracting a suitably attenuated cophasal beam from a phase sequence excitation - i.e. constant amplitude and phase varying linearly from 0 to $2n\pi$, yields a zero-crossing null, which is narrower than the tangential null obtained using the same cophasal beam. In fact, the -10dB null width of the zero-crossing null is approximately half the 3dB beamwidth (13). Also the gain ripple in the omniregion was small. Steering of the

null away from the direction of the element resulted in slight deterioration of the pattern. Maximum deterioration obviously results when the null lies midway between the elements.

Lim (14) has described another technique for the synthesis of a sharp null in an otherwise omnidirectional pattern using a circular array. In this the pattern function changes phase progressively at half the rate of change of the azimuth angle. This results in an abrupt phase reversal which results in a sharp zero-crossing null. This kind of pattern function can be synthesised by using spatial harmonics whose coefficients are given by Fourier Integrals. The nulls can then be steered in azimuth by providing linear progressive phase shifts at the input ports of the Butler Matrix used for exciting these spatial harmonics. Also the null can be scanned in the elevation plane by varying the frequency.

The null steering systems described above either involve complex steering mechanisms or are useful for large circular arrays (4). A particularly simple type of null steering system employing a circular array is described by Davies and Rizk (17) and Rizk (18). It was shown that a single null in an otherwise omnidirectional pattern can be obtained by adding any two adjacent phase modes. The system studied employed zeroth and the first phase modes resulting in a zero-crossing but broad null.

The zeroth mode has to be attenuated before being added to the first mode, because their relative amplitudes are given by zeroth and first order Bessel functions respectively. Relative phase shift between the two phase modes will produce rotation of the null through 360^{o} in the azimuth. The null direction being given by the phase shift value. The method was experimentally demonstrated (17) on a model antenna consisting of 4 dipole elements disposed about a circle of radius 0.16λ at 153MHz. Pattern characteristics, such as null depth, null width etc. are affected when the null is steered between the elements. However, overall performance was satisfactory. Further, the antenna was operated over $\pm$20% bandwidth with little effect on null characteristics.

In ref. (18) a technique for independently steering multiple nulls in the directional pattern of a circular array is also described. The technique is translated from that used for linear arrays described earlier in this section. This technique is described in detail in Chapter IV (section 4.4). The method was experimentally demonstrated for two nulls on the 4-element model circular array.

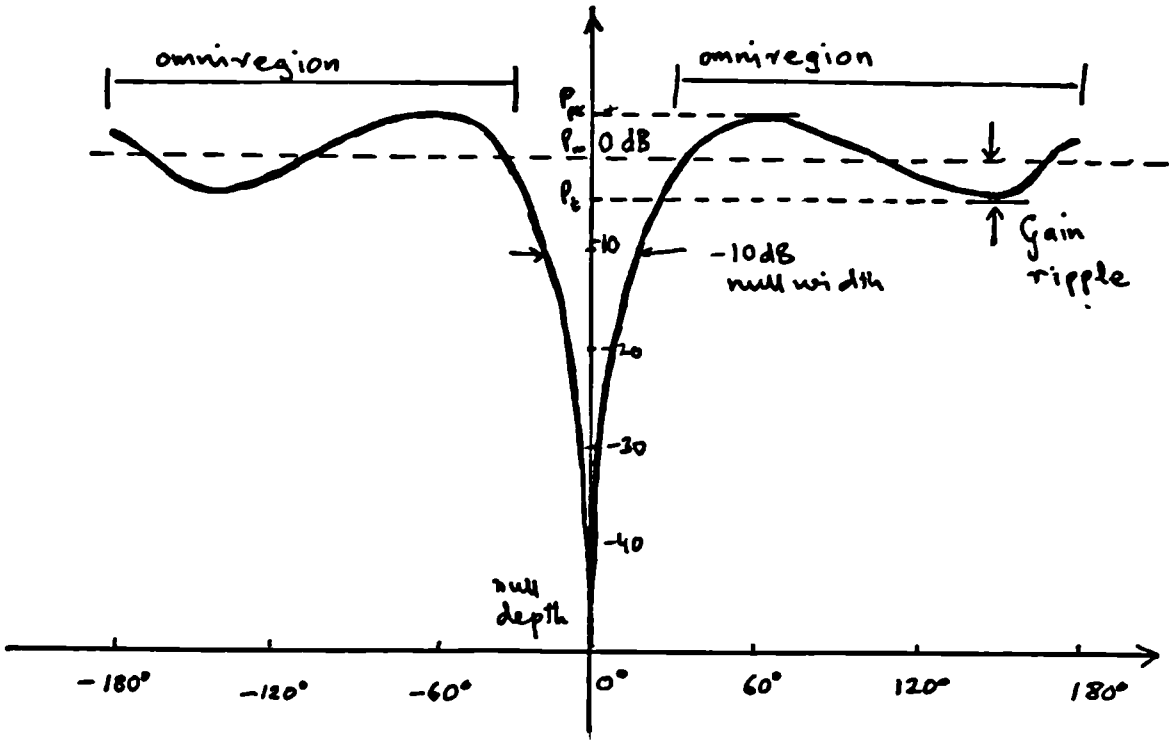

(a) NULL PATTERN

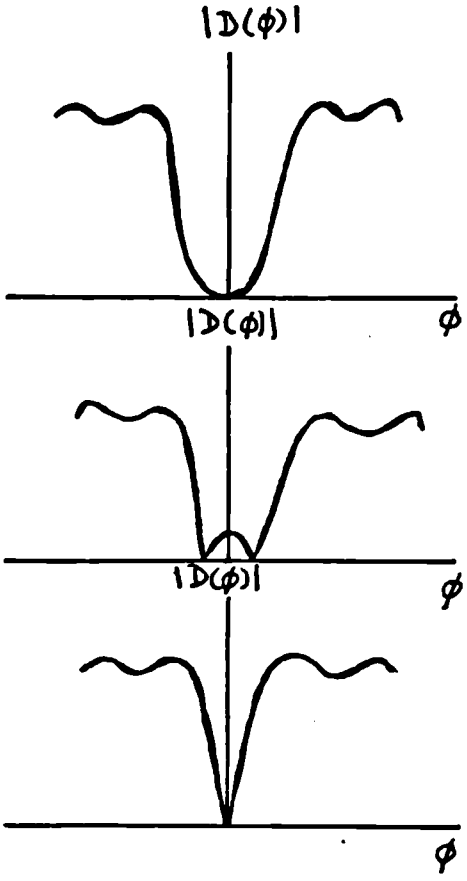

A tangential null in which the directional response touches the axes giving two simultaneous zeros

Two displaced zeros resulting in change of sign D(φ) at each zero

A zero crossing null

(b) THREE TYPES OF NULL PATTERNS

FIGURE 1.1

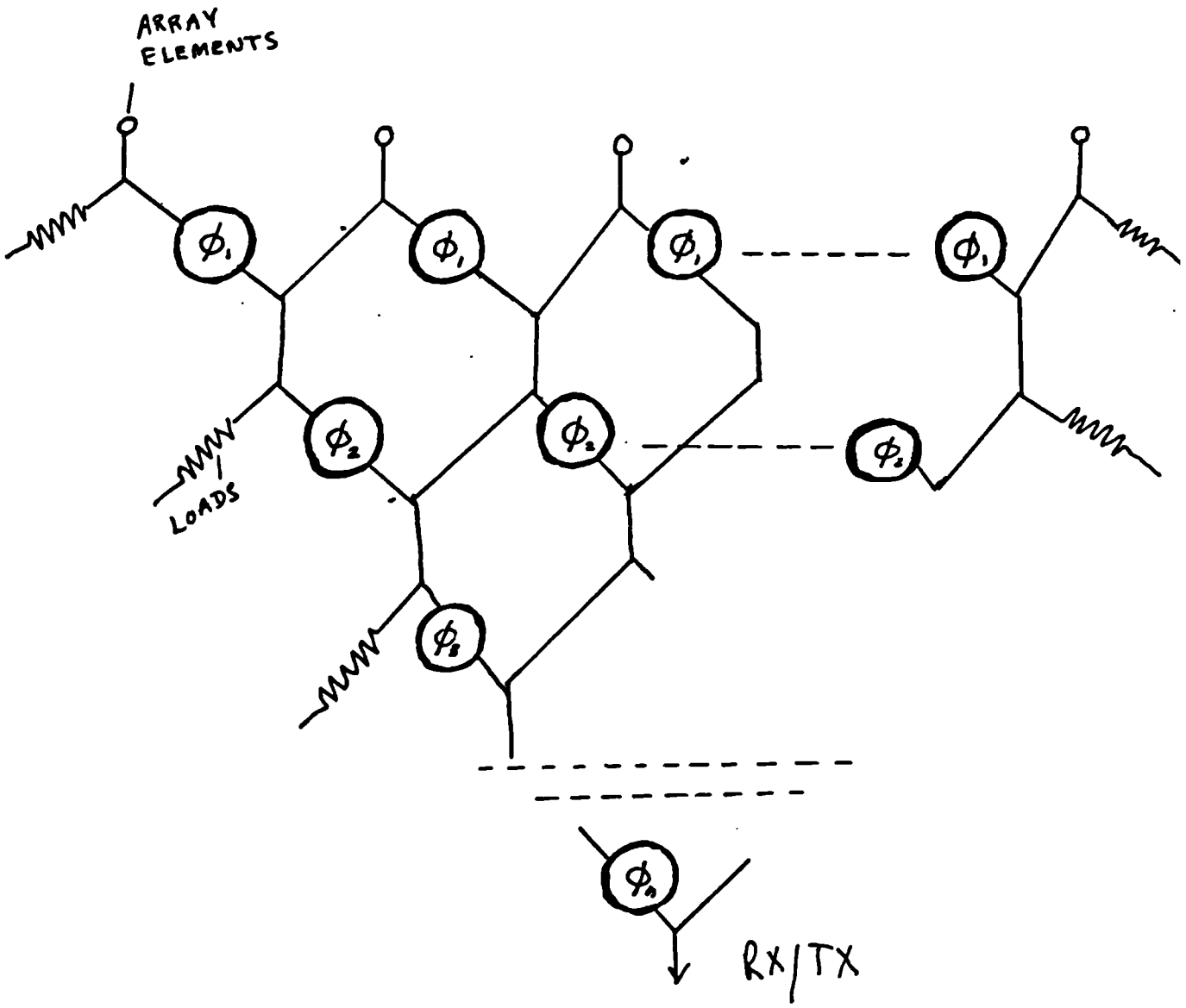

DAVIES NULL STEERING NETWORK FIGURE 1.2

CHAPTER II

THEORY OF CIRCULAR ARRAYS OF DIRECTIONAL ANTENNAS

2.1 Introduction

This chapter describes a mathematical analysis of circular arrays of directional antennas. The analysis is an extension of mode-analysis or Fourier Harmonic analysis used for synthesis of horizontal directional patterns in circular apertures and circular arrays of omnidirectional elements (2). The analysis has revealed some important mode properties of circular arrays of directional antennas, which are found helpful in synthesis of the horizontal directional patterns. The effect of using directional elements on the vertical radiation pattern of circular arrays is also described.

The chapter also describes the effect of random amplitude and phase errors in the excitation of circular arrays. Finally the effect of mutual coupling is described with reference to directional pattern synthesis.

2.2 Mode-Analysis of Continuous Circular Arrays

The horizontal far field directional pattern '$F(\phi)$' of a continuous circular aperture is a periodic function with period 2π. Hence it can, mathematically, be expressed as a complex Fourier series. A complex series is used because the far field $F(\phi)$ is a function of both amplitude and phase. Thus

$$F(\phi) = \sum_{-M}^{M} C_m e^{jm\phi} \qquad 2.1$$

where

$$C_m = \int_0^{2\pi} F(\phi) e^{-jm\phi} d\phi \qquad 2.2$$

and ϕ = azimuth angle

In order, therefore, to synthesise any far field directional pattern 'F(ϕ)' we need to produce an mth phase mode '$e^{jm\phi}$' in the far field. It is shown in ref. (2) that the mth phase mode can be produced in the far field by exciting the same mode excitation on the continuous circular array. That is, if excitation on the array is given by

$$i = I_m e^{jm\phi} \qquad 2.3$$

where

I_m = mth sequence excitation current
then the far field directional pattern $F_m(\phi)$ is given by

$$F_m(\phi) = j^m J_m(\beta r)\ I_m e^{jm\phi} \qquad 2.4$$

where

$J_m(\beta r)$ = Bessel function of order m

$\beta = \frac{2\pi}{\lambda}$, λ = wavelength of operation

r = radius of the array

Therefore if it is required to produce a far field mode

$$F_m(\phi) = C_m e^{jm\phi} \qquad 2.5$$

then the current excitation on the continuous circular array is given by

$$i = \frac{C_m}{j^m J_m(\beta r)} e^{jm\phi} \qquad 2.6$$

As an illustration, consider an array with a current excitation given by

$$i = \frac{1}{J_o(\beta r)} + \frac{1}{jJ_1(\beta r)} e^{j\phi} + \ldots + \frac{1}{j^N J_N(\beta r)} e^{jN\phi} \qquad 2.7$$

then using (2.6) and (2.5), the far field $F(\phi)$ is given by

$$F(\phi) = 1 + e^{j\phi} + e^{j2\phi} + \ldots\ldots e^{jN\phi} \qquad 2.8$$

or

$$|F(\phi)| = \frac{\sin(N+1)\phi/2)}{\sin(\phi/2)} \qquad 2.9$$

Equation (2.9) is a well known beam pattern equation with beamwidth $\gamma_h = \frac{2\pi}{(N+1)}$. Thus, with a large number of modes N narrow beams are possible. Sidelobe level can be reduced by applying an amplitude taper to the modes. This is analagous to linear additive arrays in which amplitude tapers are applied to the elements except that the patterns of linear arrays are expressed in terms of a Sin θ scale. This technique is described in more detail in Appendix III.

2.3 Modes in Circular Arrays of Finite Number of Omnidirectional Elements

In practical situations it is unlikely that continuous circular arrays could be used. Circular arrays of discrete radiators are more likely to be encountered. For analysis of an array of omnidirectional radiators situated on a circle, the mode-analysis technique can be extended. This is possible as a circular array can be approximated to a discretely sampled continuous circular array. Thus, the far field in the case of a circular array will be the continuous aperture term plus distortion terms.

It is shown in ref. (2) that if a circular array of uniformly spaced omnidirectional radiators is subjected to mth sequence excitation, the current in the nth element being given by

$$i_n = I_m e^{JmV_n} \qquad 2.10$$

$$V_n = \frac{2\pi n}{N} \qquad 2.11$$

where

I_m = mth sequence current

N = total number of elements

then the normalised far field pattern $F_m(\phi)$ is given by

$$F_m(\phi) = I_m j^m J_m(\beta r) e^{jm\phi} + \sum_{q=1}^{\infty} I_m j^{Nq-m} J_{Nq-m}(\beta r) e^{-j(Nq-m)\phi}$$

$$+ I_m j^{Nq+m} J_{Nq+m}(\beta r) e^{j(Nq+m)\phi} \qquad 2.12$$

From equation (2.12) it is evident that there is a distortion of the ideal modes in the form of a Bessel series of higher order modes. It is a property of Bessel functions that for argument 'χ' less than order n the Bessel function $J_m(\chi)$ becomes smaller as the order n increases. Clearly from equation (2.12), the largest distortion term is given by $J_{N-m}(\beta r)e^{-J(N-m)\phi}$. Since $e^{-J(N-n)\phi}$ is a rapidly oscillating function of ϕ, with a maximum value of one, the coefficient $J_{N-m}(\beta r)$ is the contributory distortion factor. Mode term will dominate provided

$$J_m(\beta r) > J_{N-m}(\beta r) \qquad 2.13$$

this is true if, $m<\frac{N}{2}$ 2.14

and $N-m \gg \beta r$ 2.15

Thus modes up to half the number of elements can be obtained in the far field.

For lower order modes $N-m \doteqdot N$. Using condition 2.15 we find

$N \gg \beta r$

or $\frac{2\pi r}{N} = d \ll \lambda$ 2.16

where d = interelement spacing

Thus the lower order modes contain little distortion provided interelement spacing is less than a wavelength.

For the highest available mode, $N-m=\frac{N}{2}$

Using condition 2.15 we find

$$\frac{2\pi r}{\lambda} = d \ll \frac{\lambda}{2} \qquad 2.17$$

Therefore for all the available modes (half the number of elements) to be of good quality, interelement spacing should be less than half a wavelength.

2.4 Modes in Circular Arrays of Infinite Number of Directional Elements

Consider the circular array geometry shown in Fig. 2.1. Suppose it is subjected to mth phase sequence excitation. Then the normalised far field pattern $F(\phi)$ can be written as

$$F(\phi)=I_m\frac{1}{mN}\sum_{1}^{N} G(\phi-V_n)e^{J(mV_n+\beta r\cos(\phi-V_n))} \qquad 2.18$$

where $G(\alpha)$ is the element directional pattern. As $N\to\infty$, the far field pattern tends to

$$F(\phi)=I_m\frac{1}{2\pi}\int_{0}^{2\pi} G(\phi-v)e^{J(\beta r\cos(\phi-v)+mv)}dv \qquad 2.19$$

The element pattern $G(\alpha)$ is a periodic function with period 2π, therefore it can be expressed as

$$G(\alpha) = \sum_{-L}^{L} C_\ell e^{j\ell\alpha} \qquad 2.20$$

substituting 2.20 in 2.19 we have

$$F(\phi)=I_m\frac{1}{2\pi}\int_{0}^{2\pi}\sum_{-L}^{L} C_\ell e^{J\ell(\phi-v)}e^{J(\beta r\cos(\phi-v)+mv)}dv \qquad 2.21$$

Using the relationship {2}

$$j^m J_m(\zeta)=\frac{1}{2\pi}\int_{0}^{2\pi} e^{j(mv+\zeta\cos v)}dv \qquad 2.22$$

Equation 2.21 becomes

$$F(\phi)=I_m e^{jm\phi} \sum_{-L}^{L} C_\ell \left[\frac{1}{2\pi} \int_0^{2\pi} e^{j(m-\ell)(v-\phi)+\zeta\cos(\phi-v)} d(\phi-v)\right] \qquad 2.23$$

or

$$F(\phi)=I_m |A_m| e^{jm\phi + \psi_m} \qquad 2.24$$

where

$$|A_m| e^{j\psi_m} = \sum_{-L}^{L} C_\ell j^{m-\ell} J_{m-\ell}(\zeta) \qquad 2.25$$

Therefore when a continuous circular array of directional elements is subjected to mth phase sequence excitation, the far field is a mth phase mode. The amplitude and phase of the phase mode is given by equation 2.25 but the form of this pattern is independent of the pattern of the directional element.

2.5 Modes in Circular Arrays of Finite Number of Directional Elements

In this section the effect of using discrete elements is studied. Suppose the circular array shown in Fig. 2.1 is subjected to mth phase sequence excitation. Then the current distribution on the circular array is given by

$$I(\phi)=I_m e^{jm\phi} S(\phi) \qquad 2.26$$

where $S(\phi)$ is a sampling function which has a unit impulse at the elements. If N is the number of elements, then the spectrum of $S(\phi)$ is given by (1)

$$S(\phi)=\sum_{q=-\infty}^{\infty} e^{jNq\phi} \qquad 2.27$$

or

$$S(\phi)=1+\sum_{q=1}^{\infty} e^{jNq\phi}+e^{-jNq\phi} \qquad 2.28$$

Substituting 2.28 in 2.26 we have

$$I(\phi)=I_m e^{jm\phi}+I_m\sum_{q=1}^{\infty} e^{j(Nq+m)\phi}+e^{-j(Nq-m)\phi} \qquad 2.29$$

Thus when mth phase mode is excited on a circular array, N-m, N+m, 2N-m, 2N+m etc. are excited as unwanted ambiguous modes.

The far field for the excitation of equation 2.29 is given by (using expression 2.24 developed in section 2.4)

$$F(\phi)=I_m|A_m|e^{jm\phi\ +\psi m+D_m(\phi)} \qquad 2.30$$

where

$$D_m(\phi)=I_m\sum_{q=1}^{\infty}|A_{Nq+m}|e^{j(Nq+m)\phi+\psi Nq+m+}\left|A_{-(Nq-m)}\right|e^{-j(Nq-m)\phi+\psi-(Nq-m)}$$

$$2.31$$

The significant distortion term is given by

$$\left\{ \sum_{-L}^{+L} C_{\ell} j^{N-m-\ell} J_{N-m-\ell}(\zeta) \quad e^{-j(N-m)\phi} \right\} \qquad 2.32$$

The mode term is given by equation (2.24). For the distortion term to be small compared to the mode term

$$J_{m-\ell}(\zeta) > J_{N-m-\ell}(\zeta) \qquad 2.33$$

This condition is satisfied if, $m < \frac{N}{2}$

and if

$$\frac{N}{2} - L \gg \beta r \qquad 2.34$$

or

$$\frac{2\pi r}{N} = d \ll \lambda \left\{ \frac{1}{2} - \frac{L}{N} \right\} \qquad 2.35$$

Thus for very directional elements (large L), the element spacing should be much smaller than half a wavelength.

The analysis described above is in terms of phase modes. For 'real' directional patterns 'F(ϕ)' (i.e. only amplitude variation), it may be more convenient to

express the pattern as a sum of amplitude modes.

$$F(\phi) = \frac{a_o}{2} + \sum_{m=1}^{M} a_m \cos m\phi + b_m \sin m\phi \qquad 2.36$$

These amplitude modes can be produced in the far field by exciting the same amplitude mode of current on the circular array. It is shown in ref. (1) that for a circular array of omnidirectional elements, if the current excitation on the array is given by

$$i = I_m \cos m\phi \qquad 2.37$$

the far field response is given by

$$C_m(\phi) = j^m J_m(\beta r) I_m \cos m\phi + j^{N-m} J_{N-m}(\beta r) \cos(N-m)\phi + \ldots\ldots \qquad 2.38$$

It is shown in Appendix I that if a circular array of directional elements has an excitation

$$i = I_m \cos m\phi$$

then the far field directional pattern is given by

$$C_m(\phi) = I_m |A_m| e^{j\psi m} \cos m\phi + C_{md}(\phi) \qquad 2.39$$

where the distortion term $C_{md}(\phi)$ is given by

$$C_{md}(\phi)= \sum_{-L}^{+L} C_\ell \left\{ \sum_{q=1}^{\infty} j^{Nq+(m-\ell)} J_{Nq+(m-\ell)}(\zeta)\cos(Nq+m)\phi \right.$$

$$\left. + \sum_{q=1}^{\infty} j^{Nq-(m-\ell)} J_{Nq-(m-\ell)}(\zeta)\cos(Nq-m)\phi \right\} \qquad 2.40$$

As with phase modes, there is a limitation on the excitation of higher order modes. Amplitude modes only of an order up to N/2 may be obtained. However, a problem arises in electronically rotating the N/2 amplitude mode. This is because on rotation, the zeros of the $\cos(N/2)\phi$ excitation will periodically coincide with the positions of all the elements and hence the mode cannot then be excited. Therefore the highest amplitude mode that can be used with electronic rotation is $\cos(N/2-1)\phi$.

2.6 Comparison of Modes in Omnidirectional and Directional Element Circular Arrays

The mth phase mode for a circular array of N omnidirectional elements is given by ref. (2).

$$F_m(\phi) = J_m(\beta r)e^{Jm(\phi+\pi/2)} + J_{N-m}(\beta r)e^{-jN-m(\phi-\pi/2)} + \ldots . \qquad 2.41$$

mth phase mode for a circular array of N directional elements $G(\alpha) = \sum_{-L}^{+L} C_\ell e^{jl\alpha}$, is given by (expression developed in section 2.5).

$$F_m(\phi)=|A_m|e^{j(m\phi+\psi m)}+|A_{N-m}|e^{-j(N-m)\phi+\psi N-m}+\ldots\ldots \qquad 2.42$$

where

$$|A_\beta|e^{j\psi\beta} = \sum_{-L}^{+L} C_\ell j^{\beta-\ell} J_{\beta-\ell}(\zeta) \qquad 2.43$$

Thus the effect of using a finite number of elements both in the case of omnidirectional and directional element circular arrays is to produce distortion of higher order modes, namely, $e^{-j(N-n)\phi}$, $e^{j(N+n)\phi}$, $e^{-j(2N-n)\phi}$, etc. Also, in both cases only mode numbers up to half the number of elements may be used.

To obtain good quality modes (i.e. with small distortion), the element spacing should be less than half a wavelength for circular arrays of omnidirectional elements. However, in the case of circular arrays of directional elements smaller interelement spacing may be required. In fact, for very directional elemenets very small interelement spacing is required.

If the interlement spacing is small such that distortion is negligible then the phase mode patterns for arrays of omnidirectional and directional elements are given by equations (2.44) and (2.45) respectively.

$$F_m(\phi)= I_m J_m(\beta r)e^{jm(\phi+\pi/2)} \qquad 2.44$$

$$F_m(\phi) = I_m|A_m|e^{j(m\phi + \psi_m)} \qquad 2.45$$

It is evident from these two expressions that the phase mode for the directional element circular array is shifted in space relative to the phase mode for the circular array of omnidirectional elements. The relative spatial phase shift 'Ω_m' for the mth mode is given by

$$\Omega_m = \psi_m - \frac{m\pi}{2} \qquad 2.46$$

A formula for these shifts as given by equation 2.43 is

$$\psi_m = \arctan \frac{(\ldots + C_{-3}J_{m-3}(\zeta) - C_{-1}J_{m-1}(\zeta) + C_1 J_{m+1}(\zeta) - C_3 J_{m+3}(\zeta) + \ldots)}{(\ldots + C_{-4}J_{m-4}(\zeta) + C_{-2}J_{m-2}(\zeta) - C_o J_m(\zeta) - C_2 J_{m+2}(\zeta) + C_4 J_{m+4}(\zeta) + \ldots} \qquad 2.47$$

It is important to note that these phase shifts are both mode order and frequency dependent, and their effect will have to be compensated, at the input ports of the Butler matrix feeding the array for directional pattern synthesis.

Another significant difference between the case of a circular array of omnidirectional elements and that of directional elements is that the mode amplitude in the former case is given by a Bessel function, whereas in the latter case the mode amplitude is given by a Bessel function series. For some Bessel arguments 'βr' (where βr is

dependent on frequency and radius) $J_m(\beta r)=0$, hence the mth mode will be missing. This is a real problem in the design of patterns for circular arrays, particularly for applications in which wideband performance is desirable. Because all the modes may be present at the design frequency (centre frequency) by choosing the correct radius. But for some other frequency some mode may be absent causing pattern distortion. However, in the case of an array of directional elements, mode amplitude is given by

$$C_0 j^m J_m(\beta r) + j^{m+1}\left(C_{+1} J_{m+1}(\beta r) - J_{m-1}(\beta r) C_{-1}\right) + \ldots\ldots \qquad 2.48$$

Using the relationship ref. (20)

$$\frac{1}{2}\left\{J_{m+1}(\beta r) - J_{m-1}(\beta r)\right\} = J_m'(\beta r) \qquad 2.49$$

where $J_m'(\beta r)$ is the derivative of $J_m(\beta r)$. The mode amplitude becomes

$$j^m J_m(\beta r) + j^{m+1} J_m'(\beta r) + \ldots\ldots \qquad 2.50$$

For $C_0 = 1$, $C_{+1} = C_{-1} = \frac{1}{2}$

It is clear from Fig. 2.2 that at arguments where $J_m(\beta r)=0$, $J_m'(\beta r)\neq 0$, hence the amplitude of the mode no longer goes to zero. Therefore the choice of directional element will improve the wideband performance of

circular arrays, by stabilising the mode amplitude and prevent it going to zero for any unfortunate value of array radius (or frequency).

2.7 Effect of Directional Elements on the Vertical Radiation Pattern of Circular Arrays

The analysis described in the last few sections has been concerned with modes obtained in the horizontal plane (plane of the circle). In this section the vertical radiation pattern is examined for circular arrays subjected to mth sequence excitation. For circular arrays of omni-directional elements subjected to mth sequence excitation, the far field '$F_m(\theta,\phi)$' in any direction in space is given by ref. (2).

$$F_m(\theta,\phi)= I_m J_m(\beta r \sin\theta) e^{jm(\phi+\pi/2)} + \ldots\ldots\ldots \qquad 2.51$$

θ=polar or elevation angle

ϕ=azimuth angle

The far field pattern in the case of directional elements can be written as

$$F_m(\theta,\phi)=\frac{1}{N}\sum_{n=1}^{N} G(\theta,\phi-V_n) e^{j(mV_n+\beta r \sin\theta \cos(\phi-V_n))} \qquad 2.52$$

The element directional pattern $G(\theta,\phi)$ can in general be expressed as

$$G(\theta,\phi)=\sum_{-L}^{+L} C_{\ell}(\theta)e^{j\ell\phi} \qquad 2.53$$

where

$$C_{\ell}(\theta)=\frac{1}{2\pi}\int_{0}^{2\pi} G(\theta,\phi)e^{-j\ell\phi}d\phi$$

This is justified because for any fixed elevation direction θ, $G(\theta,\phi)$ is periodic as ϕ varies.

Using 2.53 in 2.52 we get

$$F_m(\theta,\phi)=\frac{1}{N}\sum_{n=1}^{N}\sum_{-L}^{+L} C_{\ell}(\theta)e^{j\ell\phi}e^{j(mV_n+\beta r\ \sin\theta\ \cos(\phi-V_n))} \qquad 2.54$$

Equation 2.54 is analogous to equation 2.18. The only difference being that for C_{ℓ} in 2.18 we have $C_{\ell}(\theta)$ and for βr we have $\beta r\sin\theta$. Therefore by following the analysis outlined in section 2.5 we find that

$$F_m(\theta,\phi)=.....+C_{-1}(\theta)J^{m-1}J_{m-1}(\beta r\sin\theta)+C_0(\theta)J^{m}J_m(\beta r\sin\theta)$$

$$+C_1(\theta)J^{m+1}J_{m+1}(\beta r\sin\theta)+....\ e^{jm\phi}+.... \qquad 2.55$$

From equation 2.55 it is clear that the elevation directional pattern for a circular array of omnidirectional pattern is given by a Bessel function. Thus, apart from the zeroth mode which has maximum radiation in the vertical direction (sin(0)=0), the rest of the modes do not radiate in the

vertical direction. Also for lower order modes the elevation pattern will contain nulls of the Bessel function. However, for the case of an array of directional elements, the nulls in the elevation plane will be filled; this is apparent from equation 2.55. Therefore, by appropriate choice of directional elements (choice of $...C_{-1}(\theta)$, $C_0(\theta)$, $C_1(\theta).....$) the omnidirectionality of the vertical radiaton pattern can be improved.

Another significant difference between the circular array of omnidirectional elements and that of directional elements is that there is no variation of phase in the vertical pattern for the former case, whereas phase varies in the vertical pattern for the latter case, which is evident from equation 2.55. The significance of this result in null pattern synthesis is explained in Chapter IV.

2.8 Effect of Random Amplitude and Phase Errors in the Excitation of Circular Arrays

Section 2.5 outlined the presence of 'systematic' amplitude and phase distortion terms in the phase mode pattern of circular arrays. These errors are termed systematic because their presence is due to the finite number of elements. They will take the form of variations in amplitude and phase which depart from the ideal phase mode. They can be reduced by using more elements and hence smaller interelement spacing. The

distortion terms are due to the presence of higher order modes, namely -(N-m), N+m, -(2N-m)...etc. where N = number of elements and m = mode order.

This section investigates the effect on phase modes of any 'random' amplitude and phase errors in the excitation of circular arrays. The random errors may be due to (i) tolerances of Butler matrix network feeding the current modes (ii) distortion of the element directional pattern and (iii) unequal lengths of cables feeding the elements.

Consider a circular array with amplitude and phase of the elements given by nth phase mode excitation, i.e.

$$I_n e^{jn\phi} \qquad 2.56$$

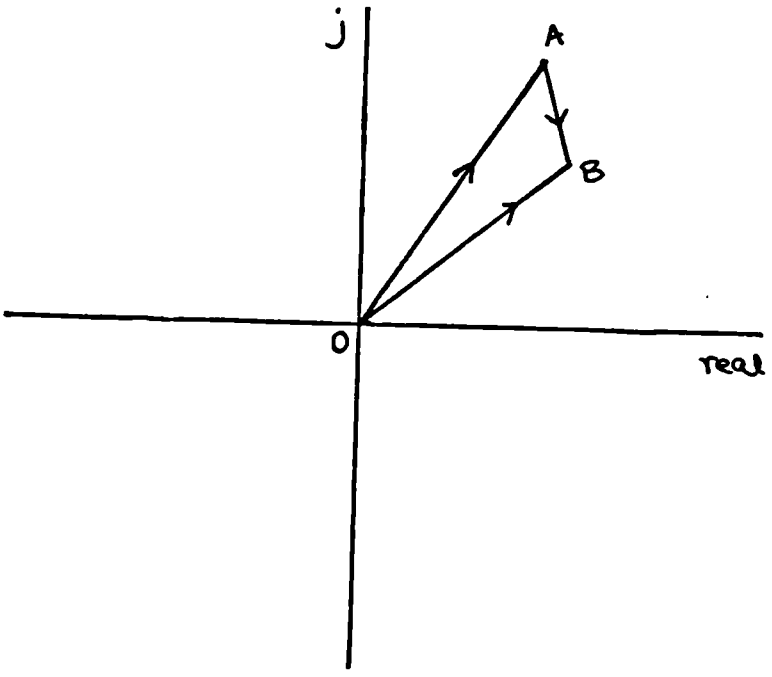

Figure 2.3

The vector $I_n e^{jn\phi}$ is represented as $\vec{OA}$ in the vector diagram shown in Fig. 2.3. Suppose there are amplitude and phase errors in the excitation. Then the excitation of the elements is given by vector $\vec{OB}$ in Fig. 2.3.

Now

$$\vec{OB} = \vec{OA} + \vec{AB} \qquad 2.57$$

$$\underbrace{I(\phi)e^{J\psi(\phi)}}_{\text{actual excitation}} = \underbrace{Ie^{jn\phi}}_{\text{phase mode term}} + \underbrace{I_e(\phi)e^{J\psi e(\phi)}}_{\text{error term}} \qquad 2.58$$

Since the excitation on circular arrays is periodic, the error term will also be periodic. Hence it can be represented as a Fourier series.

$$\therefore\ I(\phi)e^{j\psi(\phi)} = Ie^{Jn\phi} + \sum_{-K}^{K} C_K e^{JK\phi} \qquad 2.59$$

The far field '$F(\phi)$' for excitation of equation 2.59 is given by (section 2.4)

$$F(\phi) = I|A_n|e^{J(n\phi+\psi_n)} + \sum_{-K}^{K} C_K|\bar{A}_K|e^{JK\phi+\psi_K} \qquad 2.60$$

Thus the effect of random amplitude and phase errors in the excitation of circular arrays is to distort the phase modes

by the presence of higher order modes. It is interesting to note that these errors may be corrected to a certain extent by compensating at the higher order mode inputs of the Butler matrix feeding the modes.

2.9 Effects of Mutual Coupling in Circular Arrays

This section outlines the effects of mutual coupling with reference to directional pattern synthesis in circular arrays.

It has been shown in ref. (2) and ref. (3) that the effect of mutual coupling in circular arrays is to alter the element radiation impedance. For the mth phase mode the element impedance 'Z_m' is given by

$$Z_m = \sum_{i=1}^{N} Z_{1i} e^{j2\pi im/N} \qquad 2.61$$

where Z_{11} is the self impedance and Z_{12}, Z_{13}...etc. are the mutual impedances. Clearly element impedance Z_m for different modes is different. However, for any one mode, radiation impedance is the same for all the elements, due to symmetry. Z_m is also referred to as the mth mode impedance. The impedance Z_m^{BM} seen at the mth mode input of the Butler matrix network, though not the same as Z_m, will be characteristic of the mode.

Suppose e.m.f. at the input port of the mth mode is E_m. Then the current at the input port is given by

$$I_m = \frac{E_m}{Z_m^{BM}} \qquad 2.62$$

From section 2.4, the far field pattern is given by

$$F(\phi) = \frac{E_m}{Z_m^{BM}} |A_m| e^{jm\phi + \psi_m} \qquad 2.63$$

where $|A_m|$ = Bessel function series.

Thus, the mode amplitude is not only modified by a Bessel function series (different for different modes) but is also modified by the mode impedance 'Z_m^{BM}'. This is not a significant problem from the pattern synthesis point of view, because appropriate mode amplitude may be obtained by having an attenuator at the input port, and there is no need to attempt to calculate the mode impedance. Also because Z_m^{BM} is complex ($Z_m^{BM} = R_m^{BM} + jX_m^{BM}$) $\frac{E_m}{Z_m^{BM}}$ is complex. Therefore the field pattern becomes

$$F(\phi) = \left| \frac{E_m}{Z_m^{BM}} \right| |A_m| e^{jm\phi + \psi_m + \psi_{Z_m BM}} \qquad 2.64$$

Hence the phase mode would be further shifted by amount $\psi_{Z_m BM}$. This phase shift in phase mode, due to mutual coupling effects will have to be compensated for at the input port of the Butler Matrix feeding the mode. It should also be noted that $\psi_{Z_m BM}$ is frequency dependent.

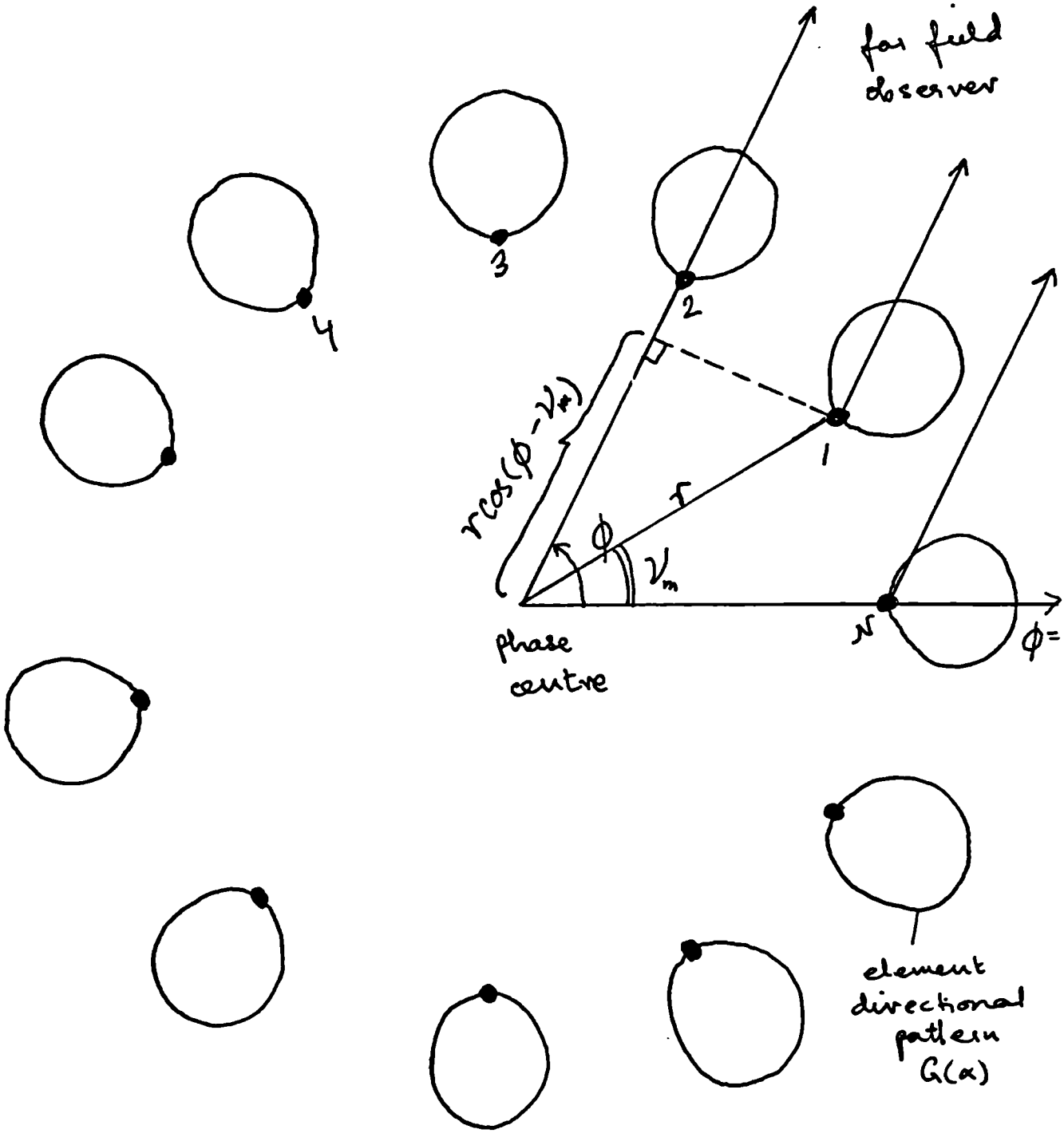

GEOMETRY OF CIRCULAR ARRAY FIGURE 2.1

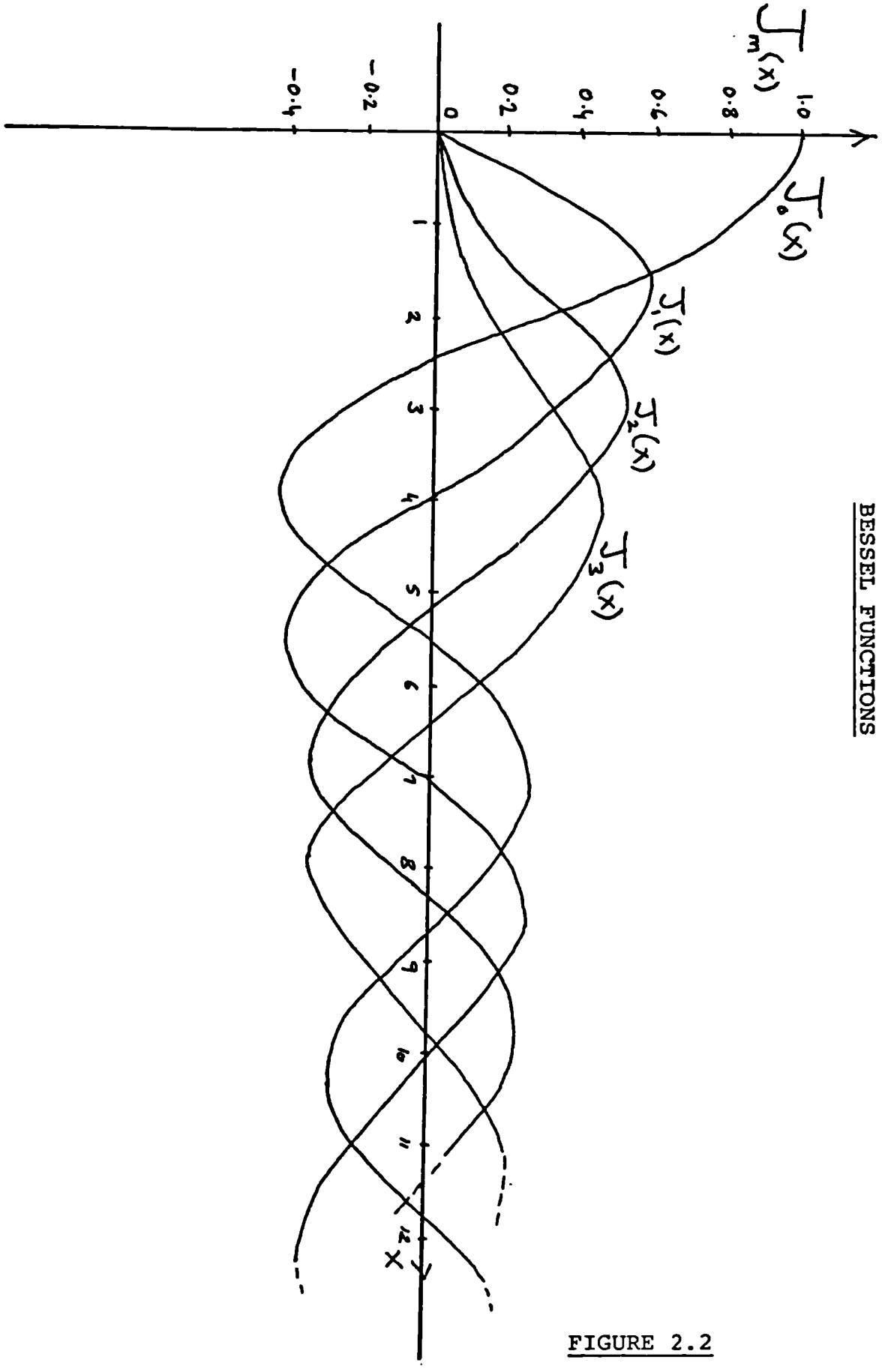

BESSEL FUNCTIONS

FIGURE 2.2

CHAPTER III

DESIGN OF CIRCULAR ARRAYS

3.1 Introduction

This chapter describes the design of circular arrays for producing desired directional patterns, for example, null or beam patterns using spatial modes. The design of circular arrays involves the choice of the number of elements, the array radius (or the interelement spacing) and the element directional pattern at the frequency of operation.

This chapter discusses the design of an experimental model circular array used for studies in conjunction with null steering. This is a 16-element array of directional elements having a pattern '1+cosϕ'. The array is to be operated at 200-400MHz band. Mode patterns are computed at 200MHz, 300MHz and 400MHz to determine the extent of distortion of the ideal modes and to study the wideband performance. The variation of amplitude and phase shift for phase modes, with frequency is also plotted. The vertical patterns for zeroth and first order phase modes are plotted for the omnidirectional element array and for the experimental array. Finally, absolute gain is computed for various modes over the frequency band 200-400MHz.

3.2 Choice of Design Parameters for Circular Arrays

This section describes a procedure for design of circular arrays for producing specified far field directional

patterns. The choice of the number of elements N depends on the highest Fourier harmonic of the directional pattern. That is, if m is the highest Fourier harmonic of the directional pattern, then the number of elements required is at least 2m, as shown in Section 2.6. The choice of the type of array element to be used will largely depend on the bandwidth requirement. Because the mode amplitude is more stable with frequency changes for the case of directional elements. In fact, for highly directional element patterns, the mode amplitude becomes very stable with frequency changes, this was established in Section 2.6. Having decided the type and number of elements to be used, the next step is to determine the array radius or inter-element spacing. It was shown in Section 2.6 that in order to avoid mode pattern degradation due to inadequate sampling the element spacing $d<\lambda\left\{\frac{1}{2} - \frac{L}{N}\right\}$, where L is the highest Fourier harmonic of the element directional pattern. In practical design of arrays, very small interelement spacing is not easy to achieve, for example, due to the size of the elements. Also there is a problem of mutual coupling between elements, resulting in element mismatch, pattern distortion, and reduced bandwidth performance. Thus the optimum choice of interelement spacing would be $\lambda\left\{\frac{1}{2} - \frac{L}{N}\right\}$. Hence the optimum choice of radius would be

$$r = \frac{\lambda}{2\pi}\left\{\frac{N}{2} - L\right\} \qquad 3.1$$

If the array is to be operated over a wideband of frequencies, then the radius should be designed at the lowest frequency. However in practical design it may be difficult to have small interelement spacing due to the size of the elements. Therefore array radius may be chosen at the centre frequency.

3.3 Design of Experimental Circular Array

For experimental investigation of the ASWE studies and the theoretical study outlined in earlier chapters a circular array has been designed. This section outlines the design of the experimental array. .The elements to be used for the circular array have been designed at ASWE. They consist of reflector backed flat plate dipoles, having a width of about half a wavelength. The elements have a good performance over the frequency band 200-400MHz. It can initially be assumed, for the purposes of calculations, that a dipole half a wavelength in front of a reflecting screen will have a directional pattern, in the horizontal plane, approximately given by (6).

$$G(\alpha)=1+\cos\alpha \qquad 3.2$$

As already mentioned, typical ship mast sizes are of the order of 8ft in diameter. Therefore the next step is to choose the number of elements. It was shown in the earlier section that for an optimum design of a circular array of

directional elements

$$r = \frac{\lambda}{2\pi}\left\{\frac{N}{2} - L\right\} \qquad 3.1$$

where

r = radius of the array

N = number of elements

L = highest Fourier harmonic of element directional pattern

λ = wavelength at centre frequency

In our case

r = 122cms

L = 1

λ = 100cms (wavelength at 300MHz)

Using equation 3.1, it is found that N=17. The experimental circular array will be fed from the N output ports of a N x N Butler matrix. A Butler matrix can be constructed for N = 4, 8, 16, 32... . Therefore the choice of a 16-element circular array seems most appropriate.

The experimental Butler matrix-fed 16-element circular array is shown in Fig. 3.1. Null and beam patterns can be synthesised by controlling the amplitude and phase of the various modes. This is achieved by controlling the attenuators A_1, A_2...etc. and phase shifters ϕ_1, ϕ_2... as shown in Fig. 3.1.

3.4 Results of Computations

In this section mode patterns are computed for the experimental 16-element array to determine the extent of distortion of ideal modes, as predicted by the analysis described in Chapter II.

Phase modes 0, ± 1, ± 2, ...± 7, computed for the experimental circular array are shown in Figs. 3.2, 3.3, 3.4. Modes are also computed (Figs. 3.2, 3.3, 3.4) for a similar array of omnidirectional elements for comparison. The modes are computed using the equation

$$F(\phi) = \sum_{n=1}^{N} G(\phi - V_n) e^{j(mV_n + \zeta \cos(\phi - V_n))} \qquad 3.3$$

$F(\phi)$ is the far field of a circular array subjected to mth sequence excitation and $G(\phi)$ is the element directional pattern. For the case of experimental array we take $G(\phi)=1+\cos\phi$, and for the case of omnidirectional elements $G(\phi)=1$.

From the computed results it can be seen that lower order modes 0, ± 1, ± 2, ± 3 are identical to 'ideal' modes, that is modes obtained for a continuous aperture. This applies to both the experimental array and the array of omnidirectional elements. But modes ± 4, ± 5, ± 6 and ± 7 get progressively more distorted. This is an expected result, because gain

ripple (i.e. variations about the mean level) is approximately given by (derived from equation 2.42)

$$\pm 10 \log \frac{|A_m| + |A_{N-m}|}{|A_m| - |A_{N-m}|} \quad \text{dBs} \qquad 3.4$$

$|A_m|$ and $|A_{N-m}|$ are given by equation 2.43. Clearly as n increases $|A_{N-m}|$ becomes comparable to $|A_m|$ making gain ripple large. Also m should be less than N/2, therefore only modes up to $\pm$ 7 are computed.

It was shown earlier that smaller interelement spacing is required for arrays of directional elements. Thus, for a constant interelement spacing, modes in a directional element circular array will be more distorted than modes in an omnidirectional element circular array. This is confirmed by the mode patterns plotted (Figs. 3.2, 3.3, 3.4). But the most significant difference between the two cases is that the fourth mode is absent in the case of circular arrays of omnidirectional elements, whereas it is present for the experimental array. This can be explained as follows: it was seen earlier that the mode amplitude for the case of arrays of omnidirectional elements is given by a Bessel function of the same order as the mode number and of argument equal to $\frac{2\pi r}{\lambda}$. In the case of 8ft diameter array operating at 300MHz, the argument is equal to 7.66. From the tables of Bessel function $J_4(7.66) \doteqdot 0$, hence the fourth mode is absent. In the case of array of '1+cosϕ'

elements, it is seen from the far field pattern equation 2.24 derived in Chapter II, that the amplitude of fourth mode is given by $J_4(7.66)\frac{j}{\pi} J_4'(7.66)$. Since $J_4'(7.66)$, the slope of $J_4(7.66)$, is not equal to zero the fourth mode is preserved in this case.

In order to investigate the wideband performance of the array, modes are computed at the lowest and highest frequencies of the band of interest, 200-400MHz. Gain ripple for various modes for 200, 300 and 400MHz is shown in Table 1 (page 74). It is clear from these results that modes numbers up to ± 7 at 200MHz and up to ± 6 at 300MHz are of good quality. These modes have gain ripple less than $\pm$2dB and phase error much smaller than 5°. Higher order modes containing large phase errors ($\pm 10^{\circ}$) and gain ripple greater than $\pm$2dB are of limited practical use. Increased distortion at higher frequencies is an expected result, since the interelement spacing at 400MHz is 0.64λ, which is much larger than 0.44λ - the required spacing for adequate sampling of higher order modes. Modes were then computed for an 8ft diameter array employing 20 elements of the type $(1+\cos\phi)$. Interelement spacing at 200MHz, 300MHz and 400MHz is 0.26λ, 0.38λ and 0.5λ respectively. In this case it was found that modes up to ± 7 are obtained, with small distortion, even at 400MHz. However, the size of flat plate dipoles chosen for the experimental array constrains the number of elements to be used to no more than 16 on an 8ft diameter array. Thus only lower modes

can be utilised at higher frequency for the experimental array.

The results for wideband operation of the experimental array showed that the amplitude and phase errors, of various modes increase as the frequency increases. Another feature determining the wideband performance of the array is the stability of mode amplitude as frequency varies. Fig. 3.5 and Fig. 3.6 show the theoretical variation of mode amplitude with frequency for the experimental array compared with a similar array of omni-directional elements. It is clear from these theoretical curves that the mode amplitude for the experimental design is much more stable than for the array of omnidirectional elements. Again, this is a predicted result (Chapter II). Thus the use of directive elements '1+cosϕ' will improve the wideband performance of circular array.

An interesting feature may be seen from Fig. 3.5 and Fig. 3.6, we saw in Chapter II that mode amplitude for the experimental array is given by

$$J_n(\beta r) - j\frac{J_n'(\beta r)}{\beta} \qquad 3.5$$

At the turning points of $J_n(\beta r)$, $J_n'(\beta r)=0$, therefore the mode amplitude becomes $J_n(\beta r)$(the same as that for an omni-directional element array). Figs. 3.5 and 3.6 confirm this result.

It was shown analytically that there is a spatial phase shift ψ_m between the excitation of phase mode on the circular array and that obtained in the far field. Using the actual far field equation (3.3) the phase was computed for the experimental array for various modes with respect to zeroth order mode. Fig. 3.7 shows a plot of these phase shifts over the frequency band 200-400MHz. For any one mode the phase shifts gradually decrease as the frequency is increased. Also, at any one frequency, phase shifts increase as the mode order is increased.

The results computed above were concerned with the mode properties in the horizontal plane. The other feature of the experimental array to be investigated is the vertical directional pattern, when the array is subjected to mth sequence excitation. For the experimental array the element reflecting screen can be replaced by an 'imaginary' element half wavelength behind it. Using pattern multiplication technique, the three dimensional element pattern is approximately given by

$$G(\theta,\phi)=\cos\left(\frac{\pi/2\cos\theta}{\sin\theta}\right)(1+\cos\phi\sin\theta) \qquad 3.6$$

Using equation 3.6, vertical radiation patterns were computed for the experimental array and also for a similar array of omnidirectional elements. Fig. 3.8 and Fig. 3.9 show the theoretical patterns for the zeroth and first

sequence excitations respectively. It is evident from these patterns that the use of directive elements, given by equation 3.6, improves the vertical radiation pattern of the circular array by filling the nulls shown for the array of omnidirectional elements. And this is also in agreement with the analysis presented in Chapter II.

3.5 Computation of Absolute Gain of Various Modes

Absolute gain of an antenna is defined as

$$\text{Gain} = \frac{\text{maximum radiation intensity}}{\text{average radiation intensity}}$$

i.e. gain of a directional antenna is the maximum power density relative to an isotropic radiator.

If the normalised far field pattern of an antenna array is given by $F_n(\theta,\phi)$ then by definition array gain is given by

$$G = \frac{4\pi}{\int_0^{2\pi}\int_0^{\pi} F_n^2(\theta,\phi)\sin\theta \, d\theta \, d\phi} \qquad 3.7$$

For a circular array of directive elements, the gain in the horizontal plane for mode 'm' becomes

$$G = \frac{4\pi \left| \int_0^{2\pi} G(\phi-v) e^{jmv+\beta r\cos(\phi-v)} dv \right|^2}{\int_0^{2\pi}\int_0^{\pi} \left| \int_0^{2\pi} G(\phi-v,\theta) e^{jmv+\beta r\sin\theta\cos(\phi-v)} dv \right|^2 \sin\theta d\theta d\phi} \qquad 3.8$$

The numerator of equation 3.8 is a Bessel function series squared. Whilst in the denominator squared Bessel function series has to be integrated twice. Analytically, this involves complicated integration. In order to avoid calculation of the denominator an alternative approach is taken.

Gain 'G_{DIR}' of mth mode for circular array of elements '$1+\cos\phi$' is proportional to the square of the field strength calculated by adding contribution from various elements. Thus

$$G_{DIR} = \text{const} \left\{ \sum_{n=1}^{N} \{1+\cos(\phi-v_m)\} e^{jmv_m+\beta r\cos(\phi-v_m)} \right\}^2 \qquad 3.9$$

Also gain 'G_{om}' of mth mode for circular array of omni-directional elements is given by

$$G_{om} = \text{const} \left\{ \sum_{n=1}^{N} e^{jmv_m+\beta r\cos(\phi-v_m)} \right\}^2 \qquad 3.10$$

The constants of equation 3.9 and 3.10 are equal if total power radiated by both the circular arrays of omni-

directional elements and '1+cosϕ' elements is equal. Therefore

$$\frac{G_{DIR}}{G_{om}} = \frac{|E_{DIR}|^2}{|E_{om}|^2} \qquad 3.11$$

where

$$E_{DIR} = \sum_{n=1}^{N} (1+\cos(\phi-v_m))e^{jmv_m+\beta r\cos(\phi-v_m)} \qquad 3.12$$

and

$$E_{om} = \sum_{n=1}^{N} e^{jmv_m+\beta r\cos(\phi-v_m)} \qquad 3.13$$

E_{DIR} and E_{om} can easily be computed. Therefore knowing G_{om}, G_{DIR} can be found from equation 3.11. A method for calculating G_{om} has been described in ref. 18. In Appendix II G_{om} is computed for zeroth mode of a 16-element array at the frequency of 300MHz. G_{om} is found to be equal to 2.76dB. For the experimental array the 3-D element pattern can be approximated to $A\sin\theta(1+\cos\phi)$ where A determines the power radiated by the single element. Both the circular array of directional elements and that of omnidirectional elements must radiate the same power. Therefore

$$A^2\int_0^{2\pi}\int_0^{\pi}\sin^3\theta(1+\cos\phi\sin\theta)^2 d\theta d\phi = \int_0^{2\pi}\int_0^{\pi}\sin\theta d\theta d\phi \qquad 3.14$$

or

$$A^2\int_0^{2\pi}\int_0^{\pi}\sin^3\theta+2\cos\phi\sin^4\theta+\cos^2\phi\sin^5\theta d\phi d\theta = 1/\pi \qquad 3.15$$

Using Wallis' Formulae

$$\int_0^{\pi}\sin^3\theta d\theta = \frac{4}{3} \qquad 3.16$$

$$\int_0^{\pi}\sin^4\theta d\theta = \frac{3}{8}\pi \qquad 3.17$$

$$\int_0^{\pi}\sin^5\theta d\theta = \frac{16}{15} \qquad 3.18$$

$$\therefore \quad A^2\int_0^{2\pi}\left(\frac{4}{3} + \frac{3}{4}\pi\cos\phi + \frac{16}{15}\cos^2\phi\right)d\phi = 4\pi$$

or

$$A^2\left[\frac{28}{15}\phi + \frac{3}{4}\pi\sin\phi + \frac{4}{15}\sin 2\phi\right]_0^{2\pi} = 4\pi$$

$$\therefore \quad A \approx 1 \qquad 3.19$$

Using this value of A, E^2_{DIR} and E^2_{om} was plotted as a function of frequency (DC to 400MHz) for an 8ft diameter

array of 16 elements (see Figs. 3.10 and 3.11). Knowing G_{om}=2.76dB at 300MHz, absolute gain for both circular array of omnidirectional elements and elements '1+cosϕ' can readily be read from Fig. 3.10 and 3.11. Since the modes are orthogonal, the absolute gain of any directional pattern can be calculated knowing the gain of individual modes.

Mode	200 MHz		300 MHz		400 MHz	
	Omnidirectional Element Array Gain ripple (dBs)	Array of (1+cosϕ) Elements Gain ripple (dBs)	Omnidirectional Element Array Gain ripple (dBs)	Array of (1+cosϕ) Element Array Gain ripple (dBs)	Omnidirectional Element Array Gain ripple (dBs)	Array of (1+cosϕ) Elements Gain ripple (dBs)
0	0	0	0	0	±0.14	±0.13
±1	0	0	0	0		±0.29
±2	0	0	0	0	±0.46	±0.7
±3	0	0	0	0	large distortion	large disortion
±4	Mode absent	±0.4	0	0	"	"
±5	±0.5	±0.6	0	0	"	"
±6	±1.0	±1.5	±0.1	±0.17	"	"
±7	±3.0	±3.5	±0.93	±1.2	"	"

TABLE 1

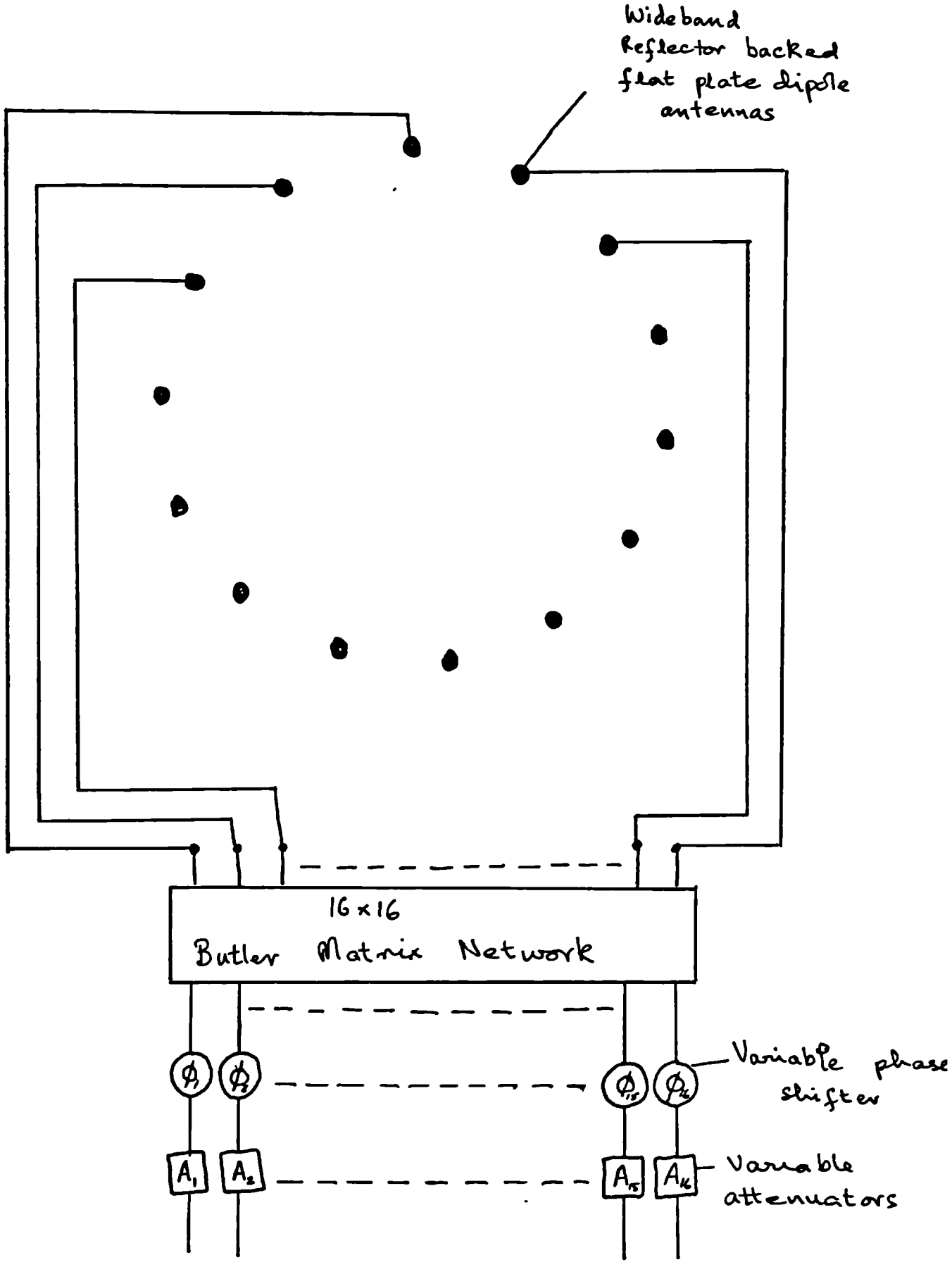

SCHEMATIC DIAGRAM OF THE EXPERIMENTAL CIRCULAR ARRAY

FIGURE 3.1

(a),(b),(c) = omnidirectional elements
(d),(e),(f) = '1 + cosϕ' elements
frequency = 300MHz

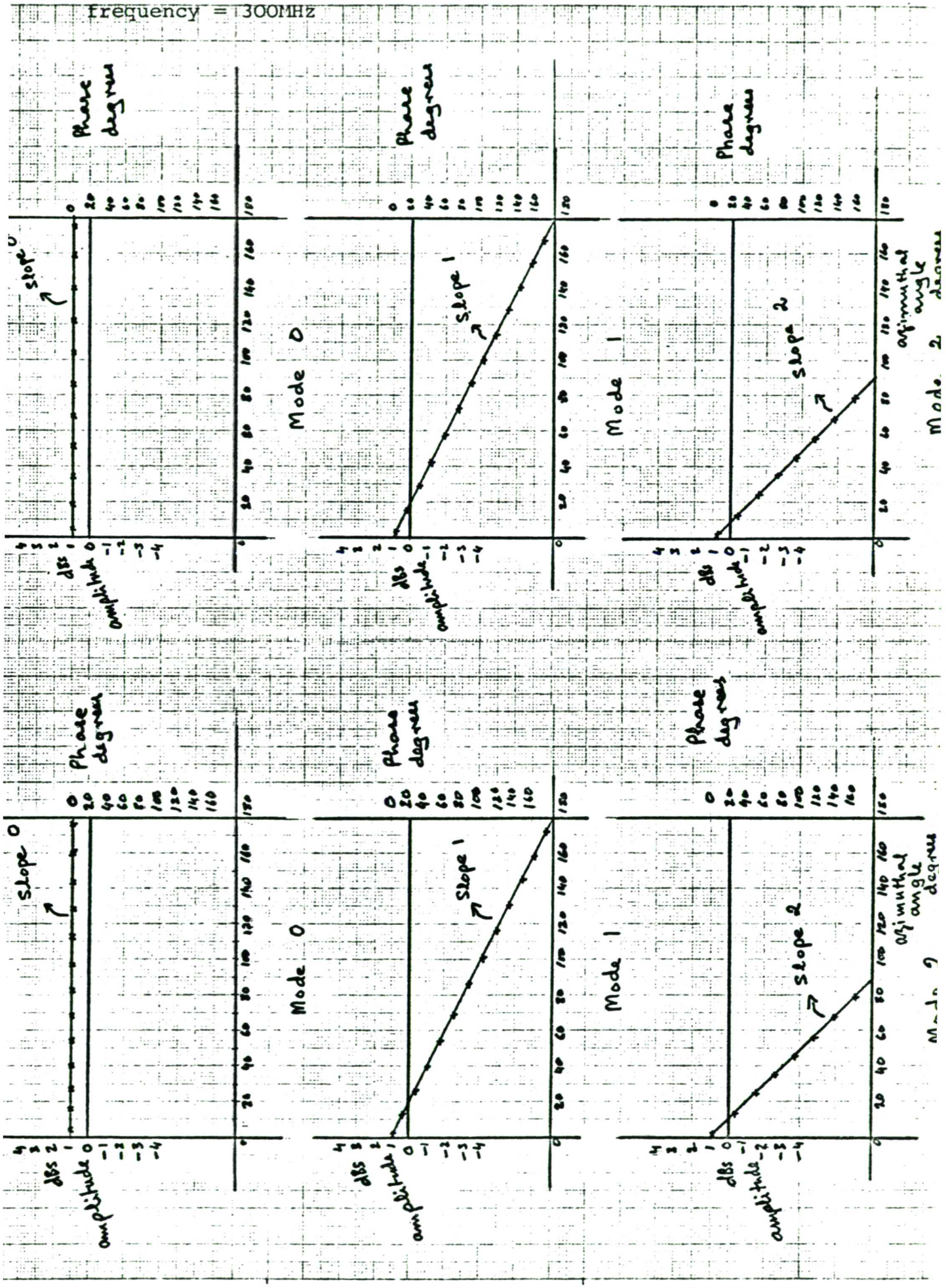

FIGURE 3.2

Phase modes for 8ft diameter circular array of 16 elements
(a), (b), (c) = omnidirectional elements
(d), (e), (f) = '1 + cosϕ' elements
frequency = 300MHz

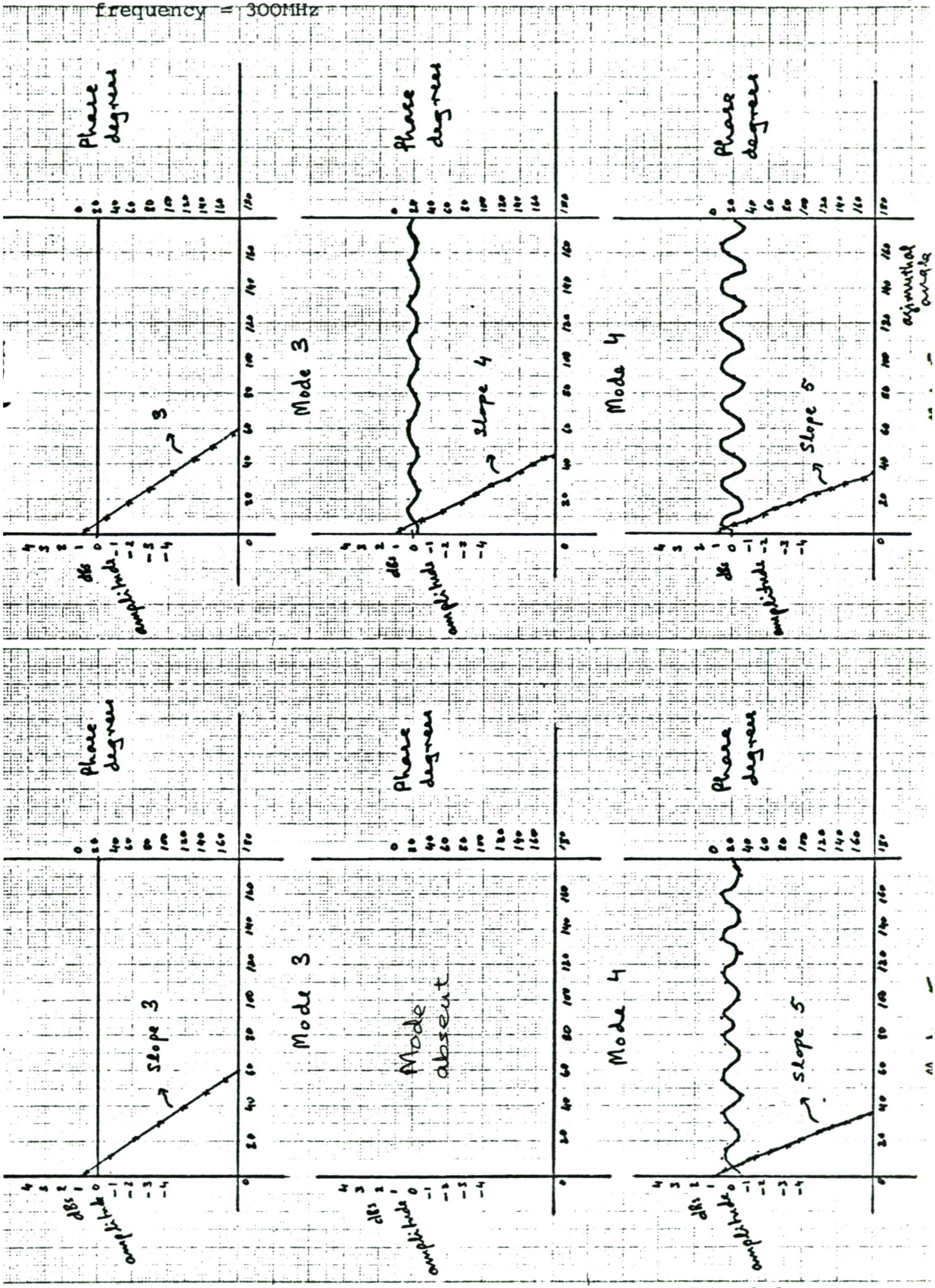

FIGURE 3.3

Phase modes for six-element circular array of omnidirectional elements
(a), (b), (c) = omnidirectional elements
(d), (e), (f) = '1 + cosϕ elements
frequency = 300MHz

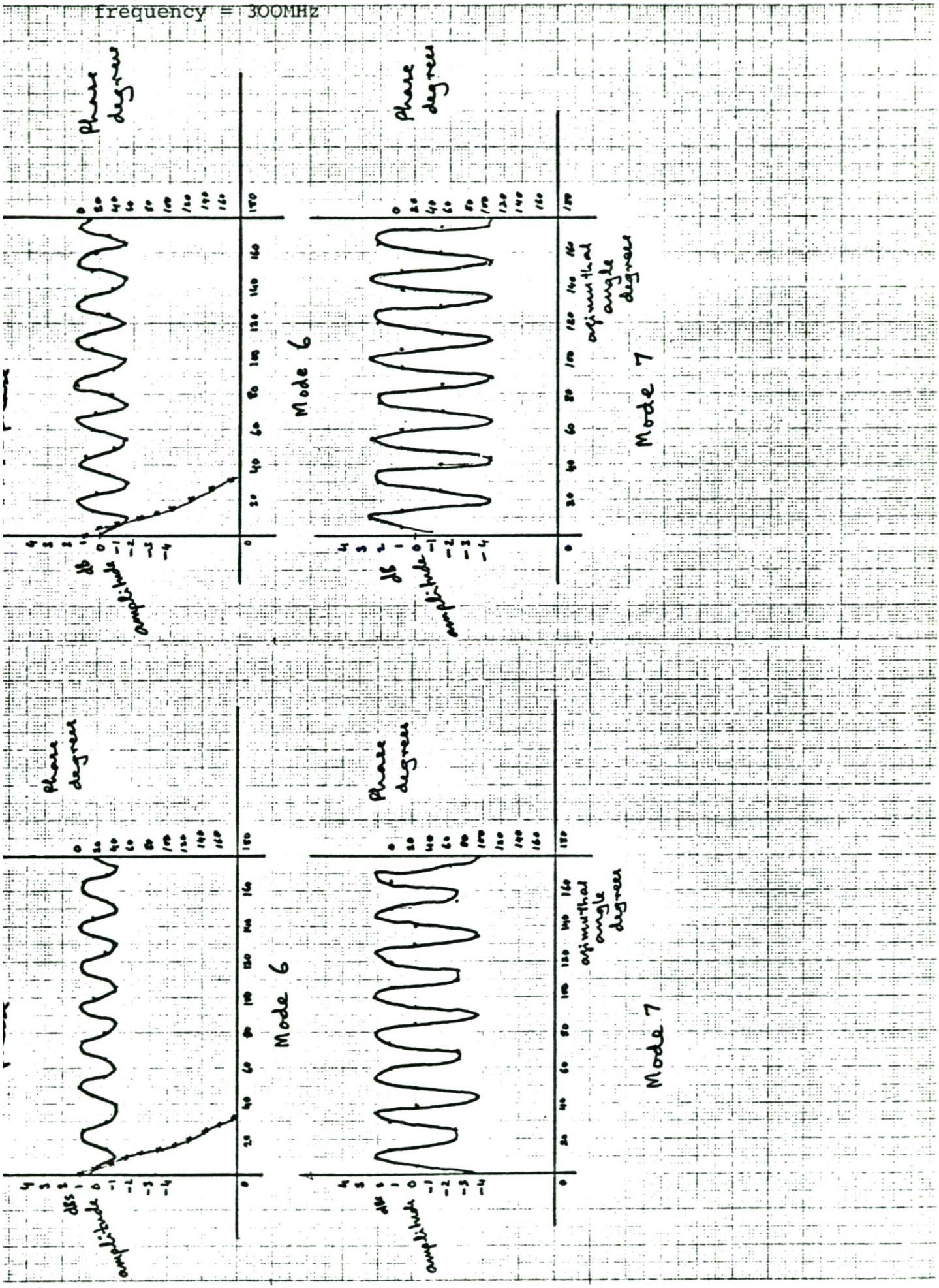

FIGURE 3.4

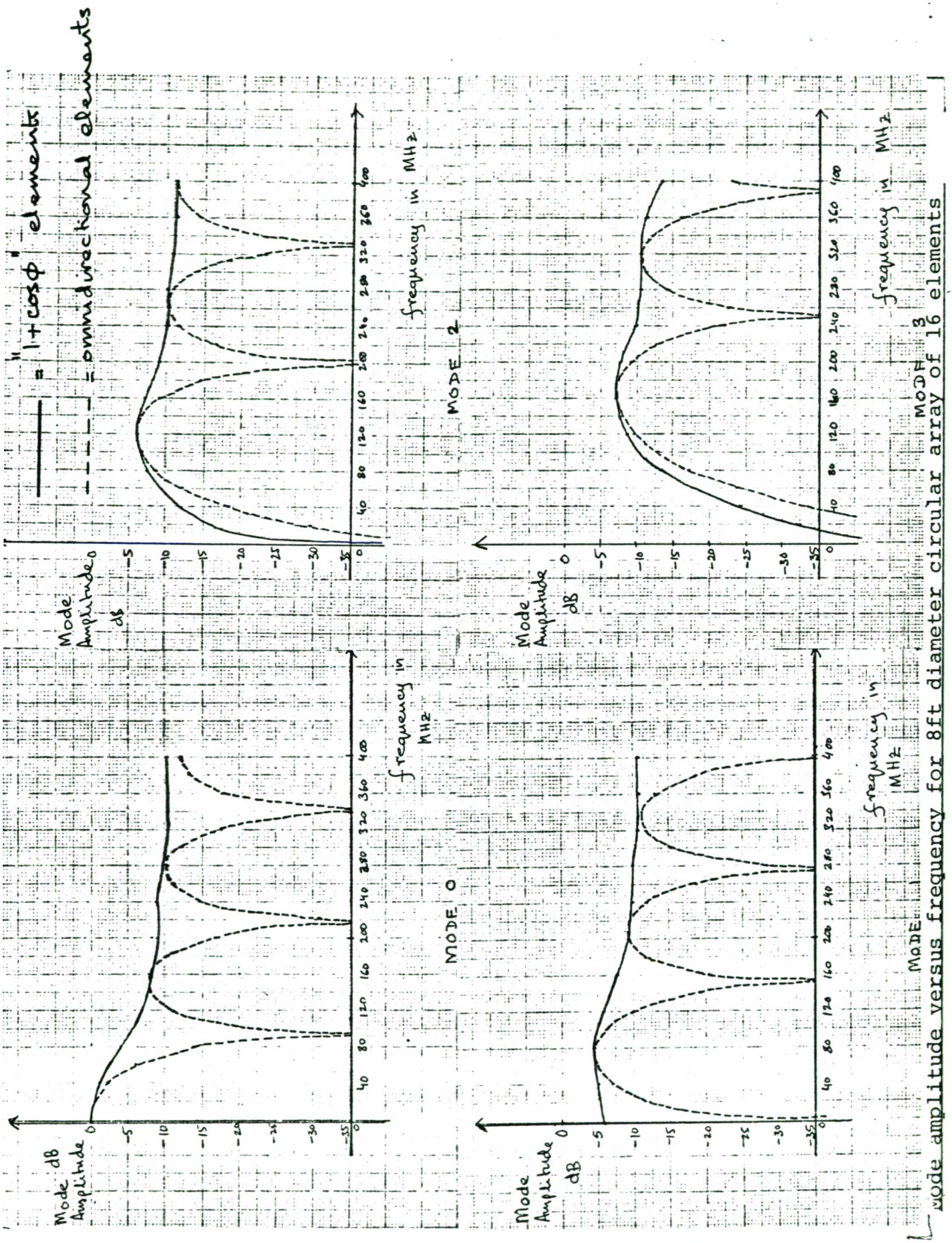

Mode amplitude versus frequency for 8ft diameter circular array of 16 elements

FIGURE 3.5

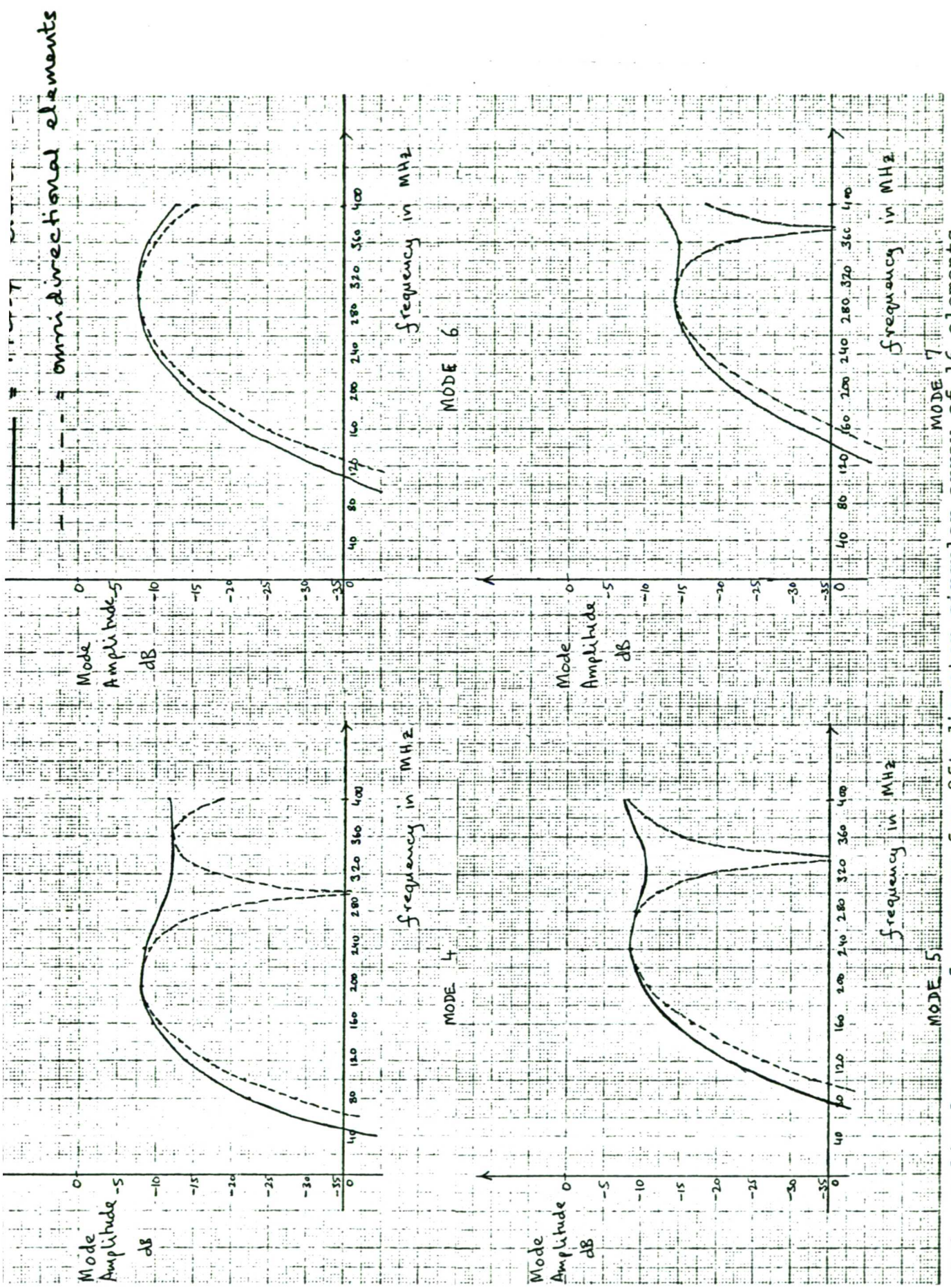

Mode amplitude versus frequency for 8ft diameter circular array of 16 elements

FIGURE 3.6

Figure 3.7 Relative phase shift versus frequency response

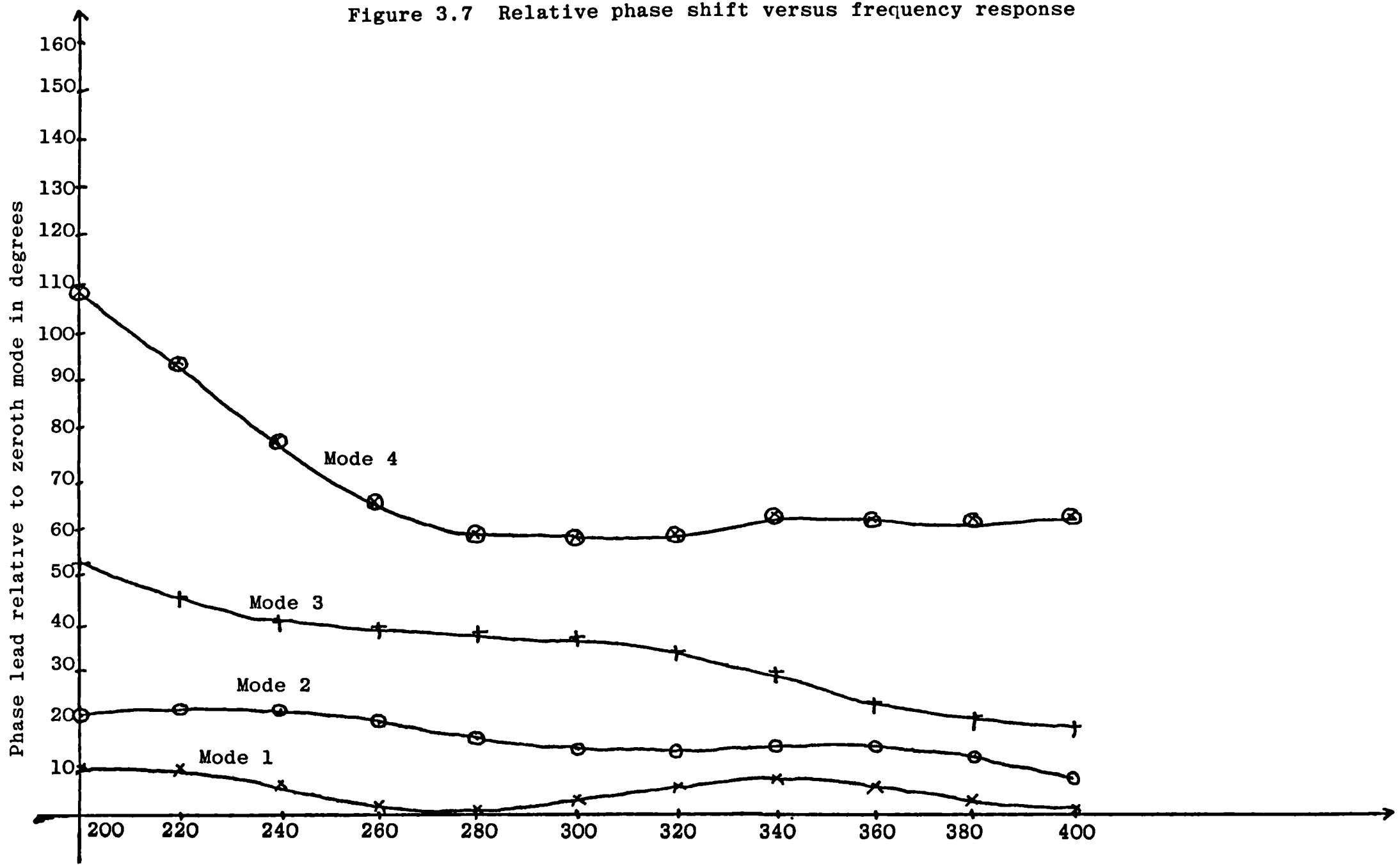

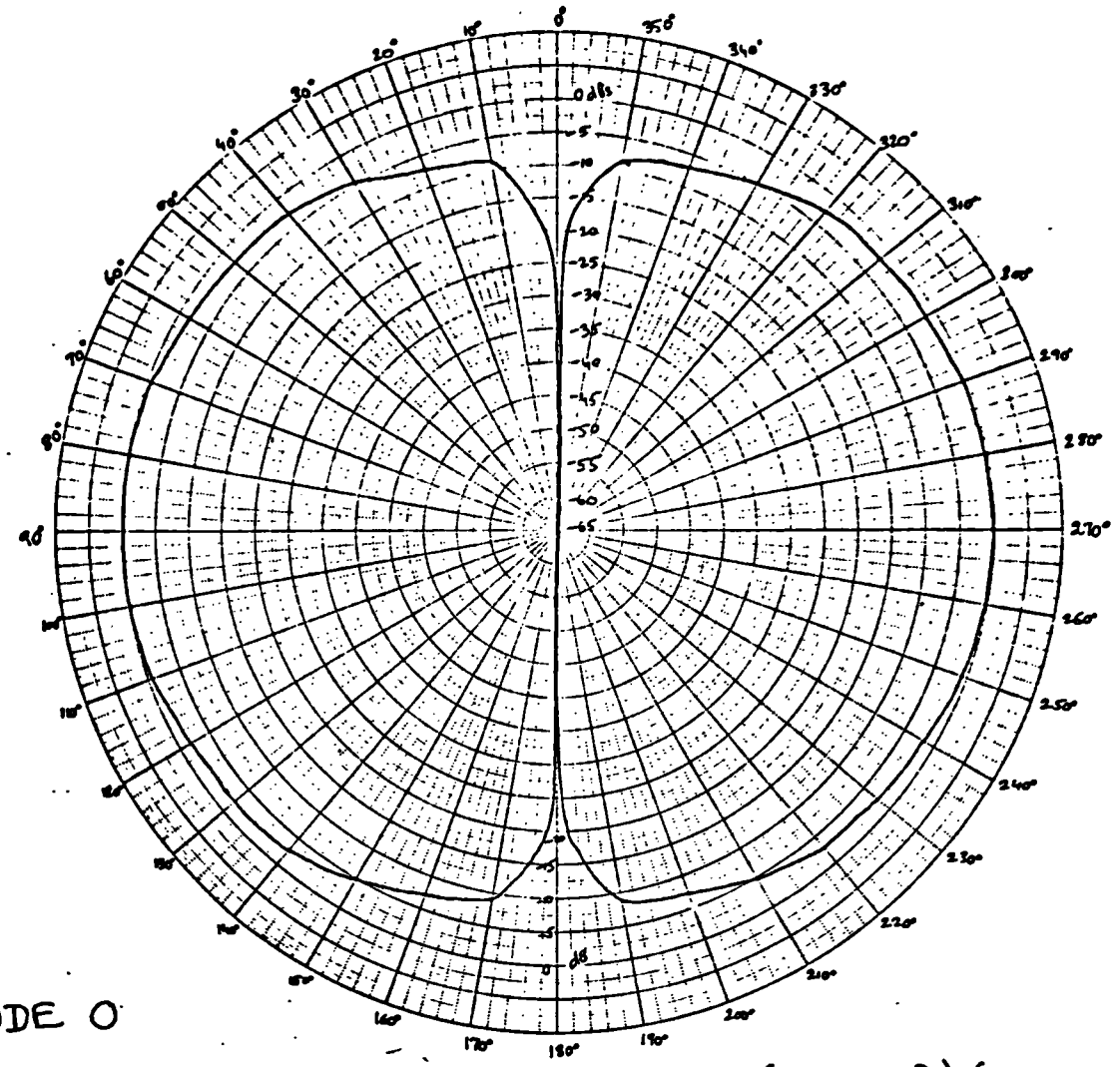

MODE 0

$$\text{ELEMENT PATTERN} = \frac{\cos(\pi/2\cos\theta)}{\sin\theta}(1+\cos\phi\sin\theta)$$

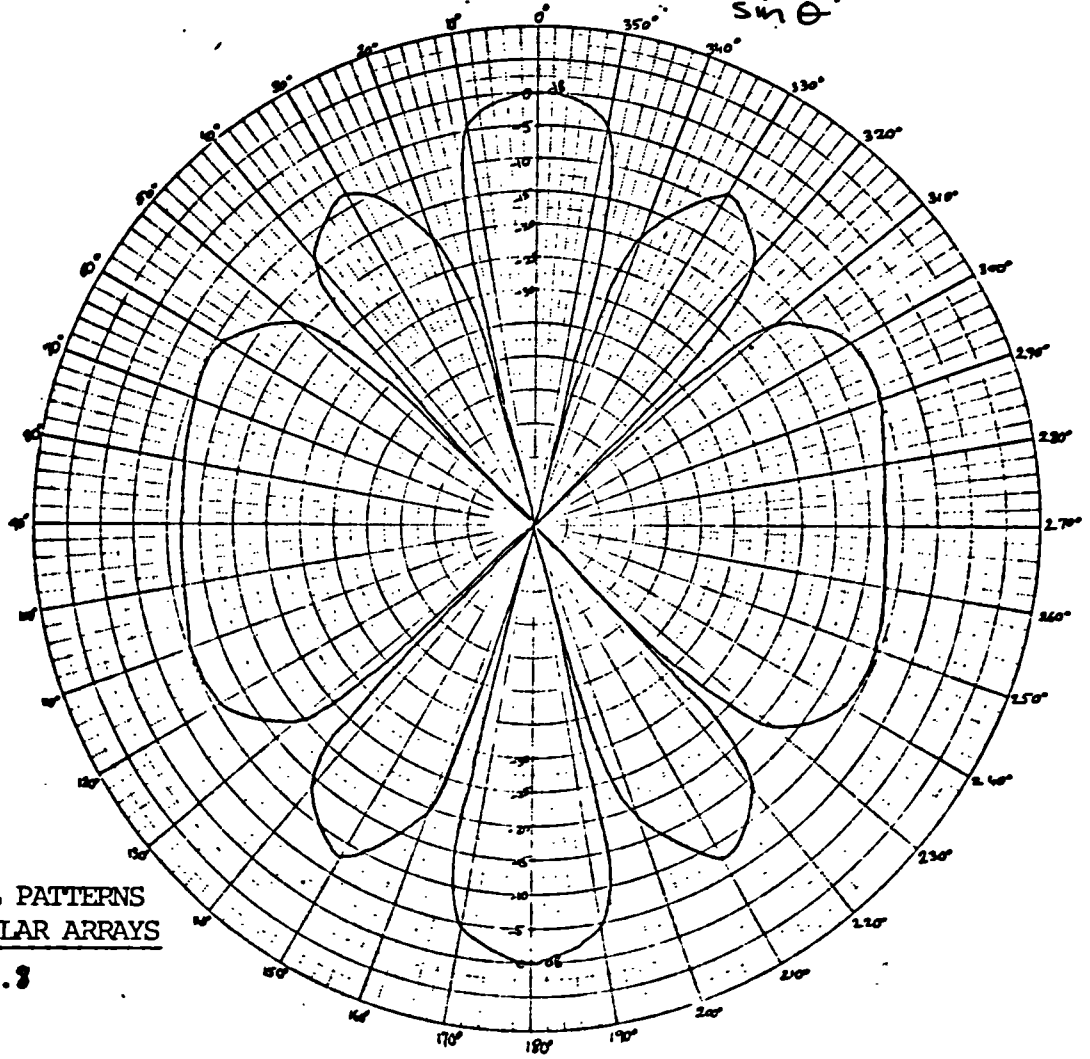

VERTICAL PATTERNS OF CIRCULAR ARRAYS

FIGURE 3.8

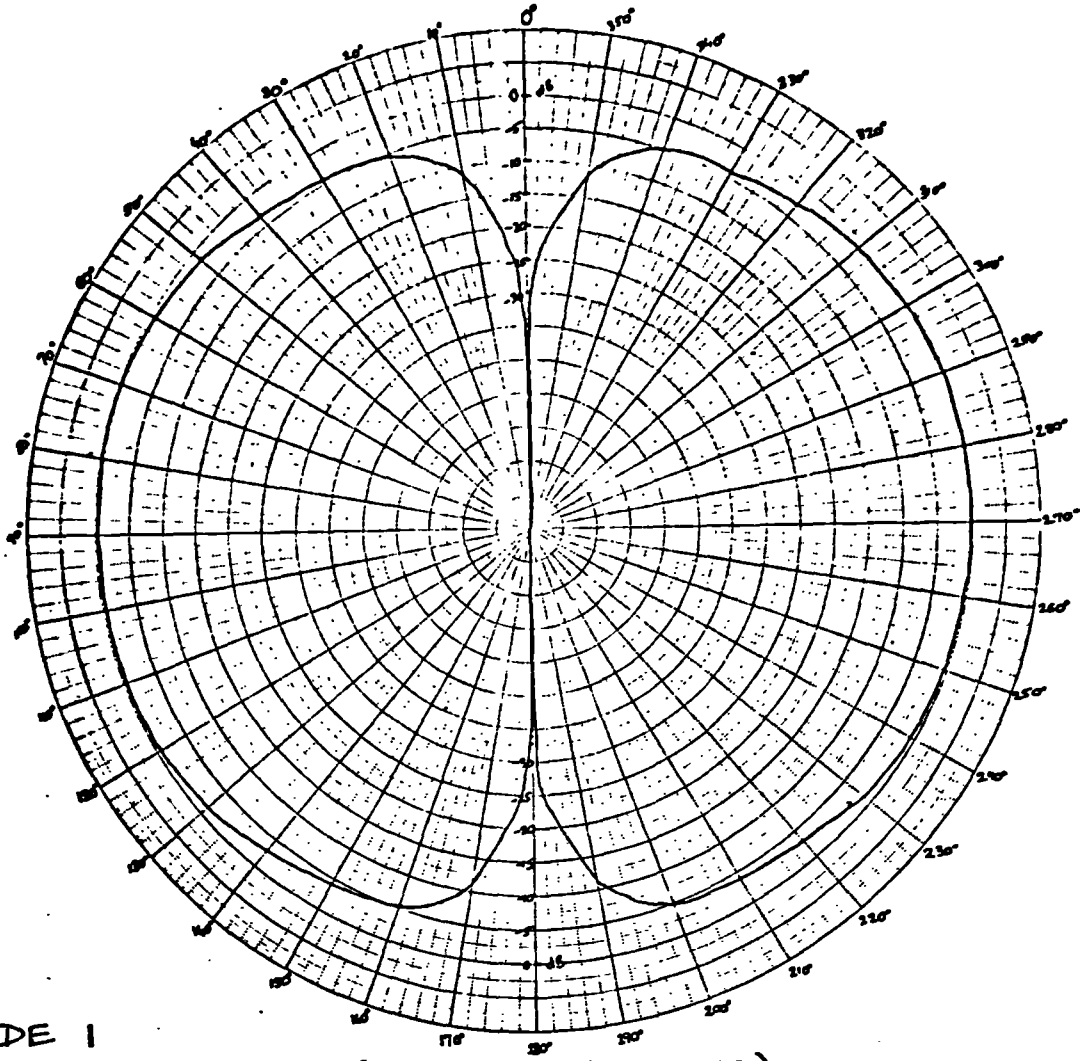

MODE 1

$$\text{ELEMENT PATTERN} = \frac{\cos(\pi/2\cos\theta)}{\sin\theta}(1+\sin\theta\cos\phi)$$

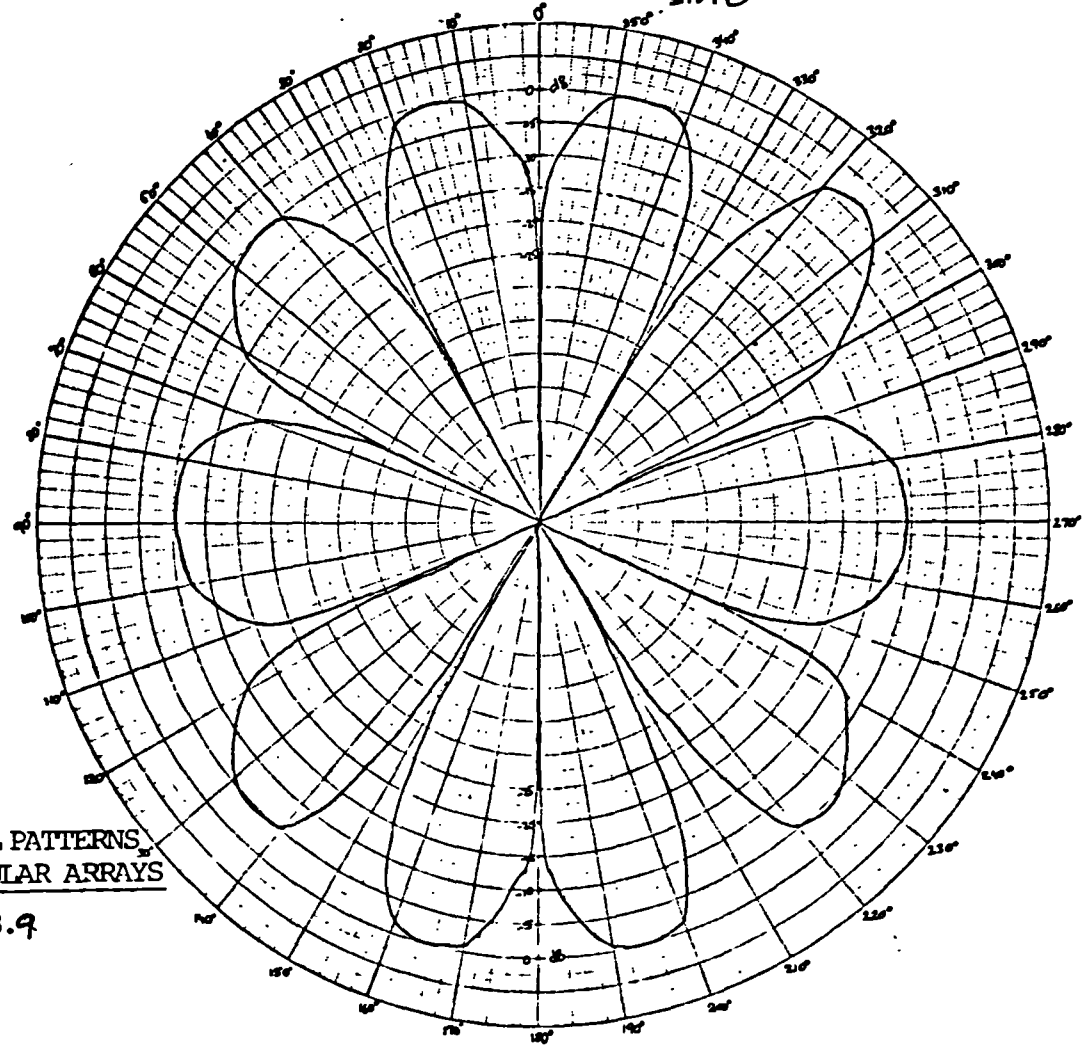

VERTICAL PATTERNS OF CIRCULAR ARRAYS

FIGURE 3.9

OMNIDIRECTIONAL ELEMENTS

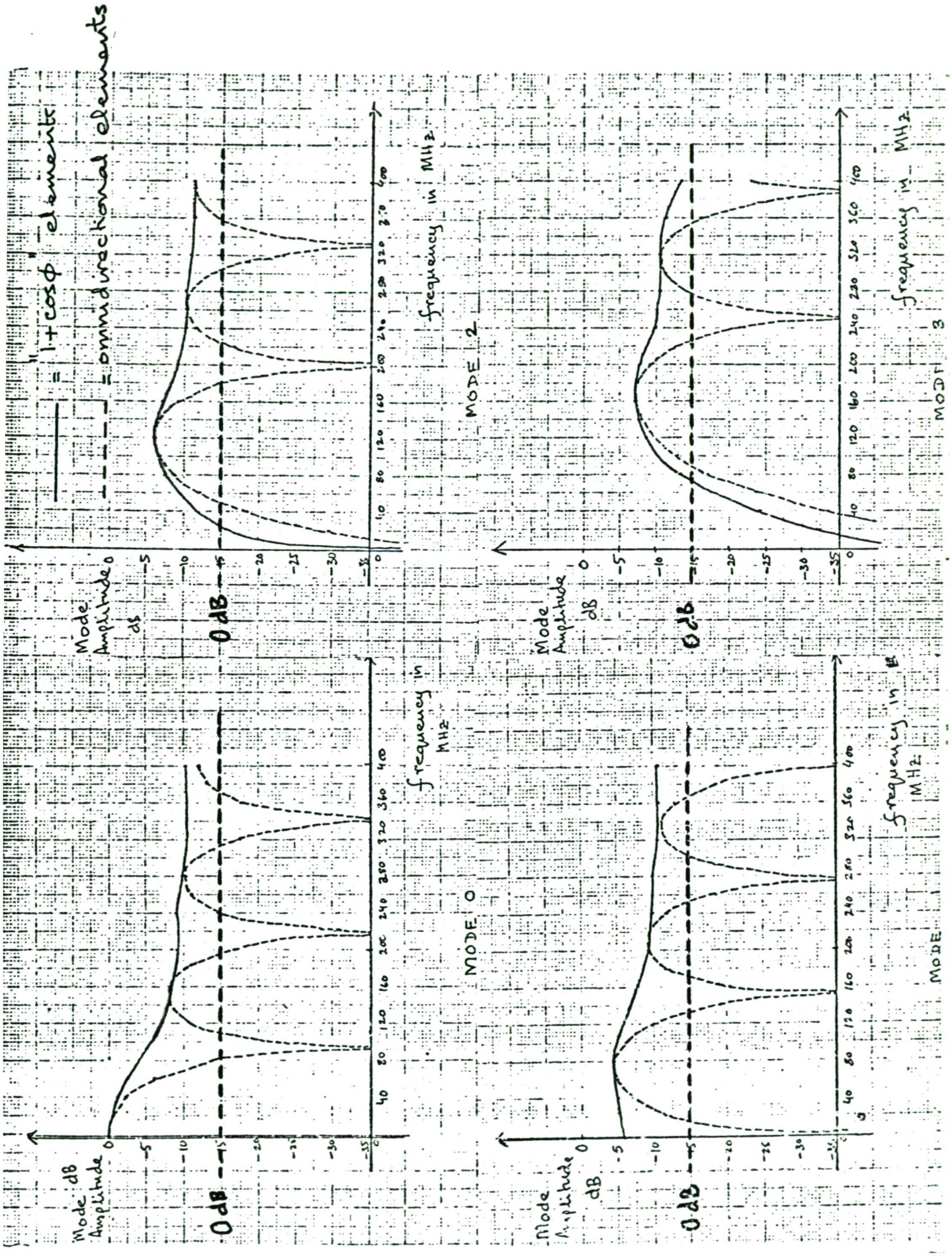

Figure 3.10 Absolute gain of various modes

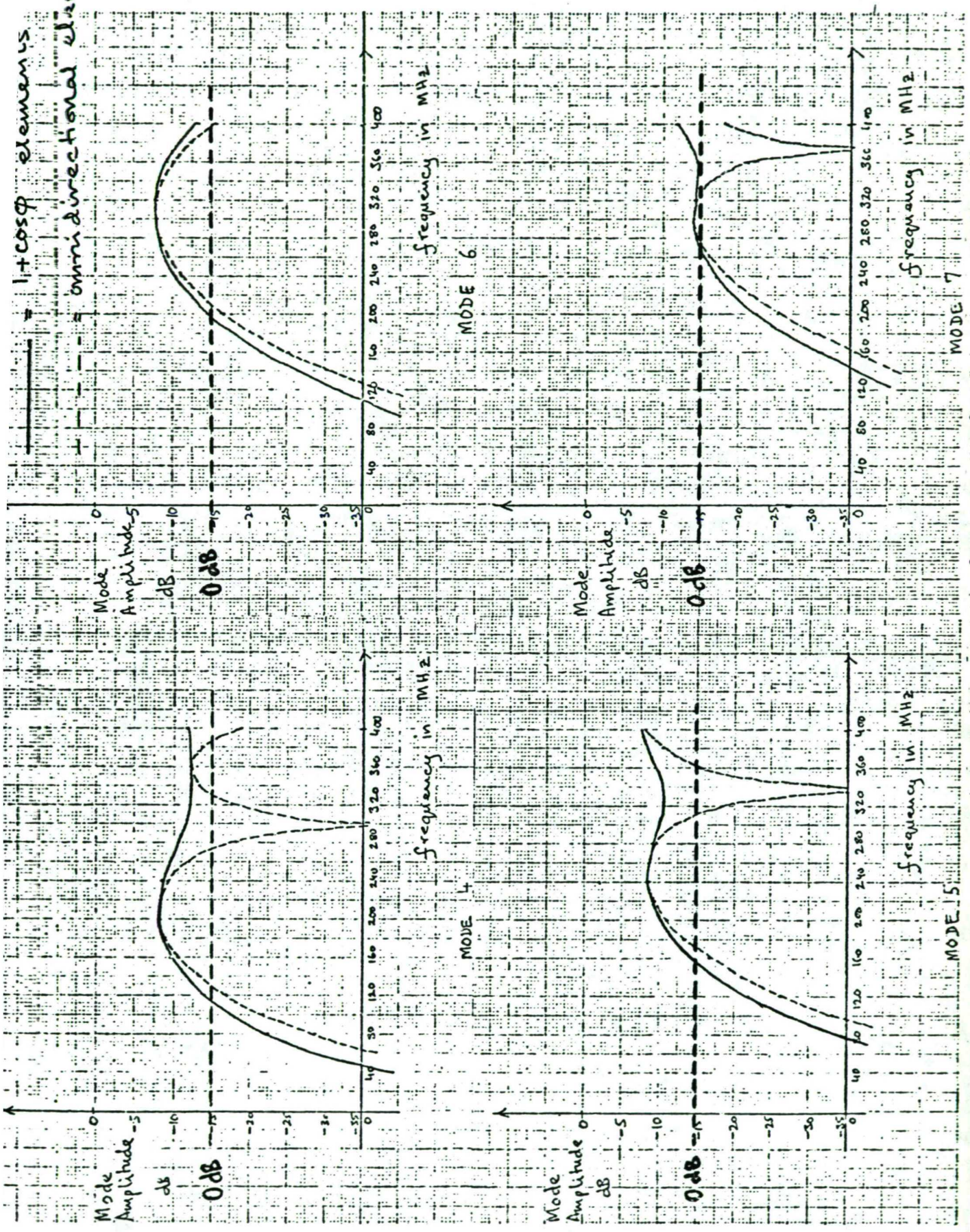

Figure 3.11 Absolute gain of various modes

CHAPTER IV

NEW TECHNIQUES FOR SYNTHESIS OF SHARP NULLS IN OTHERWISE OMNIDIRECTIONAL PATTERN OF CIRCULAR ARRAYS

4.1 Introduction

This chapter describes new techniques for synthesis of single and 2n sharp nulls in an otherwise omnidirectional pattern of circular arrays using spatial phase modes. The techniques are applicable to both circular arrays of omnidirectional and directional elements as spatial phase modes can be obtained in both the cases as shown in Chapter II. The mechanism for independent steering of 2n nulls is also described. The techniques are particularly applicable to Butler matrix fed large circular arrays. A previous technique for independent steering of multiple nulls in the directional pattern of circular arrays is also described for comparison. Section 4.6 describes a null sharpening technique using a concept of selective placement of zeros of the array polynomial in the complex Z plane.

Theoretical patterns are computed for both the new techniques and the previous technique to determine the null widths and gain ripple achievable.

4.2 Synthesis of a Single Sharp Null in an otherwise Omnidirectional Pattern

Consider a far field directional pattern 'F(ϕ)' as shown in Fig. 4.1(a). F(ϕ) has a constant phase from 0^{o} to 180^{o} and unit amplitude. At 180^{o} there is an abrupt phase reversal, resulting in a null. There is an abrupt phase reversal

again at 360^{o}, resulting in another null. It was shown in Section 2.4 equation 2.36 that $F(\phi)$ can be expressed as

$$F(\phi) = \frac{a_o}{2} + \sum_{n=1}^{N} a_n \cos n\phi + b_n \sin n\phi$$

a_o, a_n and b_n are given by

$$a_o = \int_0^{2\pi} F(\phi)d\phi \qquad 4.1$$

$$a_n = \int_0^{2\pi} F(\phi)\cos n\phi d\phi \qquad 4.2$$

$$b_n = \int_0^{2\pi} F(\phi)\sin n\phi d\phi \qquad 4.3$$

For the square wave function of Fig. 4.1(a), it can be shown that, $a_o=0$, $b_n=0$ and

$a_n=0$ for n even

$a_n=\frac{1}{n}$ for n odd

Therefore the directional pattern shown in Fig. 4.1(a) can be expressed as

$$F(\phi) = \sin\phi + \frac{1}{3}\sin 3\phi + \ldots\ldots \frac{1}{2n+1}\sin(2n+1)\phi \qquad 4.4$$

The sine harmonics for constructing the pattern $F(\phi)$ can be produced by exciting the same current harmonics on the circular array. Since in an array of finite number of elements, only a limited number of harmonics can be obtained, the field pattern $F(\phi)$ for a truncated series will be as shown in Fig. 4.1(b). The modulus of the field pattern $|F(\phi)|$ is shown in Fig. 4.1(c). Therefore there are two sharp nulls 180^{o} apart in an otherwise omni-directional pattern with small gain ripple.

In order to fill the null at 180^{o} a cardioid 'β' shown in Fig. 4.2(a) can be added to the directional pattern 'α'. Also since the field reverses sign at 180^{o}, the cardioid should be complex to produce symmetrical pattern. The resulting field pattern $|F(\phi)|$ is given

$$|F(\phi)| = |jA\left(1+\cos(180-\phi)\right)+\sin\phi+\frac{1}{3}\sin 3\phi+..\frac{1}{2n+1}\sin(2n+1)\phi| \qquad 4.5$$

FIg. 4.2(b) shows equation 4.5 plotted. The far field directional pattern is therefore a single sharp null in an otherwise omnidirectional pattern with a small degree of gain ripple.

Null depth using ideal modes is infinite, but in practical antennas there will inevitably be 'systematic' and 'random' amplitude and phase errors, which will cause loss in null

depth. The effects of amplitude and phase errors are described in Chapter II. However, the parameters null width and gain ripple in the omniregion, even when using ideal modes, will depend on two factors. Firstly, on the number of sine harmonics utilised. That is, as the number of harmonics increases the null width and gain ripple decreases. Secondly, on the relative amplitude 'A' of the cardioid.

This technique is practicable because reasonable null depths and gain ripple should be possible with a truncated sine series, since the amplitude of higher harmonics decreases as reciprocal of the harmonic order. Patterns are computed in a later section to demonstrate the feasibility of the concept.

For ship borne applications it is also desirable to maintain the null up to about 5^{o} in the vertical plane due to problems of ship roll. It was shown in Chapter II that the use of directive elements will stabilize the amplitude variation in the vertical, but will also cause phase to vary in the vertical plane as opposed to circular arrays of omnidirectional elements. Due to variation of phase in the vertical plane the null width in the vertical plane will be narrow even when broad nulls are synthesised in the horizontal plane.

4.3 Synthesis of 2n Sharp Nulls in an otherwise Omnidirectional Pattern

Consider the shifted pattern of Fig. 4.1(a) shown in Fig. 4.3(a) (shown in full line). Consider now the dotted line pattern shown in Fig. 4.3(a). This pattern can be produced by changing the mode (Fourier harmonic) excitation. Thus the second null 180^{o} away can independently be shifted to a new location 'ϕ_2', by simply controlling the mode excitation. This technique applied to circular arrays of finite number of elements is shown in Fig. 4.3(b). Also the technique can obviously be extended to produce 4,6...2n sharp nulls in an otherwise omnidirectional pattern of circular arrays (shown in Fig. 4.3(c)).

The field pattern $F(\phi)$ can be written as

$$F(\phi) = \sum_{-M}^{+M} C_m e^{Jm\phi} \qquad 4.6$$

where the mode coefficient C_m is given by

$$C_m = \int_0^{2\pi} F(\phi) e^{-Jm\phi} d\phi \qquad 4.7$$

For the case of 2n nulls, the mth mode coefficient is given by

$$C_m = \frac{(e^{-Jm\phi 1} - e^{-Jm\phi 2} + \ldots\ldots e^{-Jm\phi 2n})}{Jm} \qquad 4.8$$

where ϕ_1, ϕ_2,...ϕ_{2n} corresponds to the angular location of the first, second .....2nth null respectively. From equation 4.8 it is evident that phase shifter networks feeding a Butler matrix can be designed for appropriately phasing the various modes to independently steer the nulls.

The null width and the gain ripple between the nulls will depend on the number of modes used. Also, when two adjacent nulls are brought close together, gain between them will be reduced due to the use of a finite number of modes. This has the disadvantage that the independence between the nulls will also be lost and this will be studied later. It is also convenient to define the minimum allowable null separation as that for which the gain between the nulls is reduced not more than, say, -10dB. This definition will provide a useful means of comparison between the various synthesis techniques.

The computed results in section 4.5 study the effect of a number of ideal modes on the null width, the gain ripple and the minimum allowable null separation.

It should also be pointed out that the technique can be extended to conventional linear antenna arrays. This is possible, because in linear arrays a spatial mode is generated over 180^o on a $\sin\theta$ scale by each element. Consequently, the mode excitation of circular arrays will correspond to the element excitation in linear arrays.

4.4 A Review of the Previous Technique for the Synthesis of n nulls in the Directional Pattern of Circular Arrays

This section briefly describes the previous technique (15) for synthesis and independent steering of multiple nulls in circular arrays.

Consider an n-element circular array. If all the available modes, -n/2 through to +n/2, are excited, then the far field pattern is given by

$$F(\phi) = a_{-n/2}e^{-jn/2\phi}+....+a_{-1}e^{-j\phi}+a_o+a_1e^{j\phi}+....+a_{n/2}e^{jn/2} \qquad 4.9$$

put $Z = e^{j\phi}$

$$F(Z) = a_{-n/2}Z^{-n/2}+...+a_{-1}Z^{-1}+a_o+a_1Z+...+a_{n/2}Z^{n/2} \qquad 4.10$$

or

$$F(Z) = Z^{-n/2}\left\{a_{-n/2}+a_{-n/2+1}Z+a_{-n/2+2}Z^2+... \ ...+a_{n/2}Z^n\right\} \qquad 4.11$$

The polynomial F(Z) can be expressed as a product of n factors, i.e.

$$F(Z) = Z^{-n/2}(Z-Z_1)(Z-Z_2)(Z-Z_3).....(Z-Z_n) \qquad 4.12$$

The zeros of the polynomial Z_1, Z_2,...etc., correspond to the n zeros of the directional pattern. Thus the far field directional pattern containing n nulls can be written as

$$F(\phi) = e^{-j(n/2)\phi}(e^{j\phi}-e^{j\phi 1})\ (e^{j\phi}-e^{j\phi 2}).....(e^{j\phi}-e^{j\phi n}) \qquad 4.13$$

where ϕ_1, ϕ_2, ϕ_3,.....ϕ_n corresponds to angular location of the nulls.

Equation 4.13 can also be written as

$$F(\phi) = (e^{j(\phi_1+\phi_2+....\phi_n)}e^{-j(n/2)\phi}+.....$$

$$.....+(e^{j\phi_1}+e^{j\phi_2}+....e^{j\phi_n})e^{j(n/2-1)\phi}+e^{j(n/2)\phi} \qquad 4.14$$

Thus by appropriately phasing the various modes, nulls can be steered independently. A phase shifter network providing independent steering of the n nulls was shown (15) to be identical to that used for linear arrays (see page 33) but for circular arrays the mode outputs replace the corresponding element outputs used for linear array systems.

4.5 Results of Computations

In this section null patterns are computed to demonstrate the feasibility of synthesis techniques described in section 4.2 and 4.3 and to study the nullwidths and gain ripple achievable using a limited number of modes.

Figures 4.4(a), 4.4(b), 4.5(a) and 4.5(b) show the computed single null patterns using up to five ideal amplitude modes. These patterns demonstrate how the null width and gain ripple are affected by the relative amplitude of the cardioid. When the relative amplitude of the cardioid is unity or half (fig. 4.4(a), (b)) the -10dB null widths are 30^{o} and 17^{o} respectively and the gain ripples are $\pm$4dB and $\pm$2.3dB. Reducing the relative amplitude to 0.25 (fig. 4.5(b)) results in narrower null width (13^{o}) but the gain 180^{o} away from the null is also reduced, resulting in a gain ripple of $\pm$3.2dB. Fig. 4.5(a) shows that optimum null pattern (null width = 15^{o}, gain ripple = $\pm$2dB) is obtained for relative amplitude of 0.35. Similarly, when more amplitude modes are used narrower null widths and smaller gain ripple would be obtained, but null width and gain ripple would have to be optimised by controlling the relative amplitude of the cardioid.

To demonstrate the technique of producing 2n sharp nulls in the directional pattern of circular arrays, patterns are computed (Fig. 4.6, 4.7, 4.8) for producing two sharp nulls. Null patterns are computed using up to 10 amplitude modes. Fig. 4.6(a) shows the two nulls 180^{o} apart. Null widths and gain ripple are in the region of 8^{o} and $\pm$1.5dB respectively.

In Fig. 4.6(b), 4.7(a), 4.8(a), (b) one null is fixed at 90^{o} while the other null is steered (by controlling the

mode coefficient) towards the first null. It is evident from Fig. 4.6, 4.7 that when the second null is steered, the null sharpness and omnidirectionality in all other directions is retained. However, when the nulls are brought very near each other, say 15^{o} or 10^{o} (Fig. 4.8) the gain is reduced to -10dB and -25dB between them. This may not be a significant problem as far as practical situations are concerned. Because the likelihood of getting two interfering signals from only 5^{o} on either side of a wanted signal is small.

Minimum allowable null separation was defined earlier as that for which the gain between the null is reduced not more than -10dB. Minimum allowable null separation in the case when 10 amplitude modes are used is about 15^{o}. However, if fewer modes are used the minimum allowable null separation would be correspondingly larger. Thus, the technique is advantageous only in large circular arrays of many elements.

For comparison, null patterns are also computed using the previous technique (section 4.4). These patterns are computed (figs. 4.9, 4.10, 4.11) using phase modes 0, 1, 2 to form two nulls. The disadvantage of this technique is that the null widths are fairly broad and as the nulls are brought nearer the gain between them is considerably reduced. From fig. 4.10(a) it can be seen that even when the nulls are only 60^{o} apart, the gain between them is

reduced to -20dB. This may be a problem in situations where communication is required in the direction which lies between two interfering directions 60^{o} apart. For this null forming system, the null width is not reduced as the number of elements is increased since only 2 phase modes are used. However, the advantage of this technique is that it utilises a small number of phase modes. Consequently, it can easily be applied to small circular arrays of few elements. And for arrays of many elements, many independently steerable nulls can be synthesised.

4.6.1 Synthesis of Single Sharp Null using the Concept of Imaginary Nulls

It was shown in section 4.2 that using the Fourier Analysis technique a single sharp null may be synthesised by using n modes. However, when we apply the Schelkunoff theory to circular array modes, n modes will produce (n-1) nulls. It is shown in this section that the Fourier and Schelkunoff methods are linked through the concept of imaginary nulls and that the use of imaginary nulls will sharpen the null widths of the real null.

4.6.2 Theory

It was shown in chapter II that the far field pattern $F(\phi)'$ of a circular array can be expressed as a Fourier series

$$F(\phi) = \sum_{-M}^{+M} a_m e^{Jm\phi} \qquad 4.15$$

writing $$Z = e^{j\phi} \qquad 4.16$$

we have

$$F(Z) = a_{-M}Z^{-M} + \ldots + a_o + a_1 Z + \ldots + a_M Z^M \qquad 4.17$$

$$= Z^{-M}(a_{-M} + \ldots + a_o Z^M + \ldots + a_M Z^{2M}) \qquad 4.18$$

The polynomial inside the bracket can be expressed as a product of 2M factors. Hence

$$F(Z) = Z^{-M}(Z-Z_1)(Z-Z_2)\ldots\ldots(Z-Z_{2M}) \qquad 4.19$$

Thus the polynomial F(Z) contains 2M zeros; at Z_1, $Z_2 \ldots Z_{2M}$ where Z_1, $Z_2 \ldots Z_{2M}$ are complex numbers. Substituting the value of the nth zero in equation 4.16

$$Z_n = A_n e^{j\phi n} = e^{j\phi} \qquad 4.20$$

we have

$$\phi = \phi_n - J \log_e A_n \qquad 4.21$$

If $A_n=1$ then $\phi = \phi_n$ is real. This results in a null in the directional pattern '$F(\phi)$' at ϕ_n. However, if $A_n \neq 1$, then ϕ is complex, therefore there is no null in the directional pattern. Fig. 4.12 (below) shows the Z-plane representation of the zeros of the polynomial F(Z).

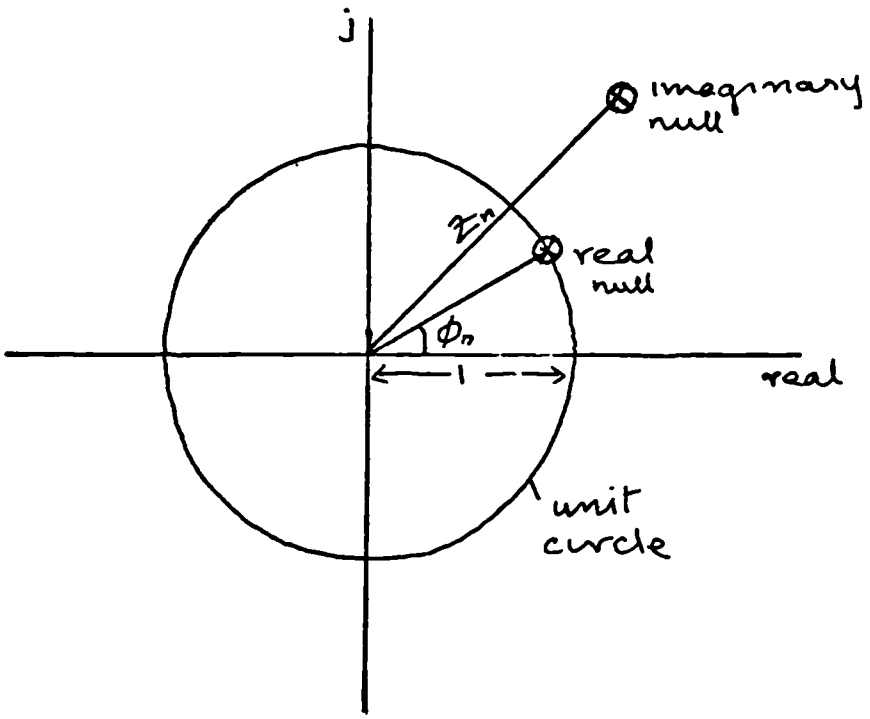

Diagram 1 Complex Z-plane

If the Schelkunoff analysis is applied to the phase modes of a circular array we see that the angular location of the zeros of the directional pattern represents the roots of the polynomial and if there are n-1 zeros for n phase modes the location of the zeros completely defines the polynomial and hence defines the mode excitation of the array.

We see from the above that when a root of the polynomial lies on the unit circle in the complex Z plane it gives rise to a real zero in space. Roots which are not located on the unit circle do not produce zeros but those located very near to the unit circle can produce minima. It is convenient to refer to roots located off the unit circle as giving rise to imaginary zeros in the directional pattern. It will now be shown that the location of these roots (or imaginary zeros) effects the shape of the directional pattern in real angles. In particular we may use such imaginary nulls to reduce the null width of a real null without introducing any additional zeros into the pattern.

4.6.3 Results of Computation

In this section it is shown that by the use of imaginary nulls, nullwidths of the real null may be sharpened.

Fig. 4.12 shows the directional pattern for null positioning as shown in diagram 2 (below)

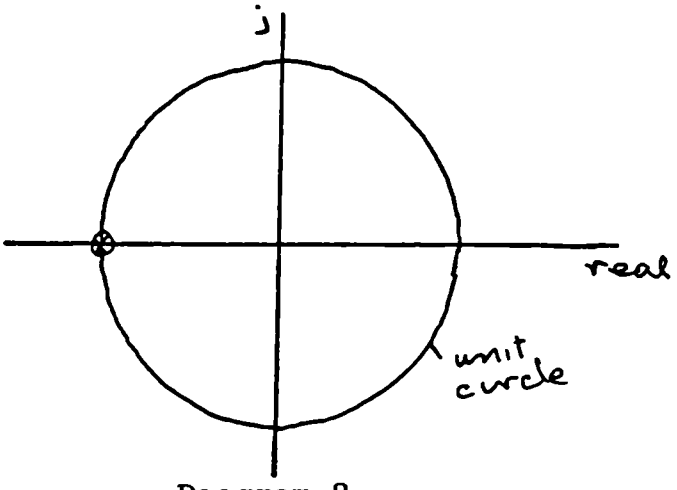

Diagram 2

Fig. 4.13, fig. 4.14 and fig. 4.15 show computed directional patterns for null positioning as shown in diagrams 3, 4 and 5 respectively.

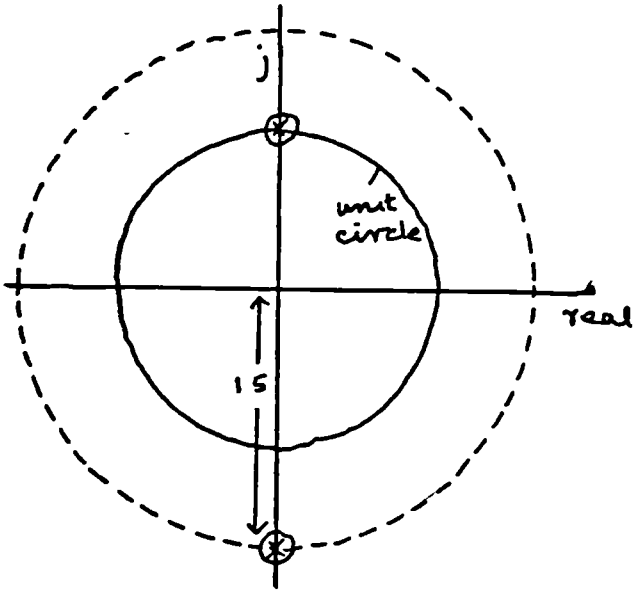

Diagram 3

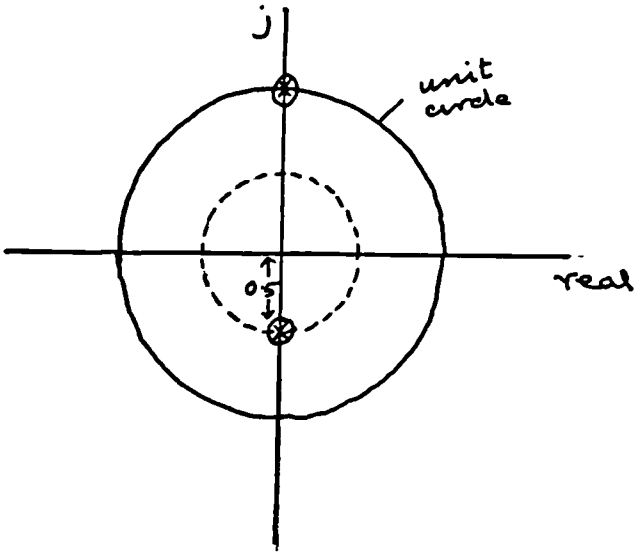

Diagram 4

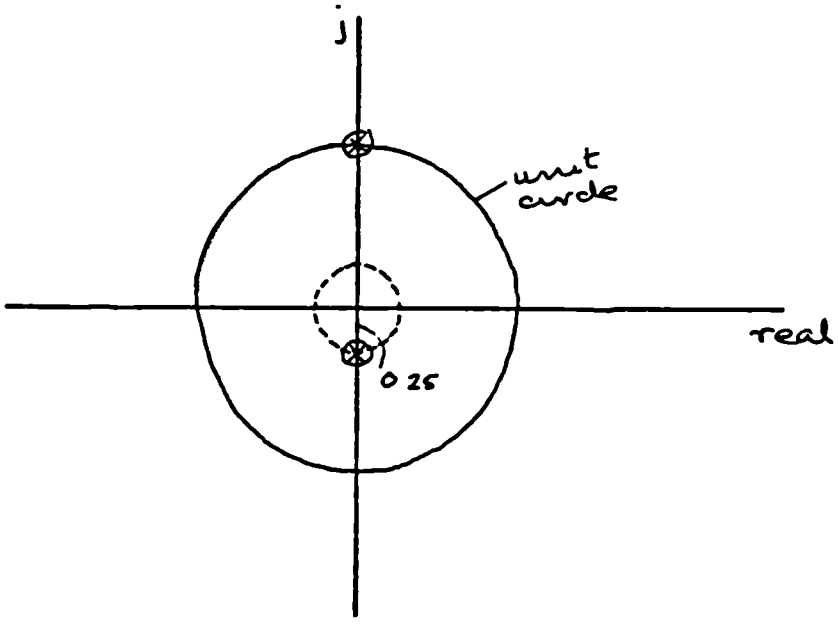

Diagram 5

Using imaginary nulls (off the unit circle) we find that the 10dB nullwidth has been reduced from 68^{o} to 40.5^{o}. However, using an imaginary null gives some gain ripple in the omni-region. From figs. 4.13, 4.14 and 4.15 it is clear that 0.25 circle gives negligible gain ripple.

Fig. 4.16 shows the directional pattern with three imaginary nulls placed on the 0.25 circle. The 10dB null width is further reduced to 29.25^{o}.

To further show that the presence of imaginary nulls sharpens the nullwidths, consider the synthesis of two nulls 180^{o} apart as described in section 4.3. The field pattern $F(\phi)$ is given by

$$F(\phi) = \sin\phi + \frac{1}{3}\sin 3\phi + \ldots\ldots \qquad 4.22$$

Suppose, harmonics up to third are used. Then

$$F(\phi) = \frac{e^{j\phi}-e^{-j\phi}}{2j} + \frac{e^{j3\phi}-e^{-j3\phi}}{6j} \qquad 4.23$$

$$\text{put} \quad Z = e^{j\phi} \qquad 4.24$$

$$F(Z) = \frac{1}{2j}\{Z+Z^{-1}\} + \frac{1}{6j}\{Z^{3}-Z^{-3}\}$$

$$= -\frac{1}{6jZ}\{1 + 3Z^{2}\}-\{3Z^{4} - Z^{6}\} \qquad 4.25$$

To obtain nulls of the pattern, put F(Z)=0

$$\therefore \quad Z^6 + 3Z^{11} - 3Z^2 - 1 = 0 \qquad 4.26$$

put $\varepsilon = Z^2$

$$\therefore \quad \varepsilon^3 + 3\varepsilon^2 - 3\varepsilon - 1 = 0 \qquad 4.27$$

put $\varepsilon = 1$ in equation 4.27

$$1 + 3 - 3 - 1 = 0$$

$\therefore$ $\varepsilon = 1$ is a root of the equation

or $Z^2=1$

$\therefore$ $Z = \pm 1$ (two real nulls in the Z-plane)

To find the remaining four roots, put

$$(\varepsilon-1)(a\varepsilon^2+b\varepsilon+c)=\varepsilon^3+3\varepsilon^2-3\varepsilon-1 = 0$$

or $$a\varepsilon^3+(b-a)\varepsilon^2+(c-b)\varepsilon-c=\varepsilon^3+3\varepsilon^2-3\varepsilon- 1$$

comparing the coefficients on either side, we have C=1,

c-b=-3

$\therefore$ b = 4

Also $b-a=3$

$\therefore \quad a=1$

thus $\varepsilon^2+4\varepsilon+1 = 0$

$\therefore \quad \varepsilon = -2 \pm \sqrt{3}$

Using equation 4.26

$Z^2 = -2 \pm \sqrt{3}$

$Z = \pm j0.52$
$Z = \pm j1.93$
} remaining four nulls in the Z-plane

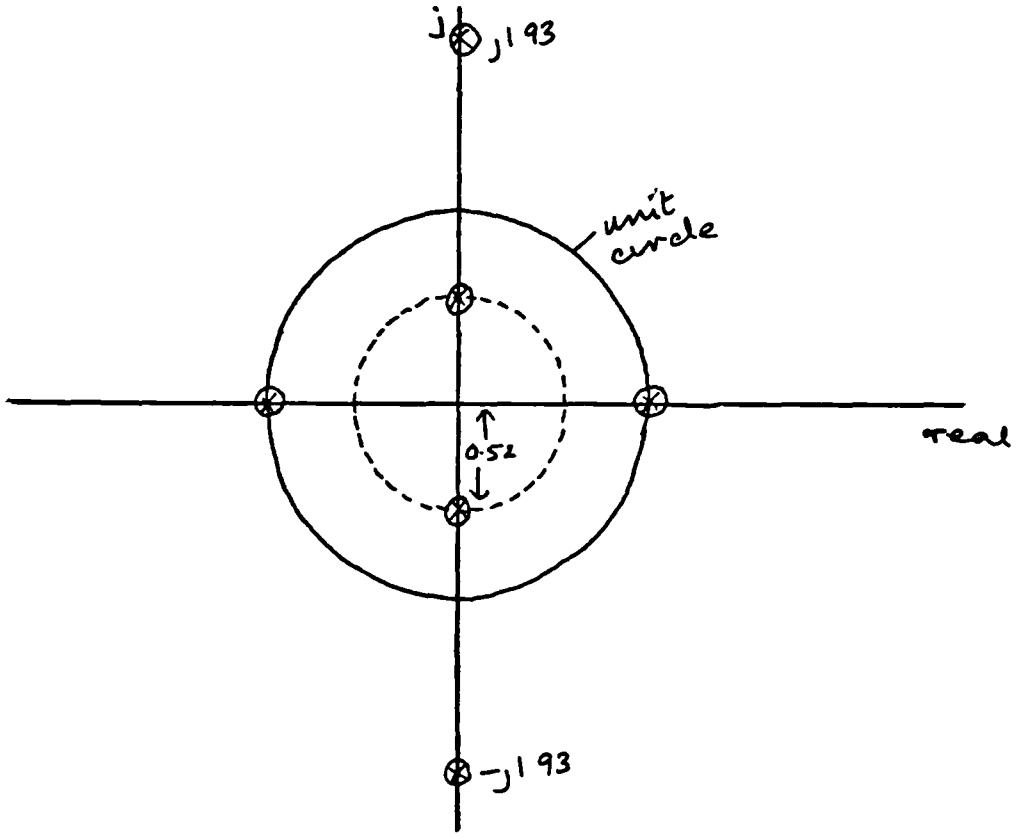

Fig. 4.17 shows a pattern using two real nulls only and fig. 4.18 shows a pattern using the four imaginary nulls as well. It is evident from these patterns that it is the presence of imaginary nulls which sharpen the null widths.

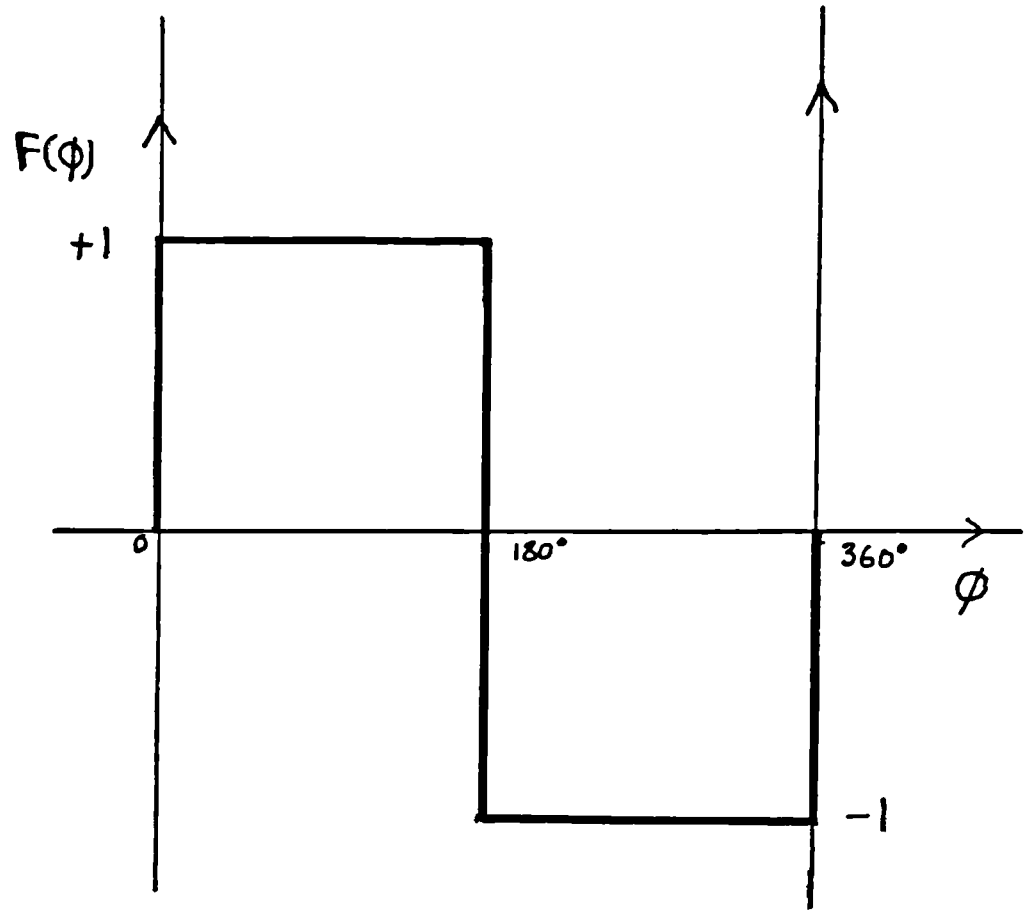

(a)

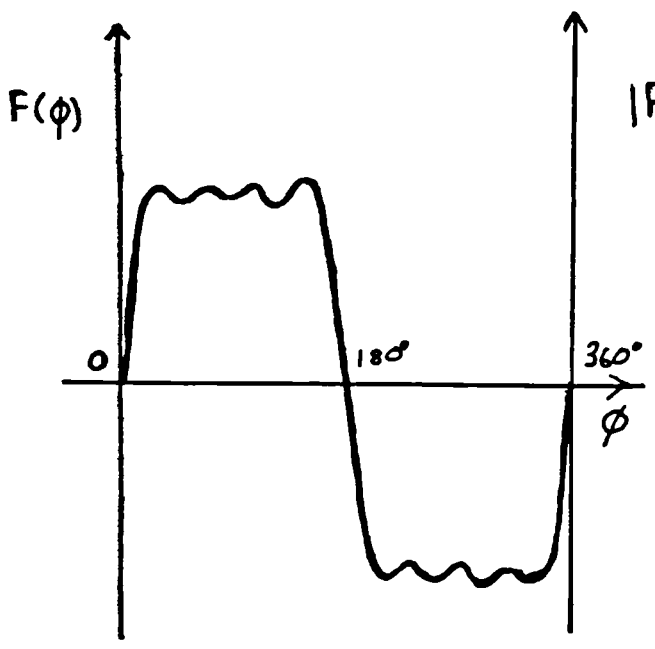

(b)

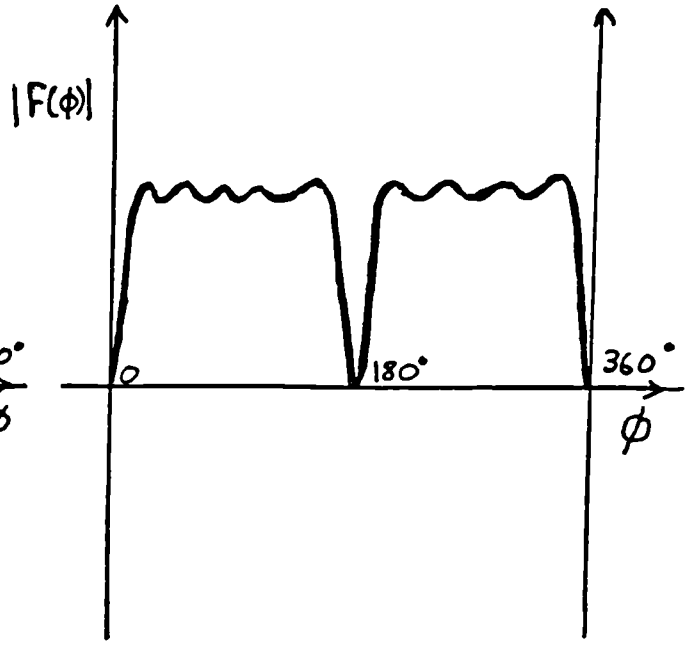

(c)

FIGURE 4.1

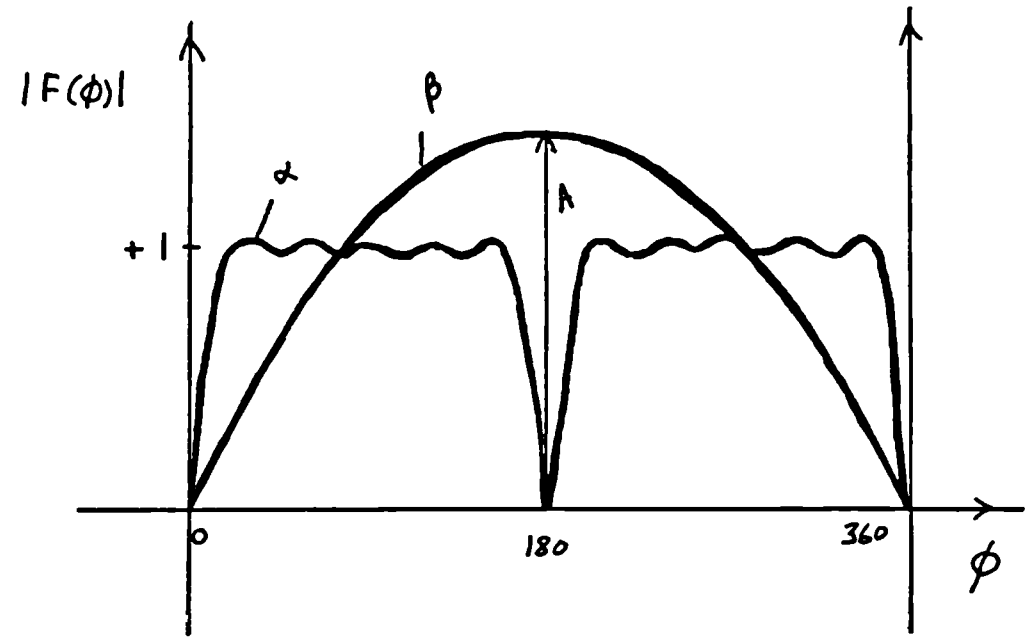

(a)

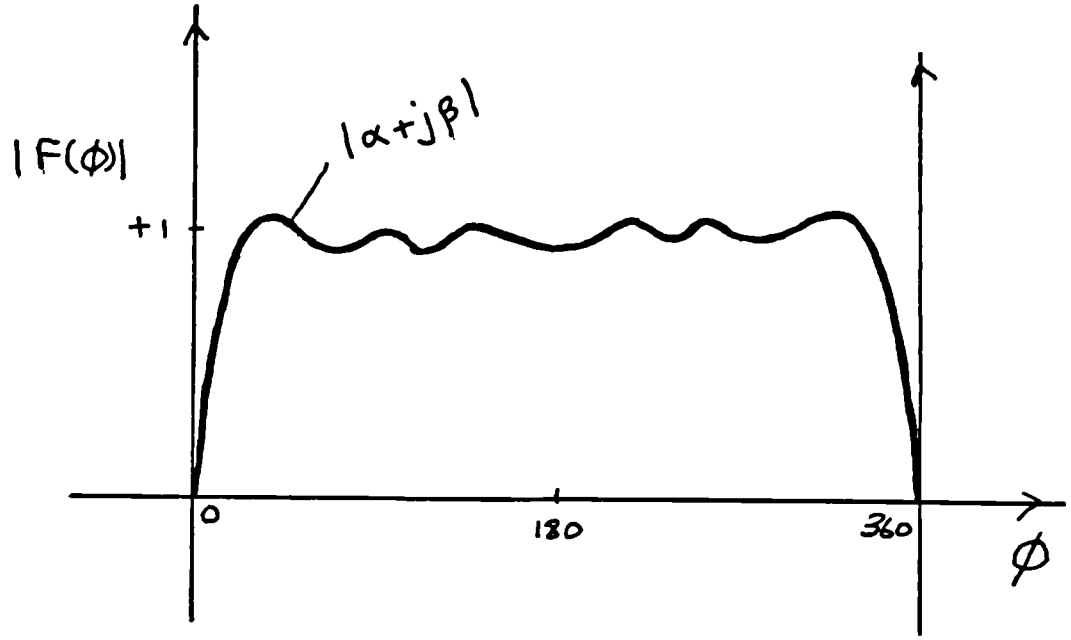

(b)

FIGURE 4.2

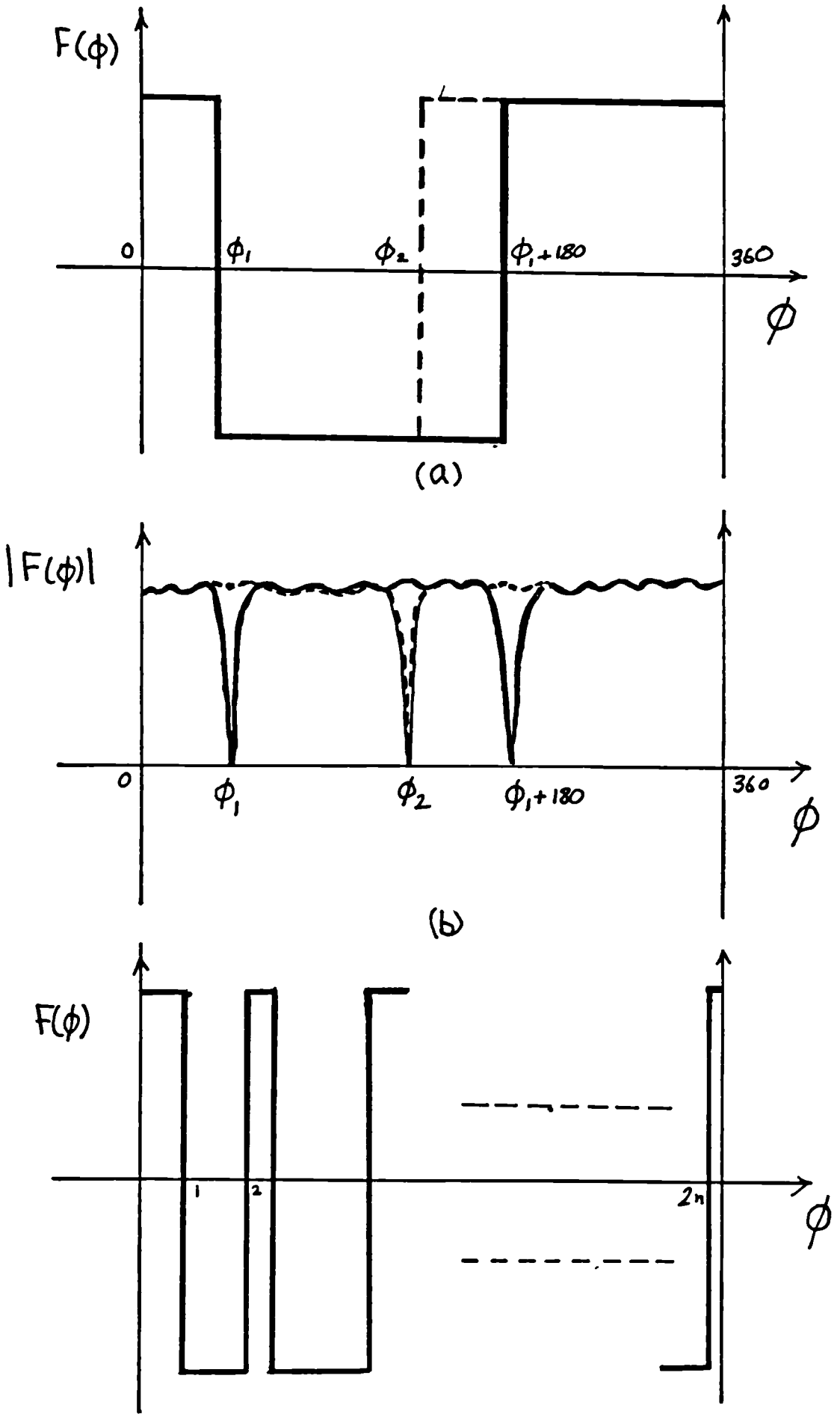

FIGURE 4.3

Synthesis of single null in otherwise omnidirectional pattern

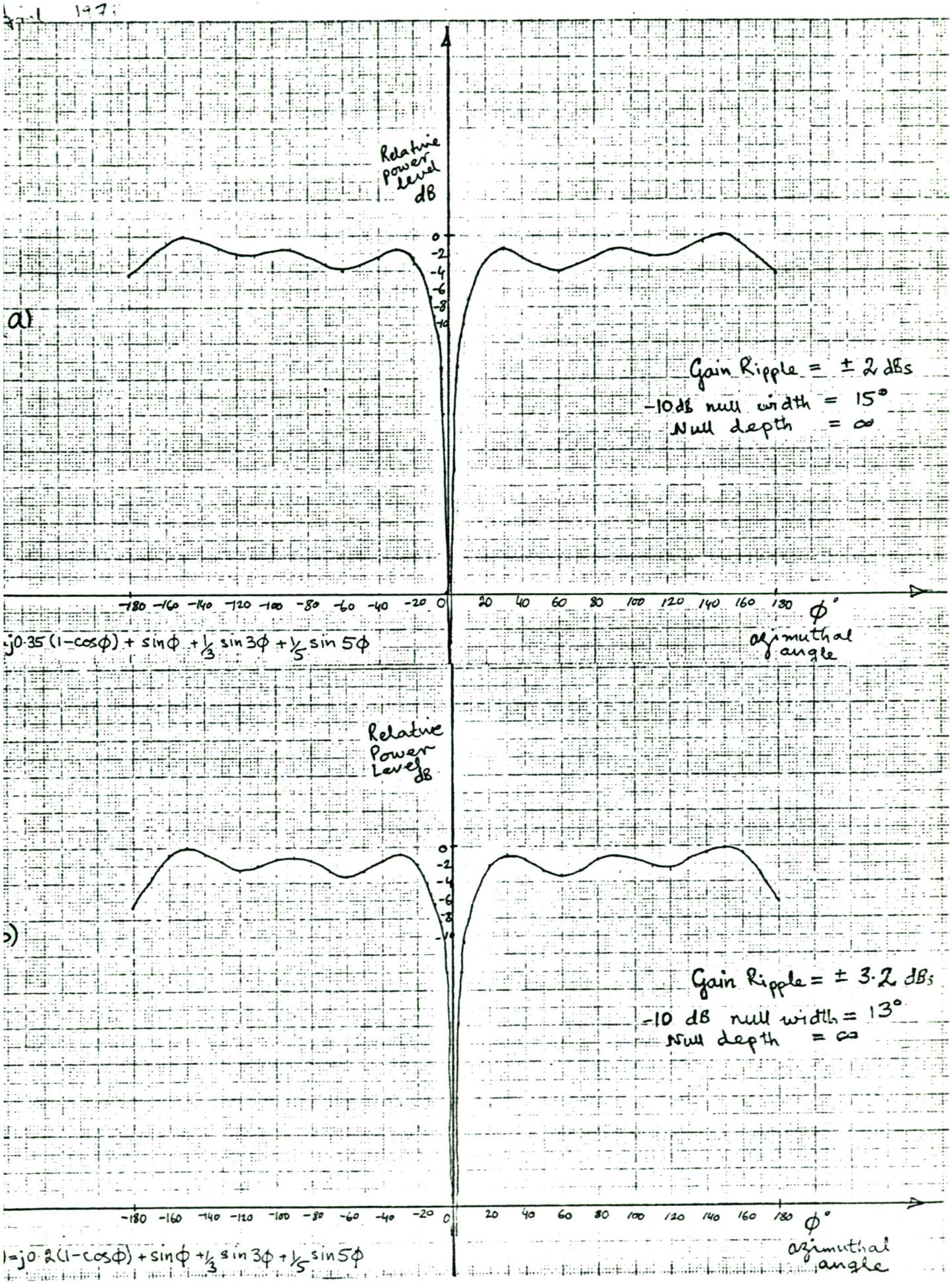

FIGURE 4.4

Synthesis of single null in otherwise omnidirectional pattern

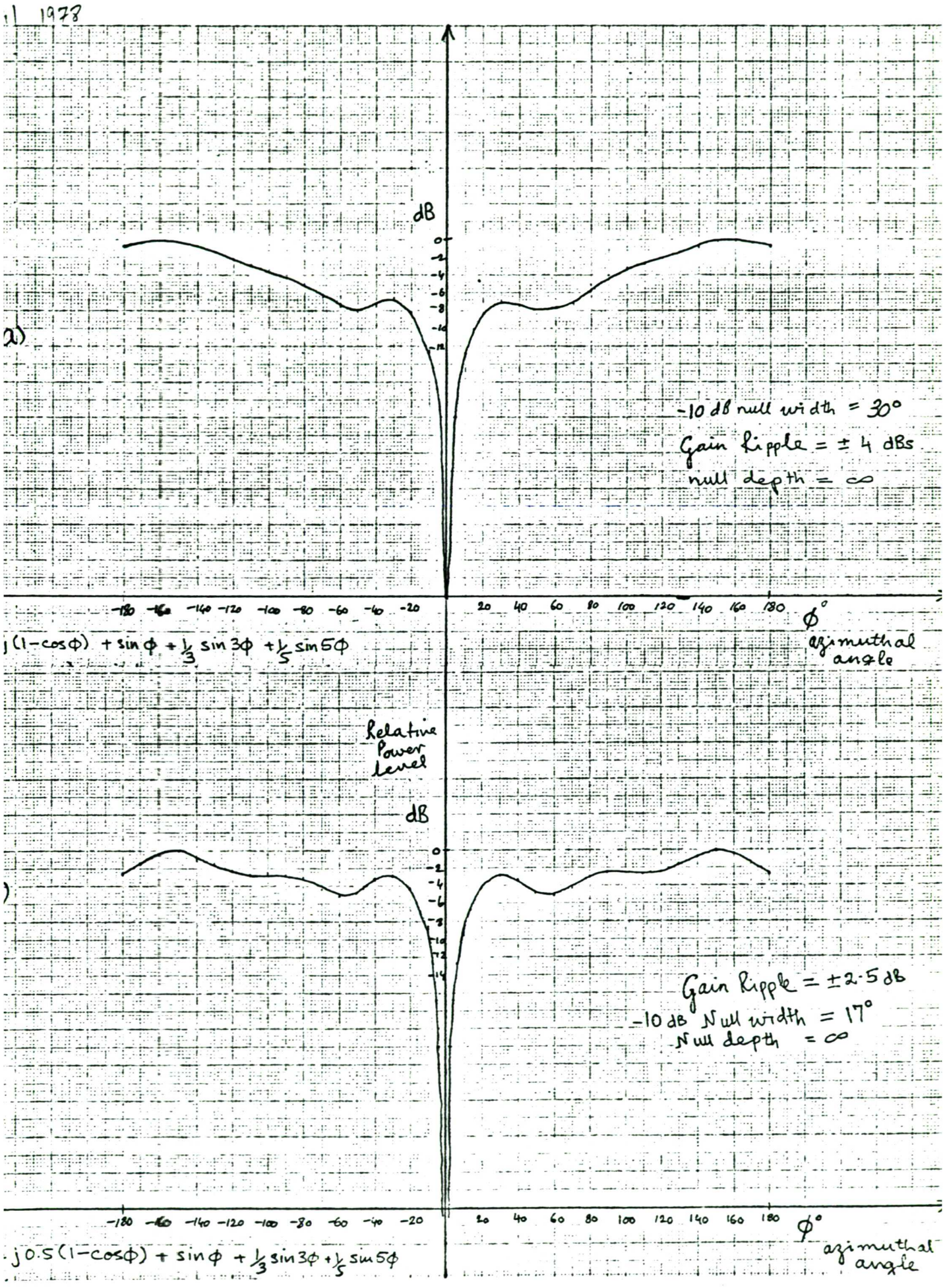

FIGURE 4.5

ew technique for synthesis of two nulls in otherwise omnidirectional attern

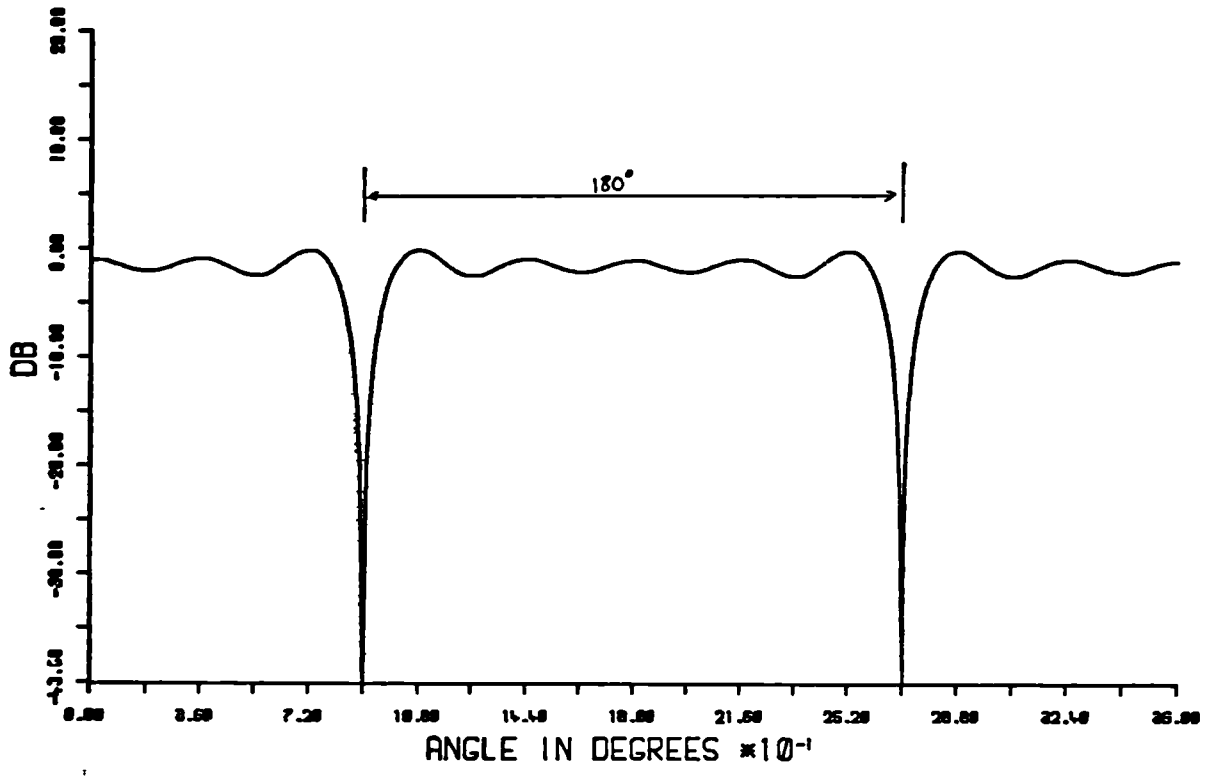

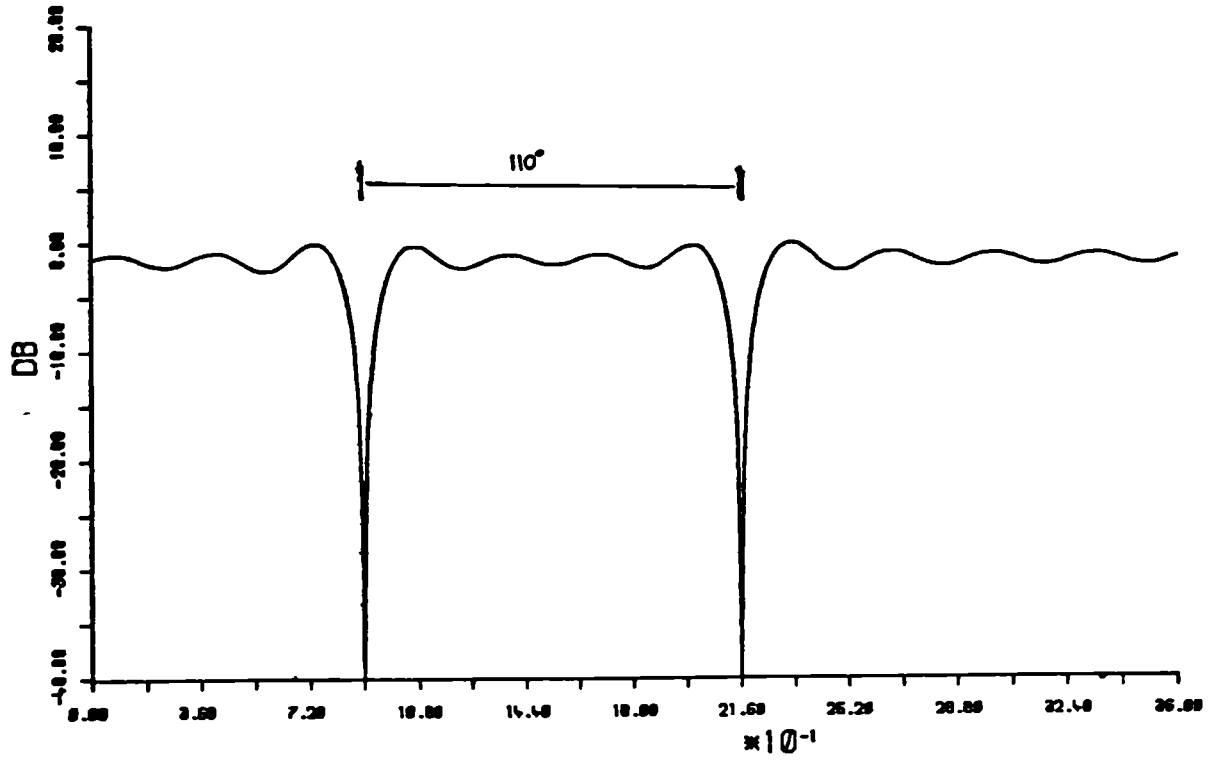

FIGURE 4.6

ew techniques for synthesis of two nulls in otherwise omnidirectional attern

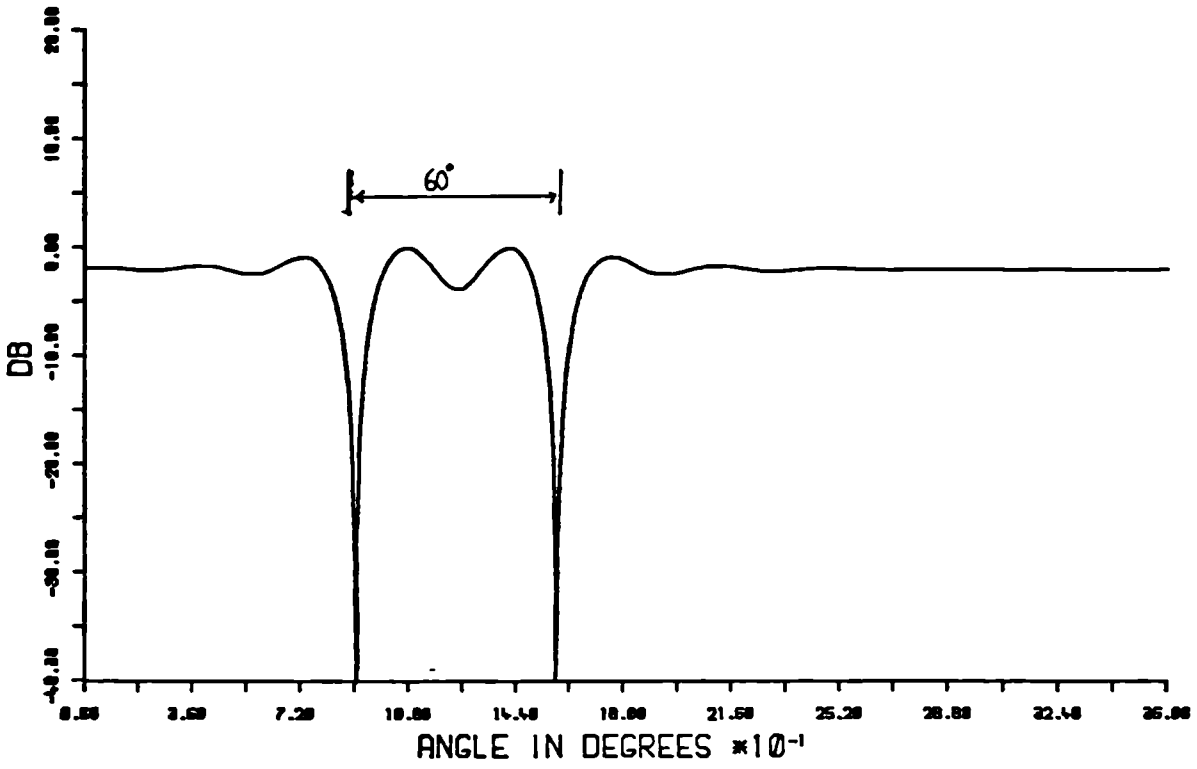

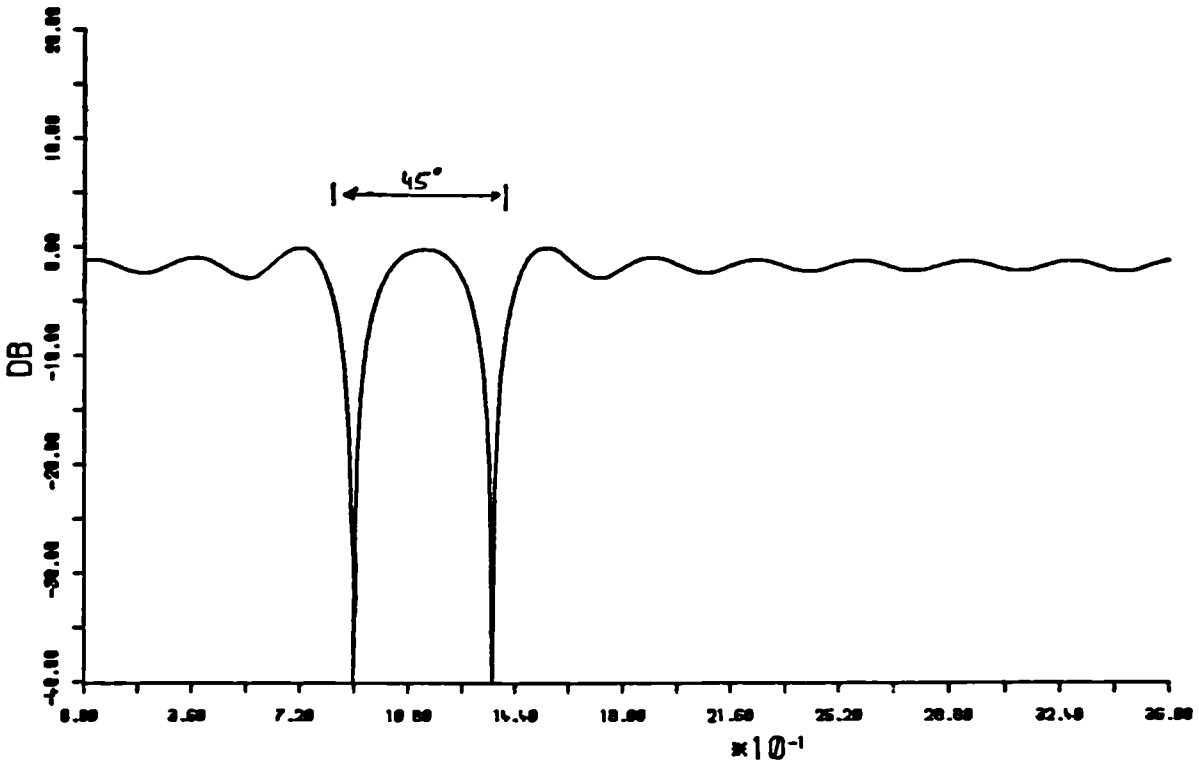

FIGURE 4.7

ew technique for synthesis of two nulls in otherwise omnidirectional attern

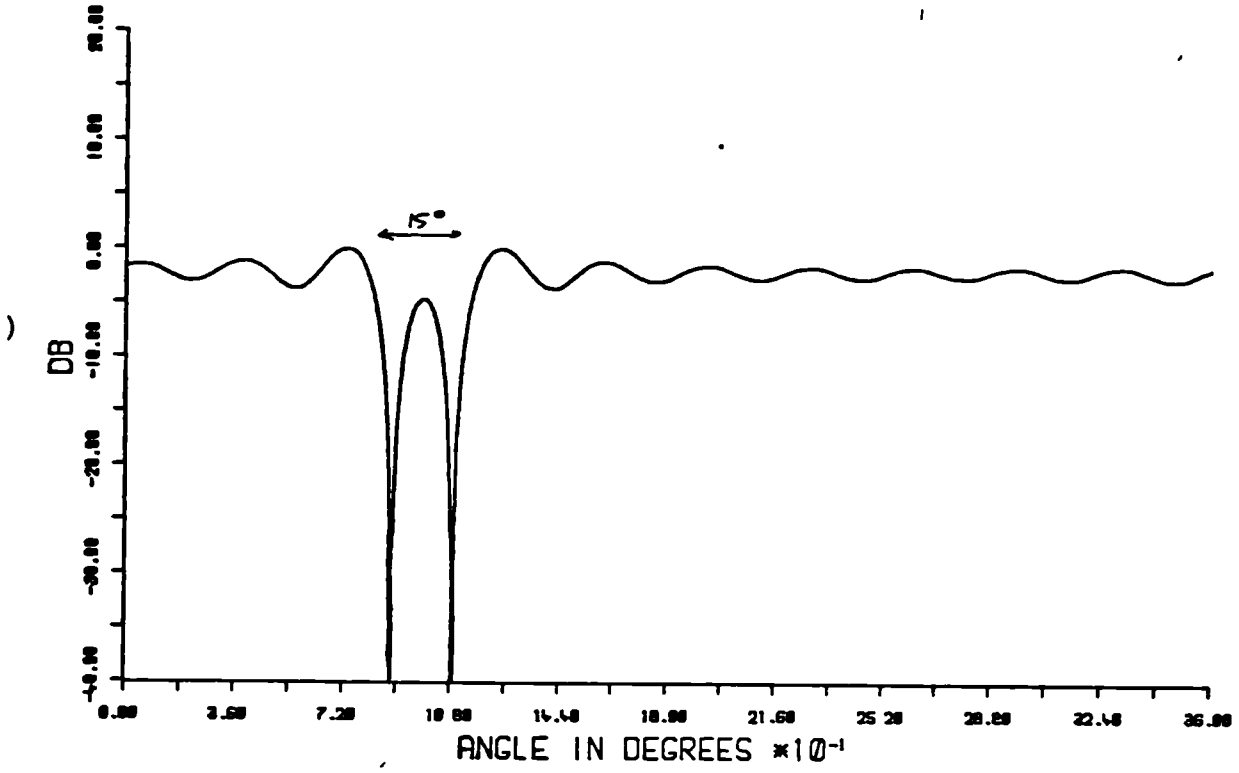

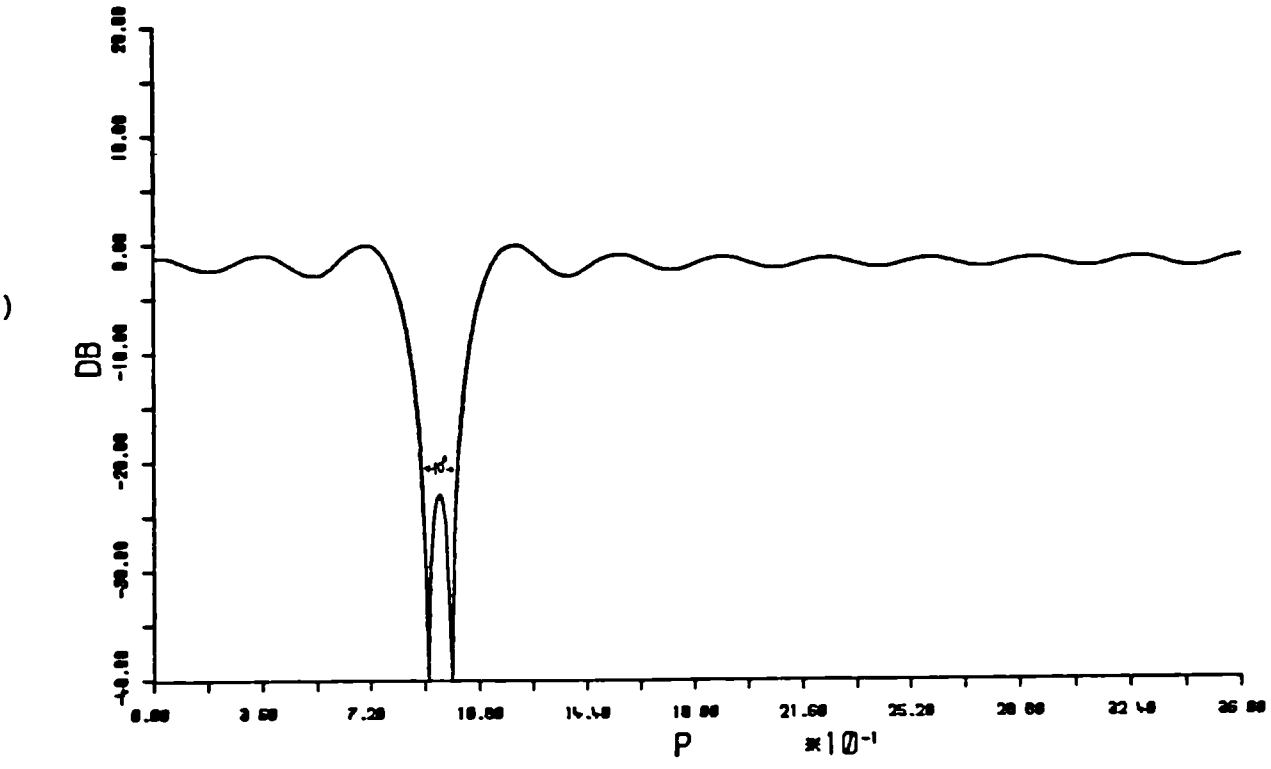

FIGURE 4.8

revious technique for synthesis of two nulls in the directional attern of circular arrays

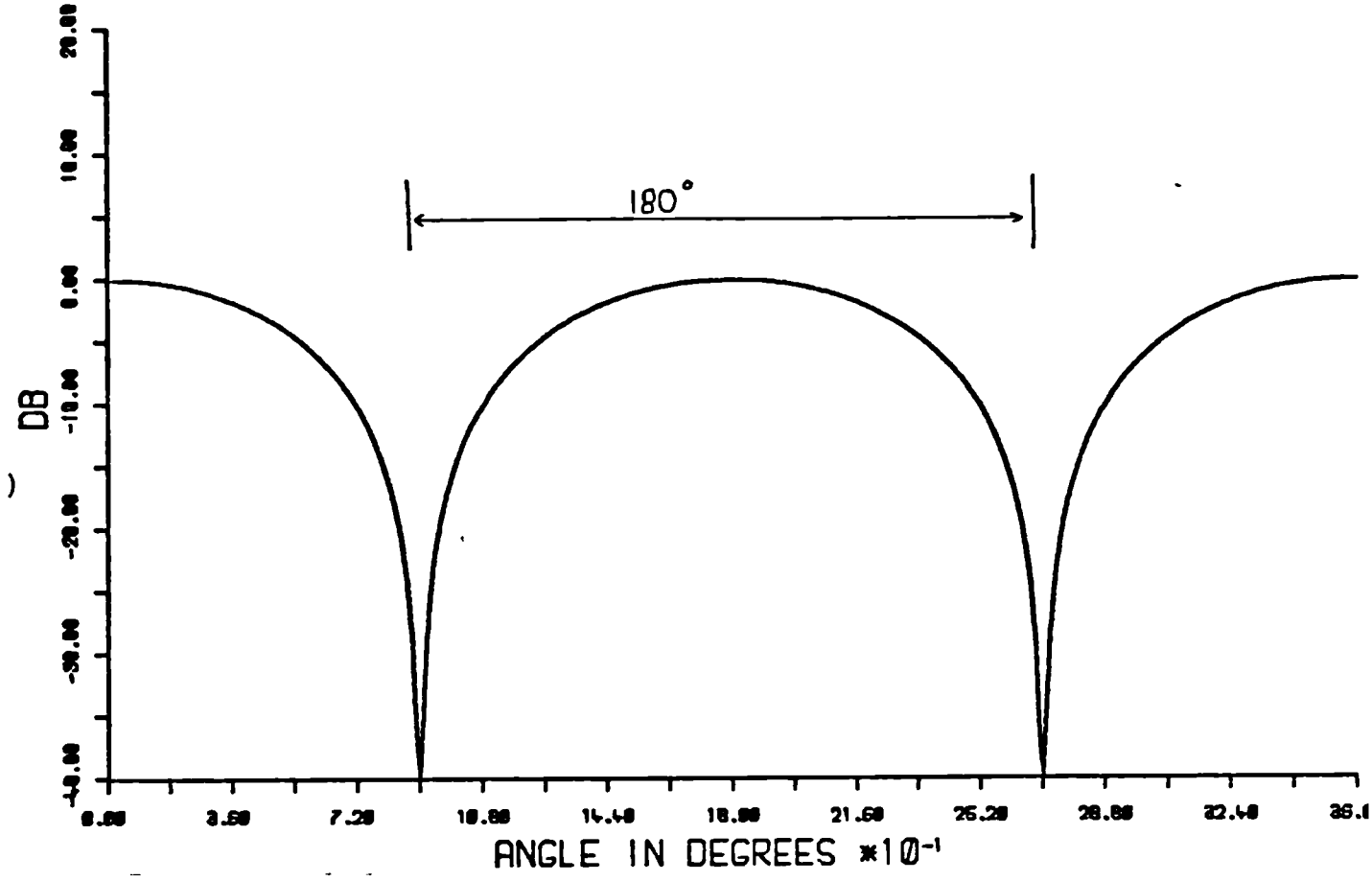

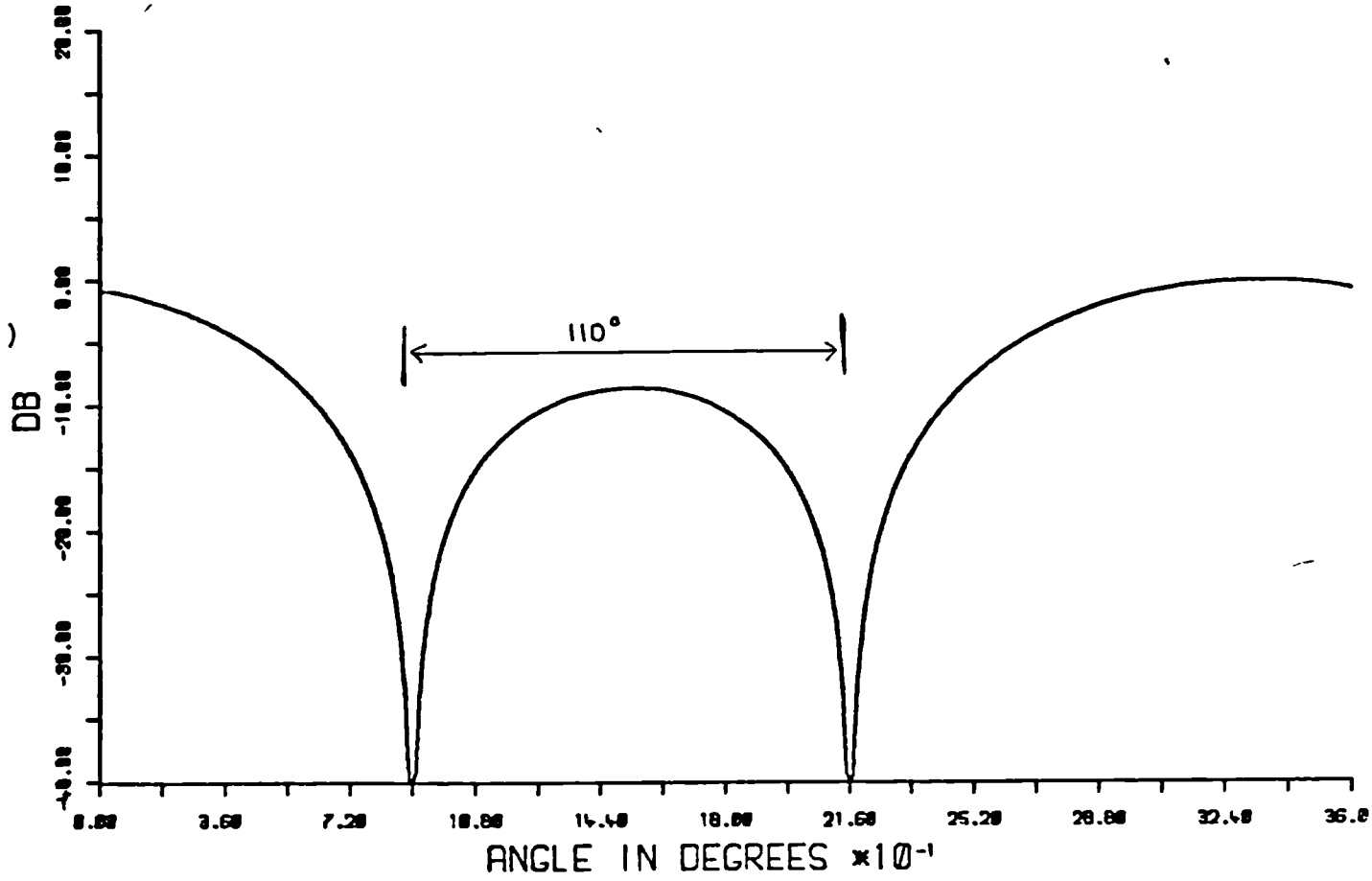

FIGURE 4.9

revious technique for synthesis of two nulls in the directional attern of circular arrays

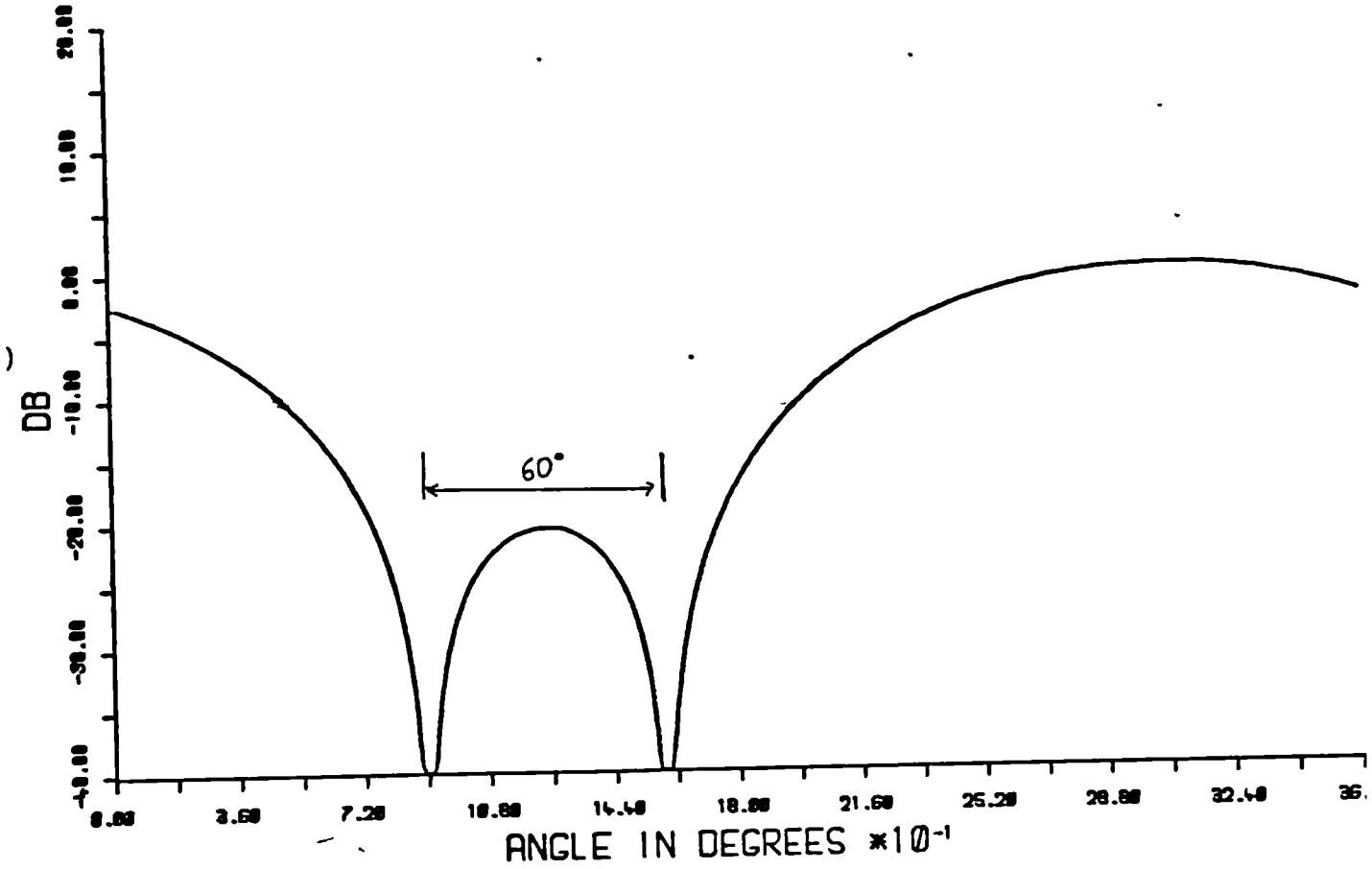

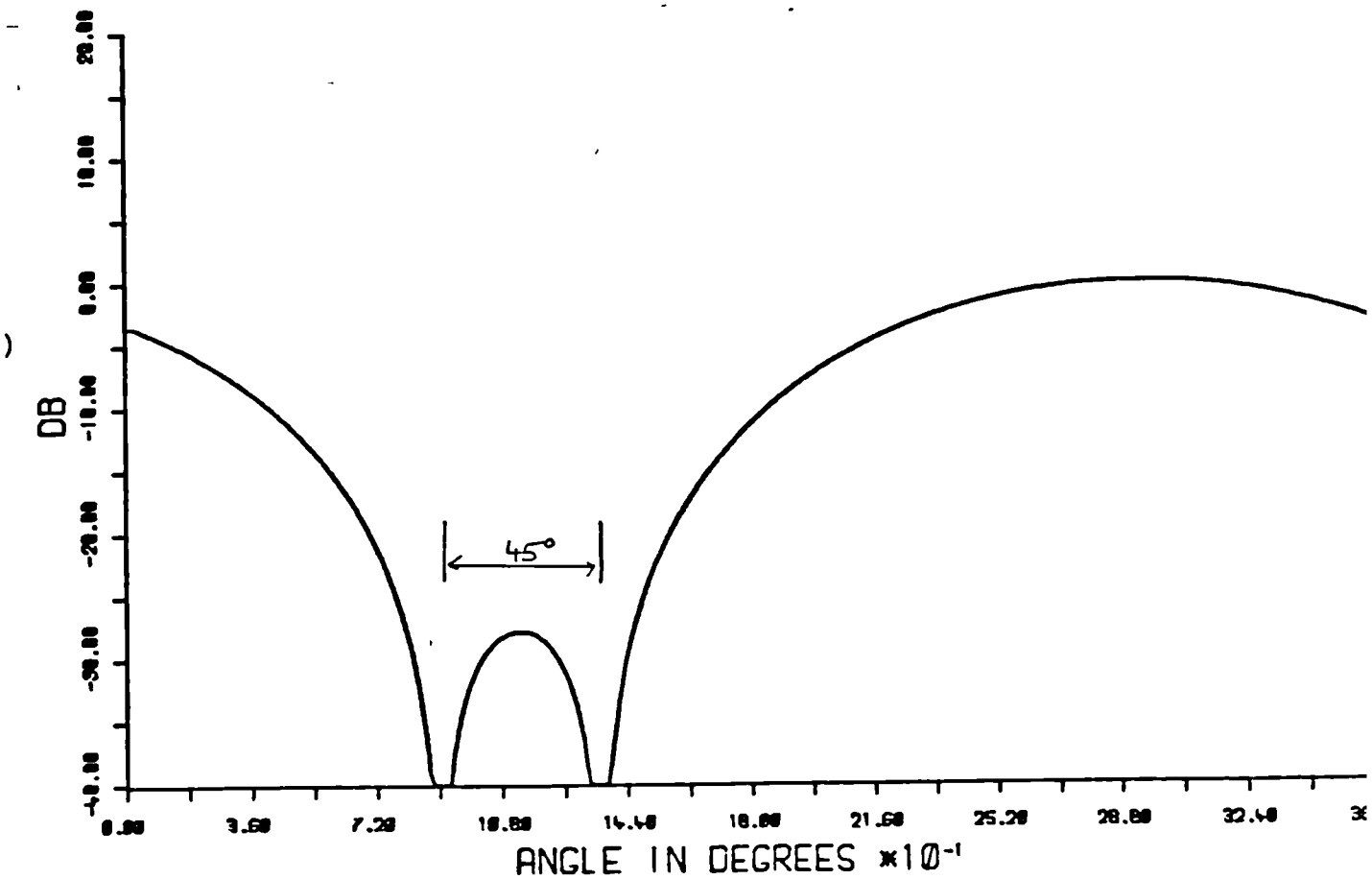

FIGURE 4.10

revious technique for synthesis of two nulls in the directional attern of circular arrays

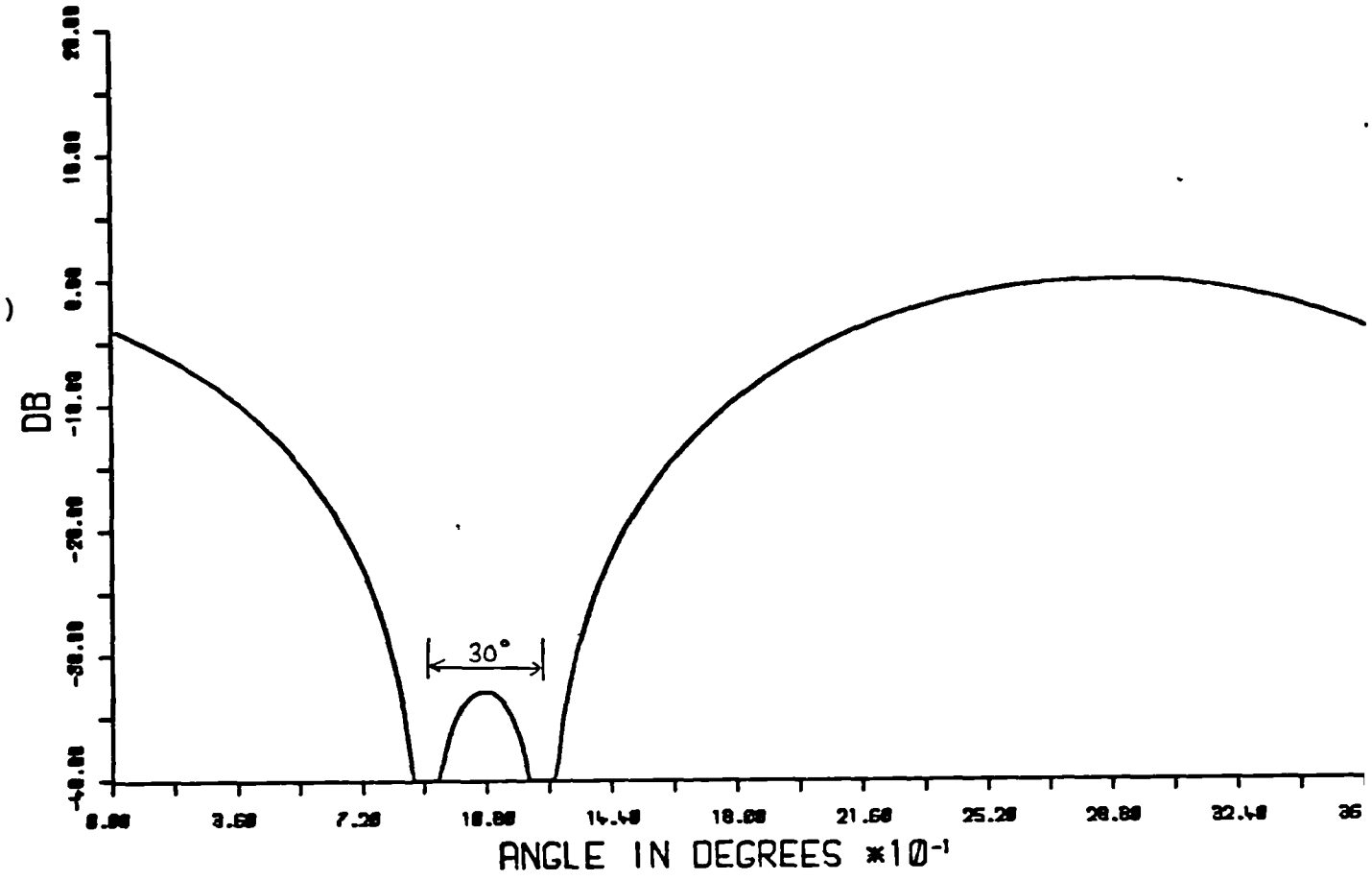

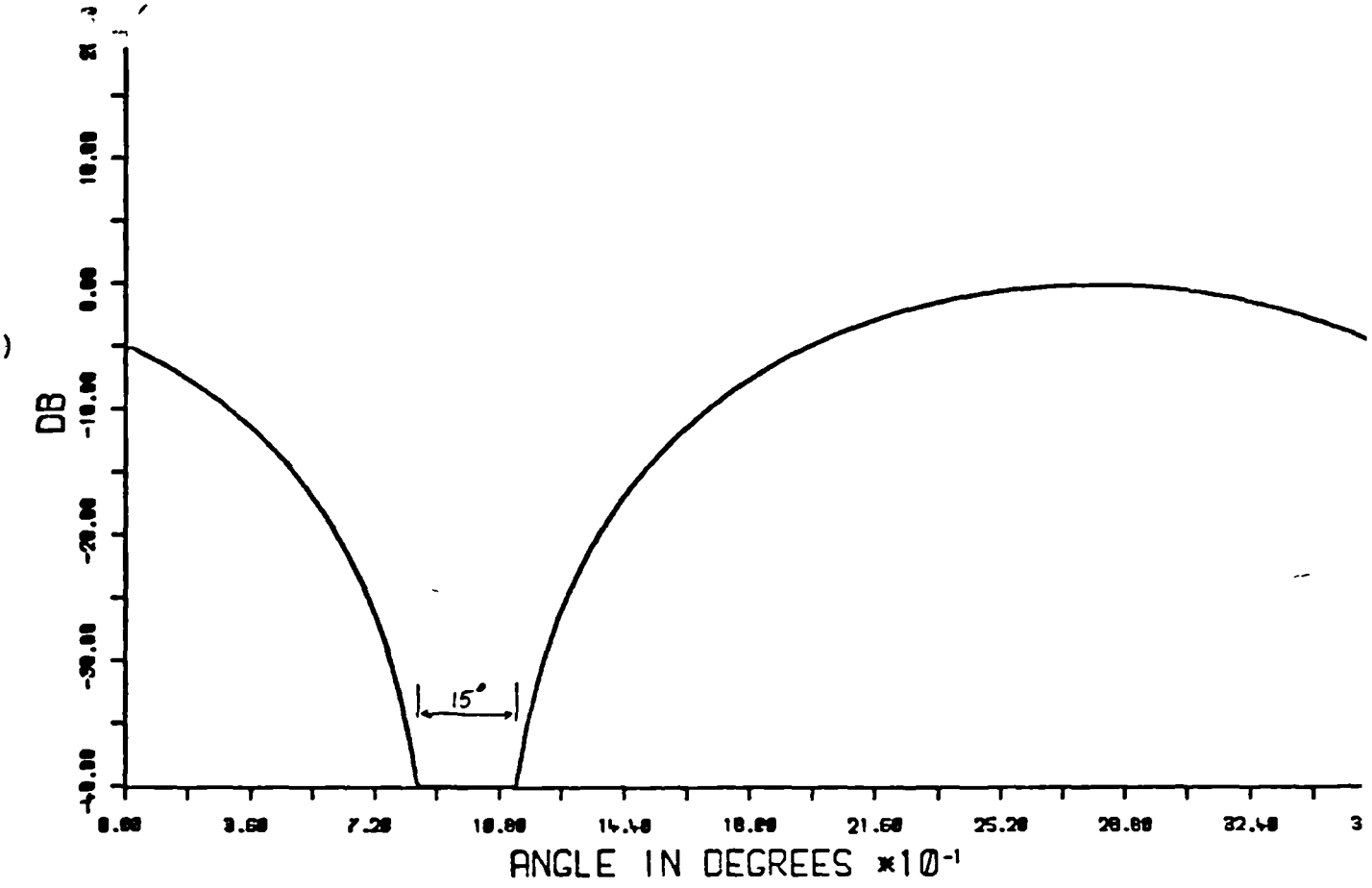

FIGURE 4.11

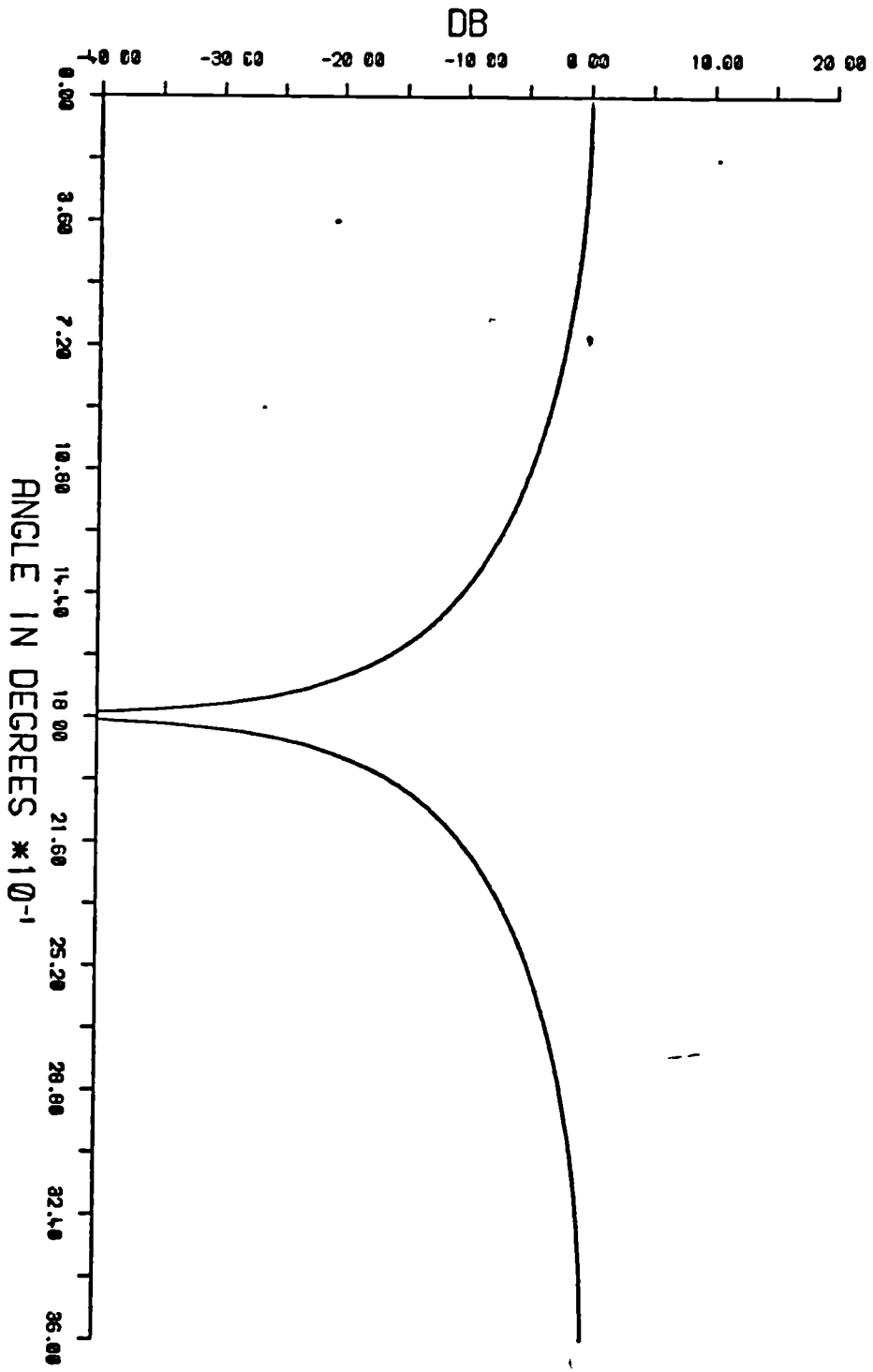

Figure 4.12 Directional pattern with one real null at. at 180^{0}

Figure 4.13

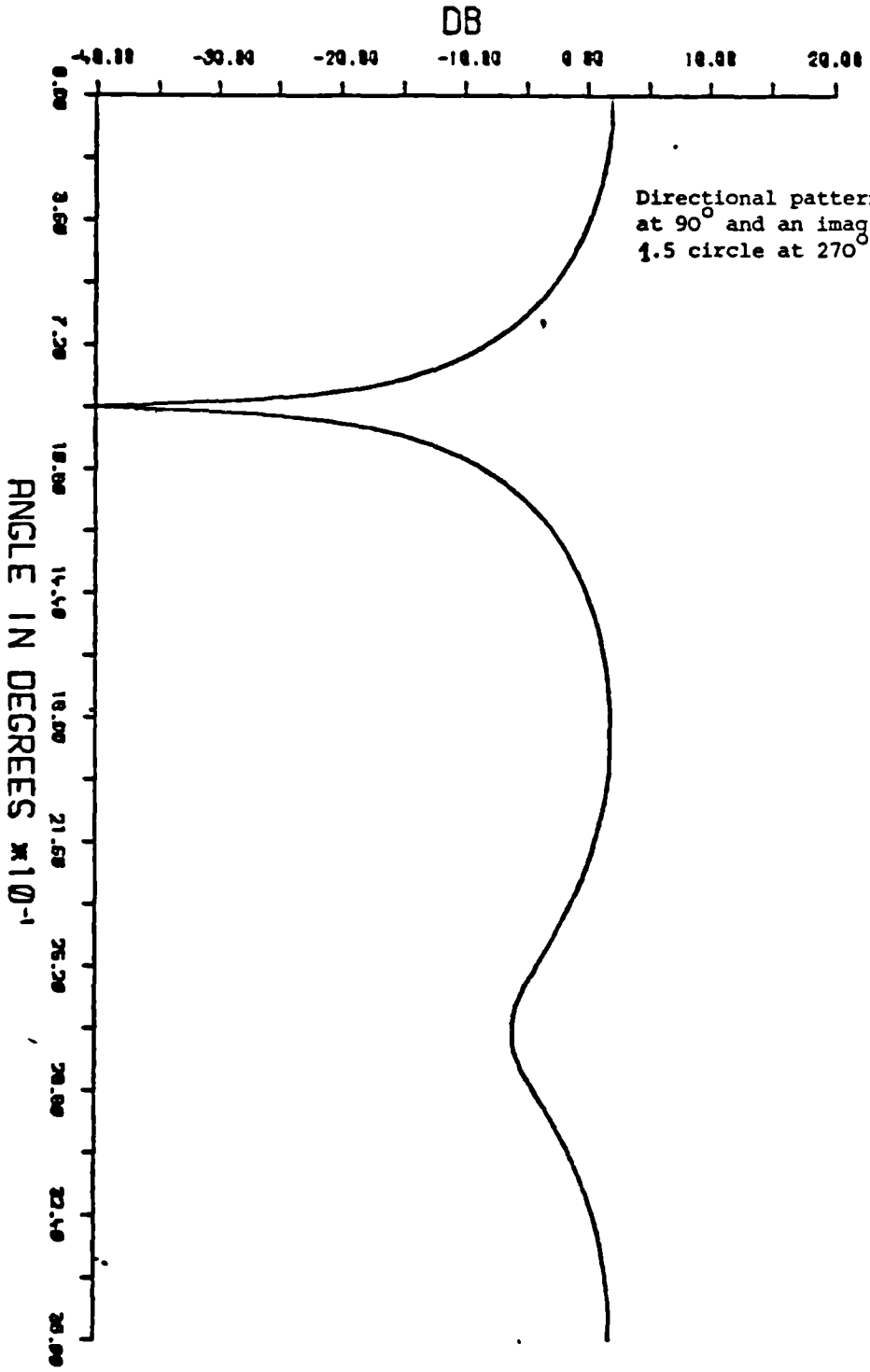

Directional pattern with one real null at 90° and an imaginary null on the 1.5 circle at 270°.

Figure 4.14

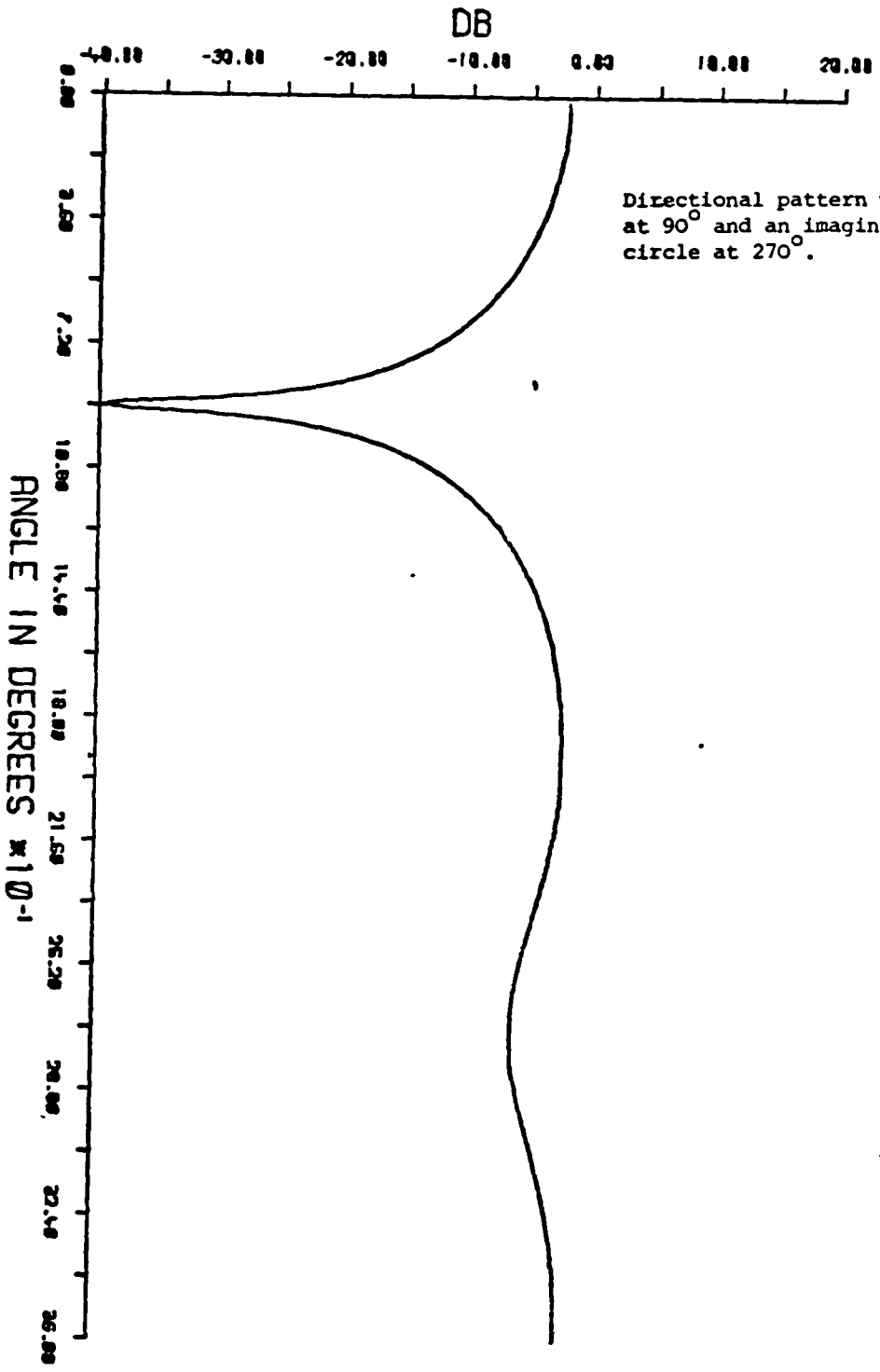

Directional pattern with one real null at 90° and an imaginary null on the 0.5 circle at 270°.

Figure 4.15

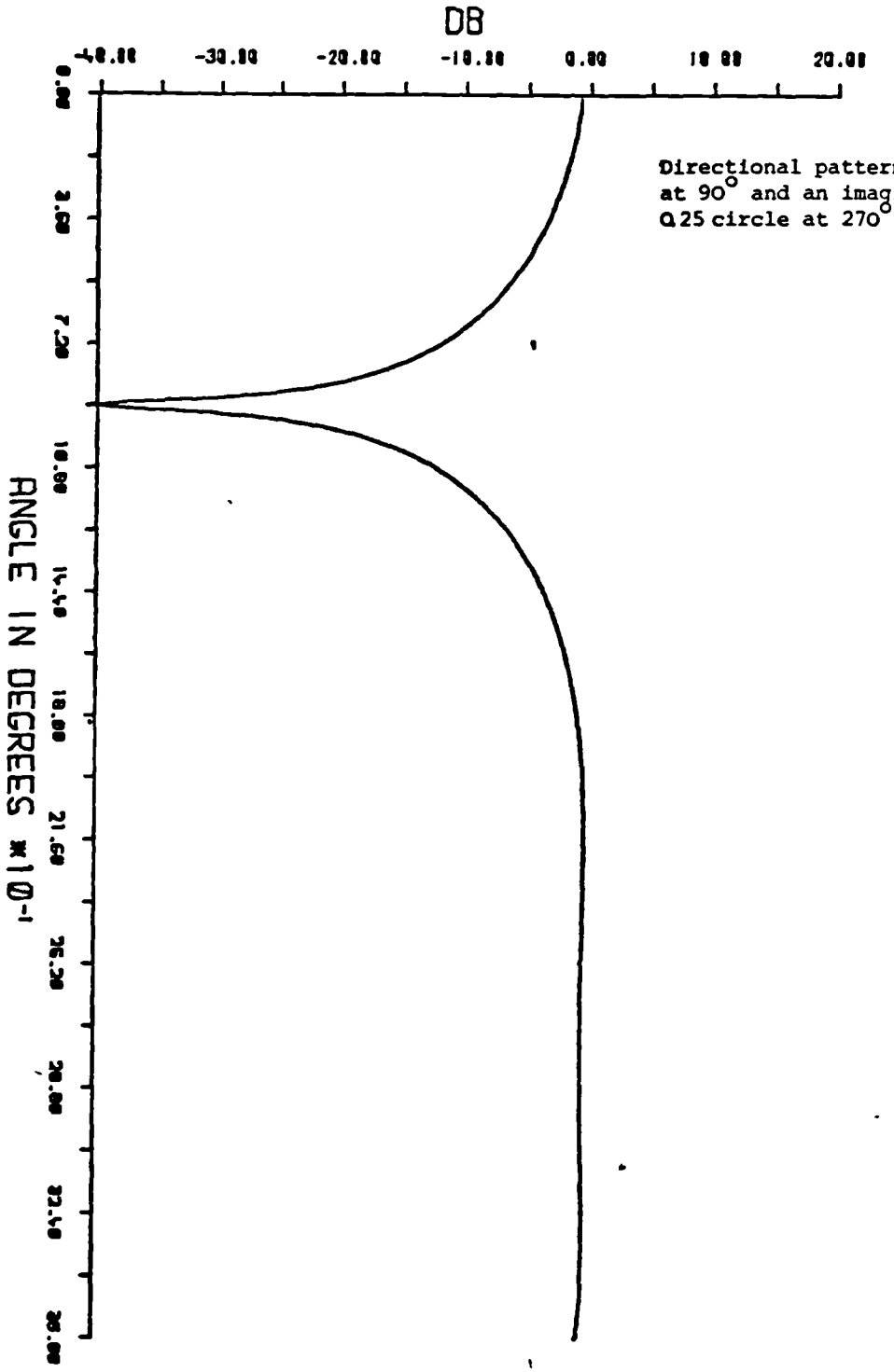

Directional pattern with one real null at 90° and an imaginary null on the 0.25 circle at 270°.

Figure 4.6

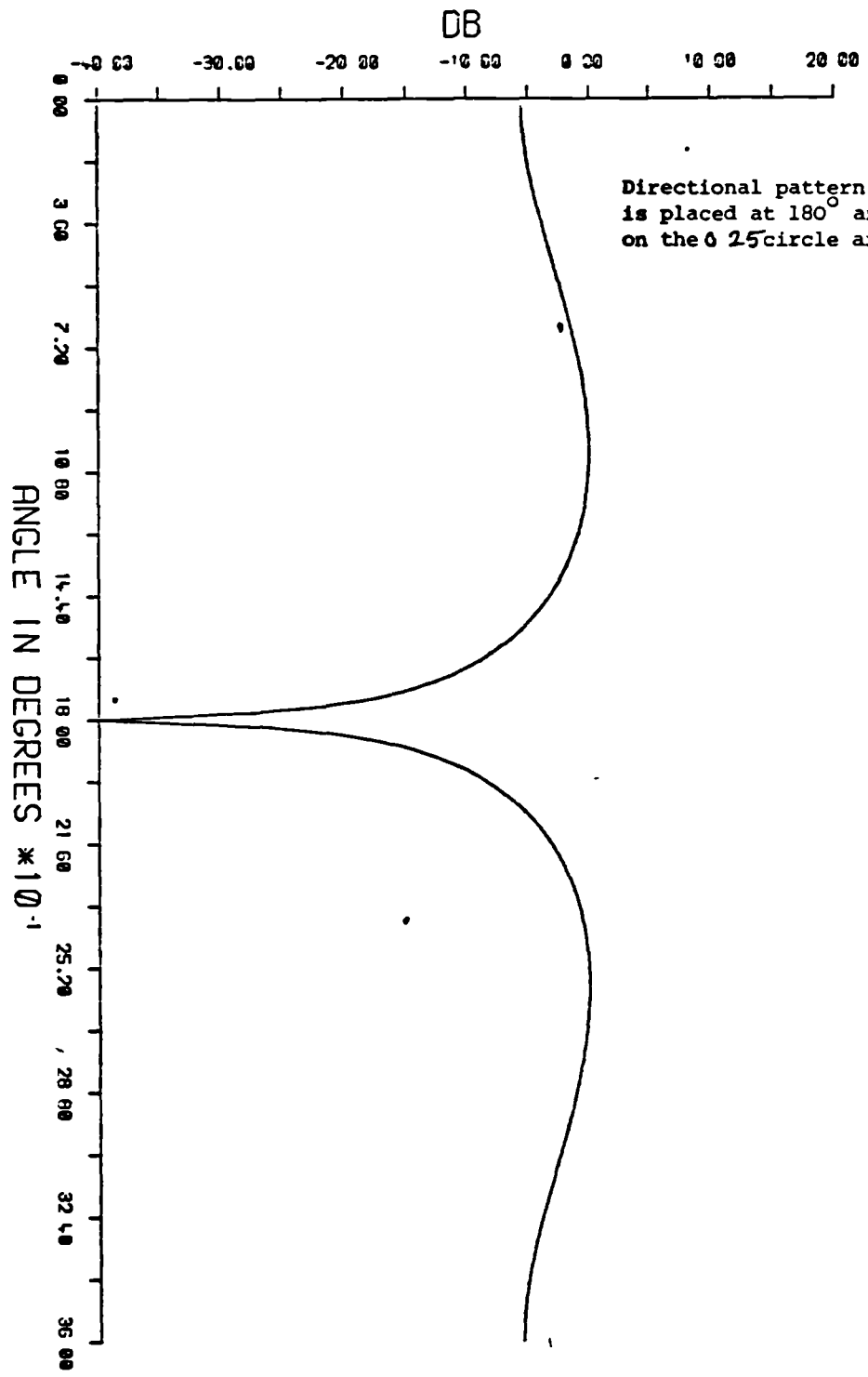

Directional pattern in which one real null is placed at 180° and three imaginary nulls on the 0.25 circle are placed at 0°

Figure 4.17

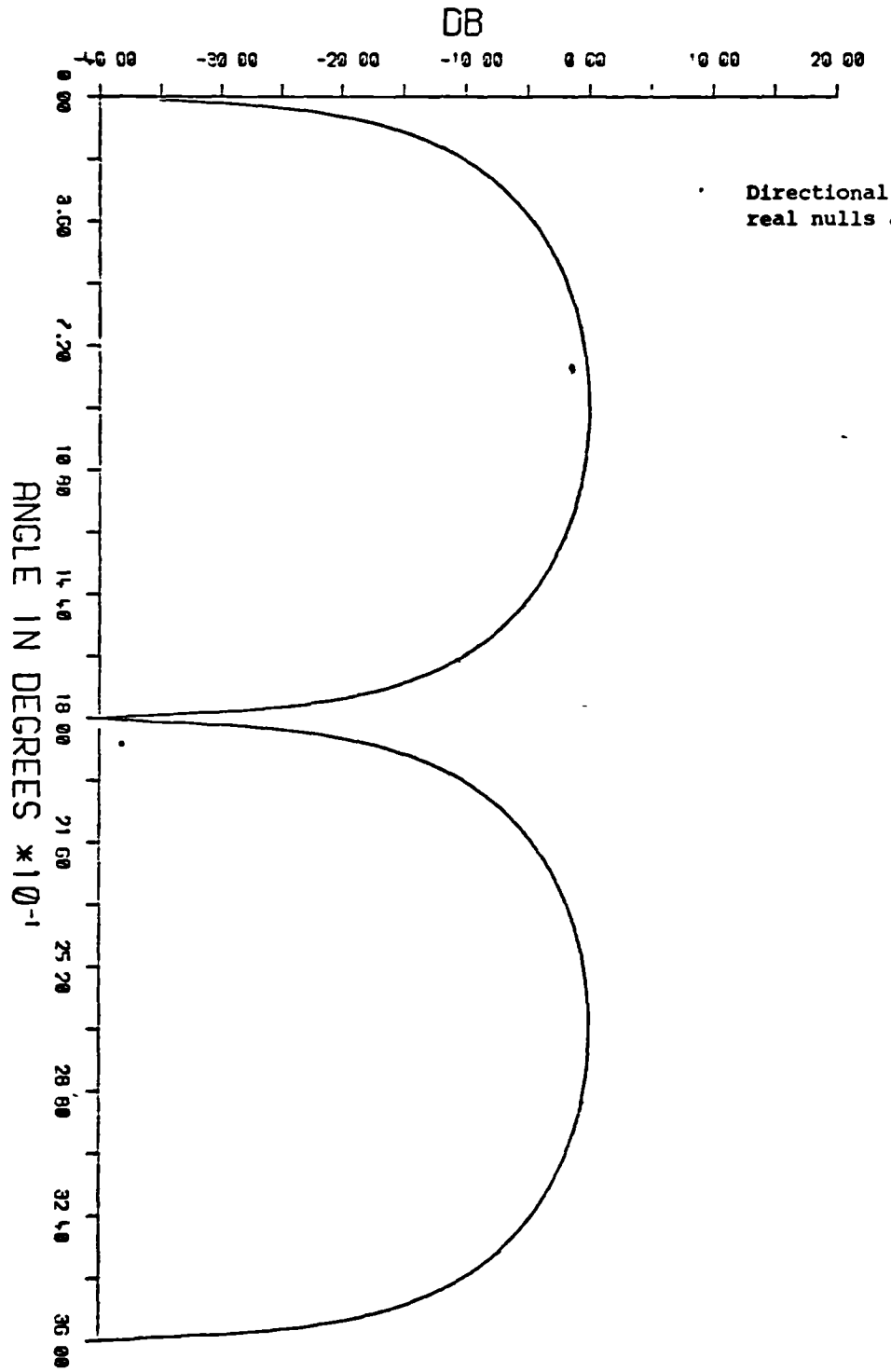

Directional pattern in which two real nulls are at 0^{o} and 180^{o}

Figure 4.18

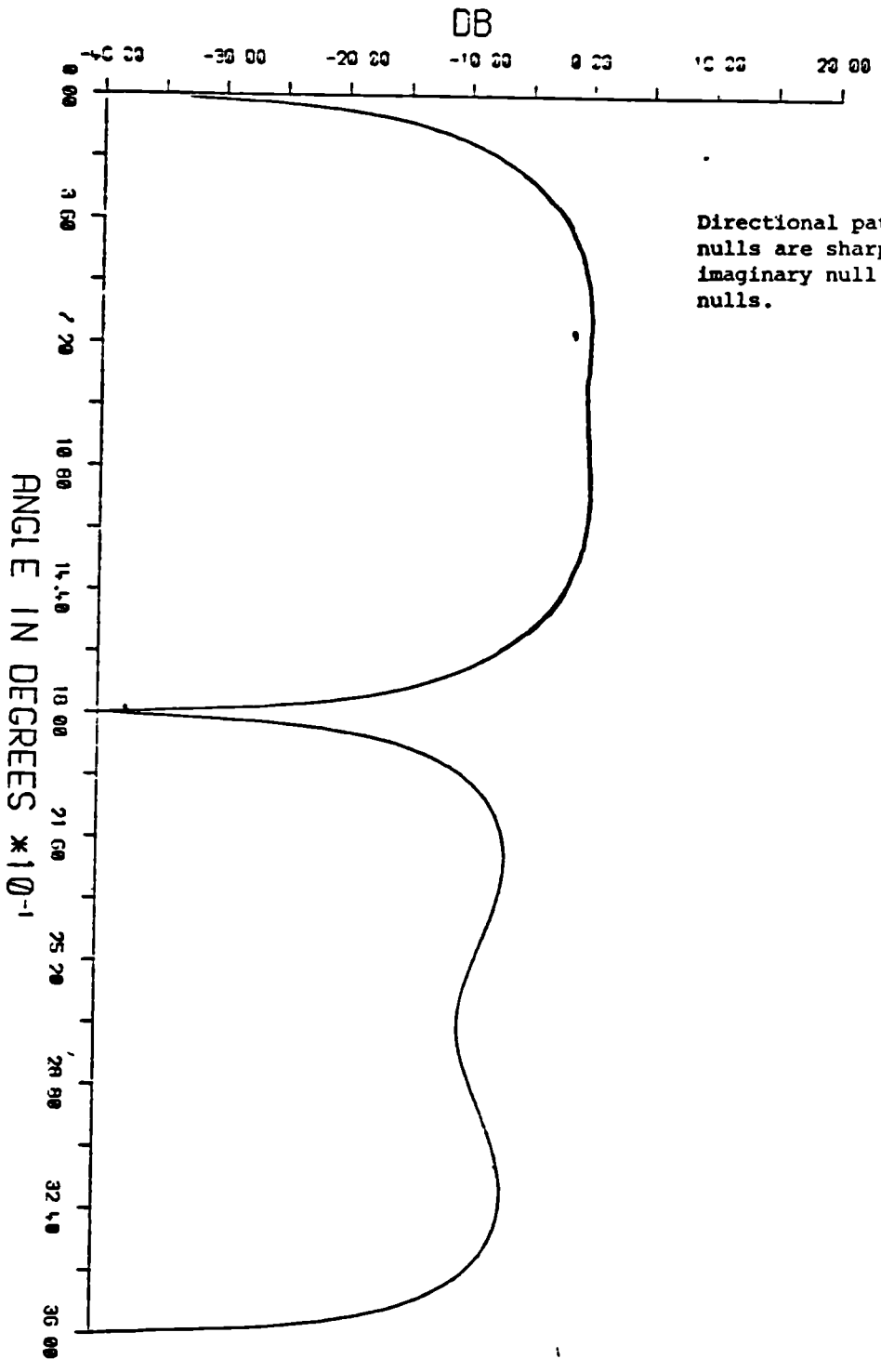

Directional pattern in which two real nulls are sharpened by placing imaginary null in between the two real nulls.

CHAPTER V

EXPERIMENTAL MEASUREMENTS CARRIED OUT AT ASWE (FUNTINGTON) ON THE 16 ELEMENT CIRCULAR ARRAY

5.1 Introduction

In this chapter experimental measurements are presented which were carried out at ASWE (Funtington) on the 16-element circular array. The array elements which are reflector backed flat plate dipoles were designed and constructed by ASWE making use of one of their standard wide band dipole designs for the 225-400MHz frequency range. Chapter II described how the directional pattern of a circular array of directional antennas can be synthesised in terms of phase modes and amplitude modes. This chapter presents results of measured phase modes and amplitude modes to experimentally verify their characteristics. Further, it was shown that phase modes are distorted (i.e. gain ripple) due to the use of a finite number of elements and also due to amplitude and phase errors in the array excitation. Measured results show the purity of phase modes that can practically be obtained. It was shown theoretically that mode gain is stabilised with frequency changes for directive element arrays. Measurements are given to verify this result.

Chapter IV described techniques for synthesis of null patterns. In this chapter measured null patterns are given to study the null depths that can be achieved. It is also shown experimentally how a single broad null may be steered to a new position in the azimuth.

5.2 Description of Circular Array and Associated System

The circular array shown in Fig. 5.1 consists of 16 wide-band flat plate reflector backed dipoles. The dipoles are operable over the frequency band 200-400MHz (shown in Fig. 5.2). The material used for these dipoles is tin plated brass. The lengths of the arms on which the elements are mounted can easily be varied (as seen in Fig. 5.1) in order to vary the array radius. The minimum diameter of the circular array is 8 ft (2.44λ) and the maximum diameter is 12 ft (3.66λ). The cables from the elements are cut to provide equal electrical lengths, they pass through the cylindrical structure, supporting the array, and are available for excitation under the covers at the bottom of the cylinder. The Butler matrix network feeding the array together with variable attenuators, phase shifters (General Radio trombone lines) and a power combiner are placed under the covers as shown in Fig. 5.3. The output from the power combiner is connected to the receiver input which lies at the centre of the turntable on which the entire array assembly is placed.

5.3 Description of the Antenna Measurement Site

The ASWE (Funtington) antenna measurement site has a large turntable at the centre of which is the receiver input. The turntable movement can be controlled from a control point which is clear of the measurement site. The polar

diagram plotter is a standard Scientific Atlanta type equipment. To ascertain accurate measurements the site is kept clear of reflectory surfaces. The circular array which is used as a receiver antenna is placed on the turn-table. The transmitter antenna which is a log-periodic dipole array is placed 99 ft ($>2D^2/\lambda$) in the far field of the circular array. The ground plane is covered with aluminium sheet which roughly provides a reflection coefficient equal to that of the sea. Fig. 5.4 shows a picture of the receiver and transmitter antennas. This arrangement provides means of measuring horizontal directional patterns of circular arrays.

The site also has the facility for measuring vertical directional patterns. A log-periodic array is mounted on a boom which moves over a 90^{o} arc in the vertical plane of the receiving antenna. The boom movement is controlled remotely.

5.4 The Wideband Butler Matrix Network

Butler matrix networks are in general used for forming multiple beams from linear arrays. It was further shown (5) that the Butler matrix network may also be used for exciting phase modes on circular arrays. The input ports of Butler matrix networks excite phase modes on a circular array by connecting the output ports of the matrix to the circular array. For an N-element circular

array fed by an NxN port Butler matrix network the phase shifts required between two adjacent output ports is a multiple of $2\pi/N$ depending on the input port excited. For a 8x8 port network the incremental values of phase shifts required are 45^{o} and for a 16x16 port network the incremental phase shifts required are $22\frac{1}{2}^{o}$. For wideband networks these phase shifts should be constant over a wideband of frequencies.

It is a property of a 90^{o} hybrid coupler and a 180^{o} hybrid coupler that they provide wideband 90^{o} and 180^{o} phase shifts. The function of these hybrid couplers is shown in Fig. 5.5(i) and (ii). Combination of 90^{o} and 180^{o} hybrid couplers can provide wideband 45^{o} phase shift as shown in Fig. 5.5(iv). A wideband 8x8 BMN can therefore be constructed by combination of 3 90^{o} hybrid couplers and 10 180^{o} hybrid couplers as shown in Fig. 5.6. For a 16x16 BMN wideband $22\frac{1}{2}^{o}$ phase shifts are required. $22\frac{1}{2}^{o}$ wideband phase shifts can be provided by combining 90^{o} and 180^{o} hybrid couplers together with pre-set attenuator (7.6dB) as shown in Fig. 5.5(iii). Fig. 5.6 and Fig. 5.7 show the required combination of 90^{o} and 180^{o} hybrid couplers and wideband pre-set attenuators for producing a wideband 16x16 BMN. A wideband 16x16 Butler matrix network constructed on printed circuit board using flat pack 90^{o} and 180^{o} hybrid couplers (from Merimac) was available. This Butler matrix network used in the experimental study was constructed for a different project.

5.5 The Wideband Elements

The wideband elements of the circular array are flat plate reflector backed dipoles. The directional pattern for an isolated element in the horizontal plane was provided by ASWE, at the frequencies of 225MHz, 275MHz, 350MHz and 400MHz and is shown in Fig. 5.8(a). It is seen that the element pattern is only slightly altered over the frequency band 200-400MHz. The element pattern was approximated to $1+\cos\phi$ in the theoretical calculations. Fig. 5.8(a) shows $1+\cos\phi$ pattern superimposed on the measured pattern for comparison. It is seen that some power is diffracted around the reflector.

The element pattern in the plane of the flat plate and in the plane normal to the flat plate is shown in Fig. 5.8(b).

5.6 Measurement of Phase Mode Patterns of a 16-element Circular Array

In the initial measurements the diameter of the circular array was set at 10 ft (corresponding to 3λ). For the measurement of zeroth order phase mode, the output from all the elements was connected to the input ports of the Butler matrix network. The output from zeroth mode port was connected to the input of the receiver with the rest of the mode ports terminated in 50Ω. The polar diagram in the plane of the array for the zeroth order mode was

measured at the frequencies of 225MHz, 310MHz and 400MHz and is shown in Fig. 5.9. The gain ripple in the zeroth mode at 225MHz, 310MHZ and 400MHz is $\pm$1dB, 1.5dB, 3dB respectively. Phase modes at higher frequencies contain large gain ripple which is an expected result. Because it was shown theoretically (Chapter II) that as the inter-element spacing in wavelengths is increased so does the gain ripple of the phase mode pattern. However, theoretically the zeroth order phase mode should have negligible gain ripple at 225MHz but in practice the gain for various elements is not the same in the direction of the radius. The pattern shape for various elements is also not exactly similar (see Fig. 5.27-5.34). Thus amplitude errors are present in the zeroth order mode. Further amplitude and phase errors are introduced in the Butler matrix network which has an amplitude accuracy on the input ports of $\pm$1dB and phase accuracy of $\pm 6^{o}$.

Similar sets of polar diagrams were plotted by taking outputs from the ports exciting 1, 2,.....7 modes and connecting it to the receiver input respectively. Fig. 5.10-5.16 shows mode patterns for 1, 2, ...7 modes respectively. Fig. 5.25 shows the variation of gain ripple for various modes at 225MHz, 310MHz and 400MHz. It is clear from Fig. 5.25 that as the mode order is increased the distortion of the modes is also increased. This is again a theoretically predicted result, as it has been shown (Chapter II) that ambiguous modes become significant for higher order modes.

It was shown in Chapter II that for modes to contain small distortion, the interelement spacing must be less than or equal to half a wavelength. For a 10ft diameter array, interelement spacing at 225MHz, 310MHz and 400MHz is 0.46λ, 0.62λ and 0.81λ respectively. Therefore as expected, the various modes contained little distortion at 225MHz. At 310MHz the lower order modes contained little distortion, but the higher order modes contained significant distortion. However, at 400MHz none of the modes have distortion small enough to make them useful in directional pattern synthesis.

In order to improve the quality of modes at the higher frequencies, the diameter of the 16-element circular array was reduced to 8 ft. Fig. 5.26 shows the variation of gain ripple as the mode order is increased at frequencies of 225MHz, 310MHz and 400MHz. Table 3 shows theoretical and measured gain ripple of various modes for 8 ft diameter array at the frequency of 300MHz. The difference between the theoretical and measured gain ripple (also shown in Table 3) is probably mainly due to amplitude and phase errors on the output ports of the Butler matrix network. A measure of amplitude and phase errors on the output ports of the Butler matrix network is given in Tables 3, 4, 5, and 6. Other factors which could contribute to such effects include phase errors in lengths of cable and non-identical features of the directional elements (see Figs. 5.27-5.34). Further, in the theoretical

calculations the element pattern was assumed to be $1+\cos\phi$. Fig. 5.27 shows the $1+\cos\phi$ pattern and measured pattern for comparison.

Comparing Fig. 5.25 and Fig. 5.26 it is evident that modes are of better quality in an 8 ft diameter array. However, higher order modes at 310MHz and 400MHz still contain some distortion, which can be improved by further reducing the radius since the inter-element spacing is still greater than $\lambda/2$ at 400MHz. However, because the radius cannot be further reduced due to the size of the elements, it is concluded that for an 8 ft diameter array modes up to ± 7 are usable for pattern synthesis at lower frequencies of the band 200-400MHz and only lower order modes (up to ± 3) are usable at middle and higher frequencies in the band of interest.

5.7 Measurement of amplitude modes of a 16 element circular array

It was shown in Chapter II that an amplitude mode may be excited in the far field by exciting equal and opposite current phase sequence excitations on the circular array. These amplitude modes are used in certain null pattern synthesis techniques as described in section 5.10.
Fig. 5.35-5.38 show the amplitude mode patterns measured by exciting Fig. 5.35(a) +1 and -1 input ports (b) +2 and -2 Fig. 5.36(a) +3 and -3 (b) +4 and -4 Fig. 5.37(a) +5 and -5

(b) +6 and -6 Fig. 5.38(a) +7 and -7. In the case of eighth mode, amplitude mode is automatically excited by exciting positive eighth phase mode (see Fig. 5.38(b)), this is because when positive eighth phase mode is excited the negative eighth phase mode is excited as an ambiguous mode.

5.8 Measurement of spatial phase shift of a mode in circular arrays

In this section measurements are given as experimental evidence of spatial phase shifts of modes in circular arrays, due to the use of directional elements and mutual coupling. It was shown in Chapter II that if the excitation on the circular array is given by

$$I(\phi) = I_m e^{jm\phi} \qquad 5.1$$

then the far field pattern is given by

$$F(\phi) = \left|\frac{E_m}{Z_m^{BM}}\right| |A_m| \; e^{Jm\phi \; + \psi m \; + \psi Z_m^{BM}} \qquad 5.2$$

i.e. the far field is also a phase mode which is phase shifted by '$\psi_m + \psi_{Z_m BM}$' for mth mode. Phase shift being dependent on the mode order m, radius in wavelengths, polar angle and the type of directional elements used. Let

$$\gamma_m = \psi_m + \psi_{Z_m BM} \qquad 5.3$$

To measure the relative phase shifts $(\gamma_1-\gamma_0)$ of first mode with respect to the zeroth mode, the two modes are combined. With excitation on the array given by

$$I(\phi) = I(1 + e^{j\phi}) \qquad 5.4$$

I = current amplitude

the far field as given by equation 5.2 is given by

$$F(\phi) = |B_o|e^{J\gamma o} + |B_1|e^{j(\phi+\gamma 1)} \qquad 5.5$$

$|B_o|$ is equalised to B_1 by having 1dB attenuation of the zeroth mode, therefore

$$F(\phi) = |B_1|e^{J\gamma o}\ (1 + e^{J(\phi+(\gamma 1-\gamma o))}) \qquad 5.6$$

$F(\phi)$ is a cardoid pattern with the null pointing in the direction

$$\phi_{null} = 180 - (\gamma_1-\gamma_o) \text{ degrees} \qquad 5.7$$

For 2.23 diameter ϕ_{null} is measured to be 160^o (see fig. 5.39), thus

$$\gamma_1 - \gamma_o = 20^o$$

By changing the frequency from 225MHz to 275MHz the diameter of the array is changed to 2.8λ. For this diameter $\gamma_1-\gamma_o$ remains 20^o.

Similarly, by combining higher order modes with the zeroth mode, the corresponding shift was measured for higher order modes relative to zeroth order mode for a diameter of 2.23λ and 2.8λ. These measured values are given in Table 1 below.

Mode order	radius = 2.23λ	radius = 2.8λ
1	20^o	20^o
2	36^o	36^o
3	45^o	36^o
4	40^o	40^o
5	100^o	90^o
6	156^o	114^o
7	231^o	203^o

Table 1

As expected, the phase shifts are dependent on mode order and radius in wavelength. These phase shifts will have to be compensated at the input ports of the Butler matrix network for directional pattern synthesis. These phase shifts are difficult to calculate because they depend on

the type of directional element used and on the mode impedance due to mutual coupling effects. The phase shift due to directional elements may be calculated but for calculating the phase shift due to mutual coupling one needs to know the self and mutual impedances of the elements, which is beyond the scope of this thesis.

5.9 Measurement of the variation of mode gain with frequency

In this section the relative gain of various modes is measured over the frequency band 200-400MHz. All gains being measured relative to the gain of zeroth order mode at 200MHz. The arrangement of the experimental set up was as follows the circular array connected to the Butler matrix network was placed on the turntable. The wideband log-periodic transmitting array was placed 100 ft away from the circular array. To avoid ground reflections, absorbing material was placed in the region midway between the transmitting and receiving antennas.

The power received by the test array, when zeroth mode port was connected to the receiver, as a function of frequency is shown in Fig. 5.40(a). From Fig. 5.40(a) it is clear that gain of zeroth order mode decreases very gradually with frequency. This experimental result is in agreement with the theoretical result. It was shown (see Fig. 3.5, Chapter III) that the mode amplitude is

given by a Bessel function series which stabilises the mode gain with frequency changes as opposed to the case of circular arrays of omnidirectional elements in which the mode amplitude varies as a Bessel function with frequency. Also, for higher order modes there is a good agreement between the gain/frequency response measured experimentally (Fig. 5.40-5.43) and computed theoretically (Fig. 3.5 and 3.6).

5.10 Formation and steering of single broad null in the directional pattern of circular array

A single broad null in an otherwise omnidirectional pattern of circular array can be synthesised by combining any two adjacent modes. In the experimental study a broad null was formed by combining the zeroth and first phase mode. The pattern function $F(\phi)$ is given by

$$F(\phi) = |B_o| e^{j\gamma_o} + |B_1| e^{J\phi+\gamma_1} \qquad 5.8$$

or

$$F(\phi) = |B_1| e^{J\gamma_o} \left\{ \frac{|B_o|}{|B_1|} + e^{J\phi+(\gamma_1-\gamma_o)} \right\} \qquad 5.9$$

For a 10 ft diameter array the null depth was optimised to approximately 30dB by making $|B_o| = |B_1|$ (i.e. by

attenuating zeroth mode 1dB relative to first mode) (see Fig. 5.44). The 10dB nullwidth is measured to be 90^{o} and gain ripple in the omniregion is $\pm$2dB. By introducting a phase shift "56^{o}" between the two modes, the null was steered 56 degrees (see Fig. 5.44).

A problem with steering the null is that null depth depends, to some extent, on the null pointing direction. This is because the modes are rippled. Hence, if null depth is optimized in the direction of the element then when it is steered midway between the element there will be a loss in null depth. Null depth also depends on the frequency of operation. This is because the relative mode gain is frequency dependent.

Fig. 5.45 shows the null patterns for an 8 ft diameter array at the frequencies of 225MHz and 300MHz. The null in the two cases is pointing in different directions because γ_o and γ_1 (see equation 5.9) are frequency dependent.

5.11 Formation of single narrow null in the directional pattern of circular array

In section 4.2 it was shown that single narrow null in otherwise omnidirectional pattern can be synthesised by combining a square wave pattern and a cardioid.

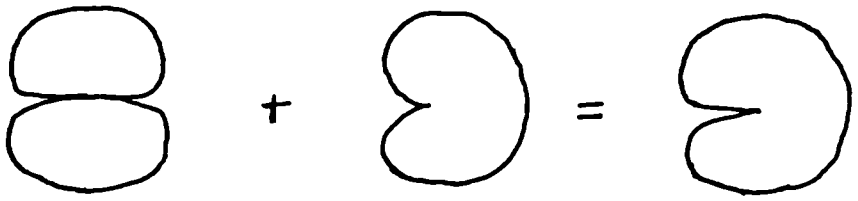

The pattern function being given by

$$F(\phi) = jA(1+\cos\phi) + \sin\phi + \frac{1}{3}\sin 3\phi + \ldots\ldots \qquad 5.10$$

It was shown that A=0.35 gave optimum nullwidth and gain ripple in the omniregion. In the experimental measurement modes only up to third were used. Attenuations and phase shifts of various modes, as given by equation 5.10 is given in Table 2.

Mode	Attenuation	Phase Shift
0	5.7dB	0^o
+1	5.4dB	180^o
-1	0dB	0^o
+3	12 dB	180^o
-3	12 dB	0^o

Table 2

After applying attenuations and phase shifts to the modes shown in Table 2 and also correcting phase shift due to the use of directive elements and mutual coupling, the output from various modes was combined in the power combiner. The output from the power combiner was then connected to the reciver input. The far field pattern thus obtained is shown in Fig. 5.46. The pattern characteristics obtained are (a) null depth = 20dB (b) -10dB null width = 20^{o} (c) gain ripple in the omni-region = $\pm$2dB.

5.12 Directional pattern in the vertical plane through the null

In order to measure vertical directional patterns of the circular array, the boom facility was used. In this the transmitting log-periodic array is mounted on the boom which moves in the vertical plane. The polarisation is always normal to the radius in the vertical plane. In the first instance absorbing material was placed on the ground plane around the array to avoid reflections. The vertical directional patterns for the zeroth and first modes are shown in Fig. 5.47 and 5.48. The vertical patterns do not contain nulls of the Bessel function which is in agreement with the theoretical result (see Fig. 3.8 and 3.9, Chapter III). Also due to some reflection from the ground plane patterns are distorted and there is radiation in the vertical direction in the case of first order mode.

Combining zeroth and first mode results in a cardioid pattern in the horizontal plane. Vertical pattern through the null is shown in Fig. 5.49. From Fig. 5.49 it is clear that the null is maintained over a large elevation angle. This is an advantage because the interfering signal may arrive at an elevation .

Further, measurements were made without the absorbing material (which is more realistic because the antenna will be above the sea). Zeroth and first order modes (see Fig. 5.50 and 5.51) contains nulls due to interference with the reflected waves. Measurement of vertical pattern through the null formed by combining zeroth and first mode is shown in Fig. 5.52. In this case elevation null width is somewhat reduced as compared to the case when absorbing material was placed around the array.

5.13 Cross polar patterns in the horizontal plane

Since the interfering signal may be horizontally polarised or circularly polarised it is important to know the cross polar performance of the circular array. The co-polar and cross polar patterns measured for zeroth, first, second and third modes are shown in Fig. 5.53 and 5.54. Since the co-polar pattern is shown attenuated by 20dB, the cross-polar level is about 30dB down on the co-polar level for various modes.

The co-polar and cross-polar patterns when zeroth and first modes are combined is shown in Fig. 5.55. The co-polar pattern is again attenuated by 20dB, therefore the cross-polar level in the direction of the null of the co-polar pattern is the same as the null depth. Hence signal with horizontal polarisation will also be rejected. However, it is interesting to note that null of the cross-polar pattern is in a different direction. This is because element directional pattern for the two polarisations is different. The element patterns for vertical and horizontal polarisations are shown in Fig. 5.56 to confirm this point.

5.14 Cross polar patterns in the vertical plane

To study the cross polar performance of the circular array in the vertical plane, zeroth and first phase modes were measured for vertical and horizontal polarisations (see Fig. 5.57 and Fig. 5.58). These results are of importance because the array may be used for communicating with aircraft or satellites and the electromagnetic waves may be of either polarisation at an elevation angle.

Mode Order	Theoretical gain ripple	Measured gain ripple
0	0	±1.5
1	0	±2.0
2	0	±3.0
3	0	±2.8
4	0	±2.8
5	0	±5.5
6.	±0.17	±4.0
7	±1.2	±6.0

Table 3

16 x 16 port 300MHz

Input port 0 (B) :- Mean overall loss = 21.4dB, standard dev. = 0.4dB

Output port No.	1	2	3	4	5	6	7	8
	-21.5dB 0°	-21.7dB -358°	-21.2dB -354°	-21.4dB -6°	-21.4dB -3°	-21.6dB -8°	-21.7dB -3°	-21.4dB -355°
Output port No.	9	10	11	12	13	14	15	16
	-21.9dB -356°	-21dB -2°	-20.6dB -359°	-21.8dB -5°	-21.2dB -4°	-20.9dB -5°	-22.3dB -359°	-20.9dB -356°

Input port +1 (1R) :- Mean overall loss = 22.1dB, standard dev. = 1.4dB

Output port No.	1	2	3	4	5	6	7	8
	-22dB -359°	-20.4dB -338°	-21.7dB -310°	-23.9dB -292°	-22.8dB -268°	-20.9dB -250°	-24.2dB -226°	-20.6dB -204°
Output port No.	9	10	11	12	13	14	15	16
	-21.7dB -180°	-20dB -159°	-22.4dB -131°	-23.3dB -115°	-23.3dB -88°	-21.1dB -65°	-23.8dB -40°	-21dB -25°

Input port -1 (1L) :- Mean overall loss = 21.4dB, standard dev. = 1.2dB

Output port No.	1	2	3	4	5	6	7	8
	-21.9dB -90°	-22.7dB -106°	-22.9dB -127°	-20.2dB -152°	-20.7dB -180°	-20.2dB -201°	-21.2dB -232°	-21.1dB -242°
Output port No.	9	10	11	12	13	14	15	16
	-21.5dB -93°	-23.4dB -289°	-23.4dB -311°	-19.6dB -332°	-21.2dB -357°	-20.5dB -16°	-20.3dB -47°	-21.5dB -63°

Input port +2 (2R) :- Mean overall loss = 22.5dB, standard dev. = 1.4dB

Output port No.	1	2	3	4	5	6	7	8
	-22.5dB -358°	-20.9dB -314°	-23dB -266°	-23.7dB -226°	-21.4dB -180°	-21.5dB -138°	-24.2dB -93°	-23.5dB -38°
Output port No.	9	10	11	12	13	14	15	16
	-22.8dB -359°	-20.2dB -317°	-22.4dB -270°	-24.3dB -225°	-20.9dB -180°	-20.9dB -138°	-24.9dB -88°	-22.9dB -39°

Table 4

Input port -2 (2L) :- Mean overall loss = 22.6dB, standard dev. = 1dB

Output port No.	1	2	3	4	5	6	7	8
	-23.2dB -85°	-23.8dB -130°	-22.1dB -180°	-22.2dB -230°	-22.3dB -274°	-23.8dB -321°	-23.1dB -2°	-21.2dB -42°
Output port No.	9	10	11	12	13	14	15	16
	-23.8dB -85°	-22.8dB -137°	-21.3dB -180°	-22.9dB -230°	-21.8dB -275°	-23.2dB -322°	-23.8dB -357°	-20.5dB -44°

Input port +3 (3R) :- Mean overall loss = 22.7dB, standard dev. = 1.6dB

Output port No.	1	2	3	4	5	6	7	8
	-22.8dB -266°	-23.3dB -201°	-25.7dB -128°	-20.4dB -64°	-22.5dB -359°	-21.8dB -295°	-22.8dB -231°	-21.5dB -185°
Output port No.	9	10	11	12	13	14	15	16
	-22.7dB -83°	-24.3dB -24°	-25.7dB -306°	-19.8dB -245°	-23.1dB -180°	-22.1dB -109°	-22.3dB -46°	-22dB -328°

Input port -3 (3L) :- Mean overall loss = 21.7dB, standard dev. = 1.1dB

Output port No.	1	2	3	4	5	6	7	8
	-20.9dB -180°	-19.5dB -247°	-20.8dB -309°	-22.6dB -23°	-21.4dB -90°	-21.9dB -163°	-23dB -216°	-22.3dB -300°
Output port No.	9	10	11	12	13	14	15	16
	-20.1dB -357°	-21dB -72°	-21.6dB -131°	-22.9dB -204°	-21.2dB -272°	-22.7dB -340°	-23dB -36°	-22.4dB -123°

Input port +4 (4R) :- Mean overall loss = 21.7dB, standard dev. = 1.1dB

Output port No.	1	2	3	4	5	6	7	8
	-22.4dB -269°	-21dB -180°	-22.6dB -82°	-21.2dB -4°	-22dB -273°	-20.3dB -180°	-22.9dB -90°	-21.8dB -356°
Output port No.	9	10	11	12	13	14	15	16
	-22.4dB -266°	-20.3dB -180°	-21.8dB -86°	-22dB -4°	-21.4dB -274°	-19.7dB -180°	-23.7dB -86°	-21.1dB -358°

Table 5

Input port -4 (4L) :- Mean overall loss = 21.7dB, standard dev. = 0.7dB

Output port No.	1	2	3	4	5	6	7	8
	-21.3dB -180°	-21.5dB -271°	-22dB -357°	-21.9dB -99°	-21.2dB -180°	-21.2dB -281°	-22.2dB -6°	-22.5dB -90°
Output port No.	9	10	11	12	13	14	15	16
	-21.6dB -180°	-21dB -279°	-21.2dB -1°	-22.7dB -99°	-20.7dB -180°	-20.6dB -278°	-23dB -1°	-21.9dB -92°

Input port +5 (5R) :- Mean overall loss = 21.4dB, standard dev. = 1.1dB

Output port No.	1	2	3	4	5	6	7	8
	-20.7dB -354°	-19.8dB -246°	-20.7dB -121°	-23.4dB -25°	-21.3dB -263°	-21.1dB -159°	-23.6dB -39°	-20.7dB -296°
Output port No.	9	10	11	12	13	14	15	16
	-20.2dB -180°	-20.2dB -70°	-21.3dB -304°	-22.2dB -204°	-21.9dB -87°	-21.5dB -335°	-23dB -213°	-21.3dB -122°

Input port -5 (5L) :- Mean overall loss = 22.4dB, standard dev. = 1.7dB

Output port No.	1	2	3	4	5	6	7	8
	-23dB -90°	-22.9dB -205°	-25.3dB -308°	-19.7dB -66°	-22dB -180°	-21.2dB -299°	-23dB -52°	-20.8dB -152°
Output port No.	9	10	11	12	13	14	15	16
	-23dB -267°	-23.2dB -27°	-25.7dB -132°	-19.9dB -247°	-22.7dB -2°	-21.7dB -115°	-22.3dB -228°	-21.2dB -332°

Input port +6 (6R) :- Mean overall loss = 22.3dB, standard dev. = 1.1dB

Output port No.	1	2	3	4	5	6	7	8
	-22.3dB -82°	-23.8dB -318°	-21.2dB -180°	-22dB -48°	-21.7dB -270°	-24dB -135°	-22.3dB 0°	-21.1dB -220°
Output port No.	9	10	11	12	13	14	15	16
	-23.1dB -81°	-23.3dB -314°	-20.5dB -180°	-22.6dB -48°	-21.2dB -270°	-23.5dB -136°	-23dB -356°	-20.5dB -222°

Table 6

Input port -6 (6L):- Mean overall loss = 22.2dB, standard dev. = 1.4dB

Output port No.	1	2	3	4	5	6	7	8
	-21.5dB -355°	-21.1dB -136°	-22.3dB -270°	-24dB -46°	-20.7dB -180°	-21.4dB -313°	-23.2dB -95°	-24dB -216°
Output port No.	9	10	11	12	13	14	15	16
	-22dB -358°	-20.5dB -139°	-21.7dB -274°	-24.7dB -46°	-20.1dB -180°	-21dB -320°	-23.9dB -90°	-23.2dB -217°

Input port +7 (7R):- Mean overall loss = 21.7dB, standard dev. = 1.3dB

Output port No.	1	2	3	4	5	6	7	8
	-22.5dB -90°	-22.8dB -287°	-23.6dB -126°	-20.4dB -332°	-21.2dB -180°	-20.2dB -22°	-21.7dB -232°	-21dB -66°
Output port No.	9	10	11	12	13	14	15	16
	-22dB -268°	-23.1dB -110°	-24.1dB -310°	-19.8dB -153°	-21.5dB -357°	-20.7dB -197°	-20.9dB -48°	-21.4dB -242°

Input port -7 (7L):- Mean overall loss = 22.3dB, standard dev. = 1.6dB

Output port No.	1	2	3	4	5	6	7	8
	-22.5dB -357°	-20.4dB -160°	-22.2dB -311°	-23.9dB -114°	-23.3dB -270°	-20.7dB -72°	-25.1dB -229°	-20.5dB -28°
Output port No.	9	10	11	12	13	14	15	16
	-22.4dB -180°	-19.8dB -342°	-22.9dB -132°	-23.4dB -298°	-23.5dB -88°	-21dB -247°	-24.2dB -42°	-20.9dB -209°

Input port -8 (8L):- Mean overall loss = 22dB, standard dev. = 0.8dB

Output port No.	1	2	3	4	5	6	7	8
	-22.2dB 0°	-21.8dB -180°	-22.6dB -354°	-21.4dB -180°	-22.5dB -6°	-21.5dB -180°	-22.7dB -6°	-21.7dB -180°
Output port No.	9	10	11	12	13	14	15	16
	-22.9dB -359°	-21.1dB -180°	-21.9dB 0°	-21.8dB -180°	-22.1dB -7°	-20.7dB -180°	-23.5dB -359°	-21.2dB -180°

Table 7

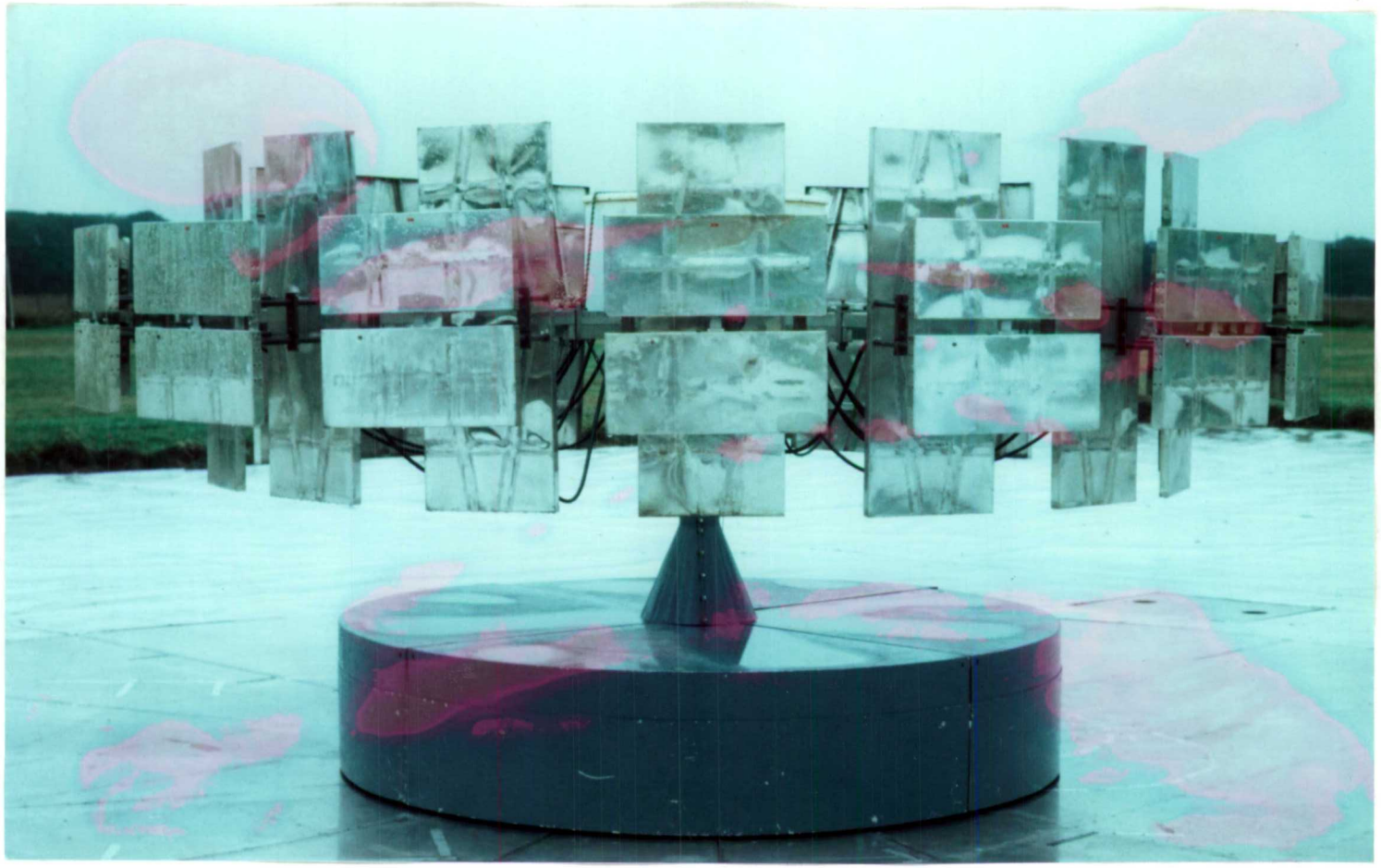

Figure 5.1 A Photograph of the 16 Element Circular Array

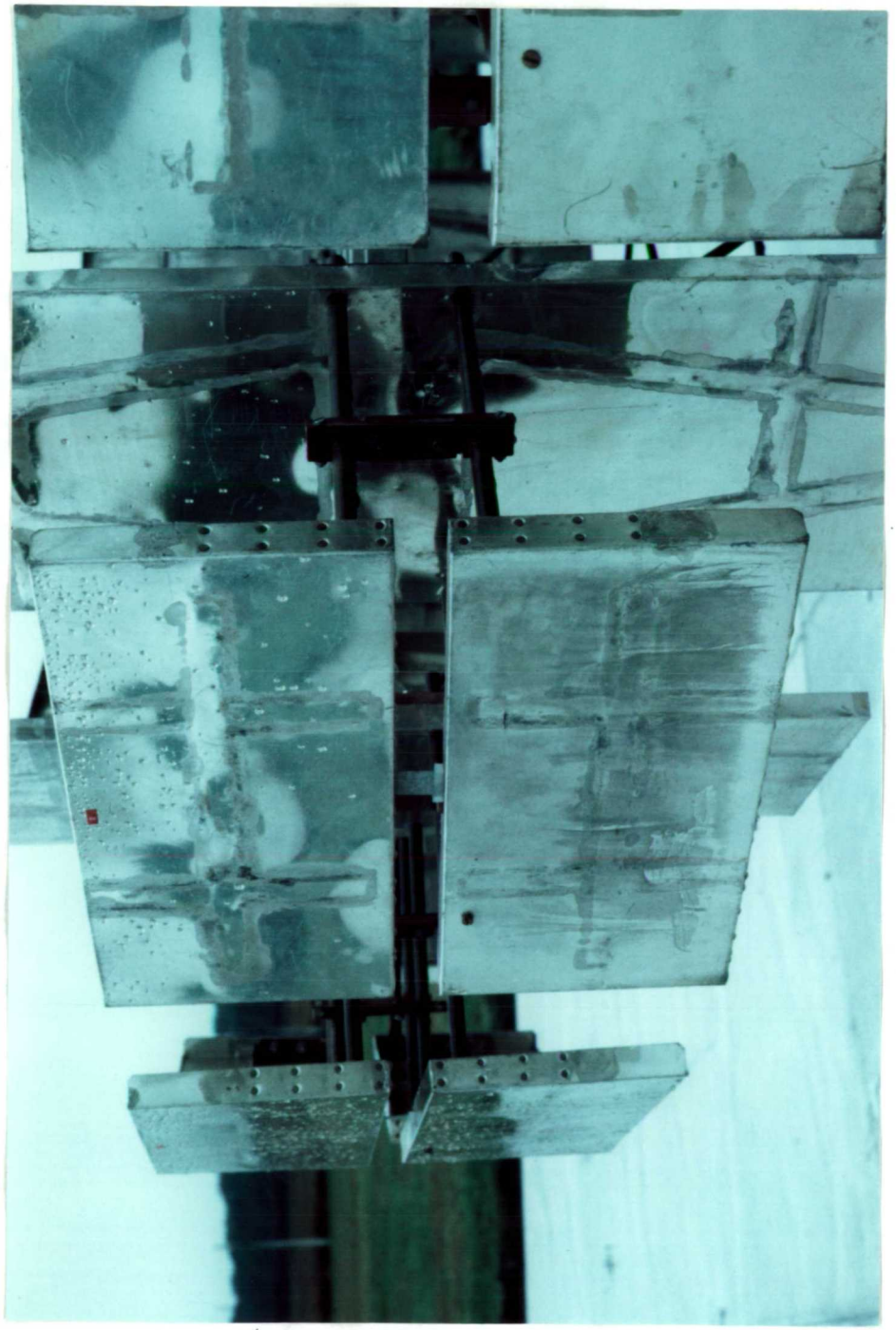

Figure 5.2 A Photograph of the Element

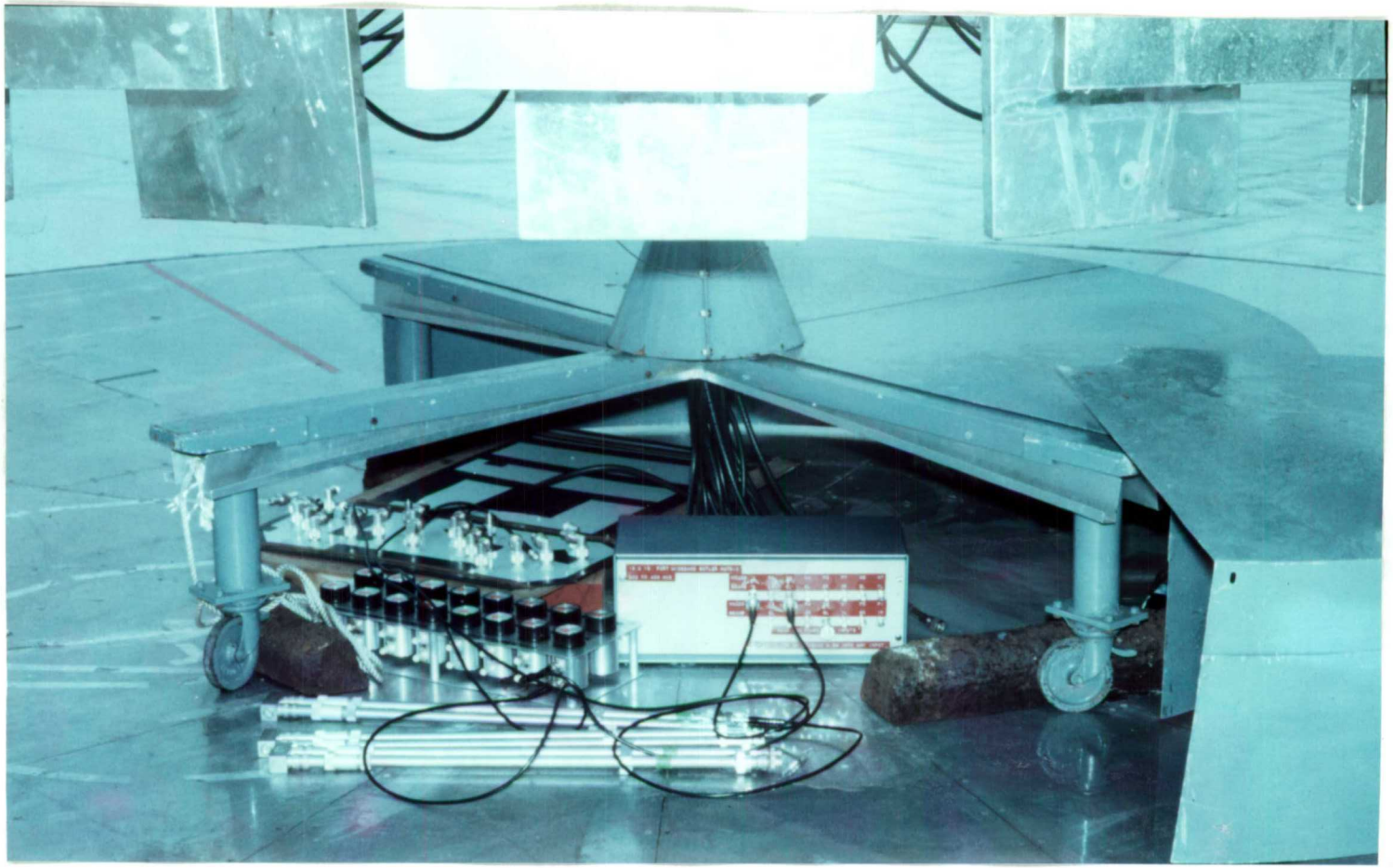

Figure 5.3 A Photograph of the Butler Matrix network and associated system

Figure 5.4 A Photograph of the Antenna Meaurement Site

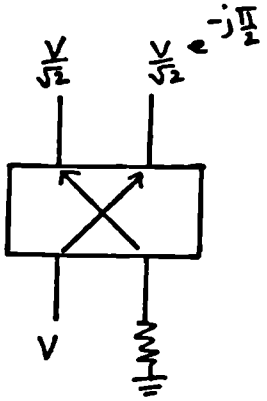

(i) 90° hybrid coupler

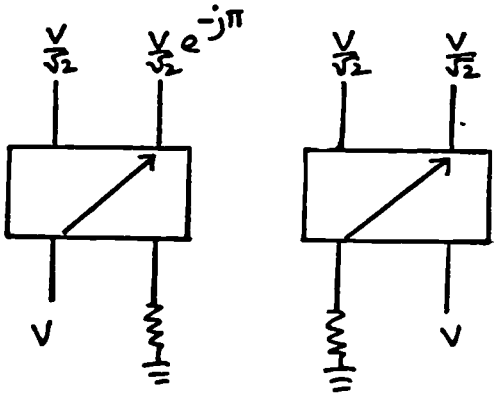

(ii) 180° hybrid coupler

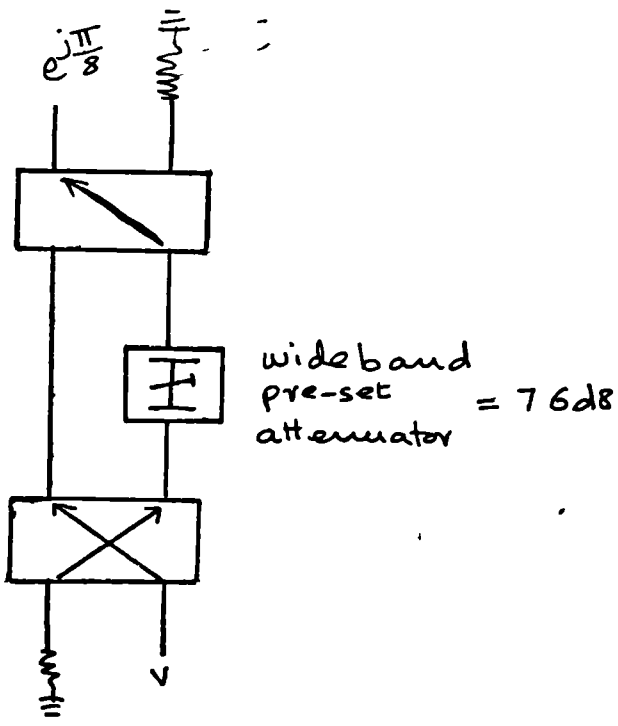

(iii) 22½° wideband phase shift

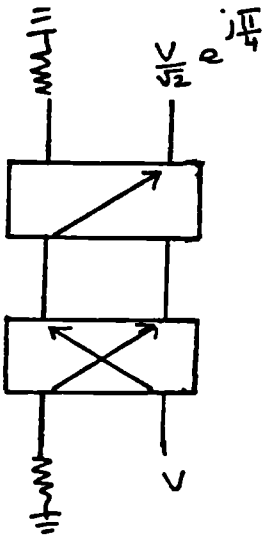

(iv) 45° wideband phase shift

Figure 5.5

Wideband 8x8 Butler Matrix

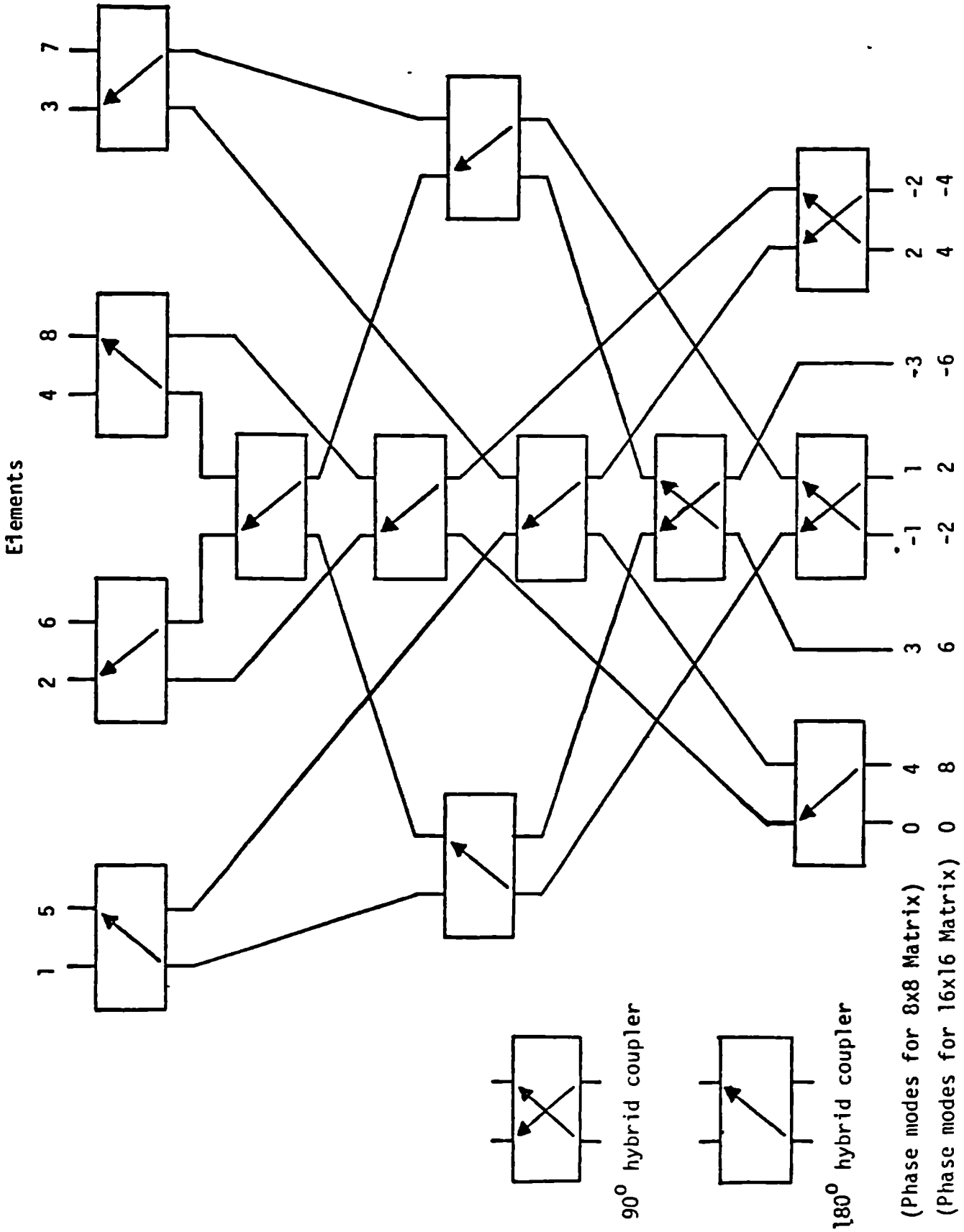

FIGURE 56

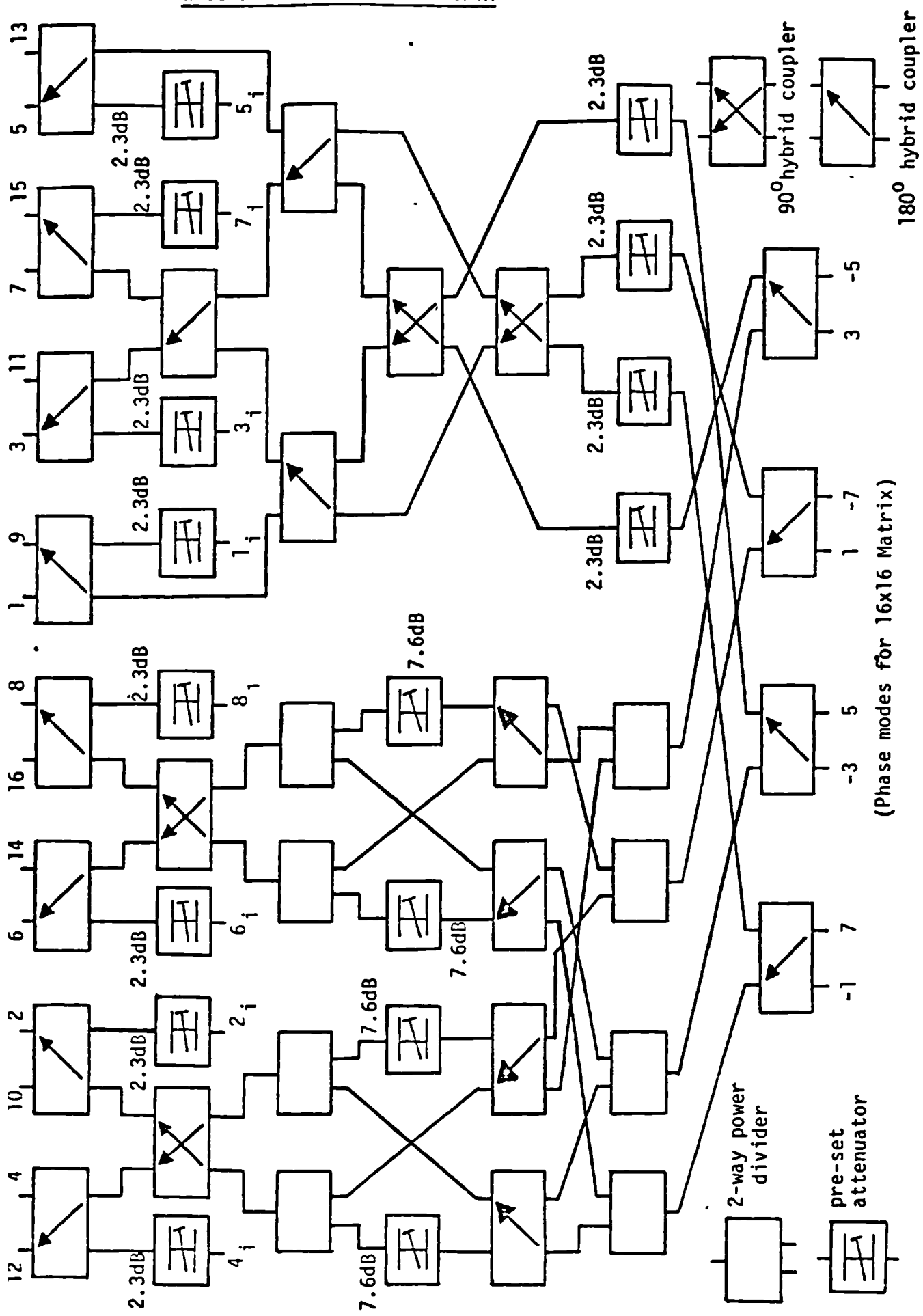
Wideband 16x16 Butler Matrix
2.3dB
7.6dB
90° hybrid coupler
180° hybrid coupler
(Phase modes for 16x16 Matrix)
2-way power divider
pre-set attenuator

FIGURE 57

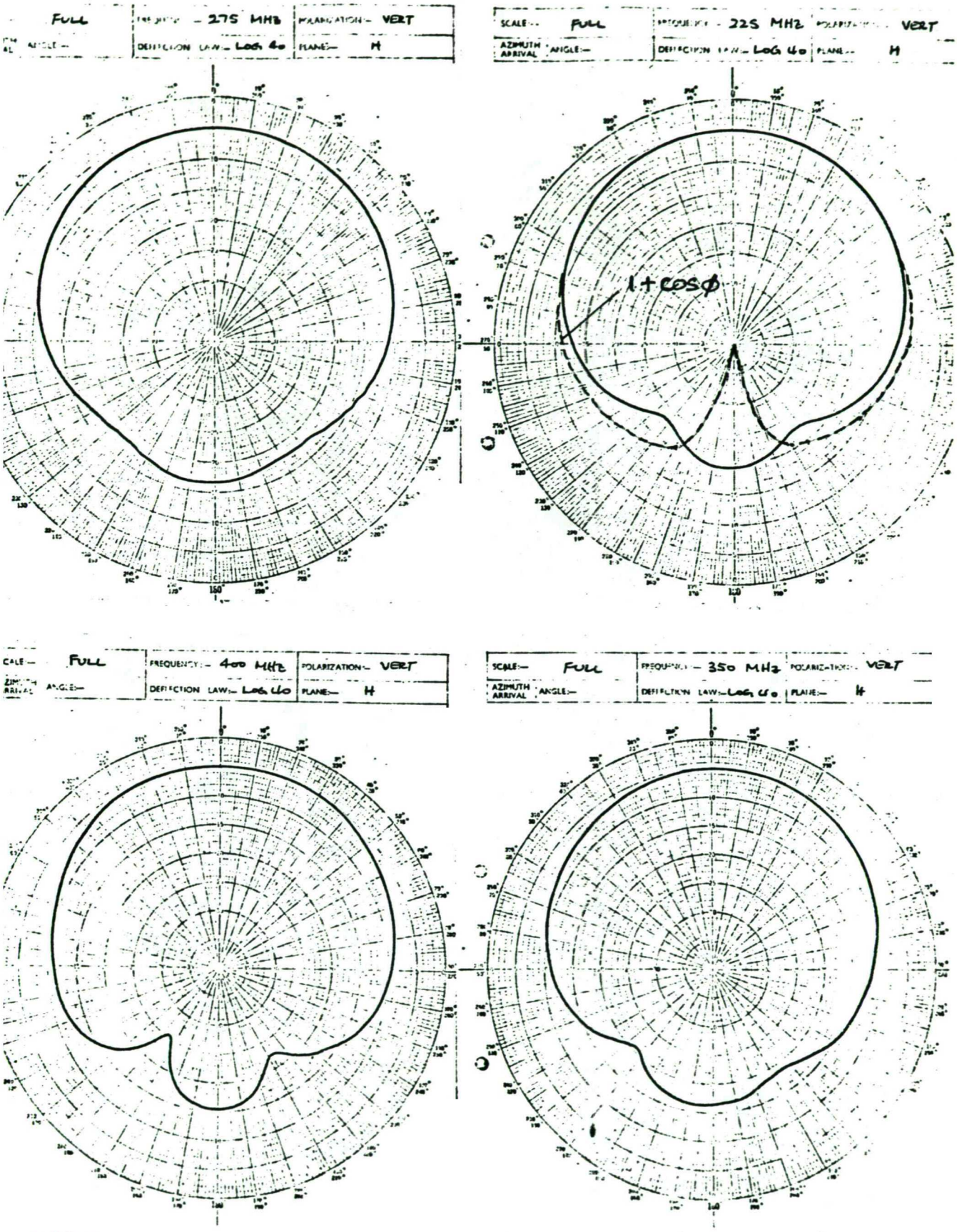

4-7-79 9 UHF ARRAY ELEMENT
C. BURGESS DESIGN.

4-7-79 7 UHF ARRAY ELEMENT
C. BURGESS DESIGN.

Measured directional pattern for isolated element

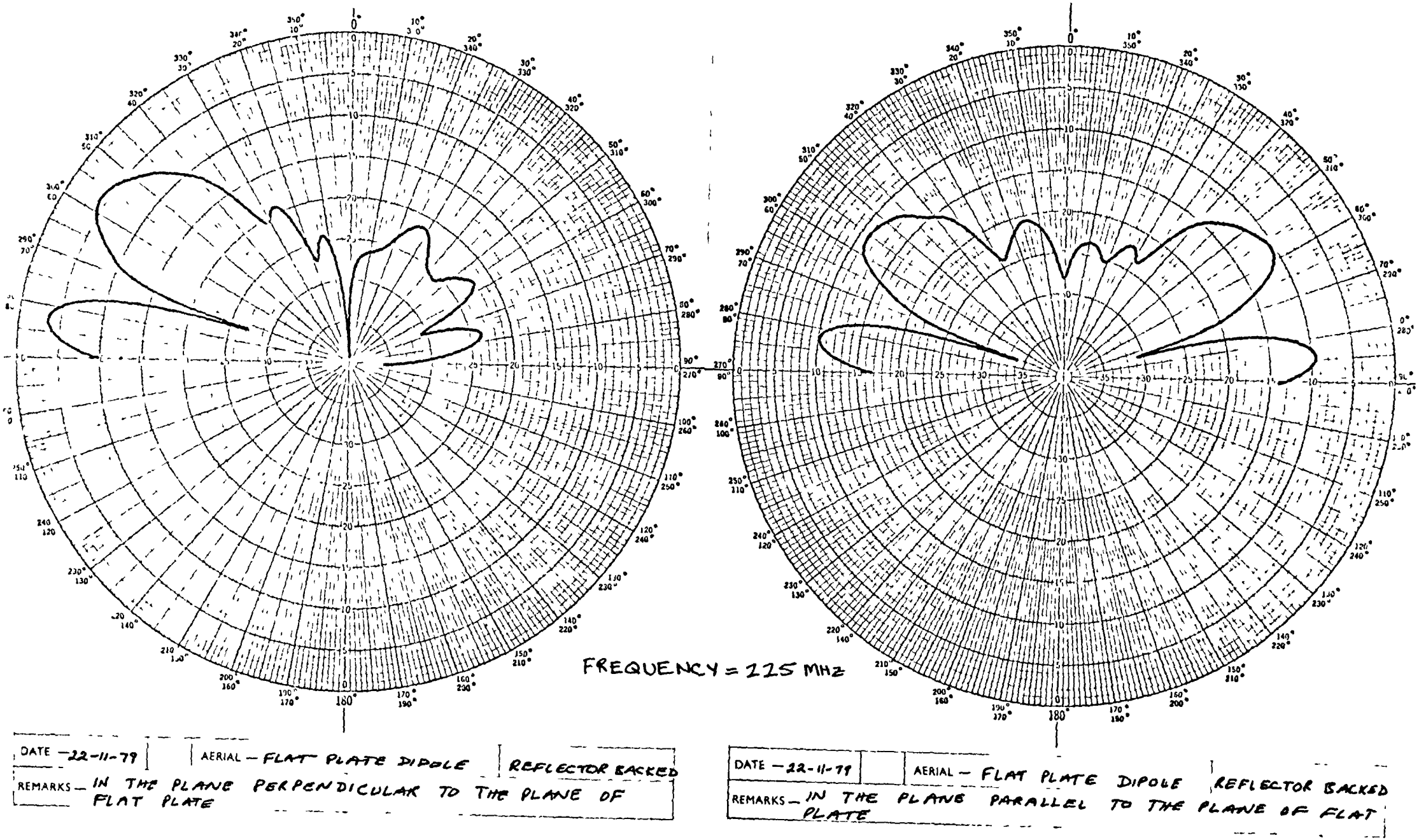

Figure 5.8(b) Measured element pattern in orthogonal planes

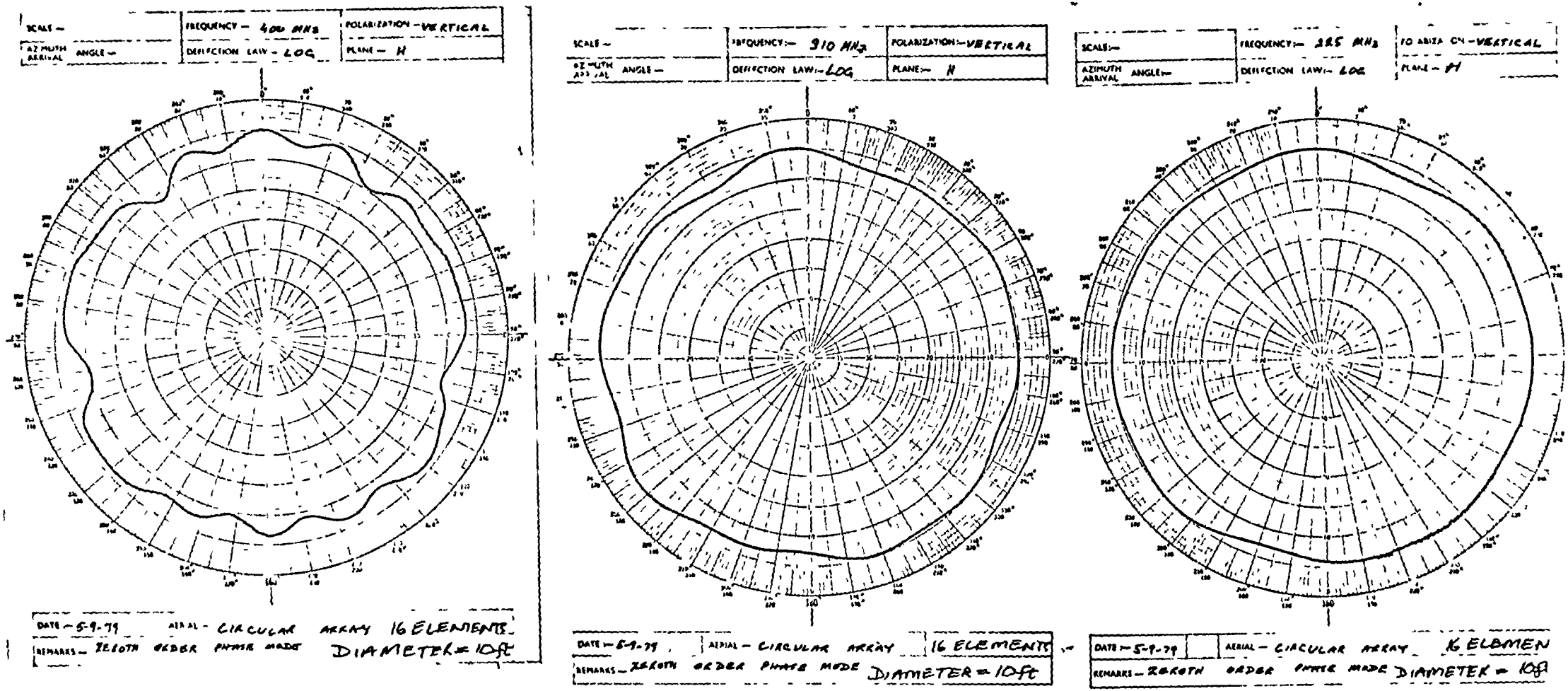

Figure 5.9 Measured zeroth order phase mode of a 10ft diameter array

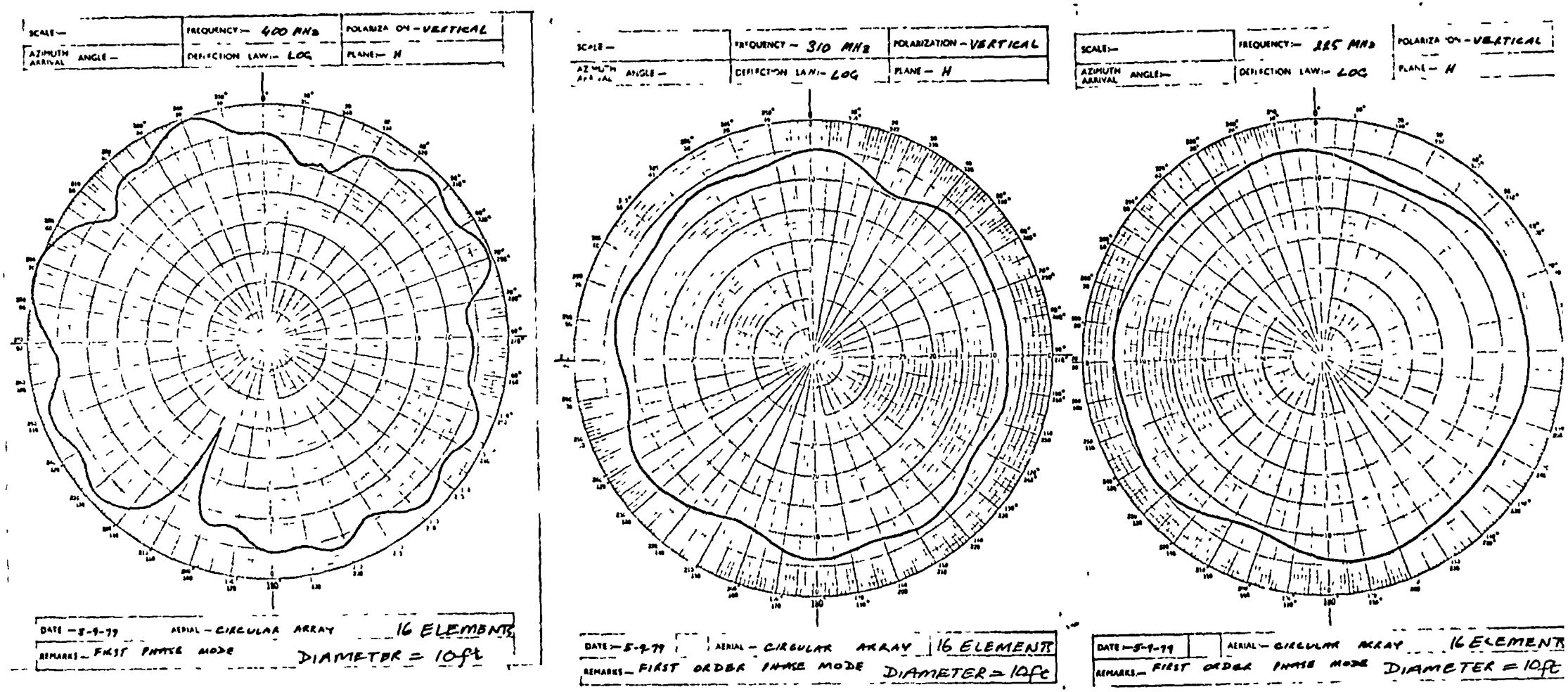

Figure 5.10 Measured first order phase mode of a 10ft diameter array

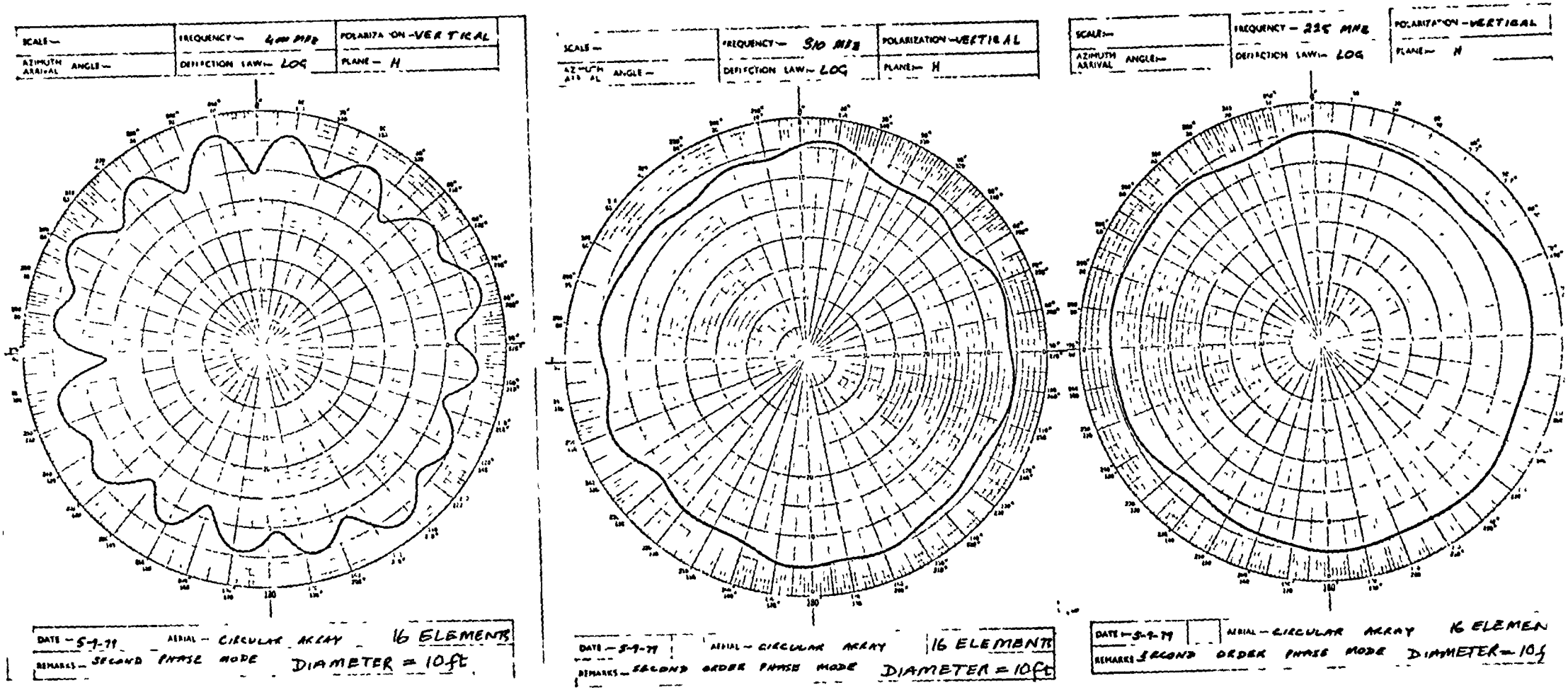

Figure 5.11 Measured second order phase mode of a 10ft diameter array

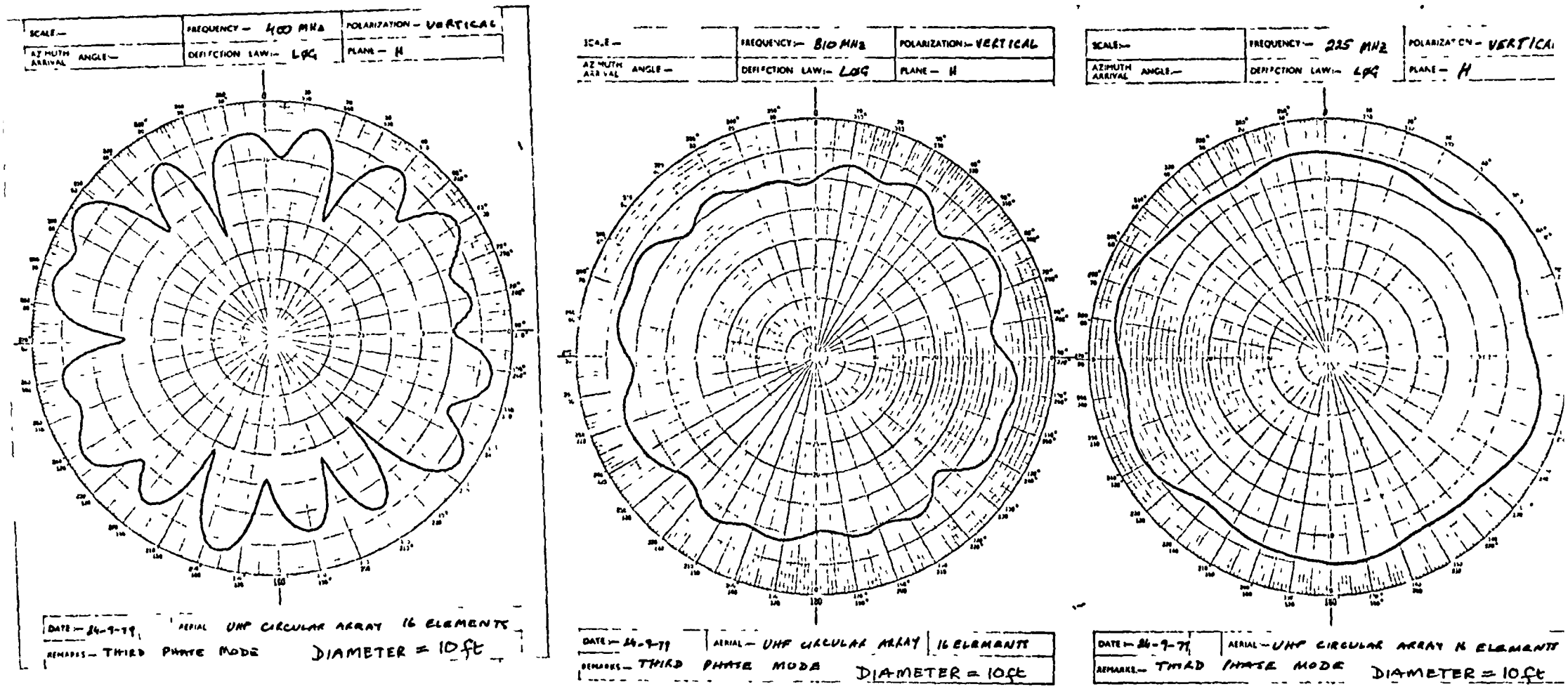

Figure 5.12 Measured third order phase mode of a 10ft diameter array

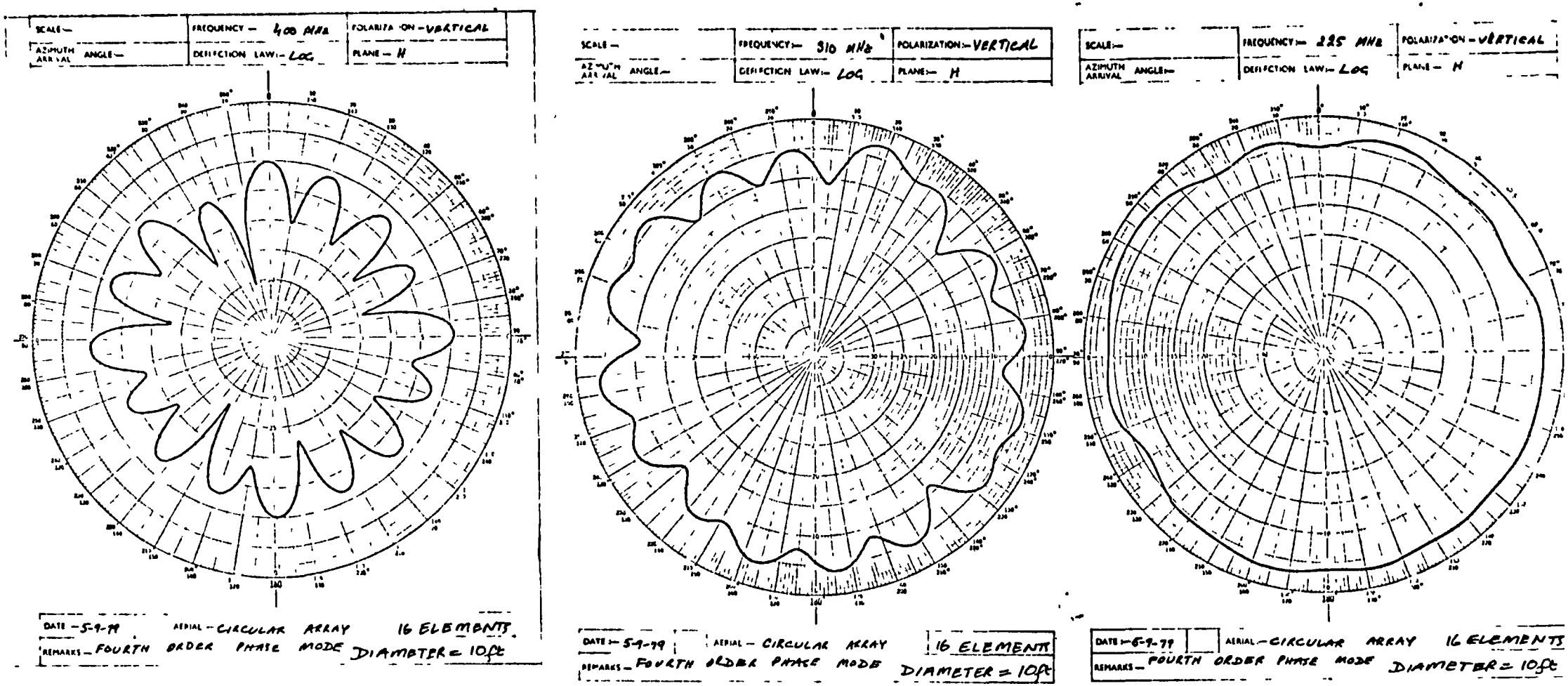

Figure 5.13 Measured fourth order phase mode of a 10ft diameter array

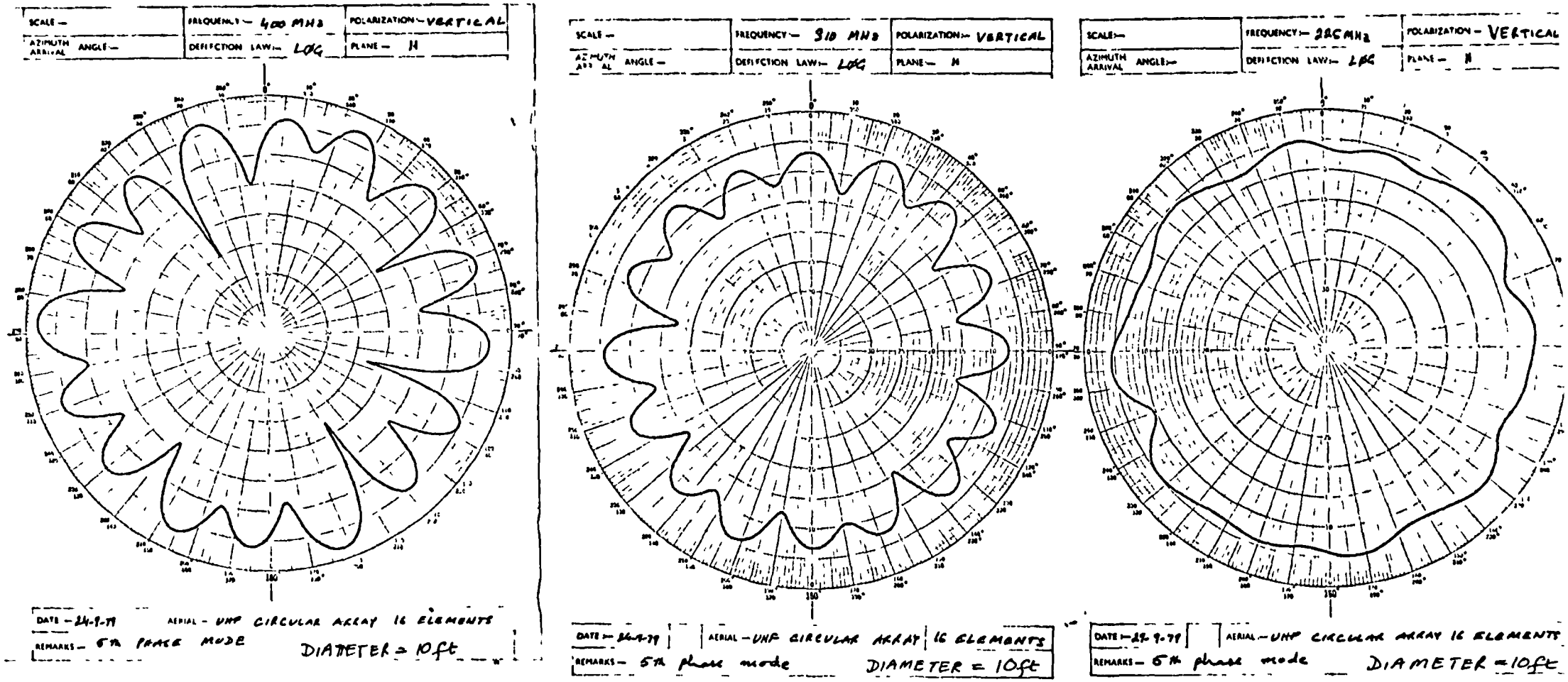

Figure 5.14 Measured fifth order phase mode of a 10ft diameter array

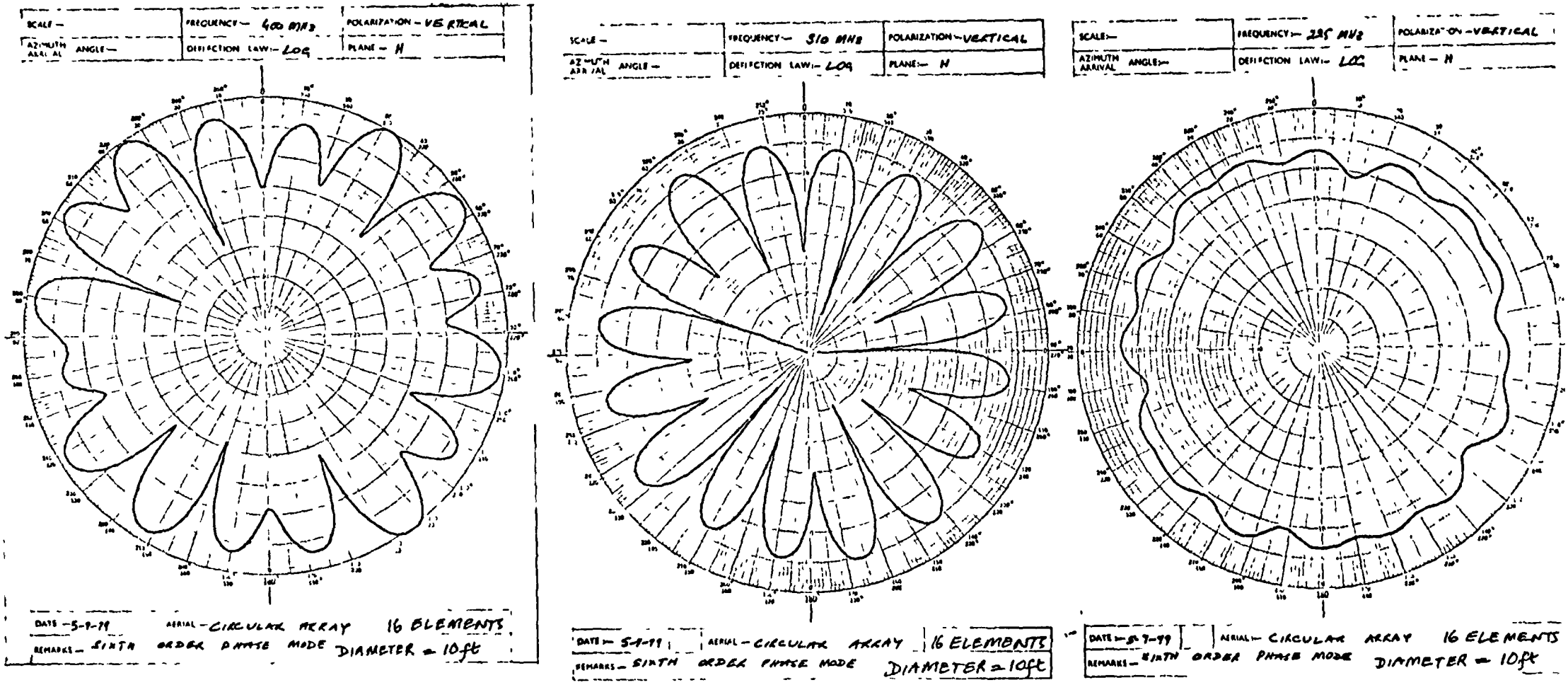

Figure 5.15 Measured sixth order phase mode of a 10ft diameter array

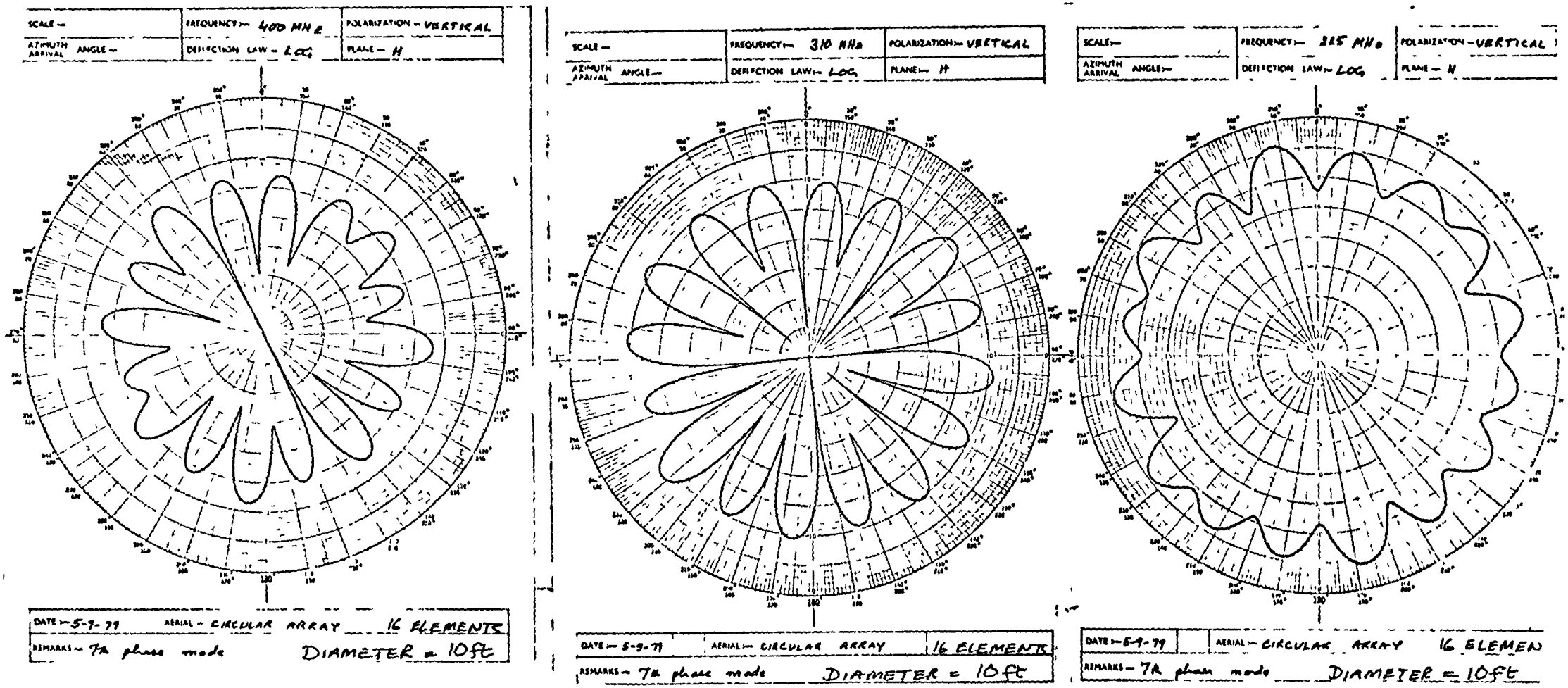

Figure 5.16 Measured seventh order phase mode of a 10ft diameter array

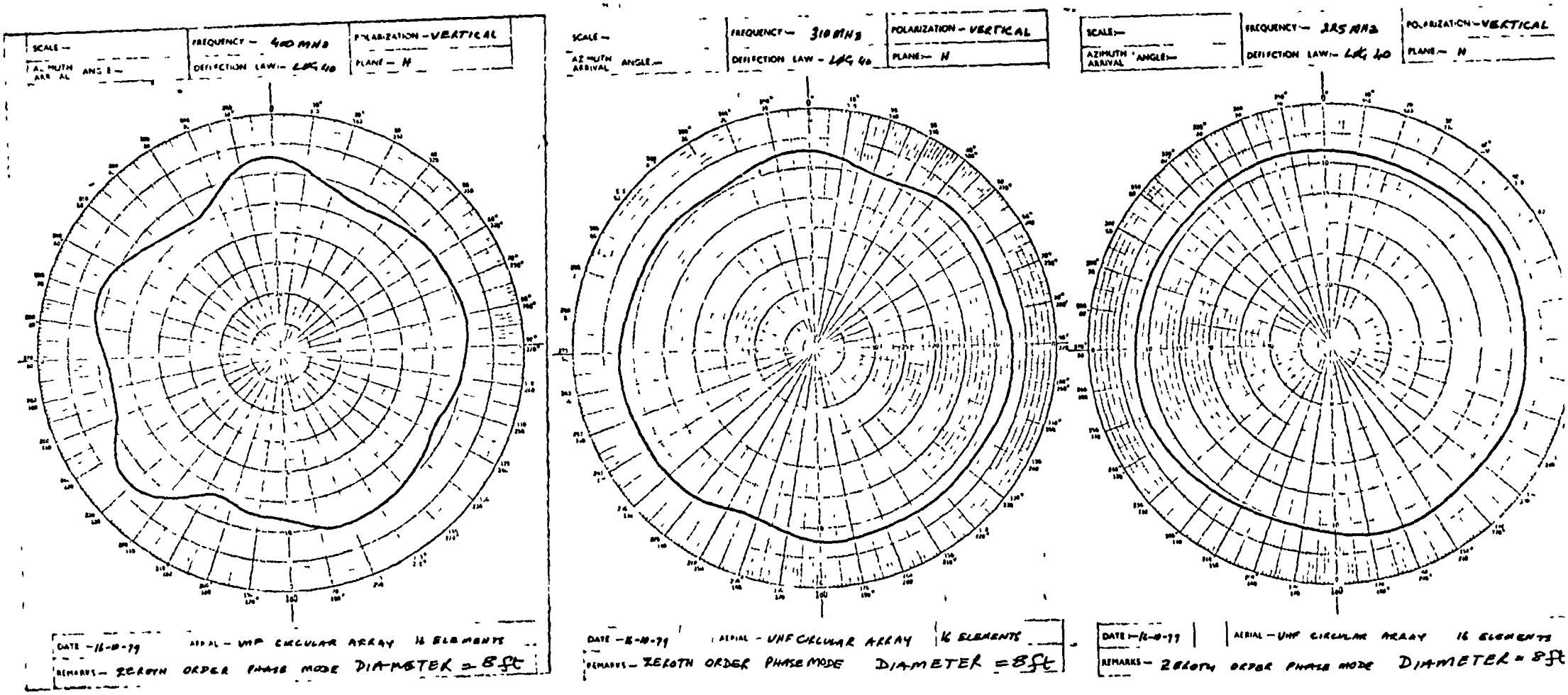

Figure 5.17 Measured zeroth order phase mode of an 8ft diameter array

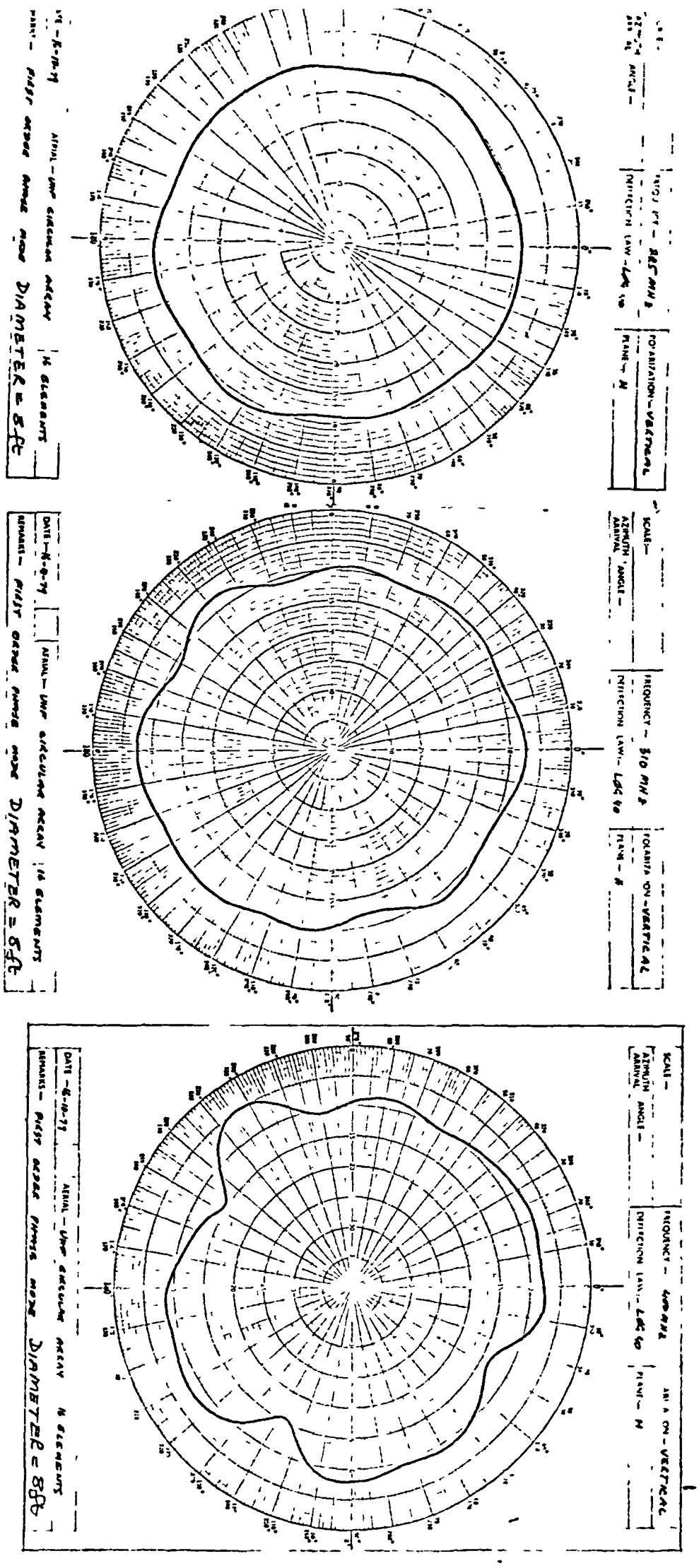

Figure 5.18 Measured first order phase mode of an 8ft diameter array

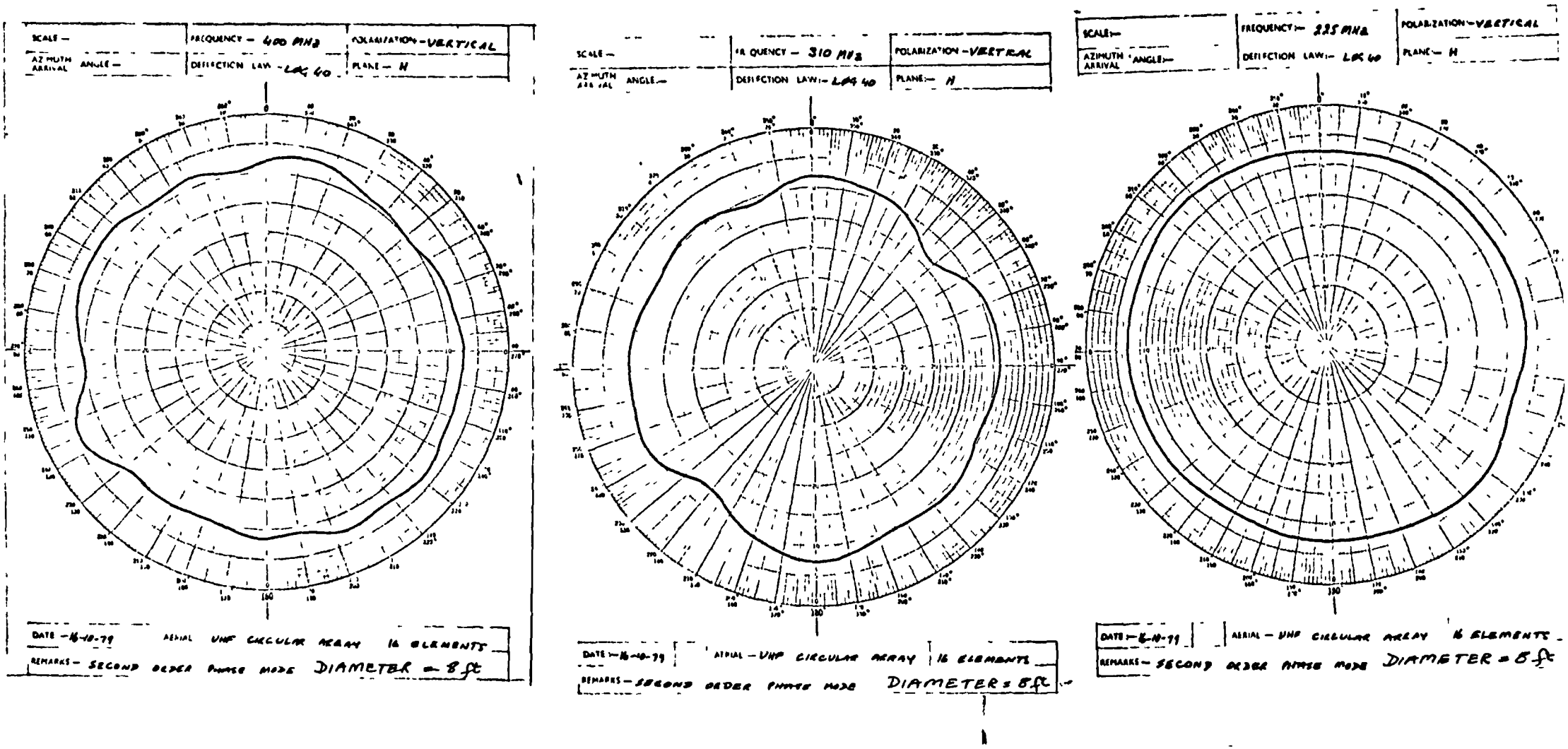

Figure 5.19 Measured second order phase mode of an 8ft diameter array

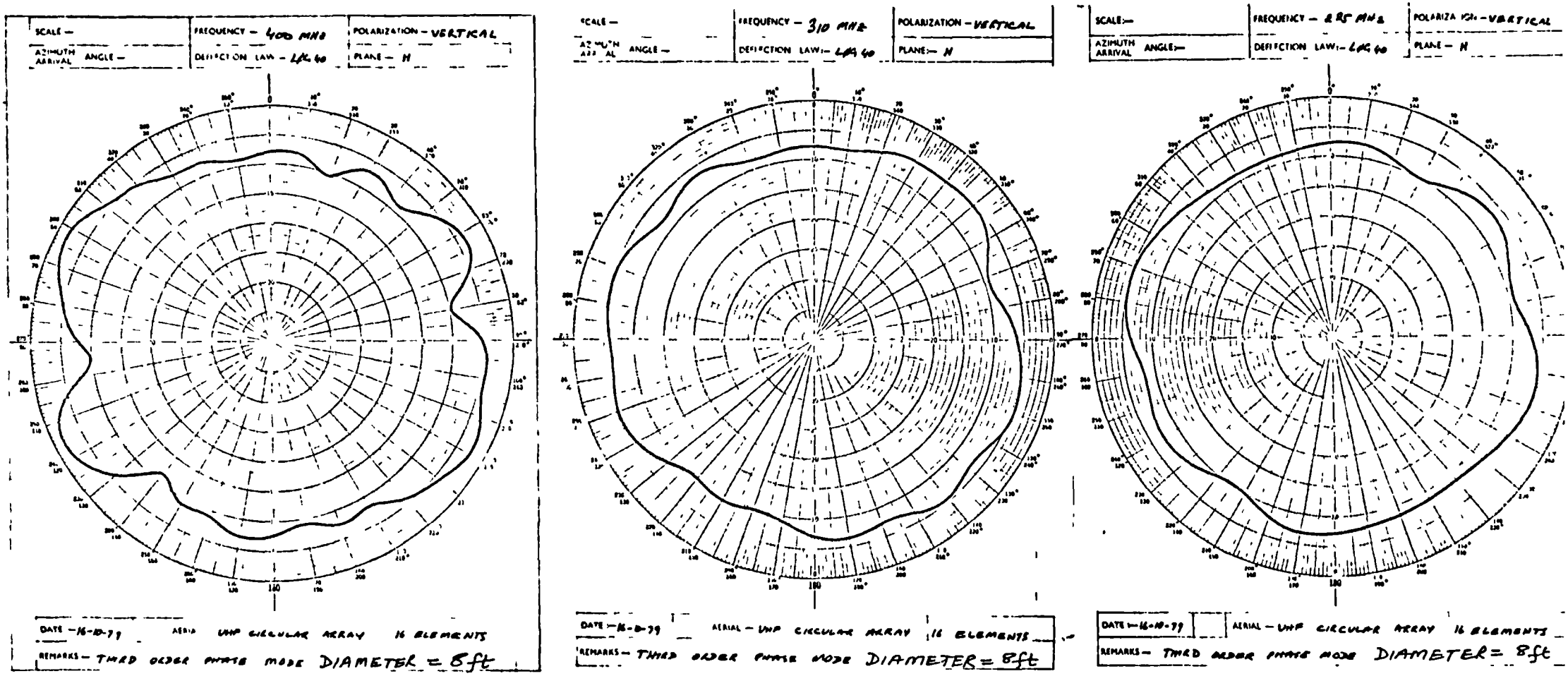

Figure 5.20 Measured third order phase mode of an 8ft diameter array

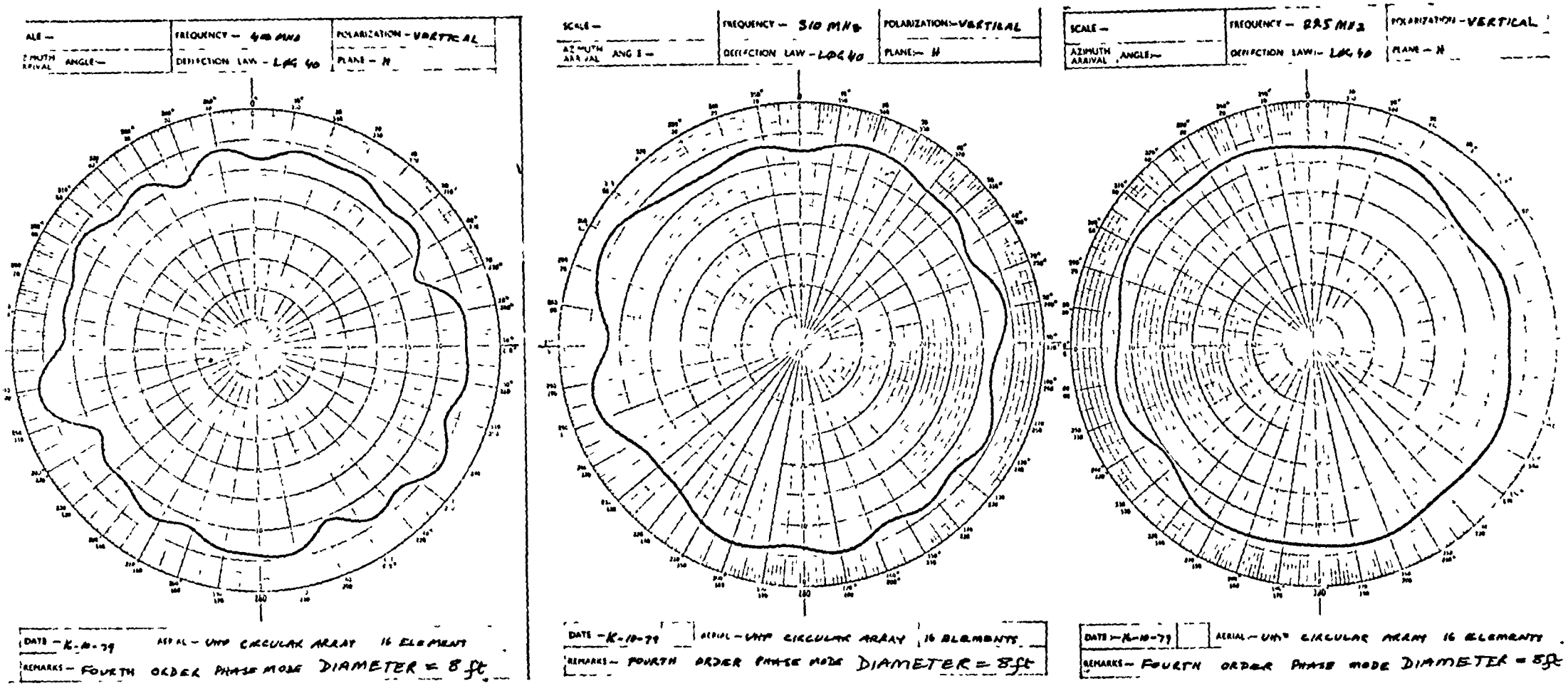

Figure 5.21 Measured fourth order phase mode of an 8ft diameter array

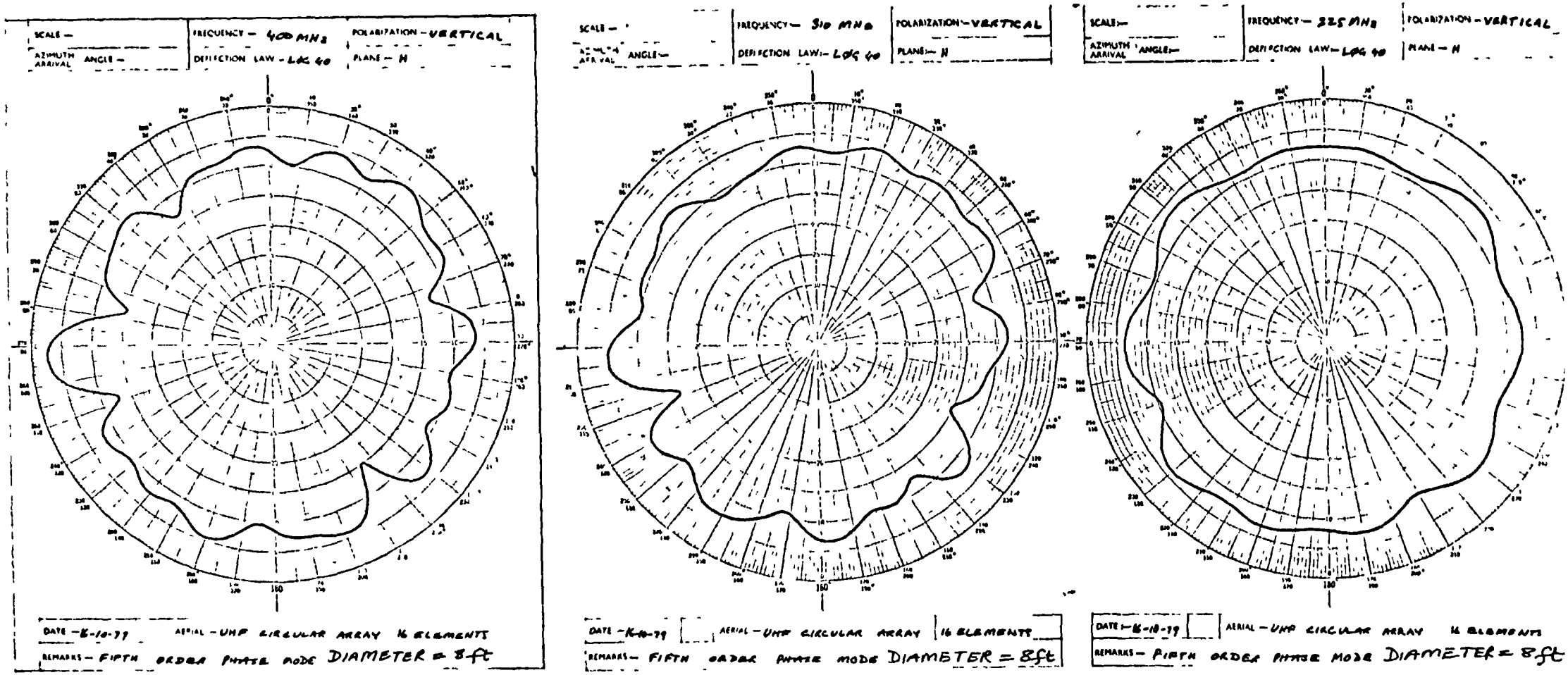

Figure 5.22 Measured fifth order phase mode of an 8ft diameter array

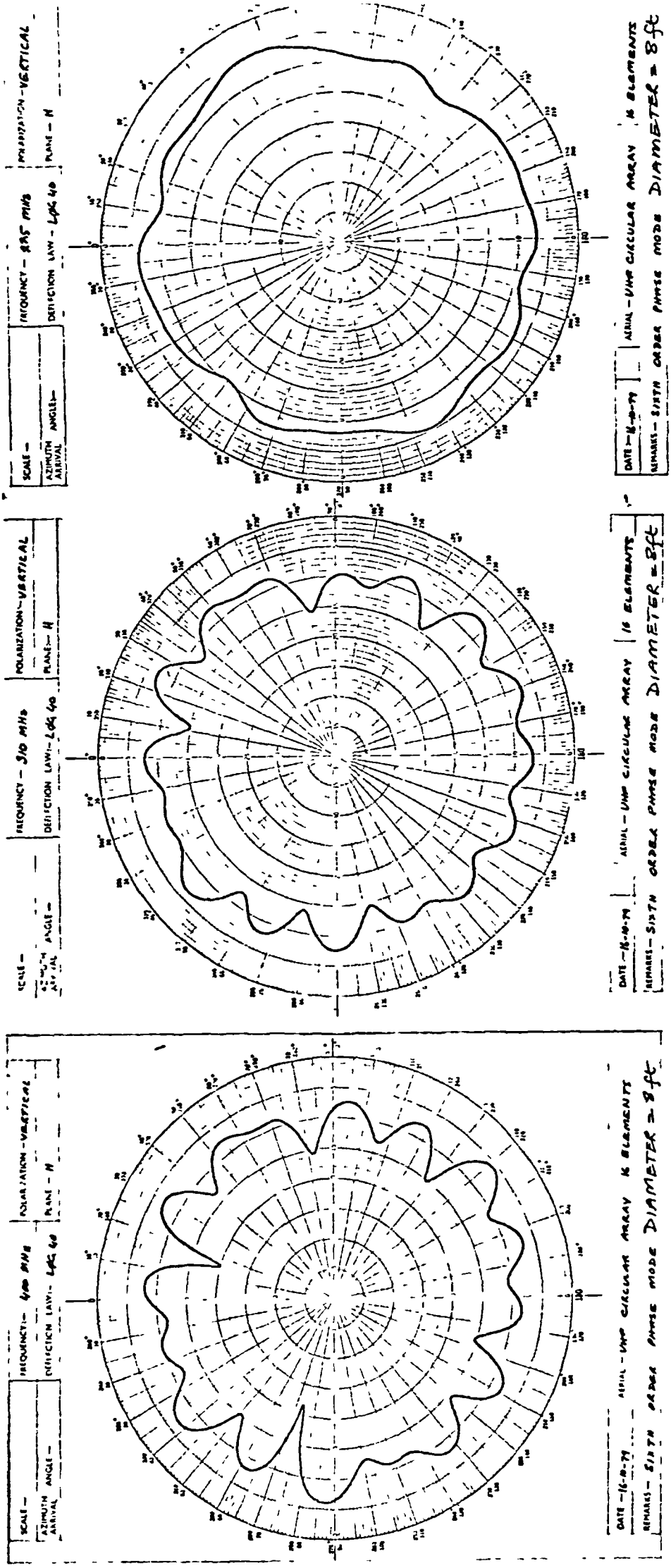

Figure 5.23 Measured sixth order phase mode of an 8ft diameter array

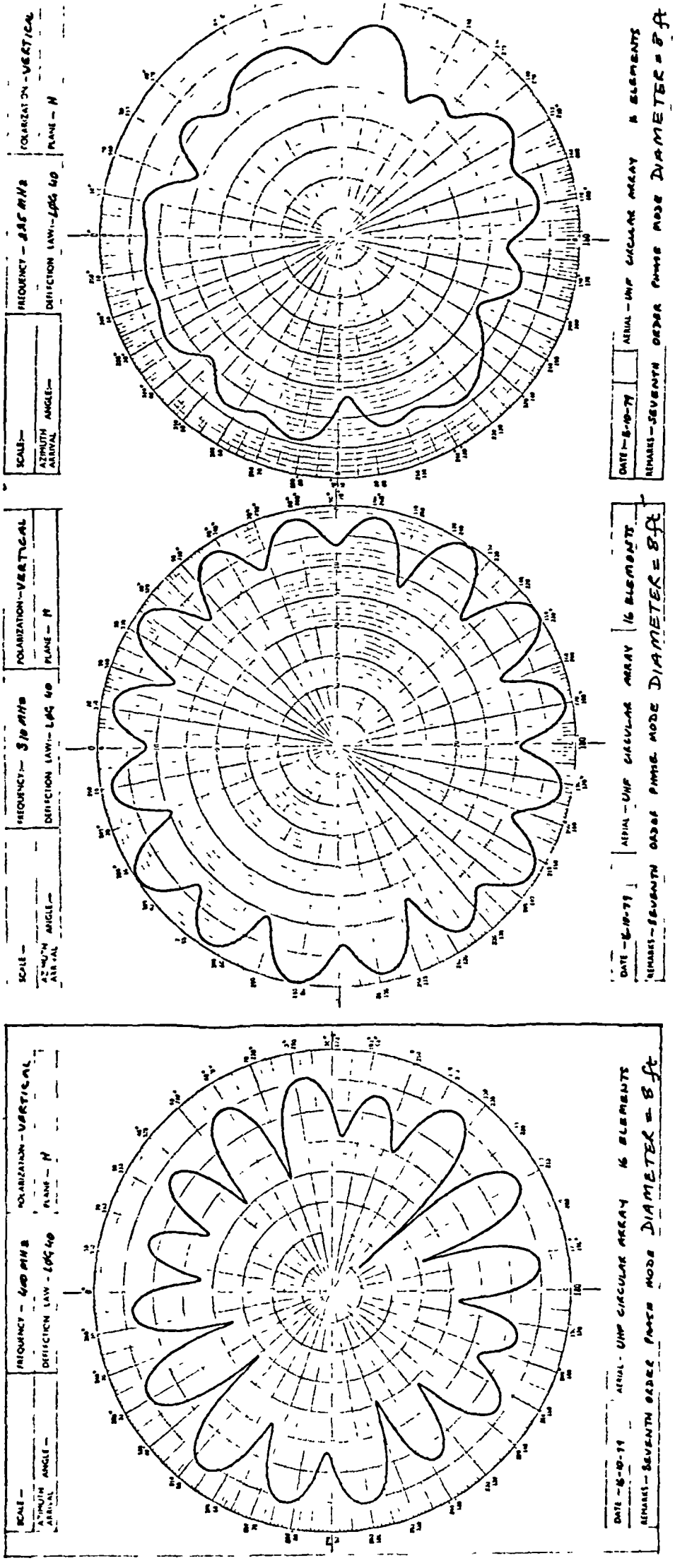

Figure 5.24 Measured seventh order phase mode of an 8ft diameter array

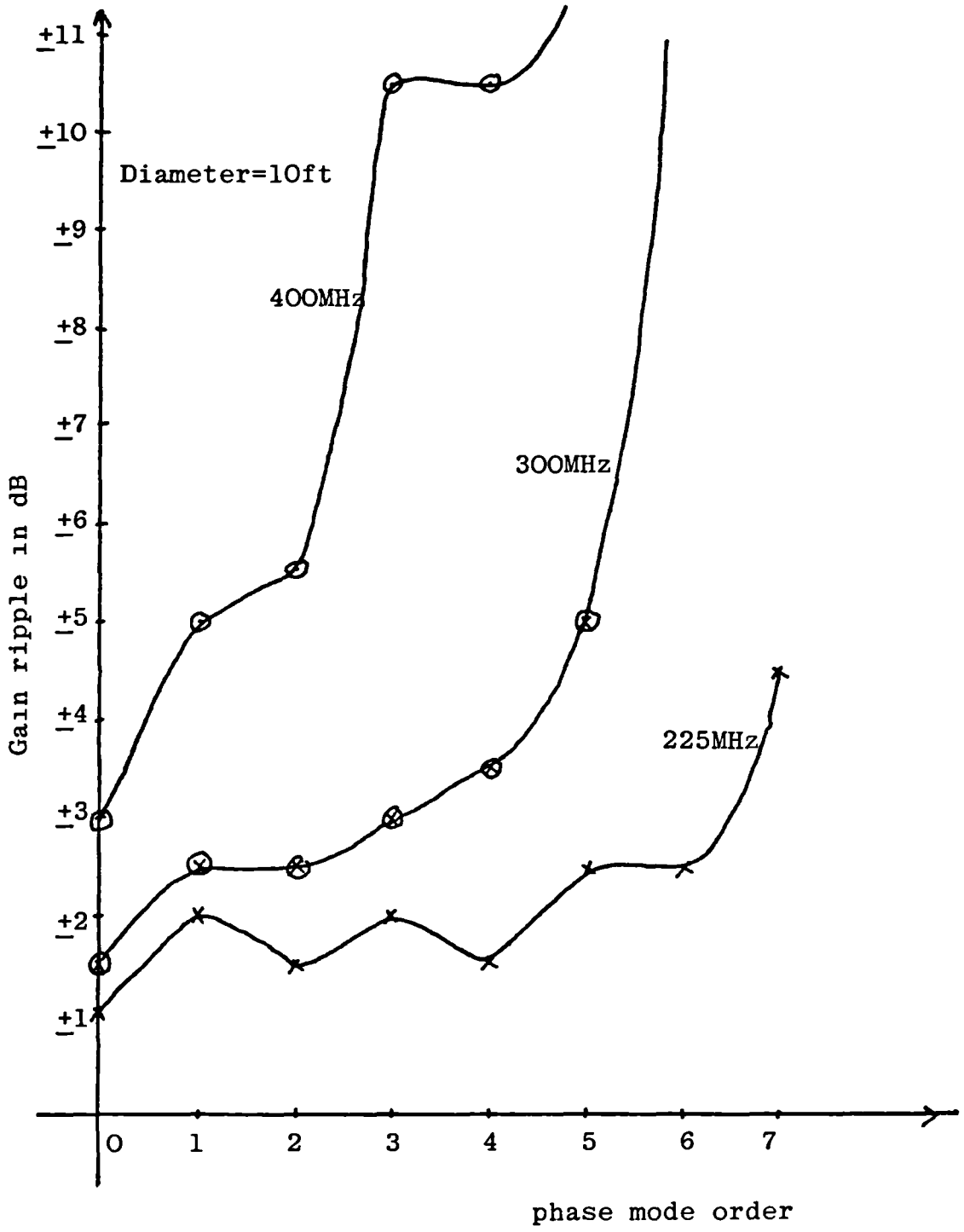

FIGURE 5·25

VARIATION OF GAIN RIPPLE WITH PHASE MODE ORDEI

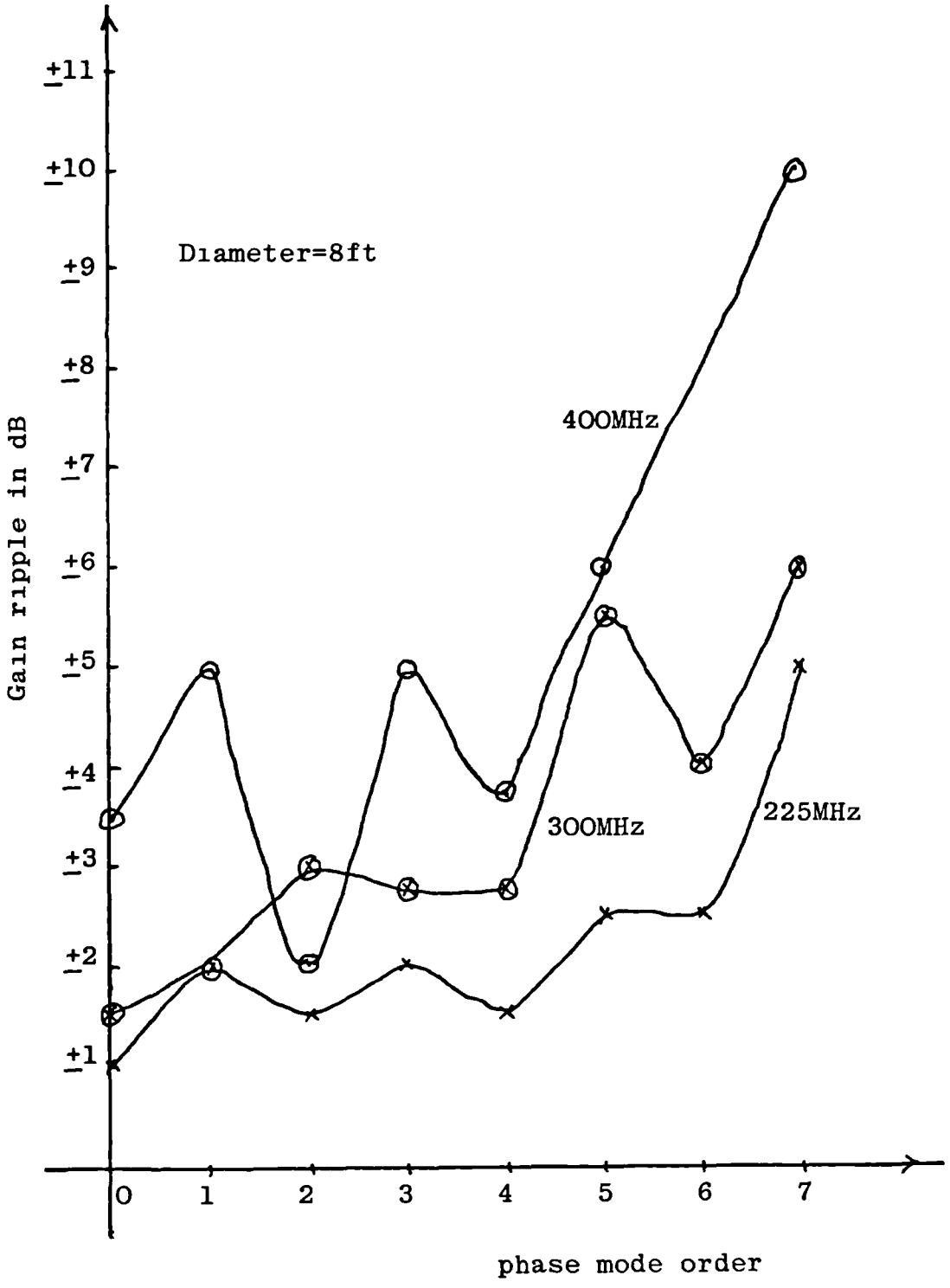

FIGURE 5.26

VARIATION OF GAIN RIPPLE WITH PHASE MODE ORDEI

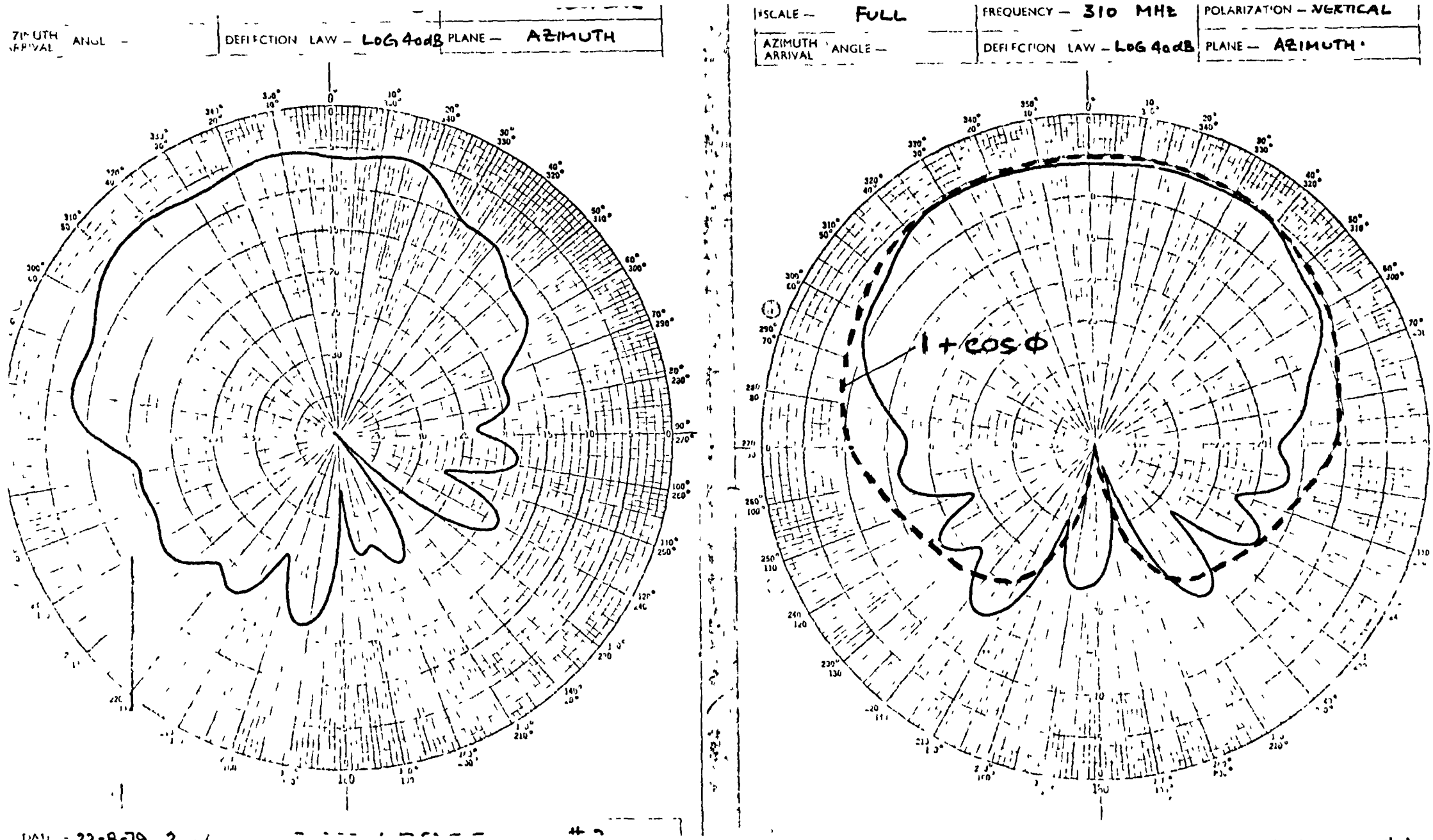

Figure 5.27 Measured pattern for elements No. 1 and 2 in array environment

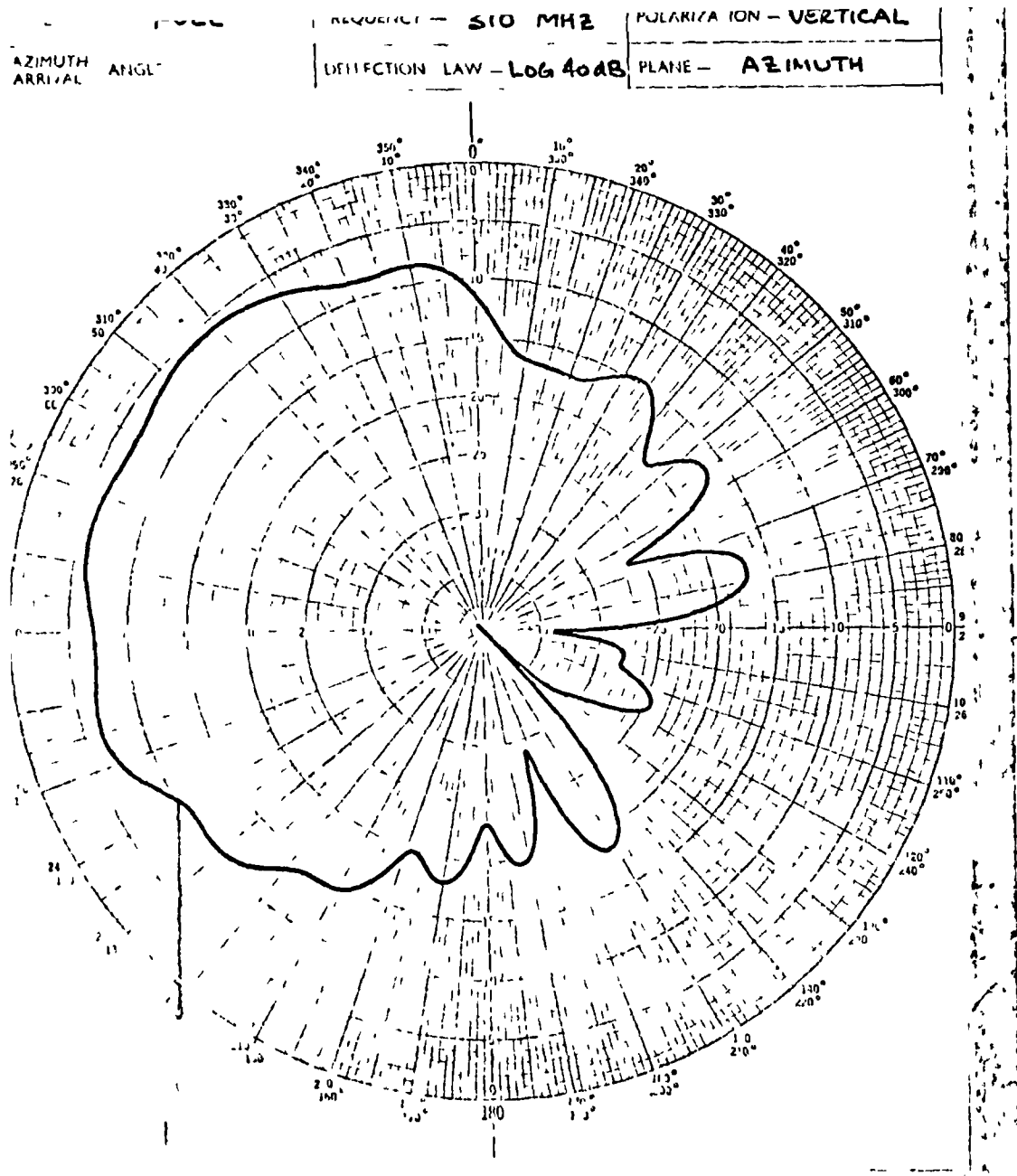

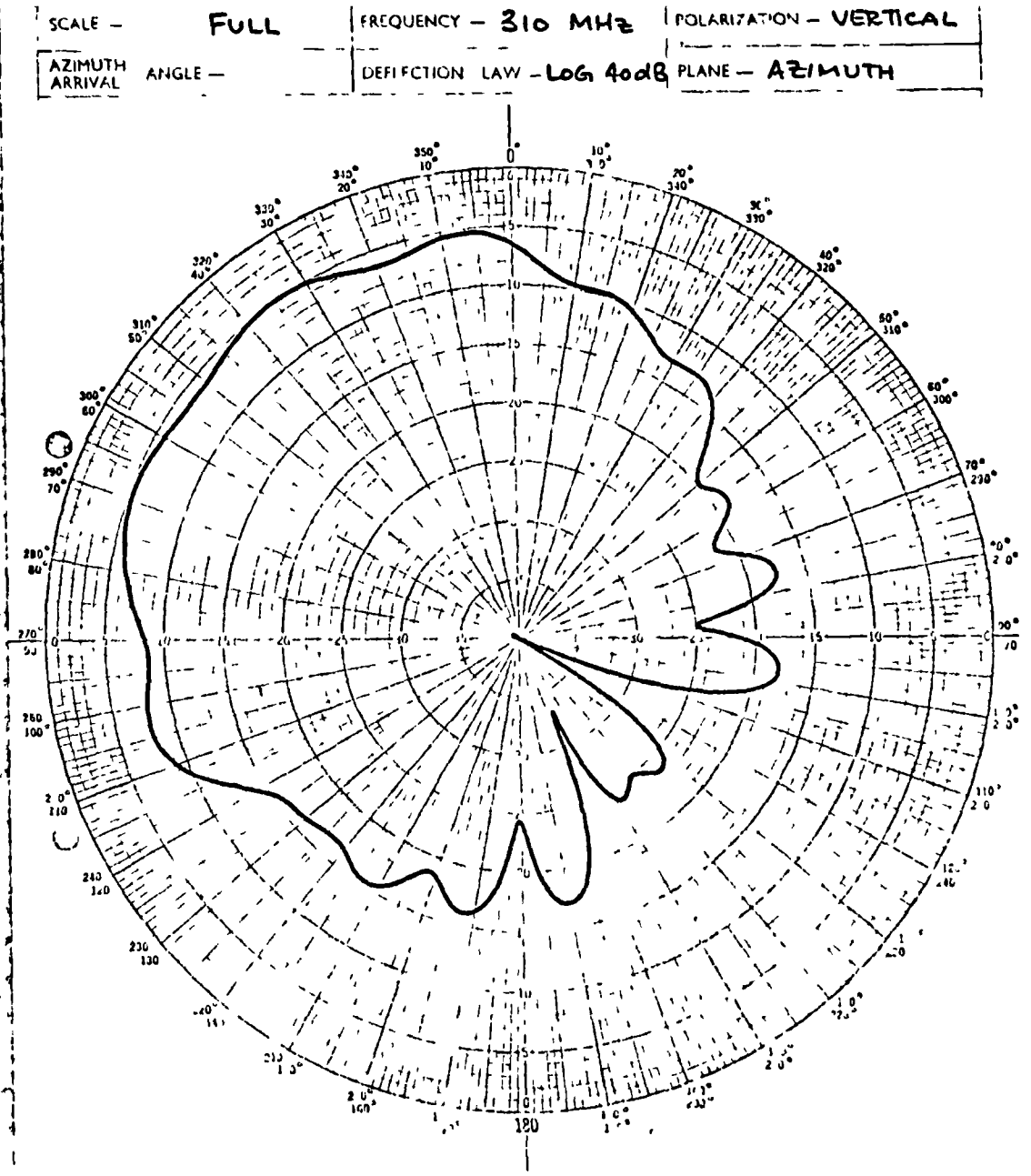

Figure 5.28 Measured pattern for elements No. 3 and 4 in array environment

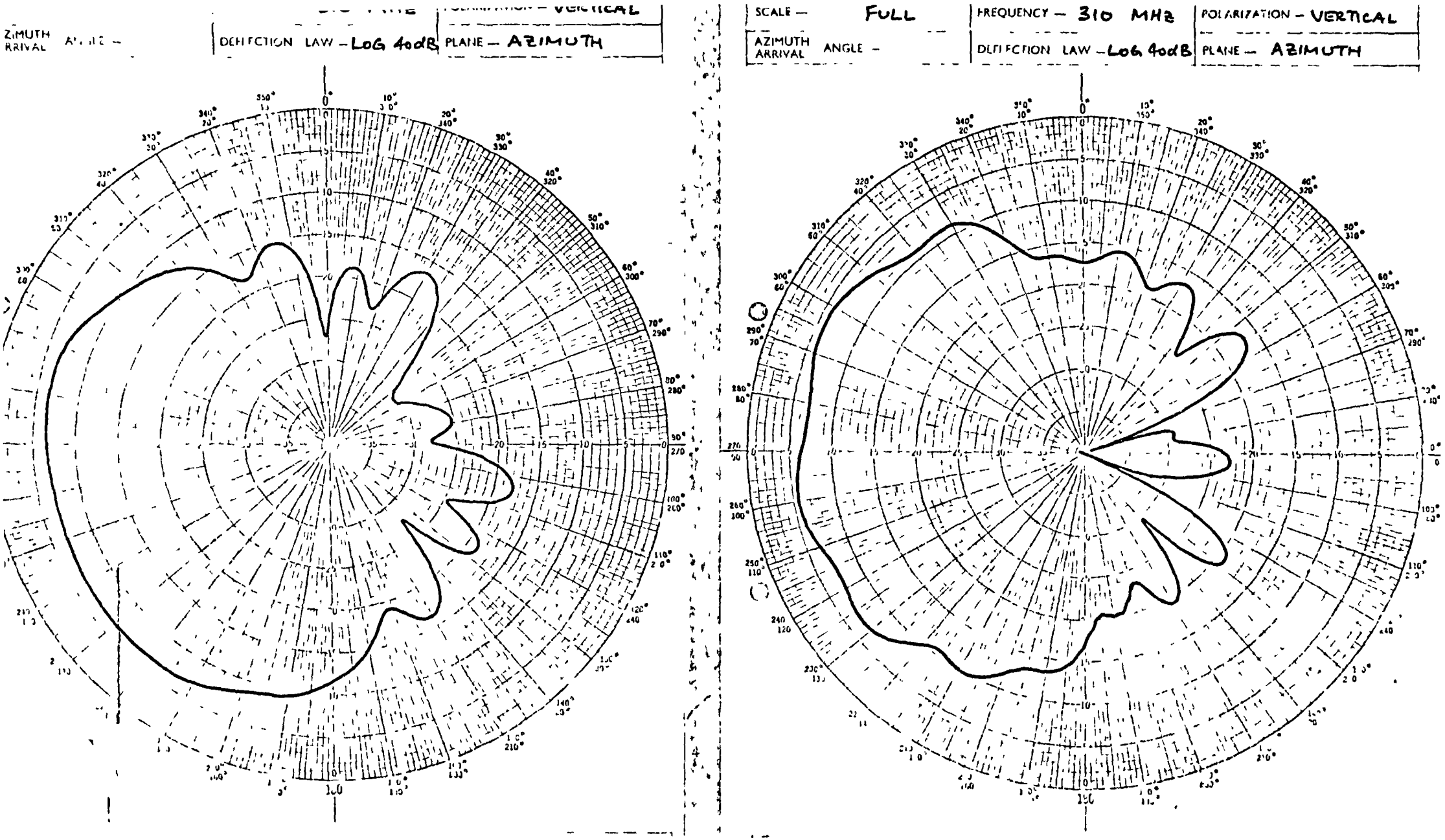

Figure 5.29 Measured pattern for elements No. 5 and 6 in array environment

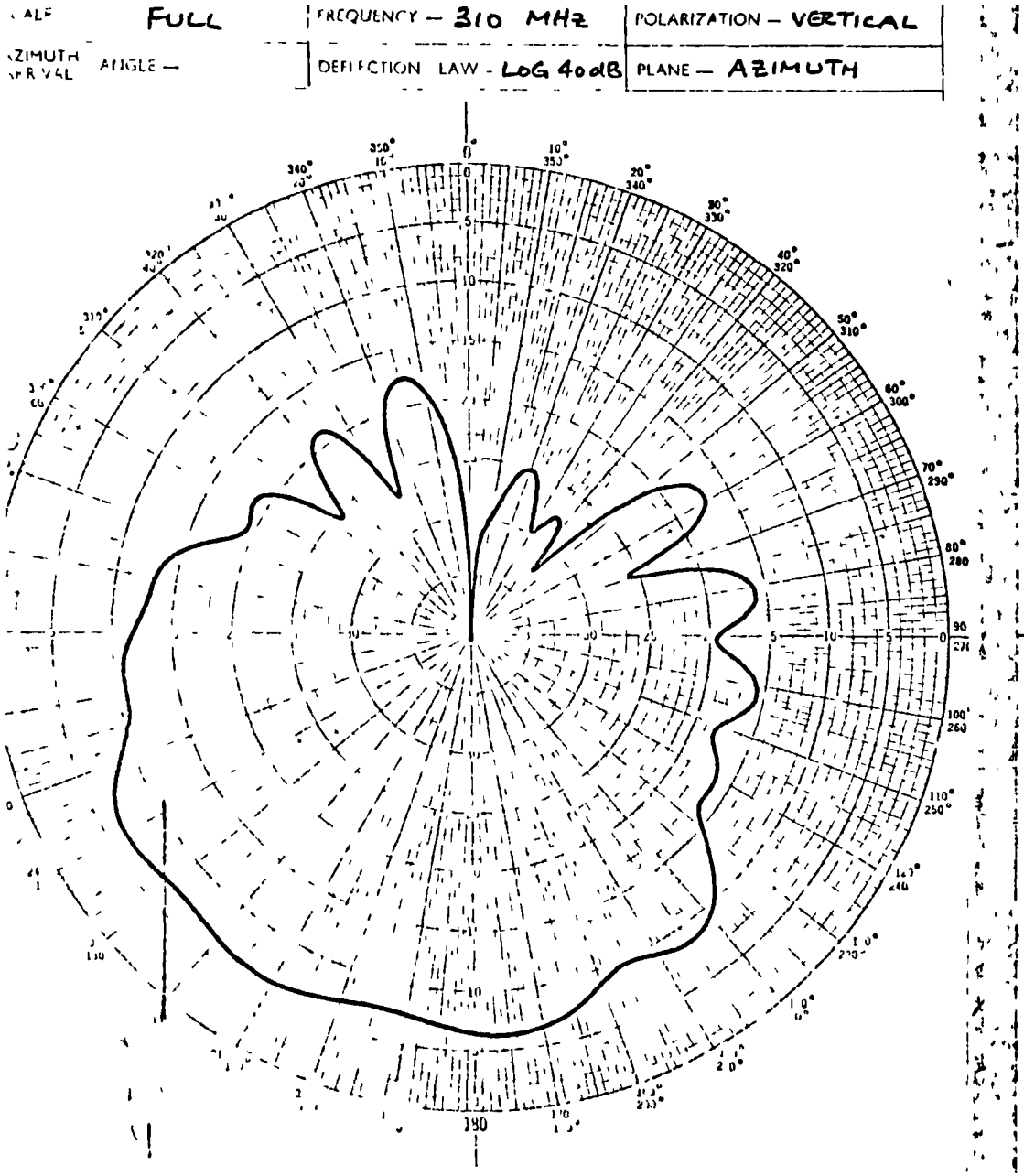

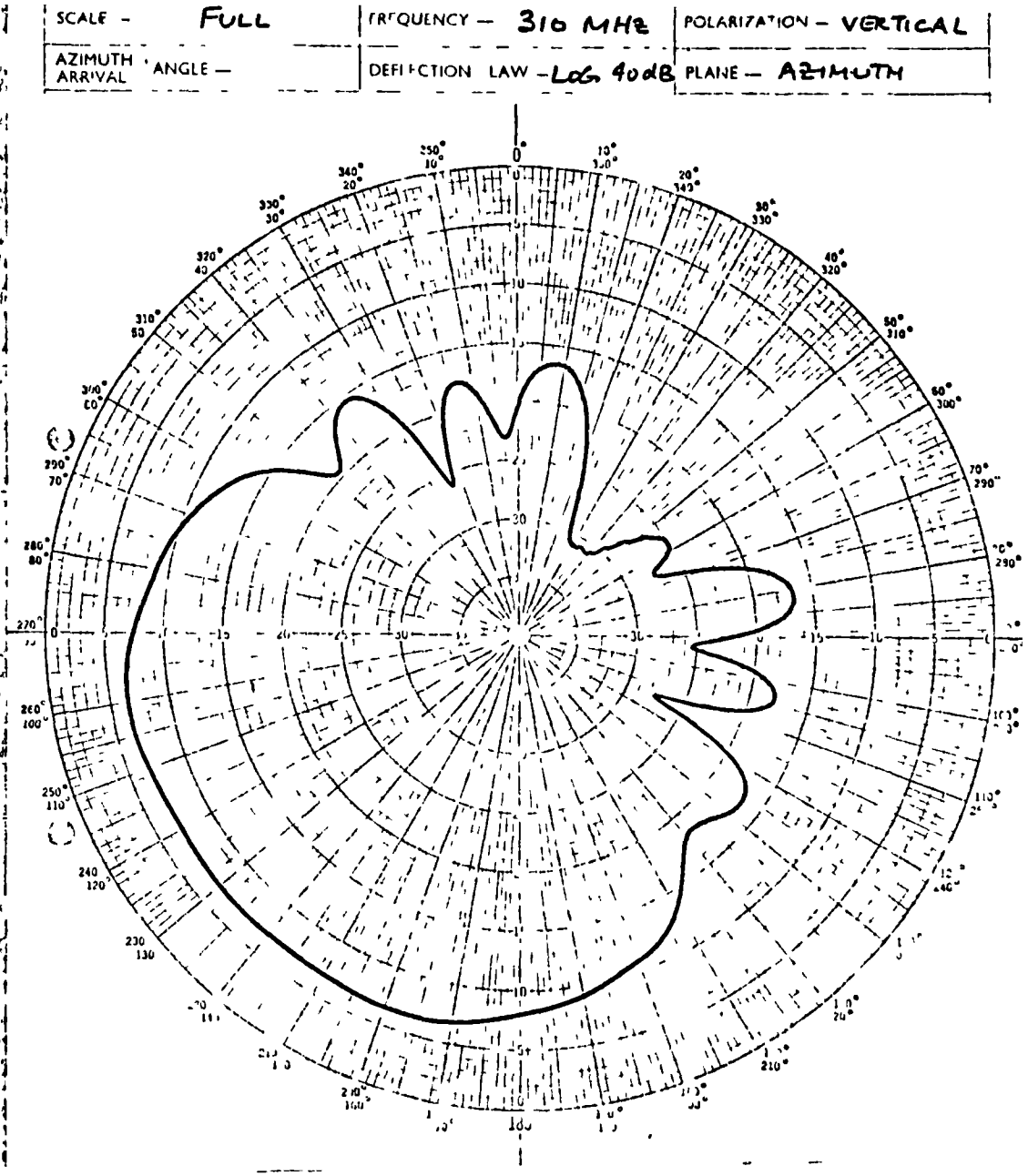

DATE 22-8-79 8

MEASURED IN

#7

IRONMENT

Figure 5.30 Measured pattern for elements No. 7 and 8 in array environment

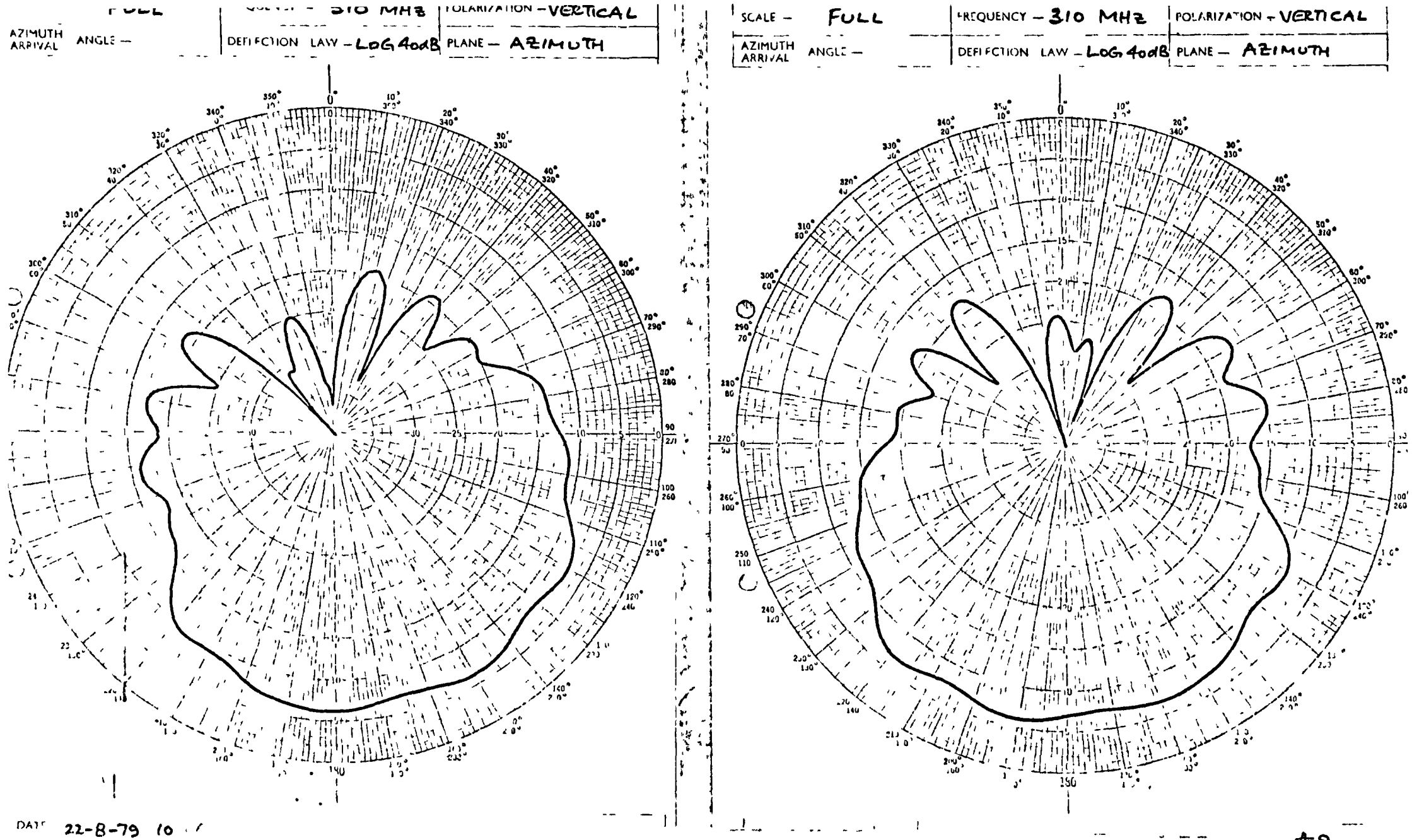

Figure 5.31 Measured pattern for elements No. 9 and 10 in array environment

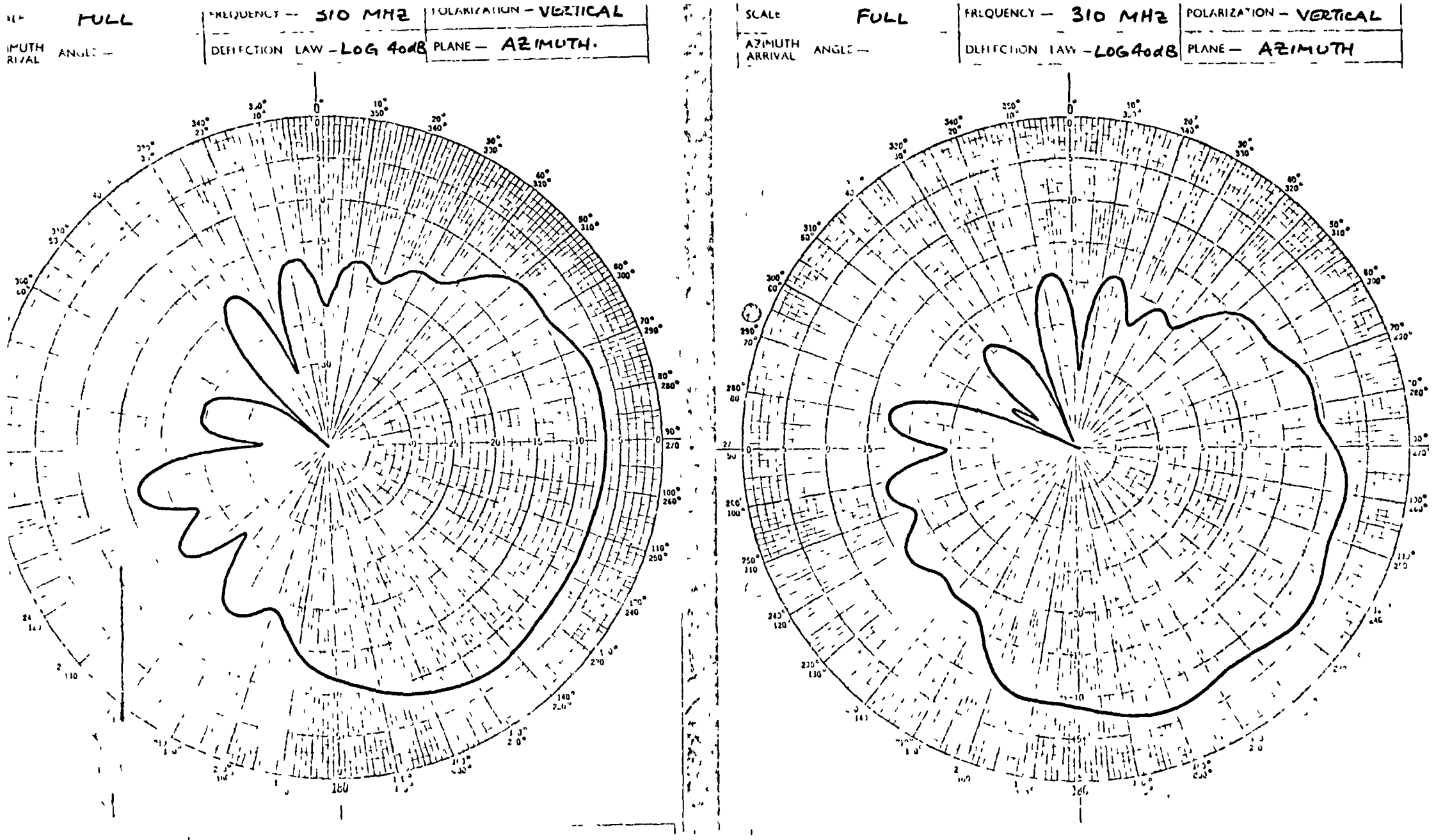

Figure 5.32 Measured pattern for elements No. 11 and 12 in array environment

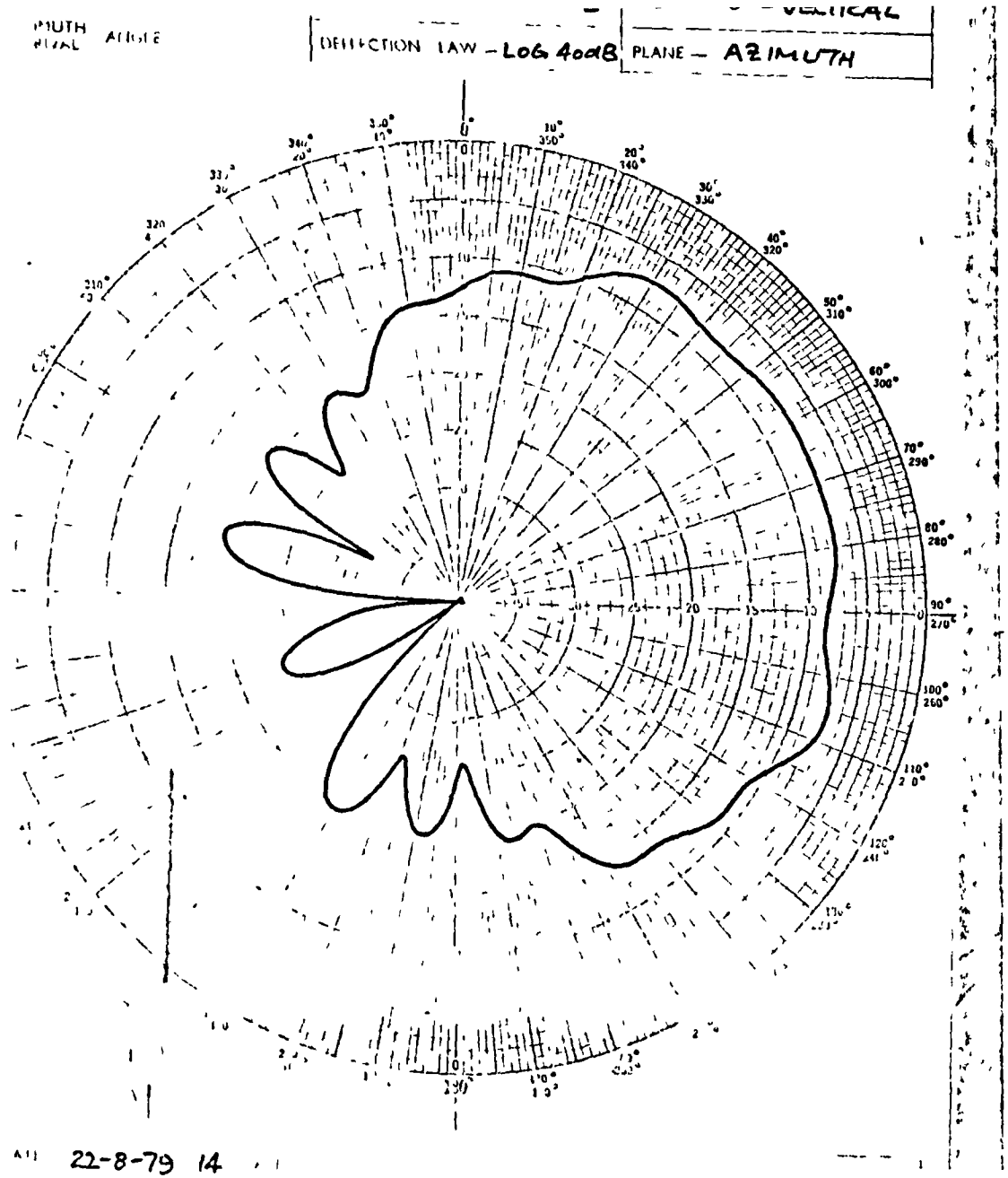

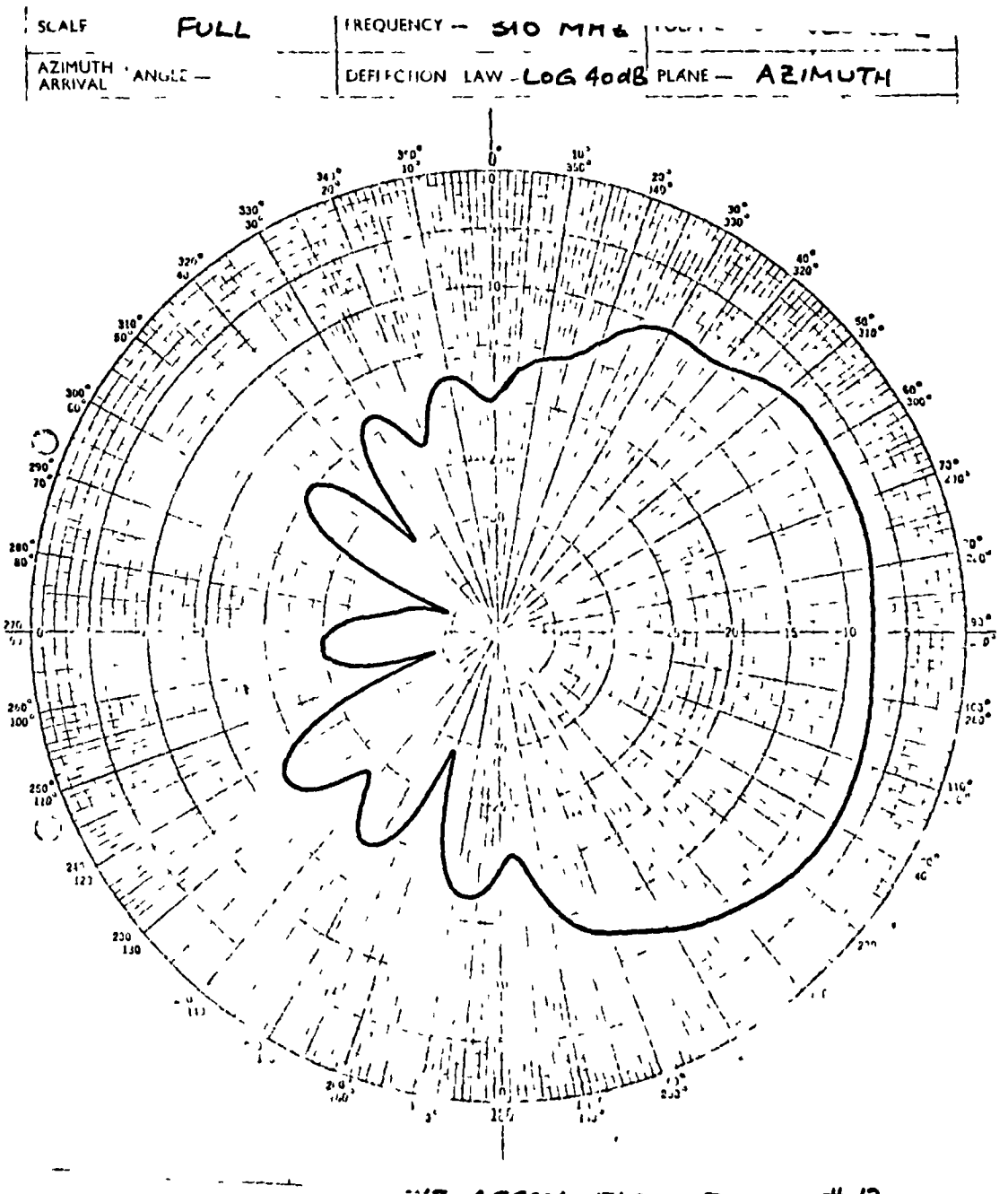

Figure 5.33 Measured pattern for elements No. 13 and 14 in array environment

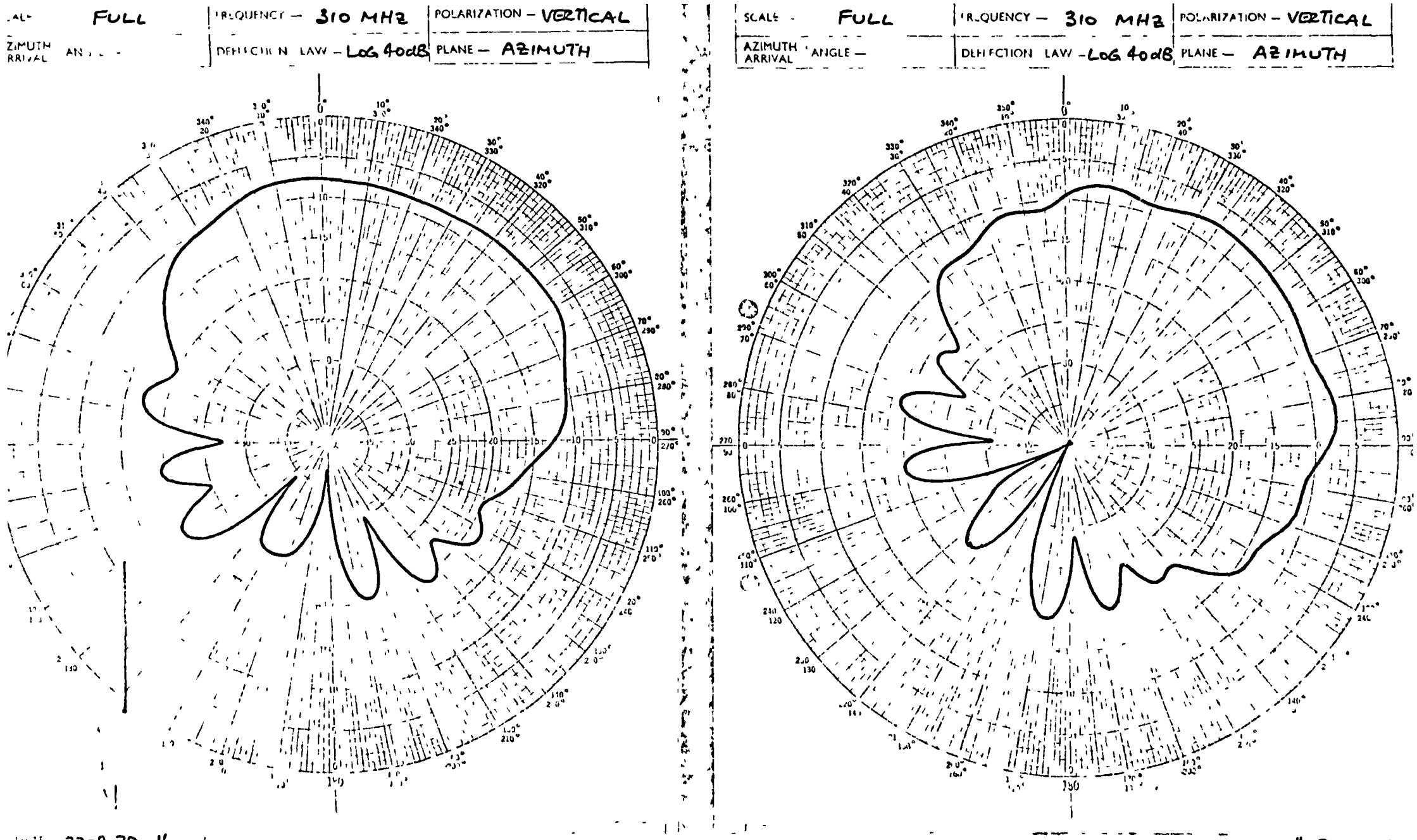

Figure 5.34 Measured patterns for elements No. 15 and 16 in array environment

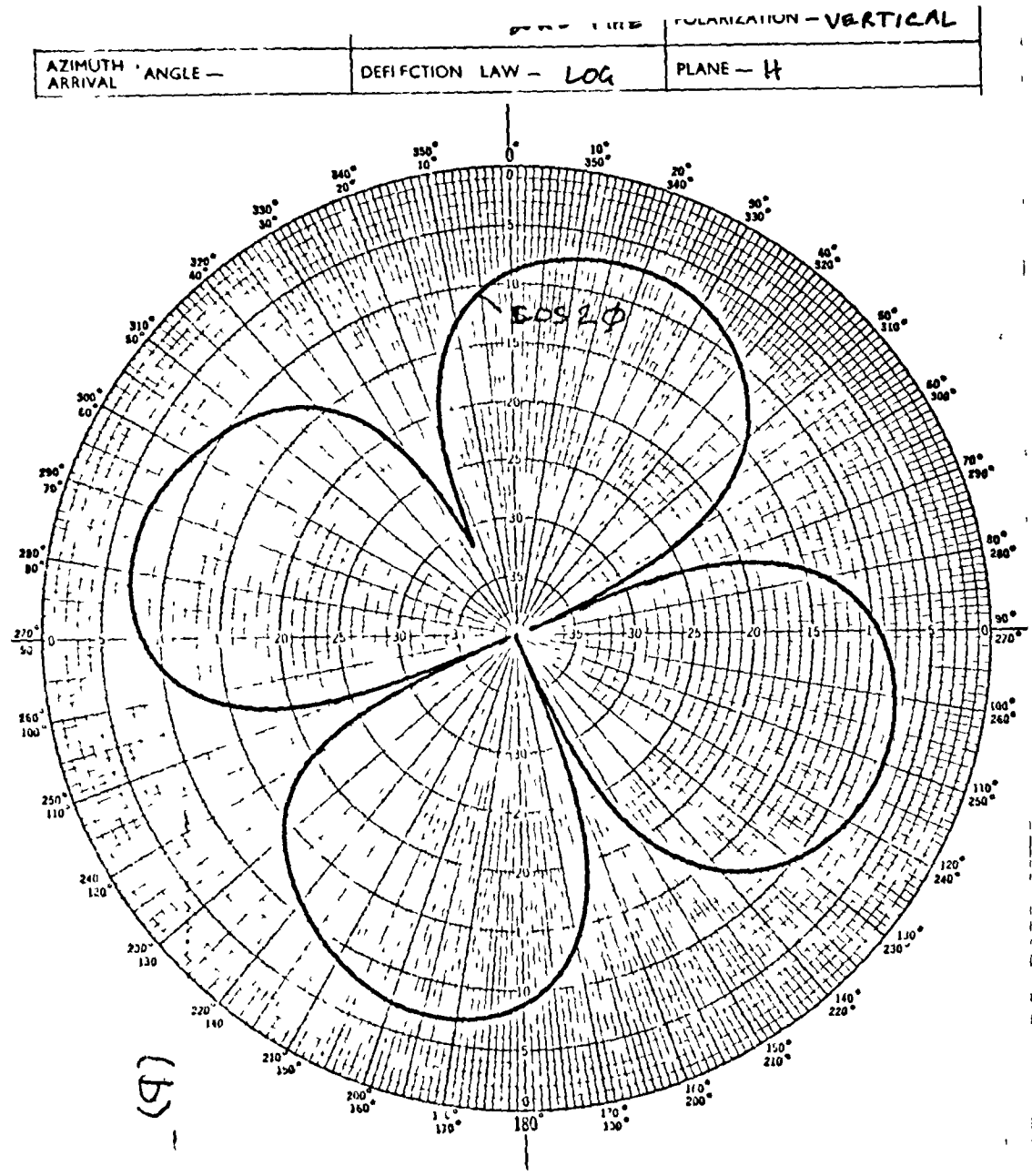

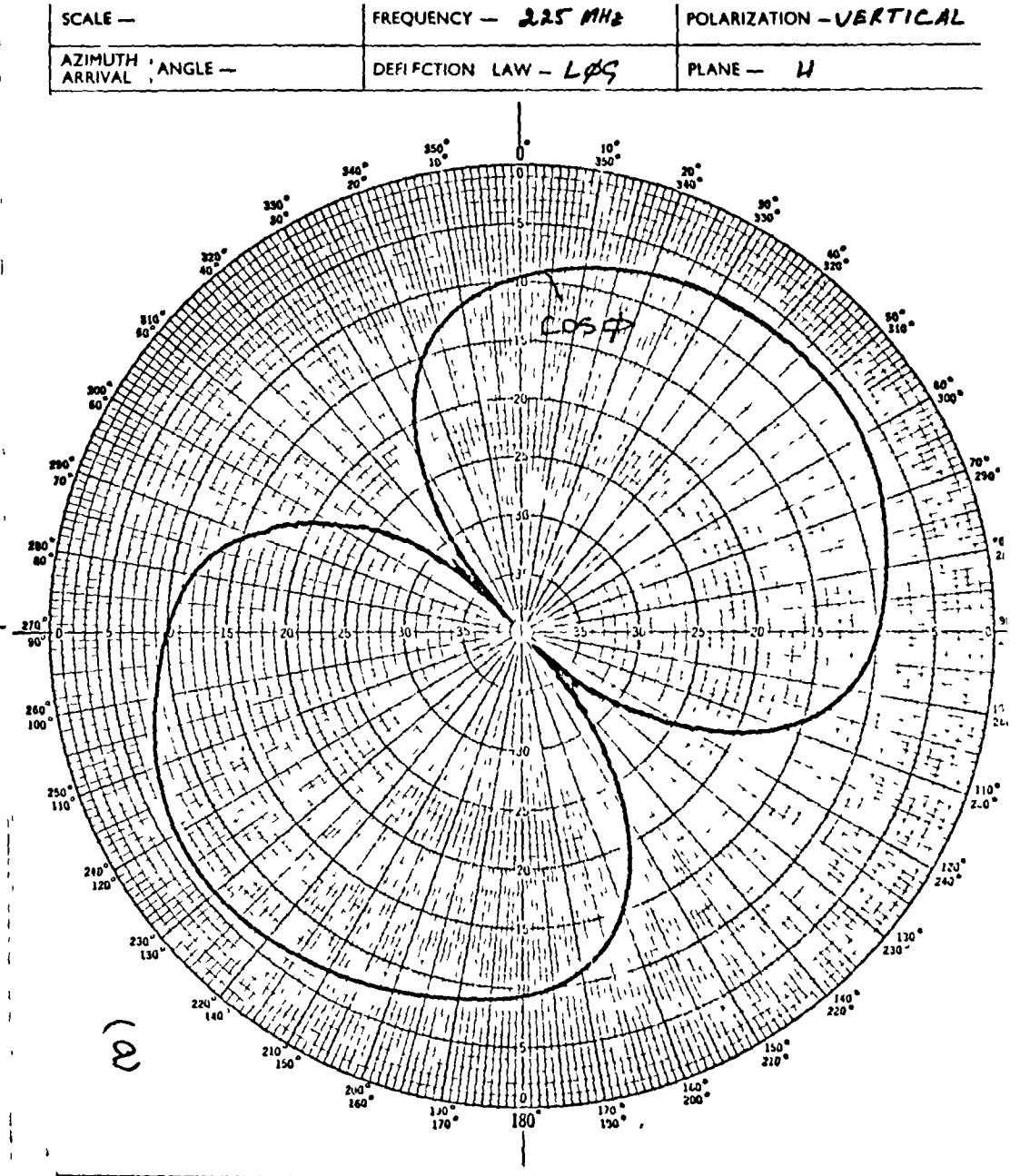

Figure 5.35 Measured first and second amplitude mode

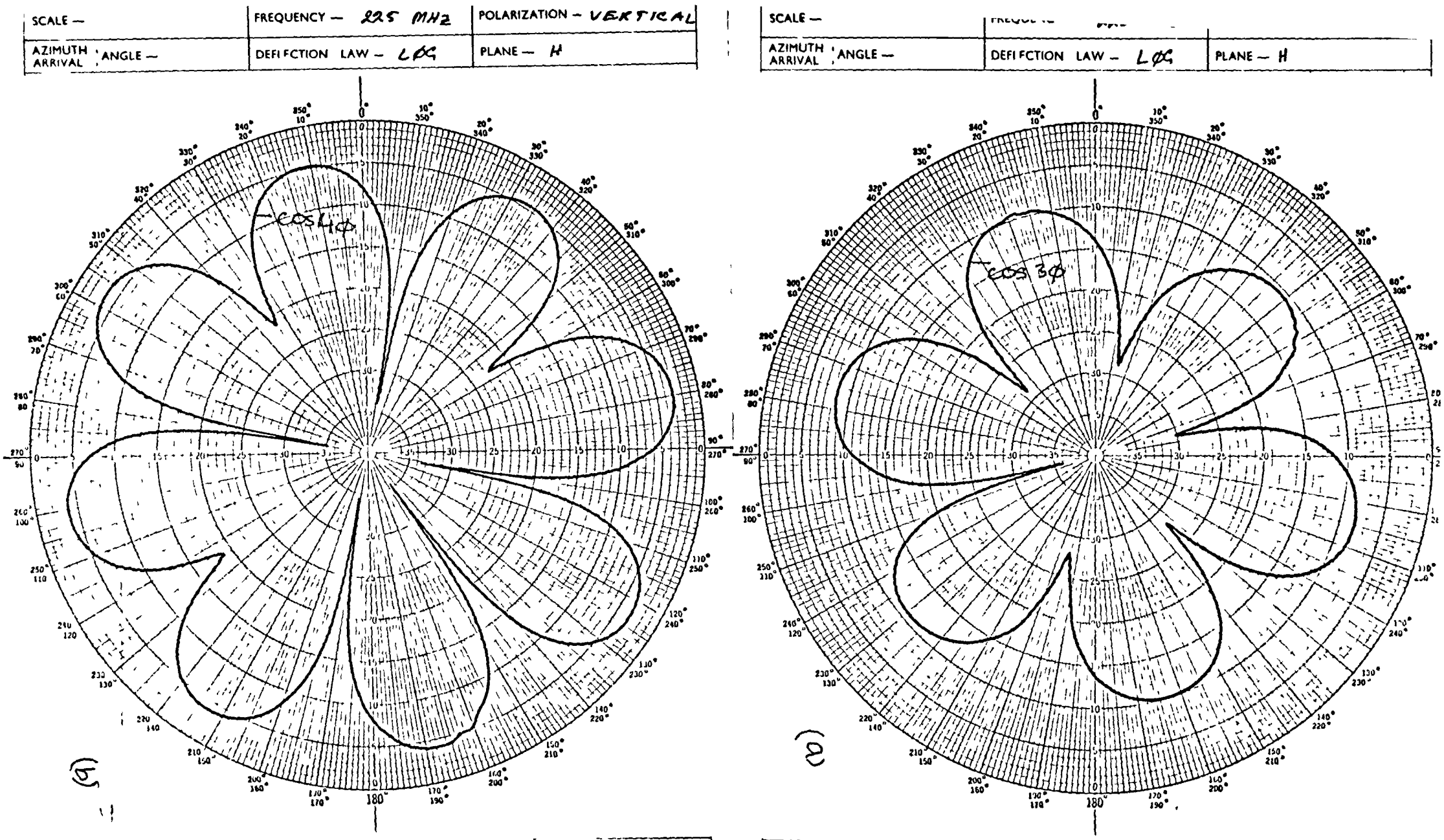

Figure 5.36 Measured third and fourth amplitude mode

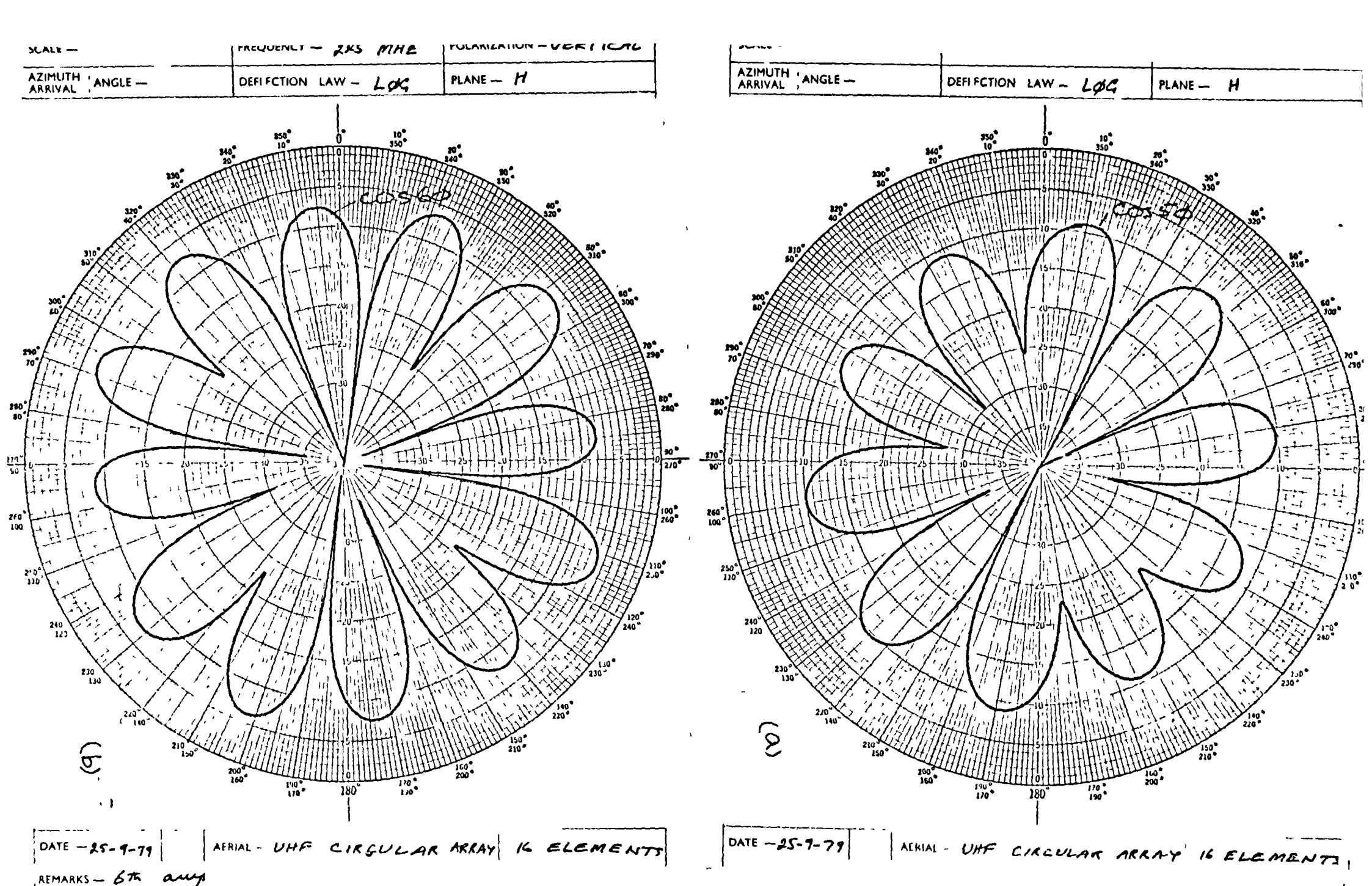

Figure 5.37 Measured fifth and sixth amplitude mode

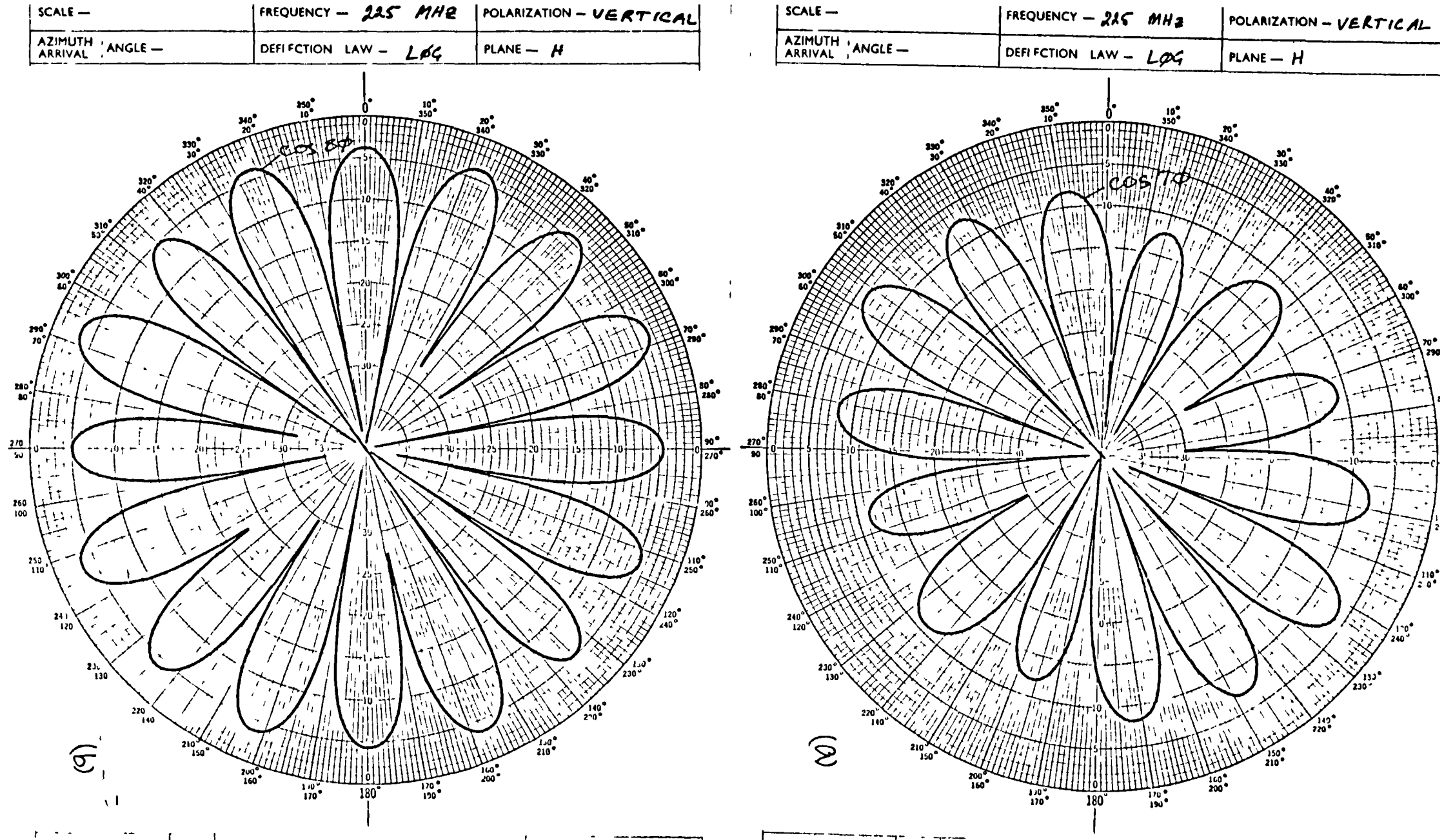

Figure 5.38 Measured seventh and eighth amplitude mode

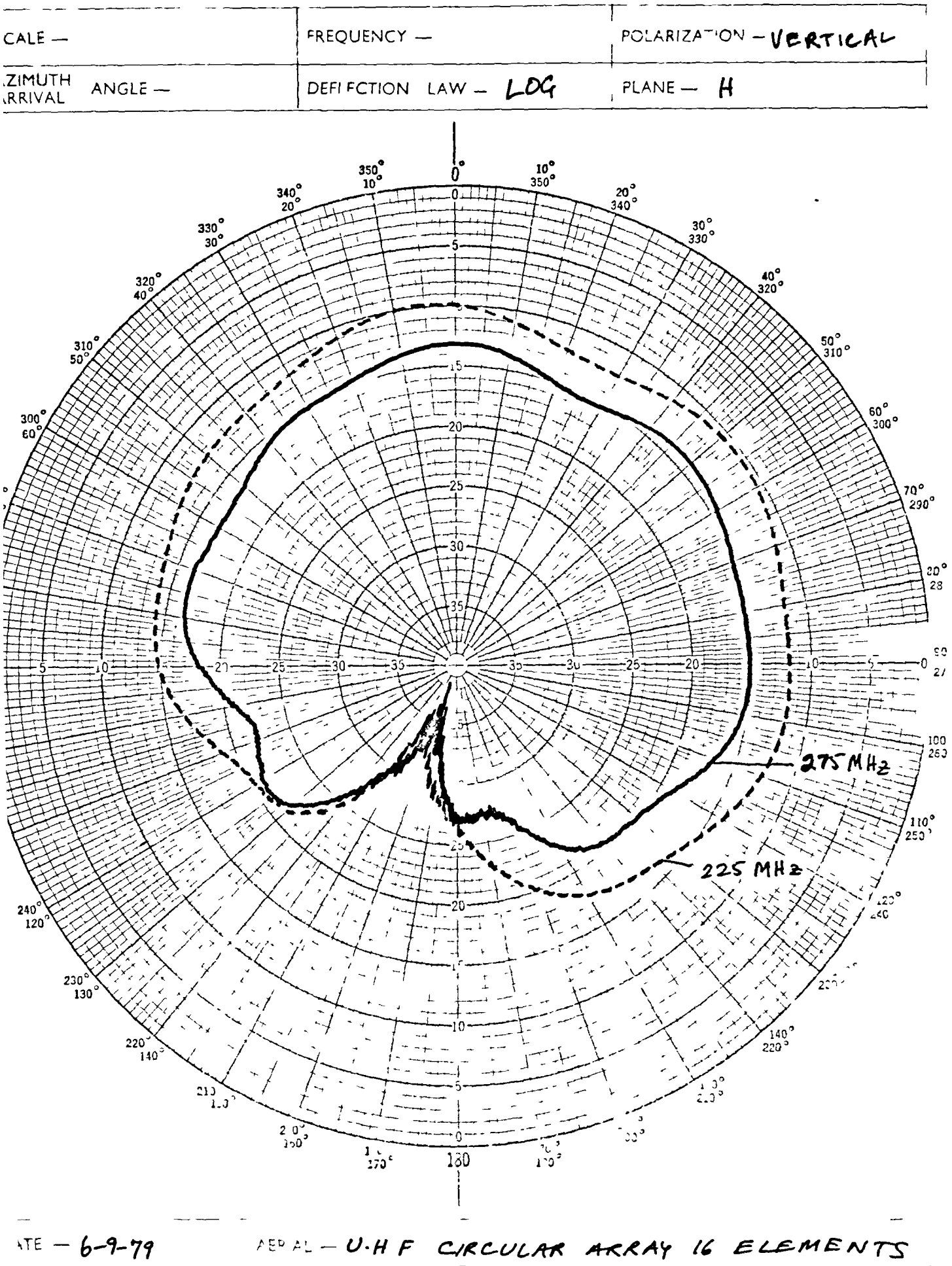

Figure 5.39 Measurement of the combination of zeroth and first order phase modes at 225MHz and 275 MHz for a 10ft diameter array

Figure 5.40

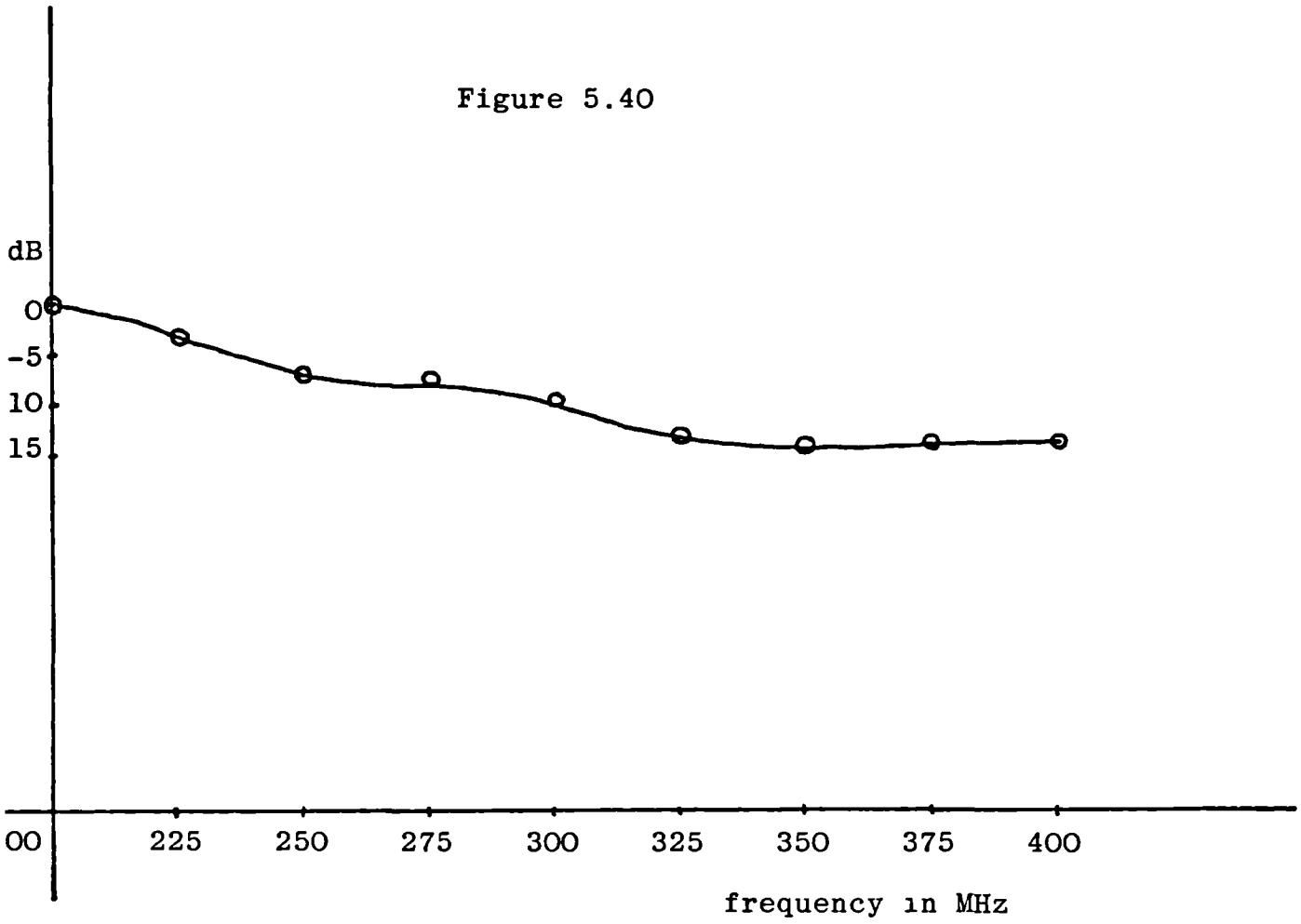

VARIATION OF ZEROTH ORDER MODE GAIN WITH FREQUENCY

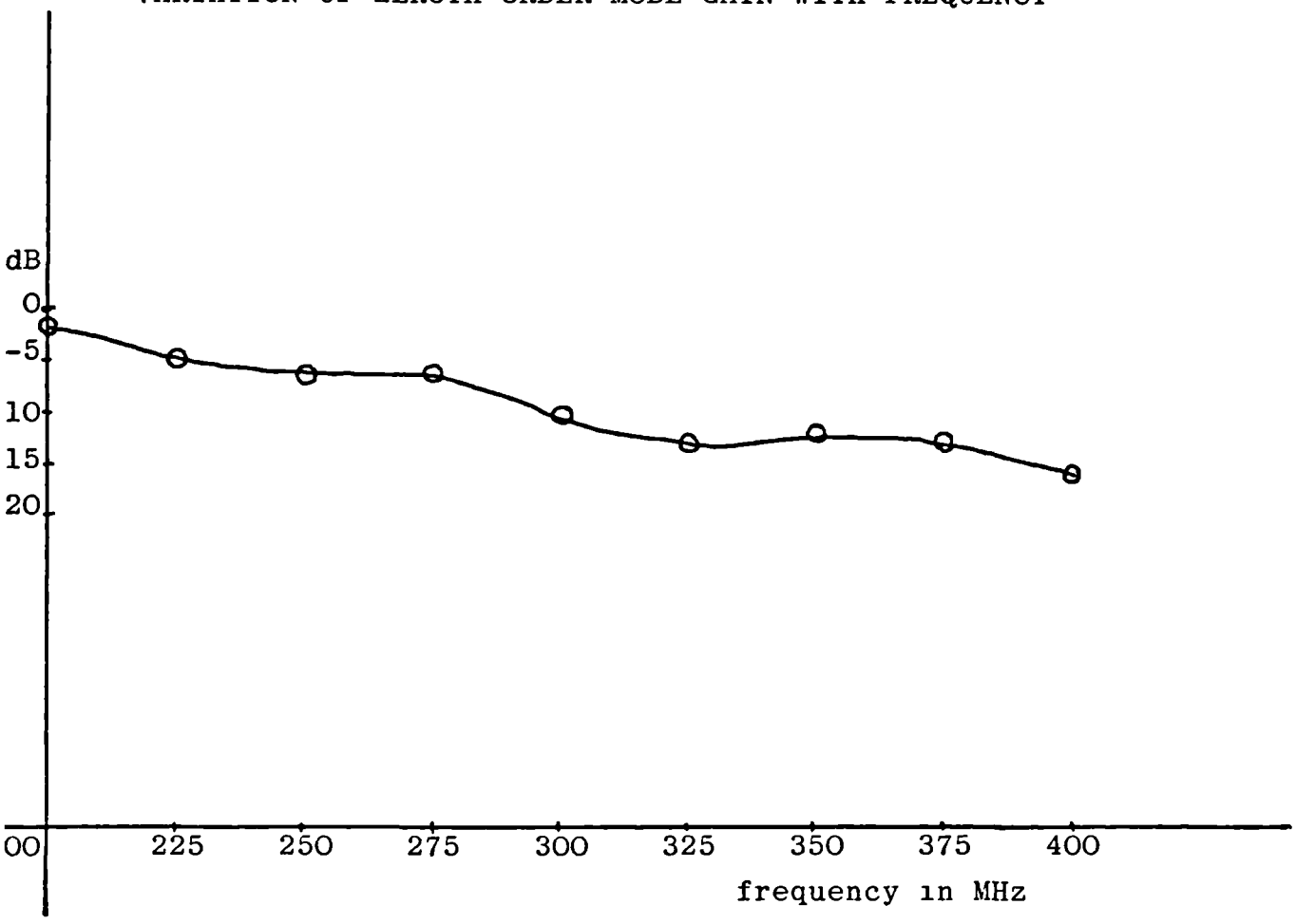

VARIATION OF FIRST ORDER MODE GAIN WITH FREQUENCY

Figure 5.41

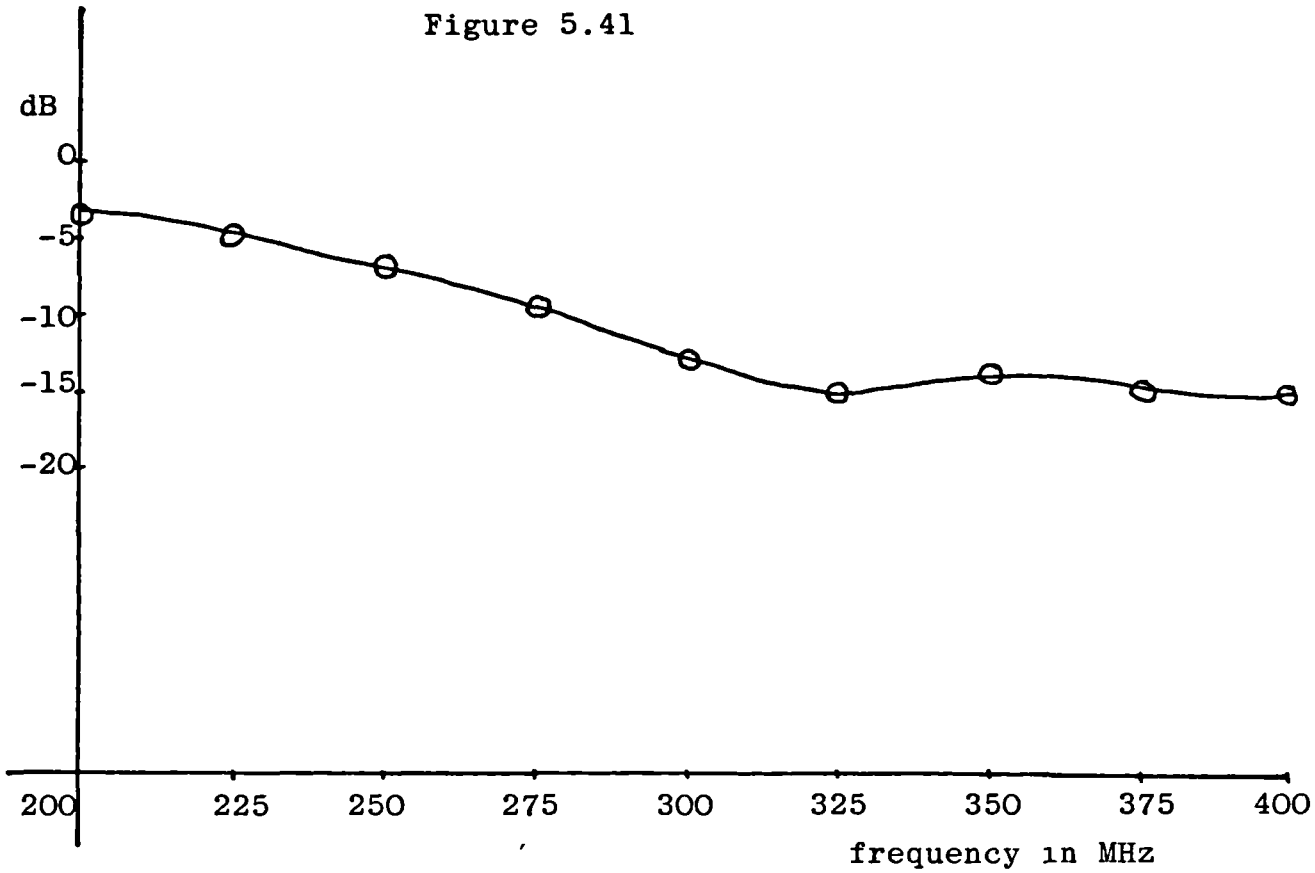

VARIATION OF SECOND ORDER MODE GAIN WITH FREQUENCY

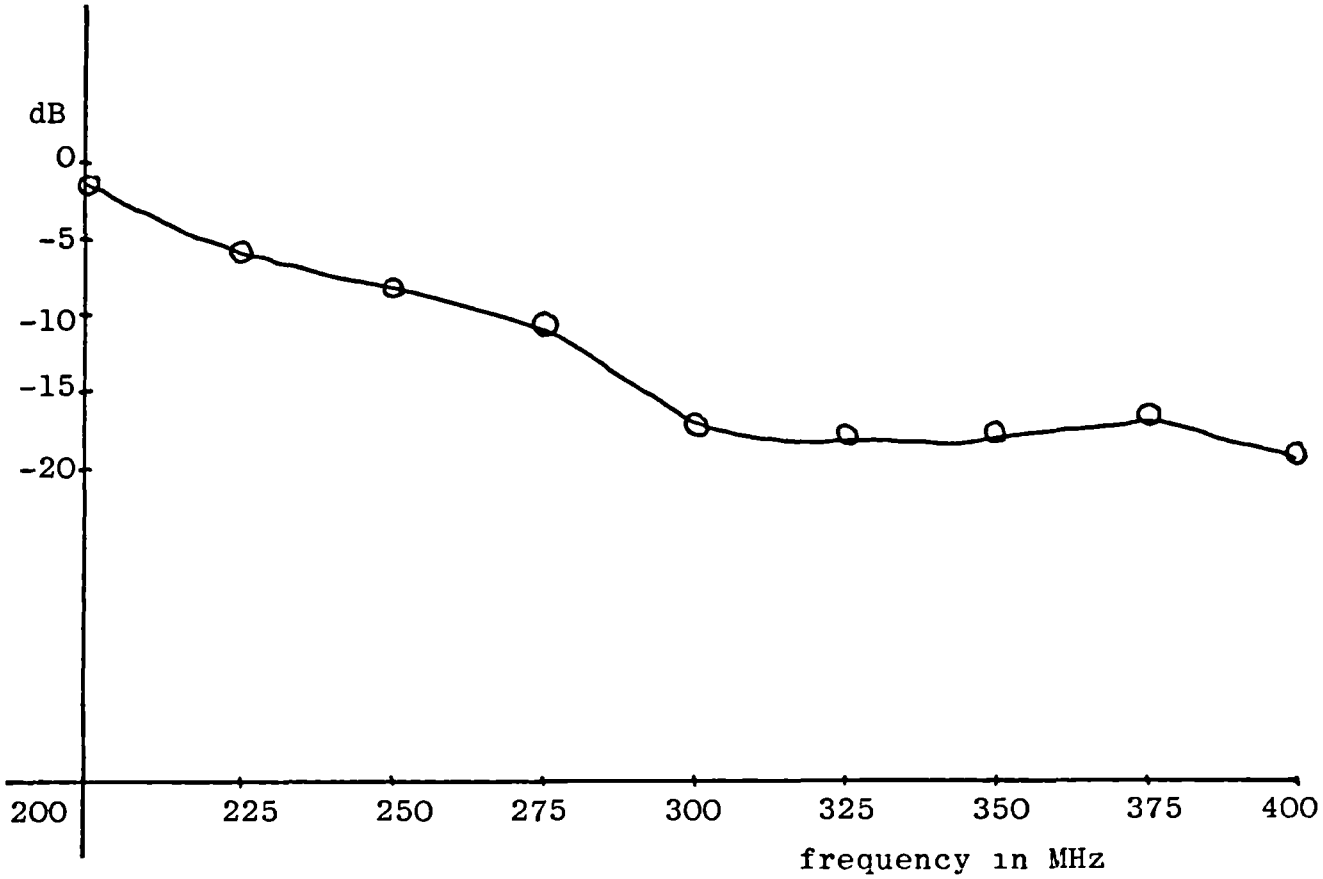

VARIATION OF THIRD ORDER MODE GAIN WITH FREQUENCY

Figure 5.42

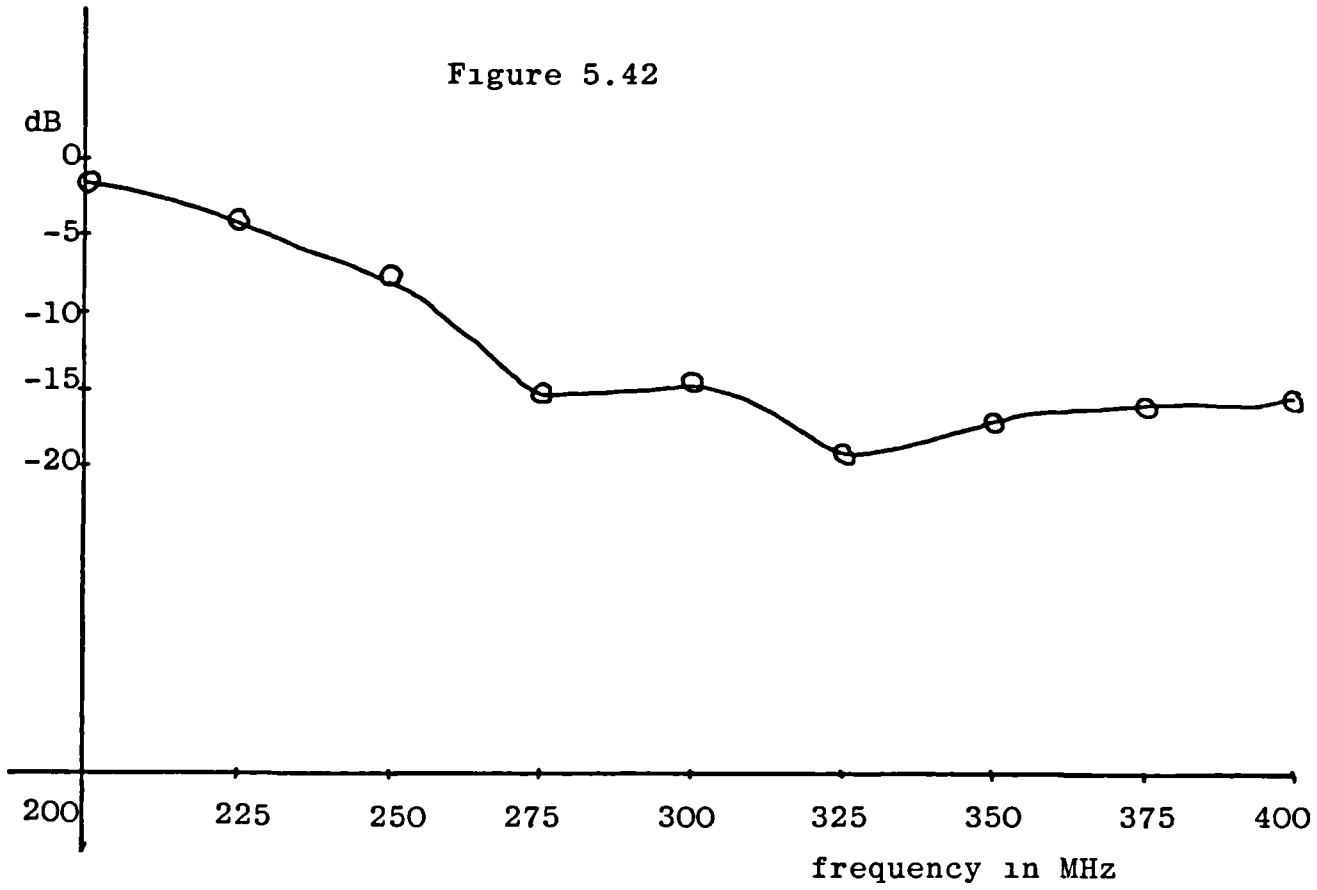

VARIATION OF FOURTH ORDER MODE GAIN WITH FREQUENCY

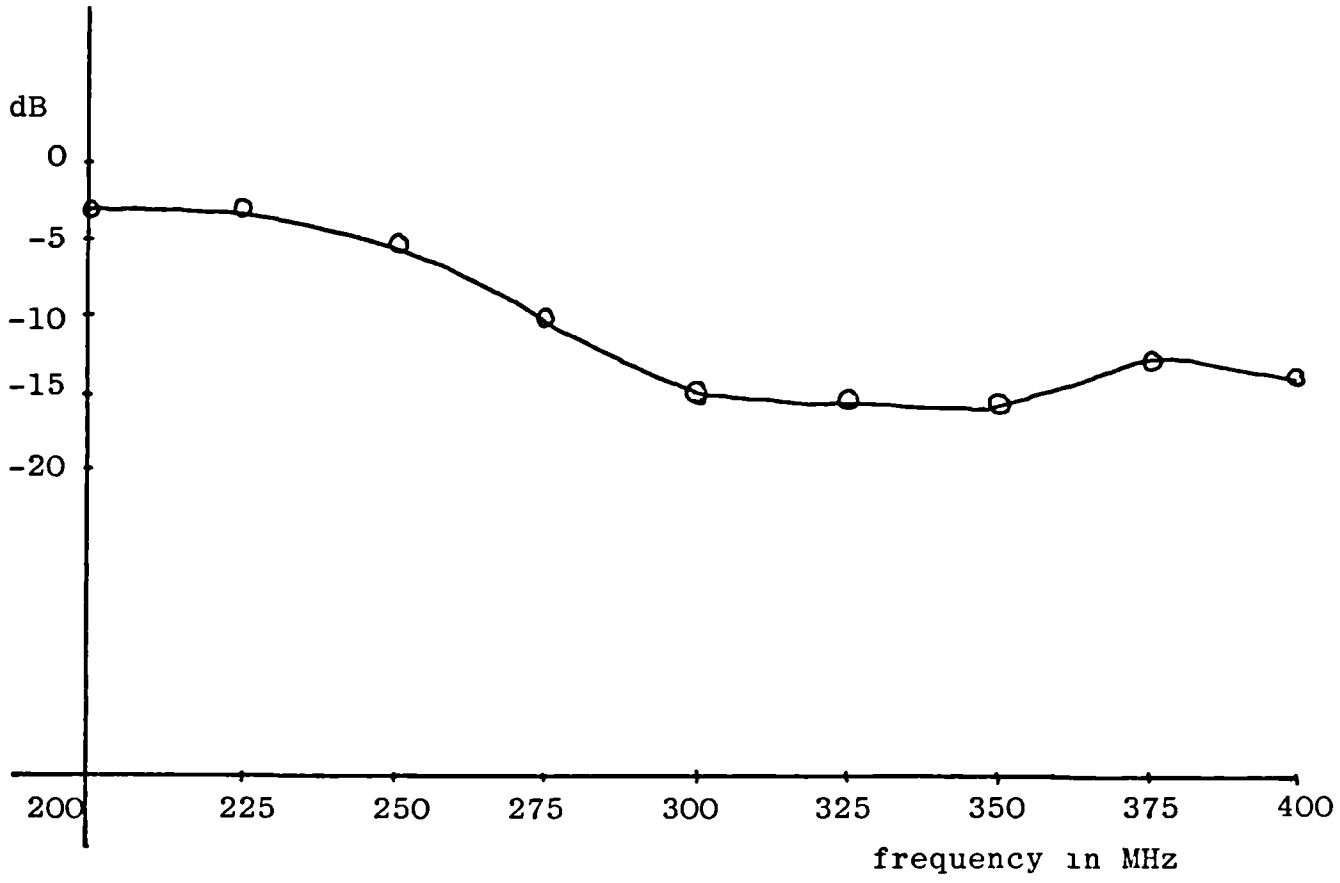

VARIATION OF FIFTH ORDER MODE GAIN WITH FREQUENCY

Figure 5.43

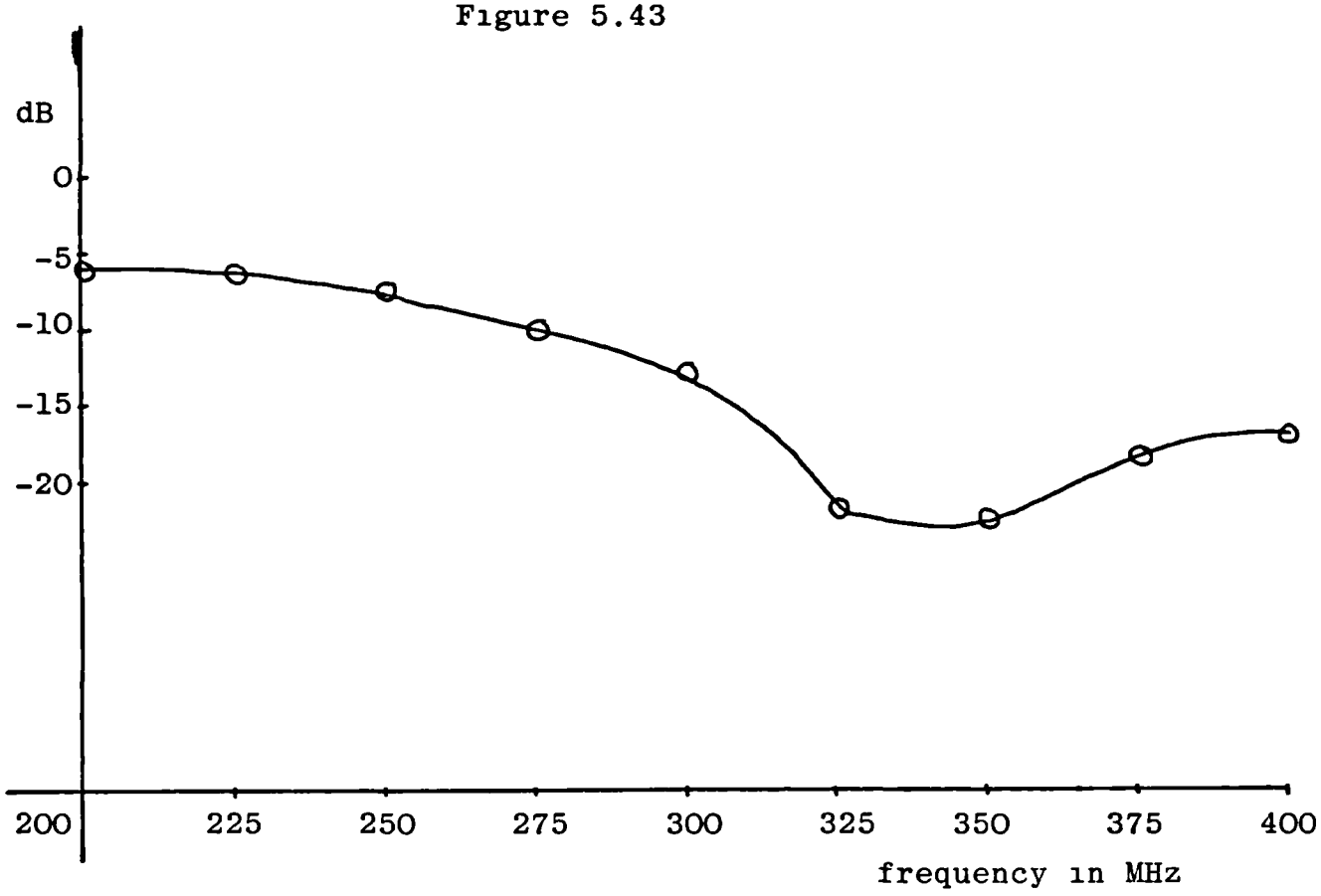

VARIATION OF SIXTH ORDER MODE GAIN WITH FREQUENCY

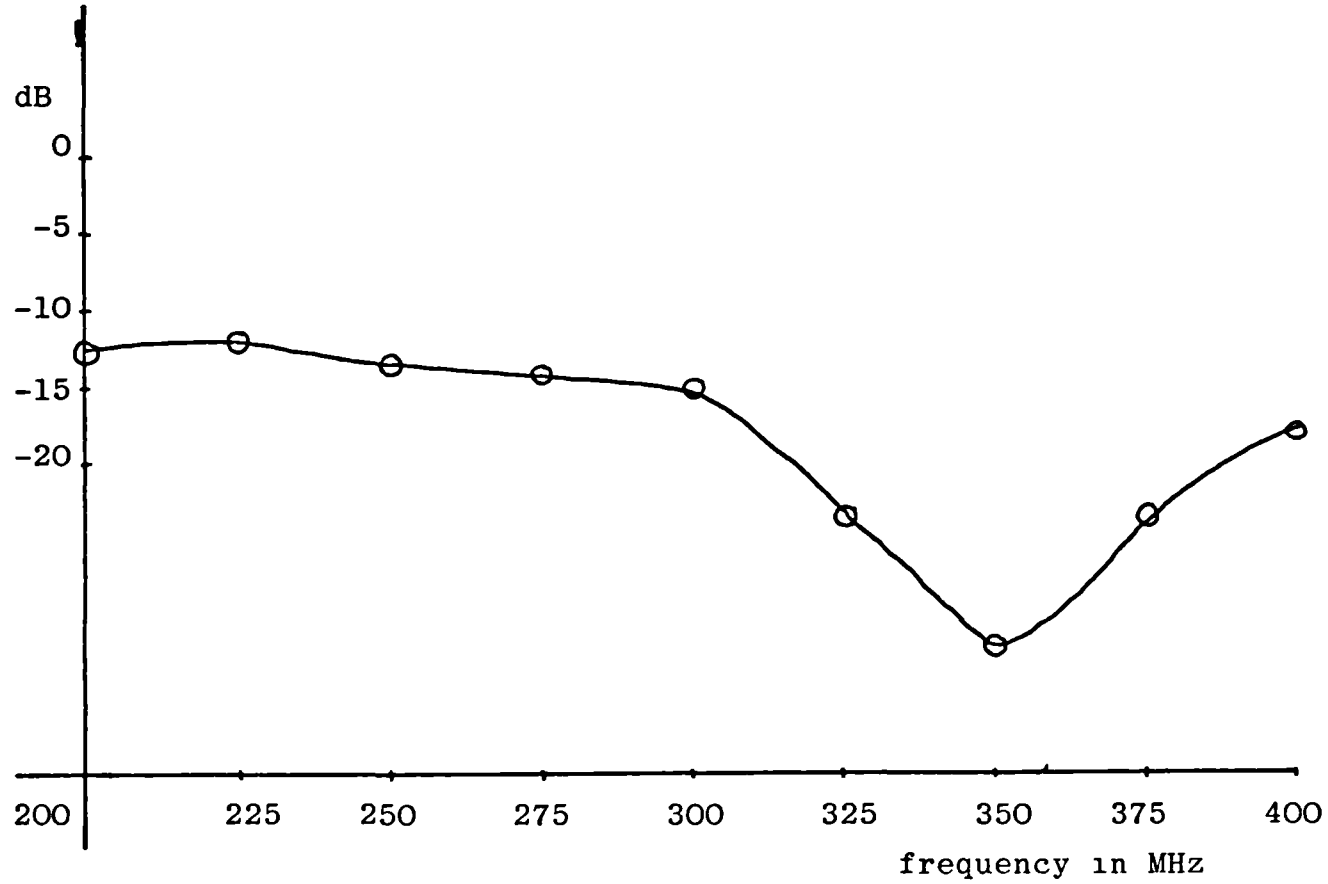

VARIATION OF SEVENTH ORDER MODE GAIN WITH FREQUENCY

CALE:—	FREQUENCY:— 310 MHz	POLARIZATION:— VERTICAL
ZIMUTH ANGLE:—	DEFLECTION LAW:— LOG	PLANE:— H

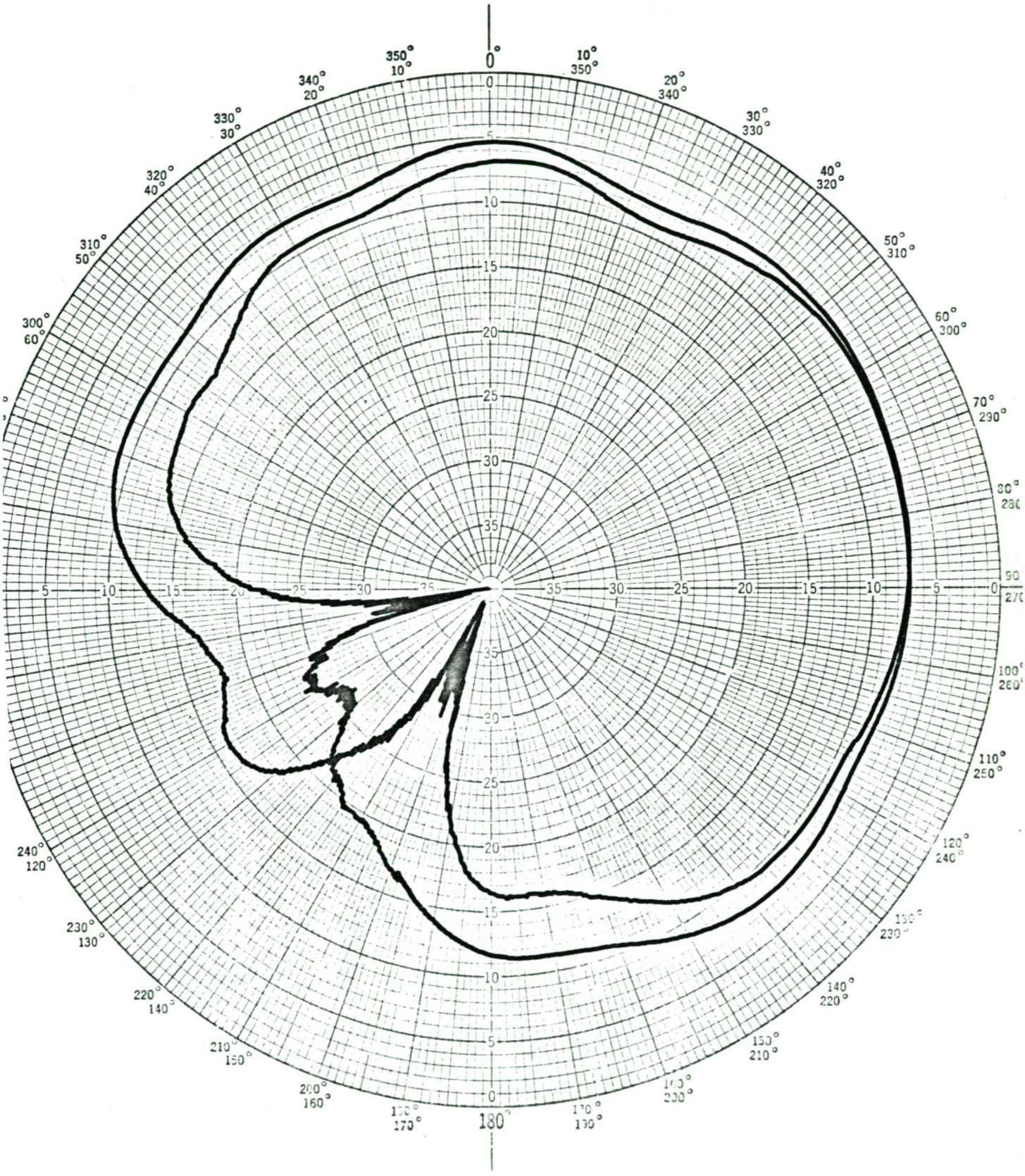

E:— 5-9-79 AERIAL:— CIRCULAR ARRAY 16 ELEMENTS

Figure 5.44 Measured null pattern by combination of zeroth and first phase modes. Null steered to a new position by having 56° phase shift in the zeroth phase mode

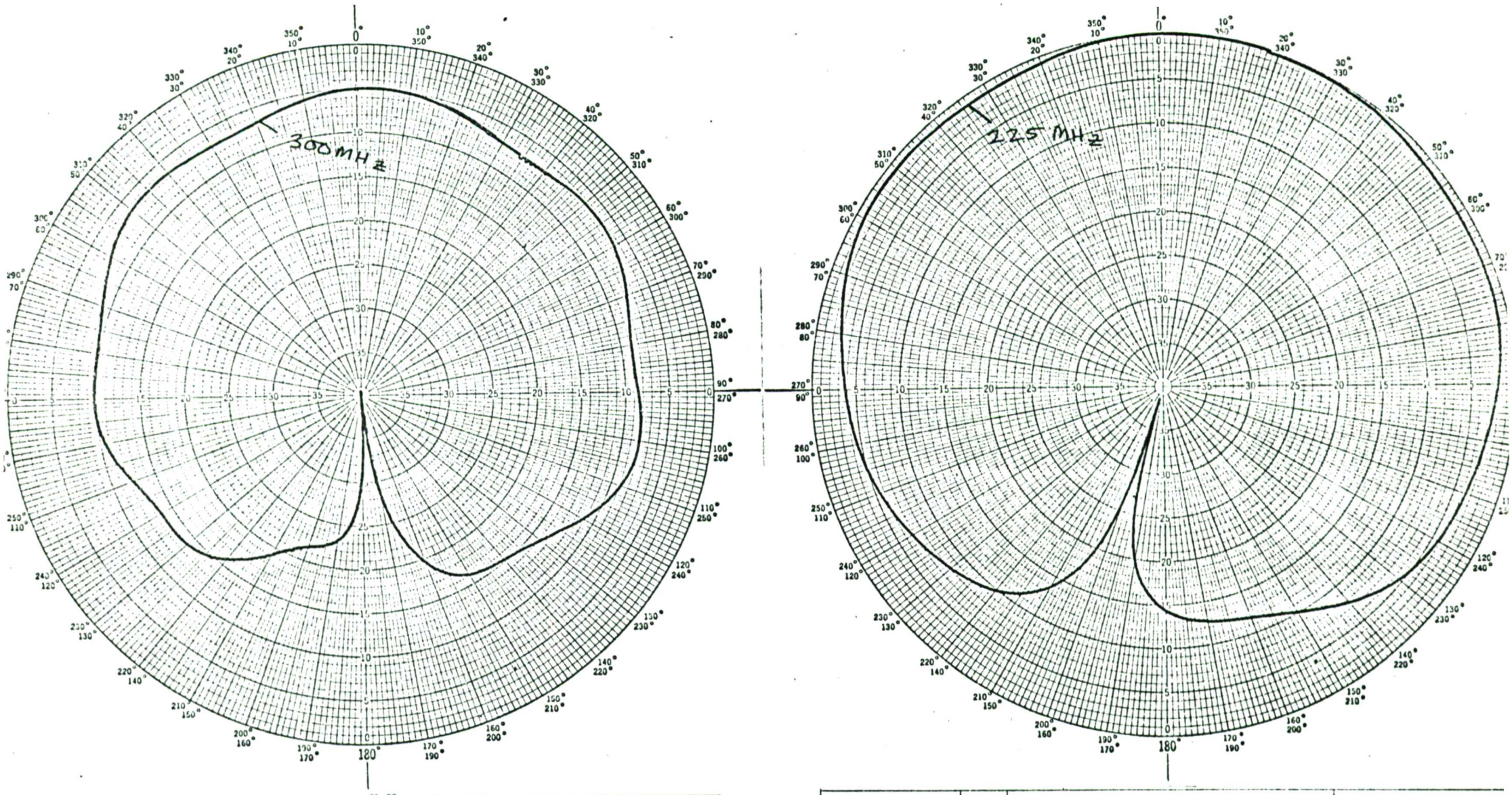

Figure 5.45 Measurement of the combination of zeroth and first phase modes at 225MHz and 300MHz for an 8ft diameter array

CALE:—	FREQUENCY :— 310 MHz	POLARIZATION :— VERTICAL
ZIMUTH ANGLE:— RRIVAL	DEFI FCTION LAW:— LOG	PLANE:— H

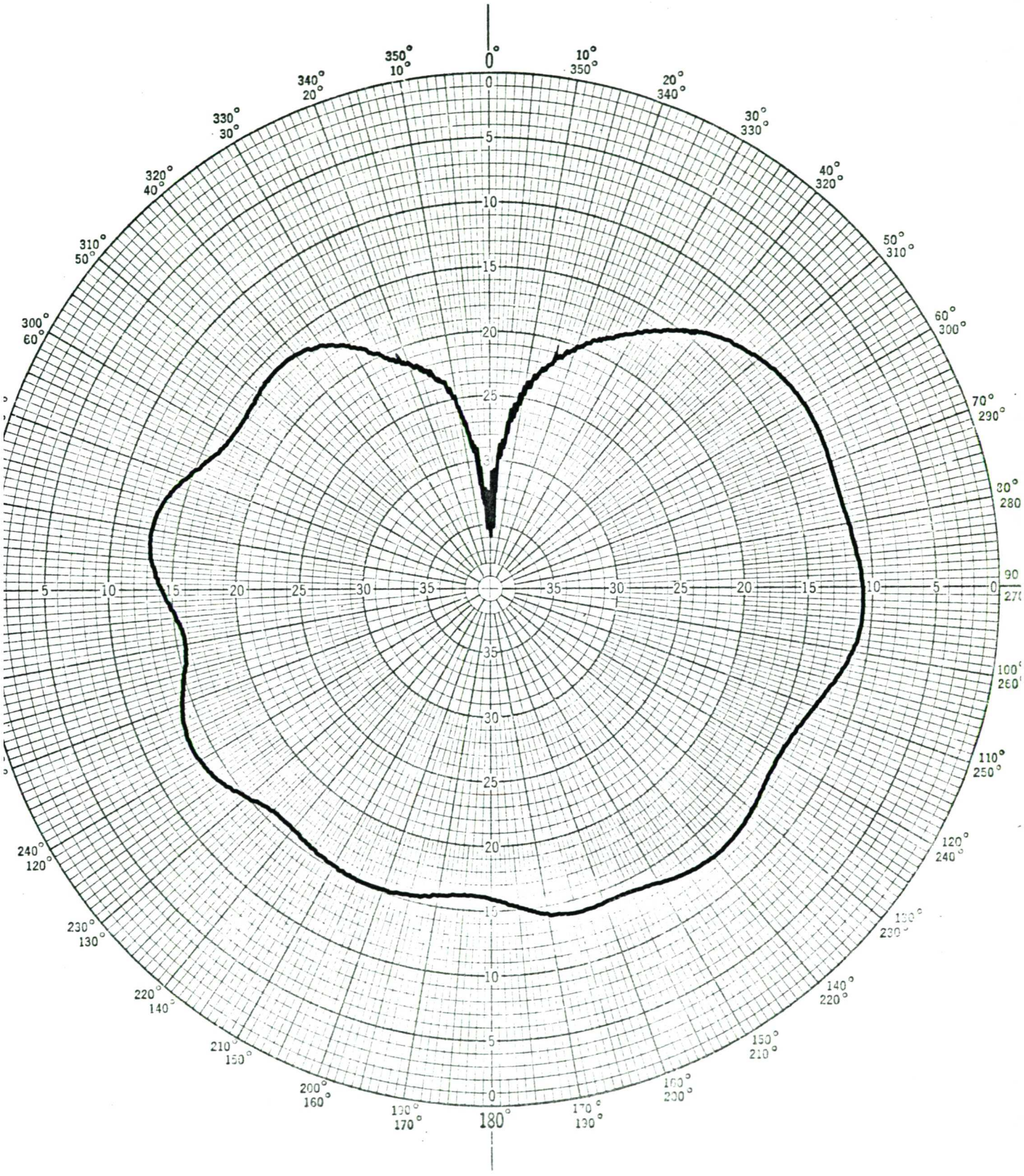

DATE :— 26-9-79 AERIAL :— UHF CIRCULAR ARRAY 16 ELEMENTS

Figure 5.46 Measured sharp null pattern

$F(\phi) = 0.35j(1-\cos\phi)+\sin\phi+1/3\sin 3\phi$

SCALE:—	FREQUENCY:— 225 MHz	POLARIZATION:— VERTICAL
AZIMUTH ARRIVAL ANGLE:—	DEFLECTION LAW:— LOG 40	PLANE:— E

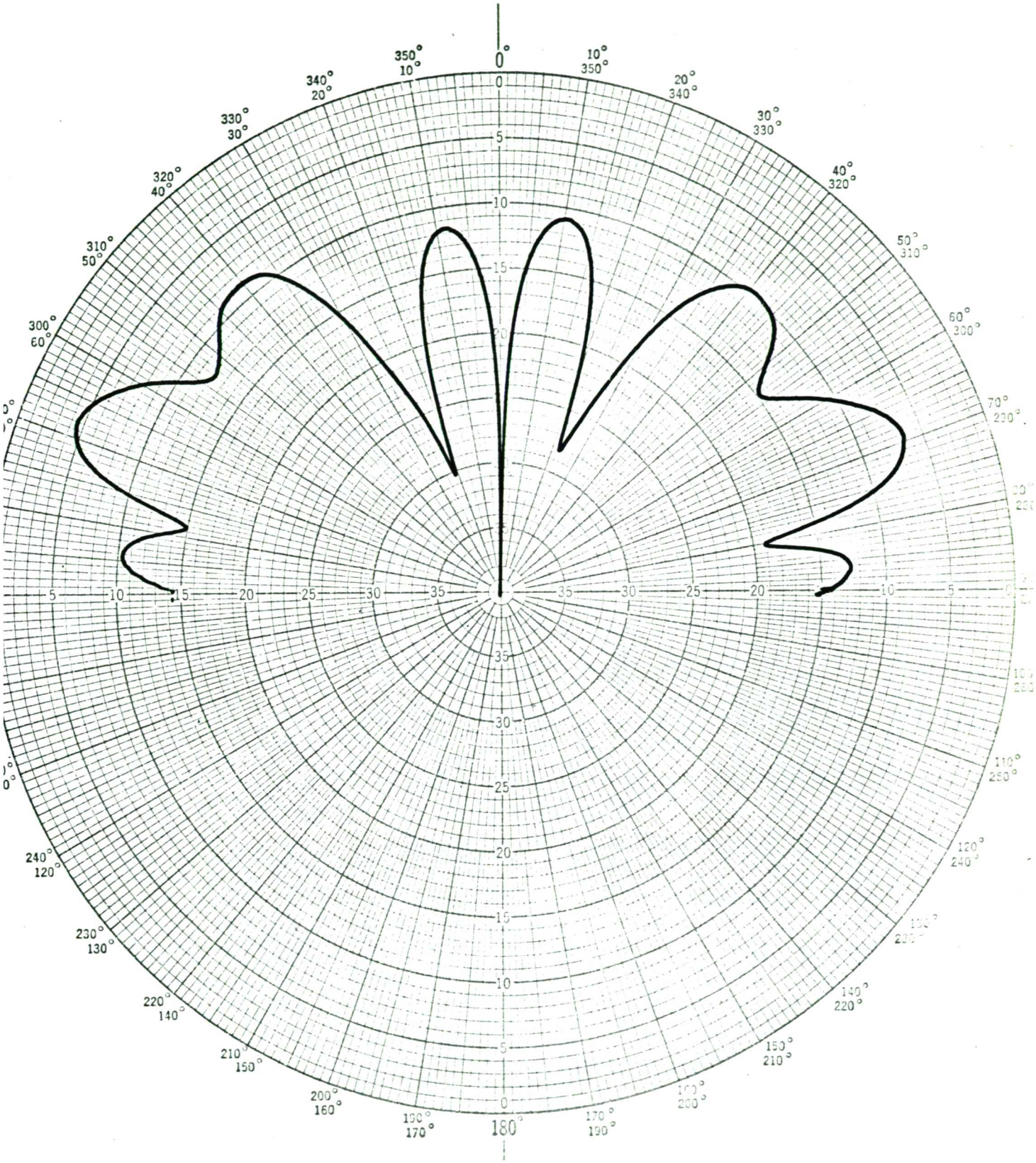

Figure 5.47 Measured vertical pattern for the zeroth phase mode. Absorbing material on the ground plane.

SCALE:—	FREQUENCY:— 225 MHz	POLARIZATION:— VERTICAL
AZIMUTH ANGLE OF ARRIVAL:—	DEFLECTION LAW:— LOG 40	PLANE:— E

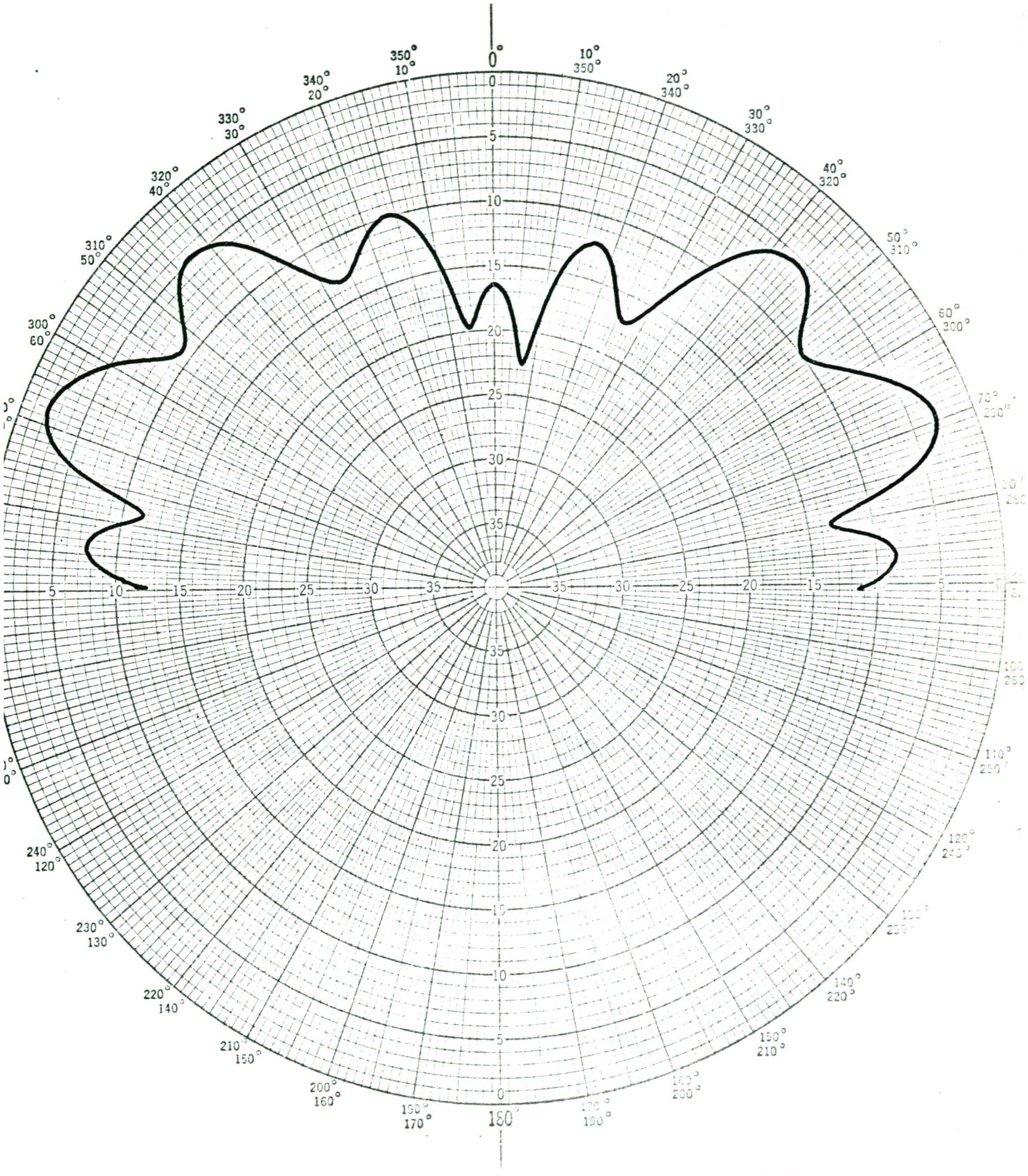

Figure 5.48 Measured vertical pattern for the first phase mode. Absorbing material on the ground plane.

SCALE:—	FREQUENCY:— 225 MHz	POLARIZATION:— VERTICAL
AZIMUTH ARRIVAL ANGLE:—	DEFLECTION LAW:— LΦG 40	PLANE:— E

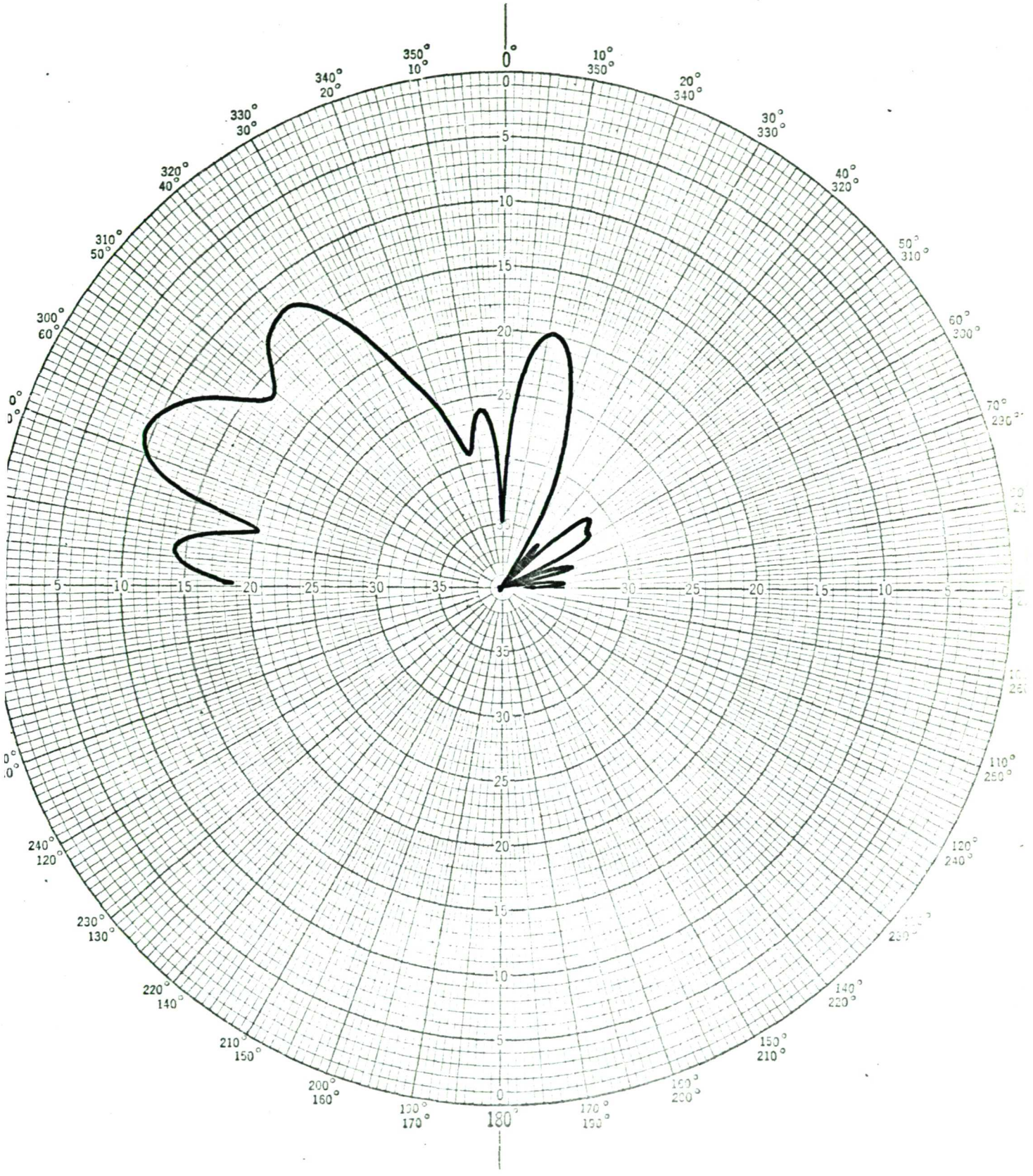

Figure 5.49 Measurement of the vertical cut through the null formed by adding zeroth and first phase mode. Absorbing material around the array.

SCALE:—	FREQUENCY:— 225 MHz	POLARIZATION:—VERTICAL
AZIMUTH ARRIVAL ANGLE:—	DEFLECTION LAW:— LOG 40	PLANE:— E

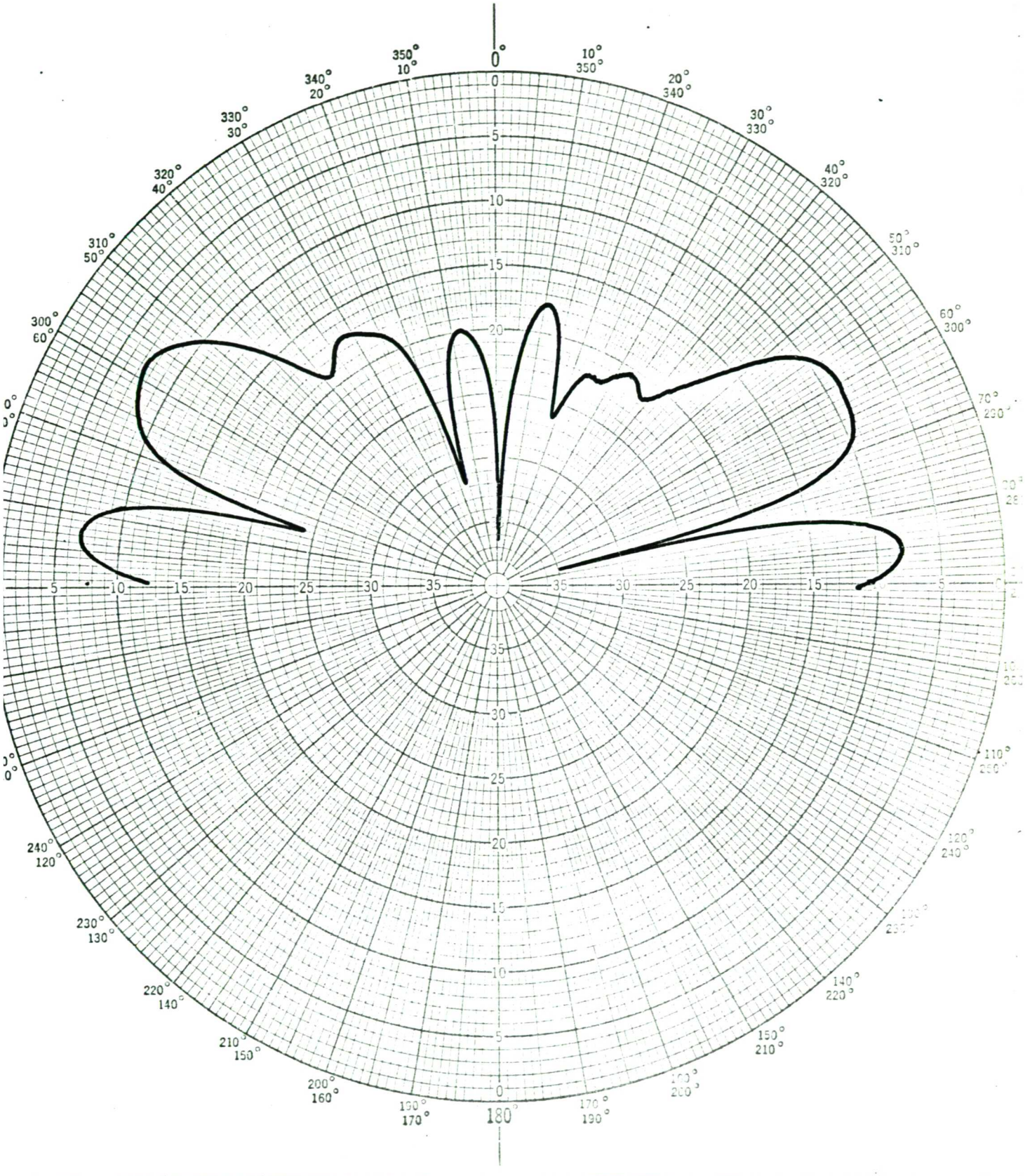

Figure 5.50 Measured vertical pattern for zeroth phase mode. Reflecting ground plane.

SCALE:—	FREQUENCY:— 225 MHz	POLARIZATION:—VERTICAL
AZIMUTH ARRIVAL ANGLE:—	DEFI FCTION LAW:— LOG 40	PLANE:— E

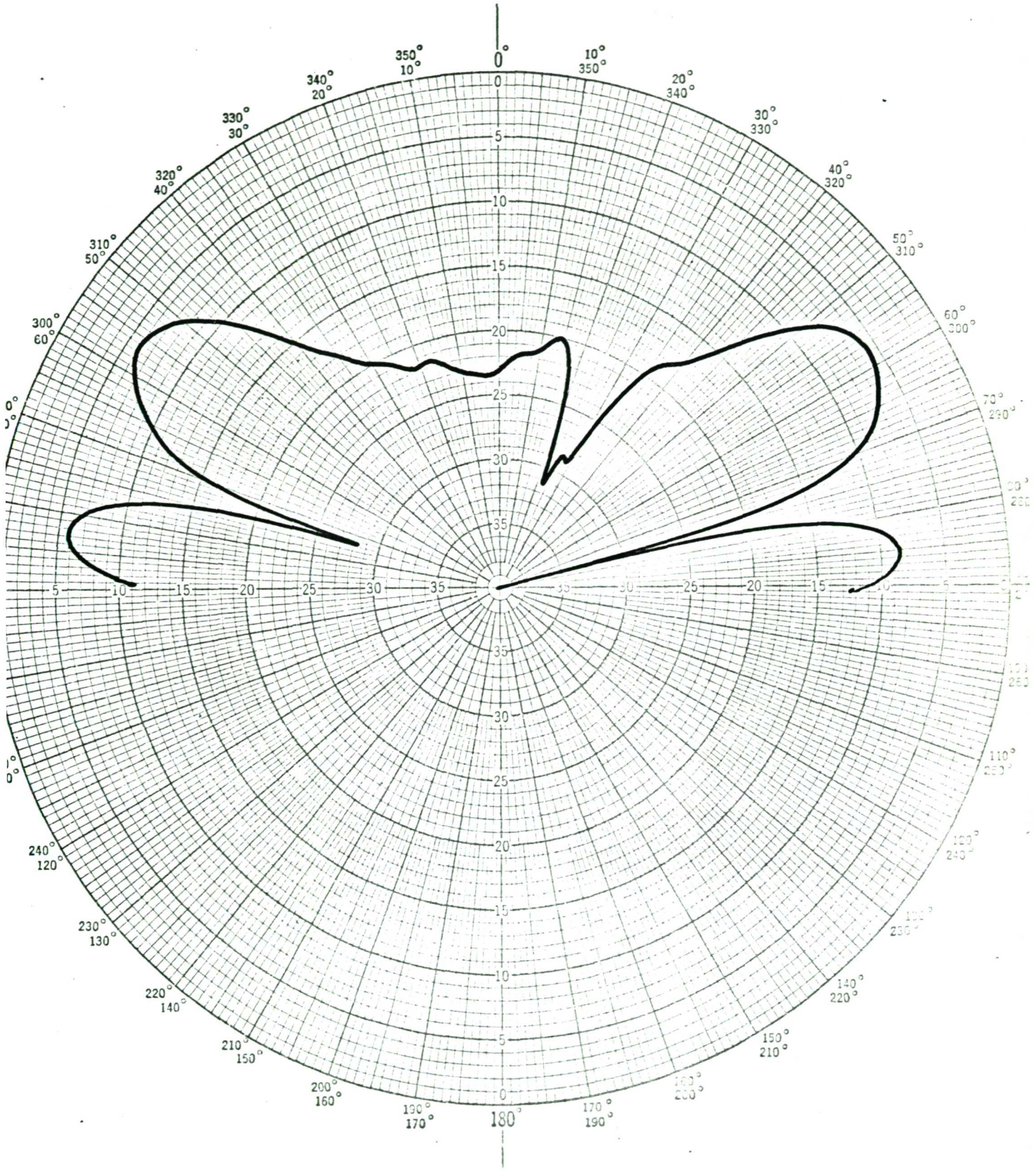

Figure 5.51 Measured vertical pattern for first phase mode. Reflecting ground plane.

SCALE:—	FREQUENCY:— 225 MHz	POLARIZATION:— VERTICAL
AZIMUTH ANGLE OF ARRIVAL:—	DEFLECTION LAW:— LOG 40	PLANE:— E

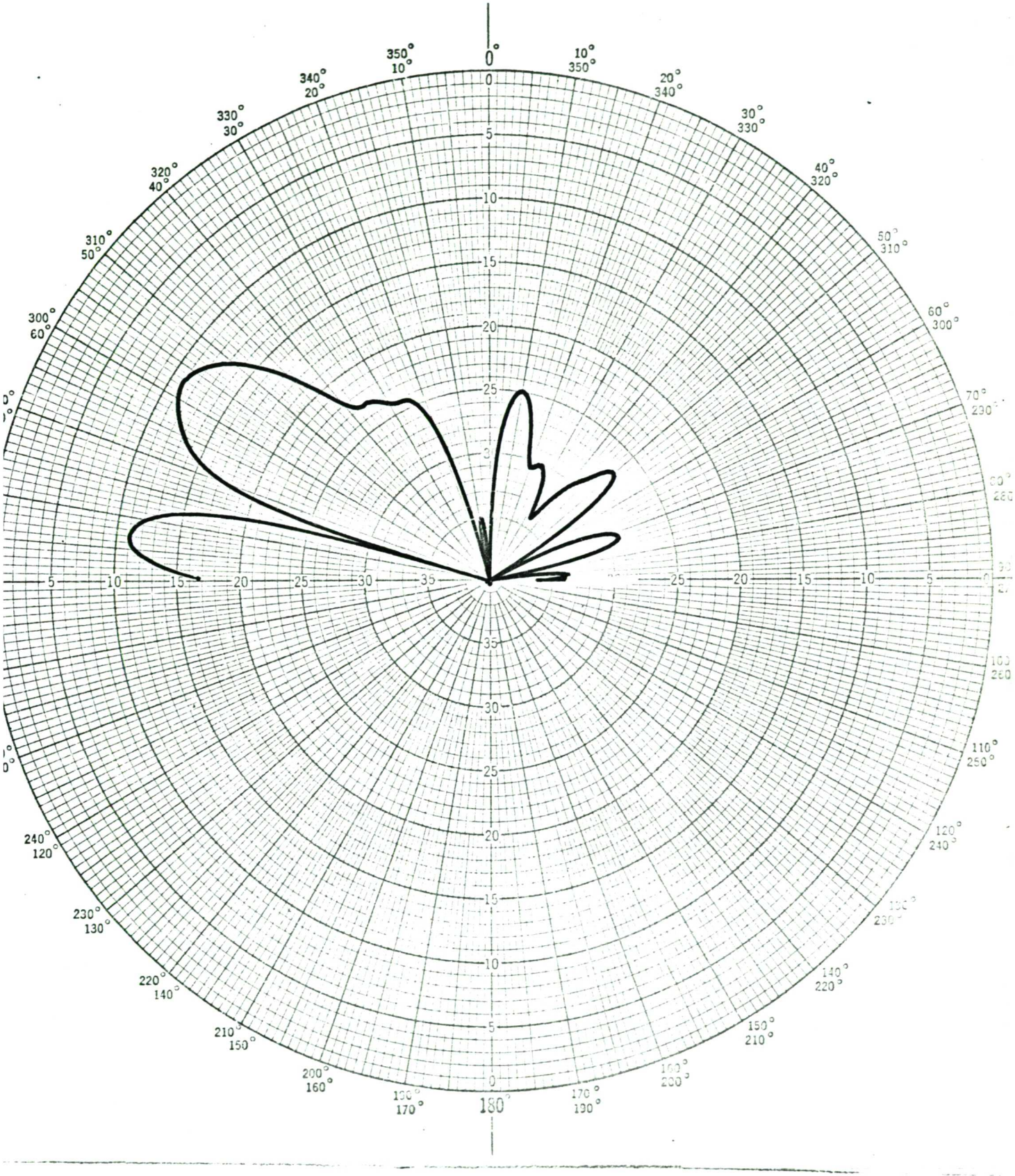

Figure 5.52 Measurement of the vertical cut through the null formed by adding zeroth and first phase mode. Reflecting ground plane.

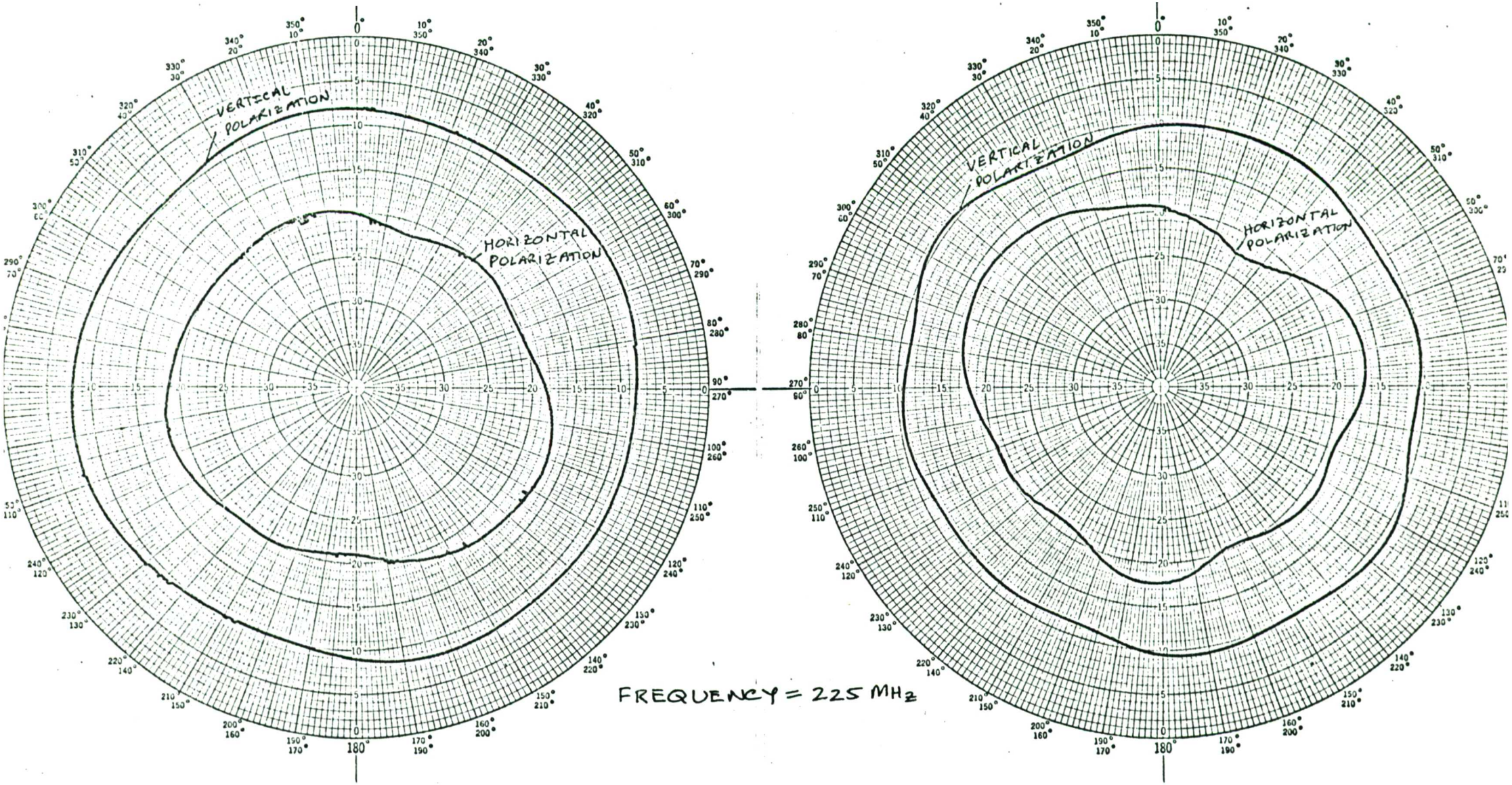

DATE :— 20-11-79 | AERIAL :— CIRCULAR ARRAY | 16 ELEMENTS

REMARKS.— MEASUREMENT OF CROSS-POLAR [illegible]
ORDER M
ATTENUATIO

DATE :— 20-11-79 | AERIAL :— CIRCULAR ARRAY | 16 ELEMENTS

TION FOR THE

20 DB

Figure 5.53 Measurement of the cross-polar patterns for zeroth and first phase modes. Attenuation of co-polar pattern = 20dB.

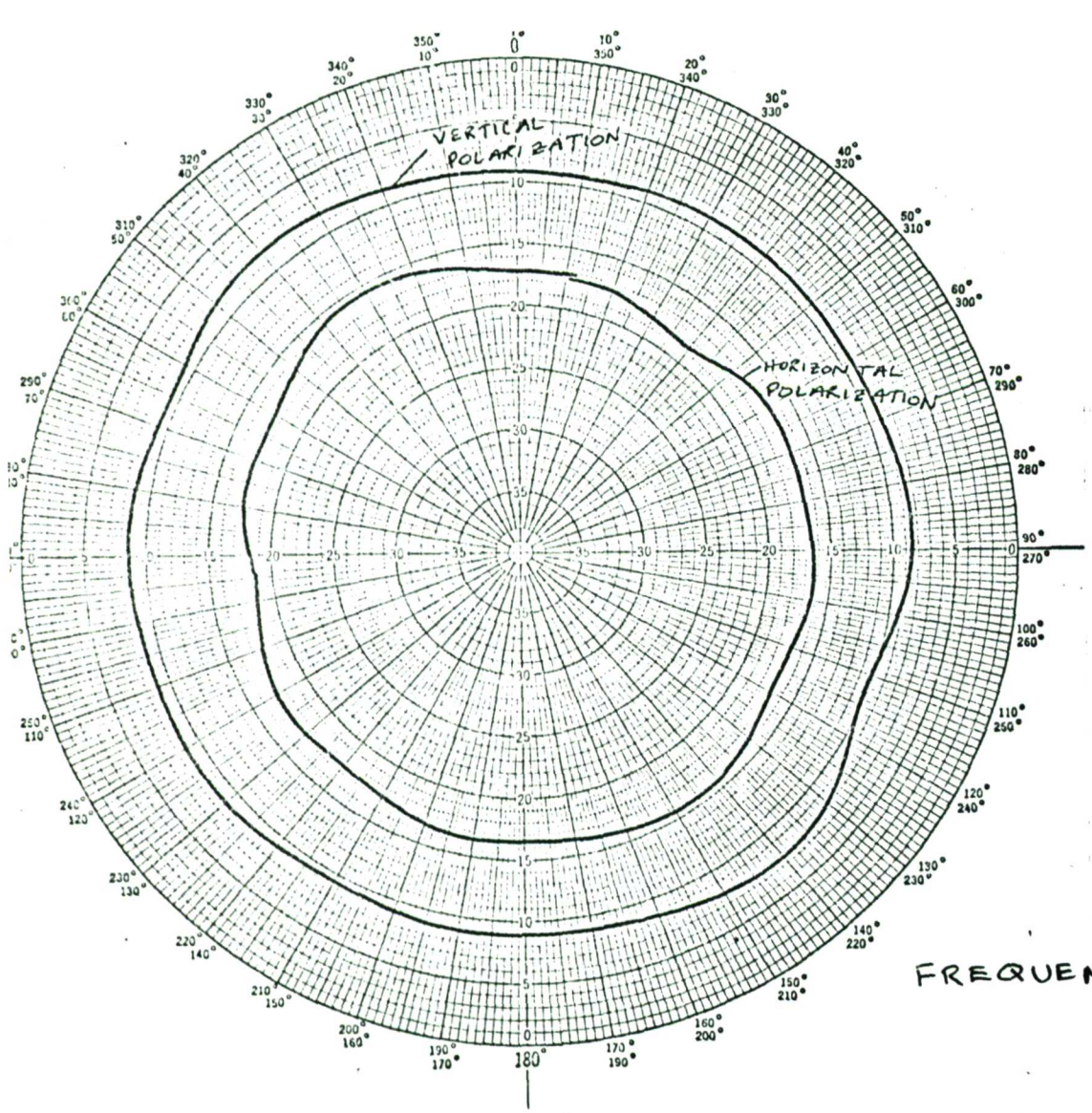

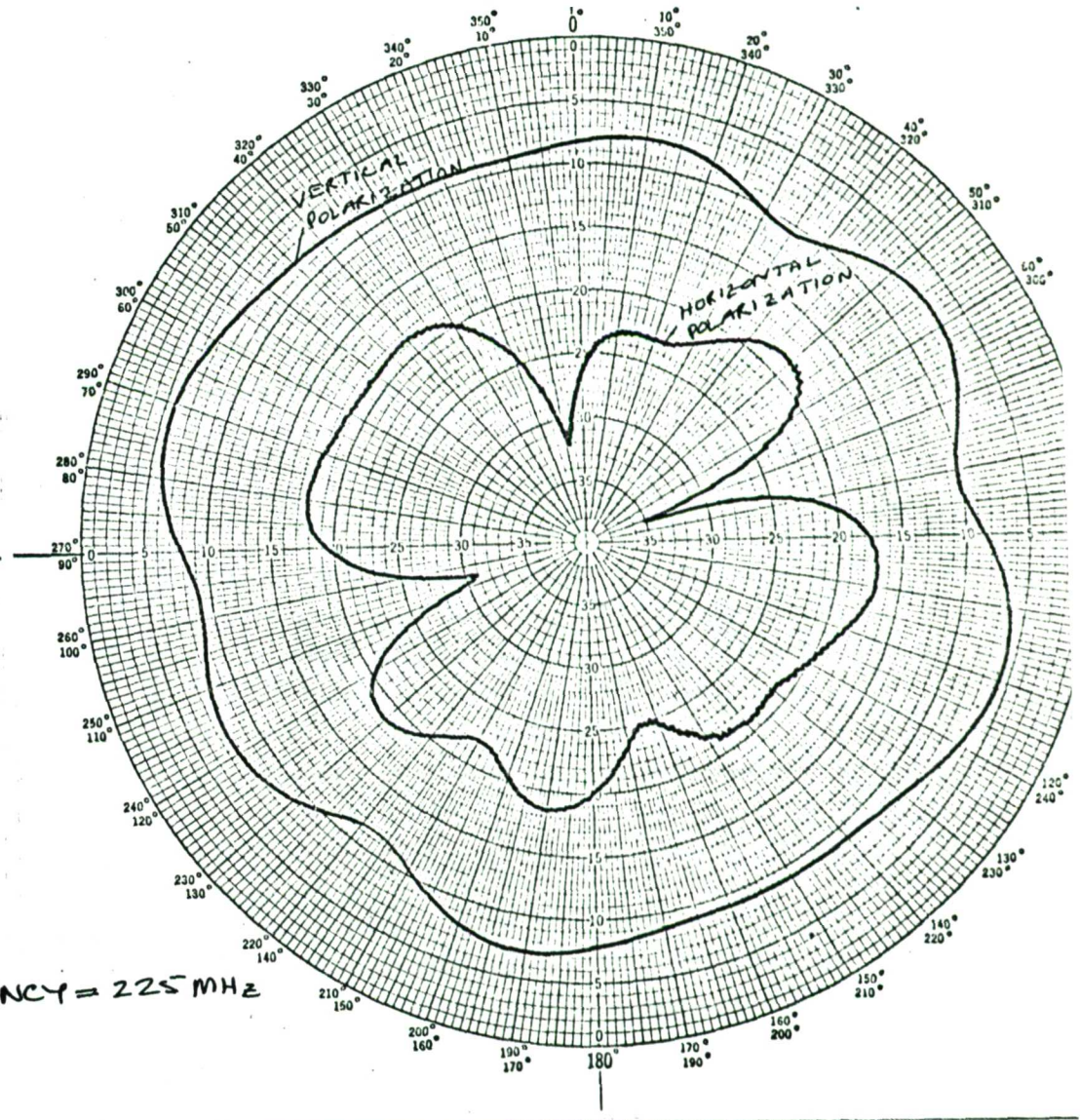

FREQUENCY = 225 MHz

DATE :— 20-11-79 | AERIAL :— CIRCULAR ARRAY | 16 ELEMENTS

REMARKS.— MEASUREMENT OF CROSS-POLAR PATTERNS FOR THE SECOND ORDER ATTENUATION OF

DATE :— 20-11-79 | AERIAL :— CIRCULAR ARRAY | 16 ELEMENTS

MEASUREMENT OF CROSS-POLAR PATTERNS FOR THE

DB

Figure 5.54 Measurement of the cross-polar pastterns for second and third phase modes. Attenuation of co-polar pasttern = 20dB.

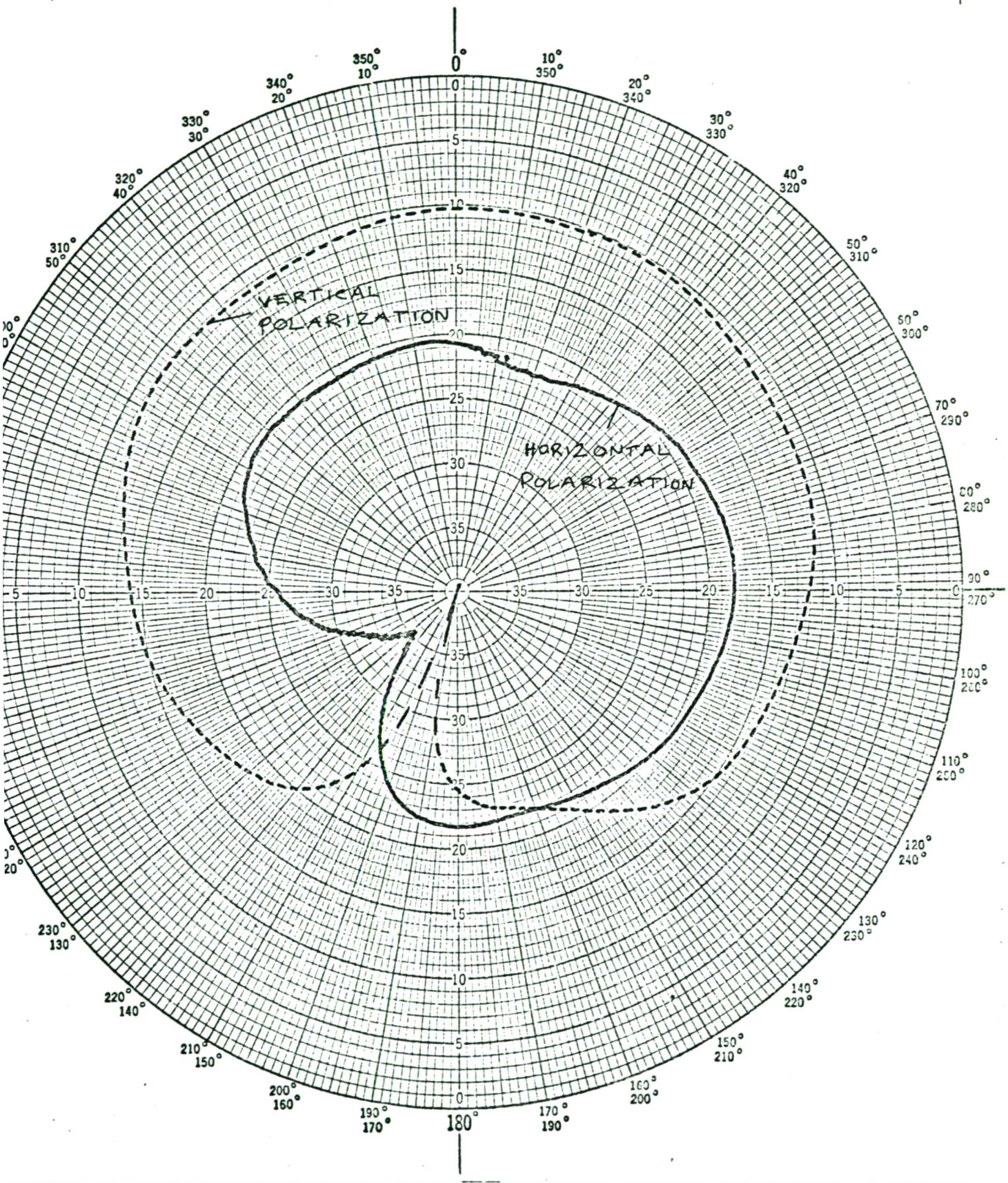

Figure 5.55 Measurement of the combination of zeroth and first phase mode for cross-polarization. Attenuation of co-planar pattern = 20dB.

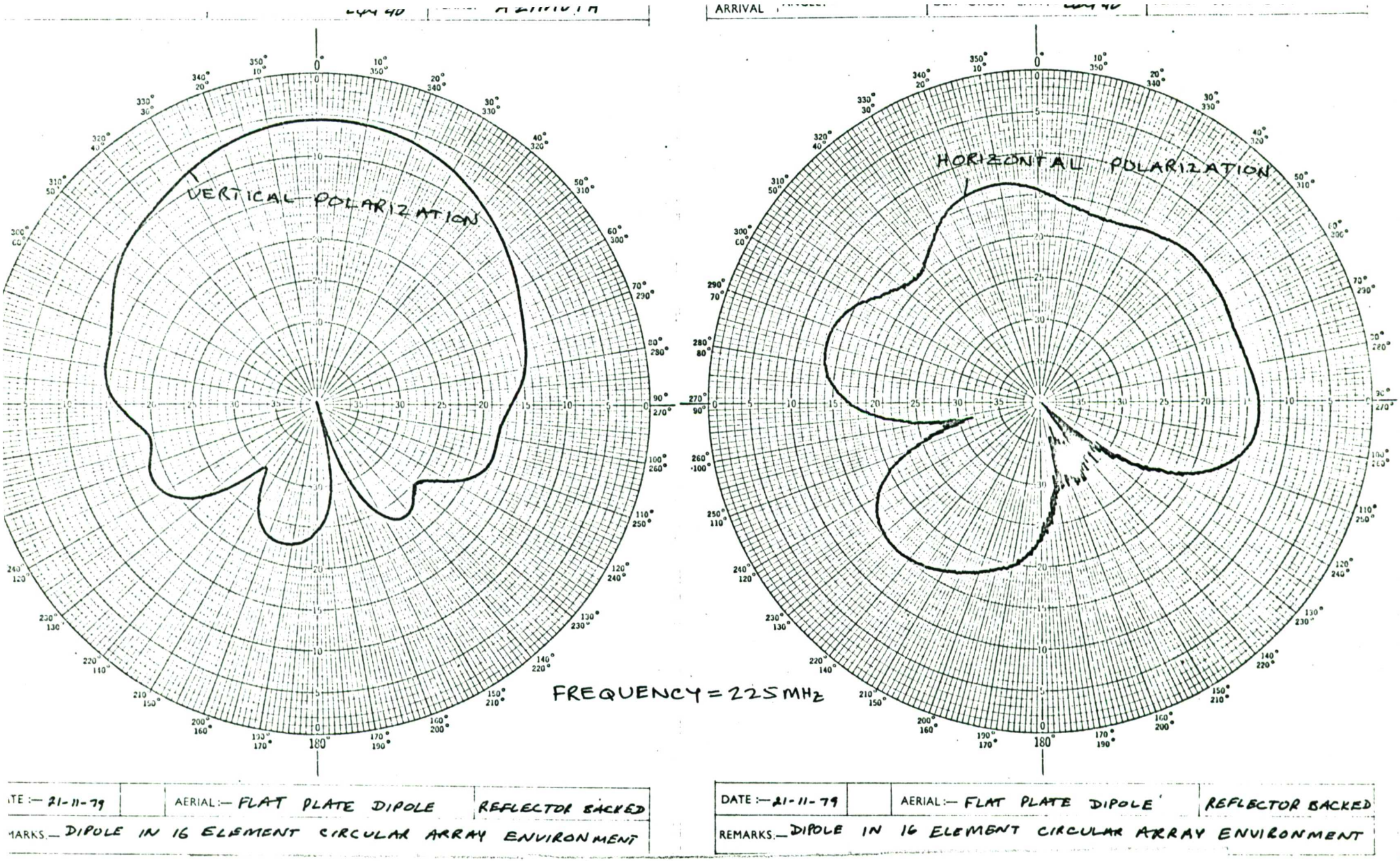

Figure 5.56 Measured element pattern for vertical and horizontal polarizations.

SCALE:—	FREQUENCY:— 225 MHz	POLARIZATION:—
AZIMUTH ANGLE OF ARRIVAL:— 0°	DEFLECTION LAW:— LOG 40	PLANE:— VERTICAL E

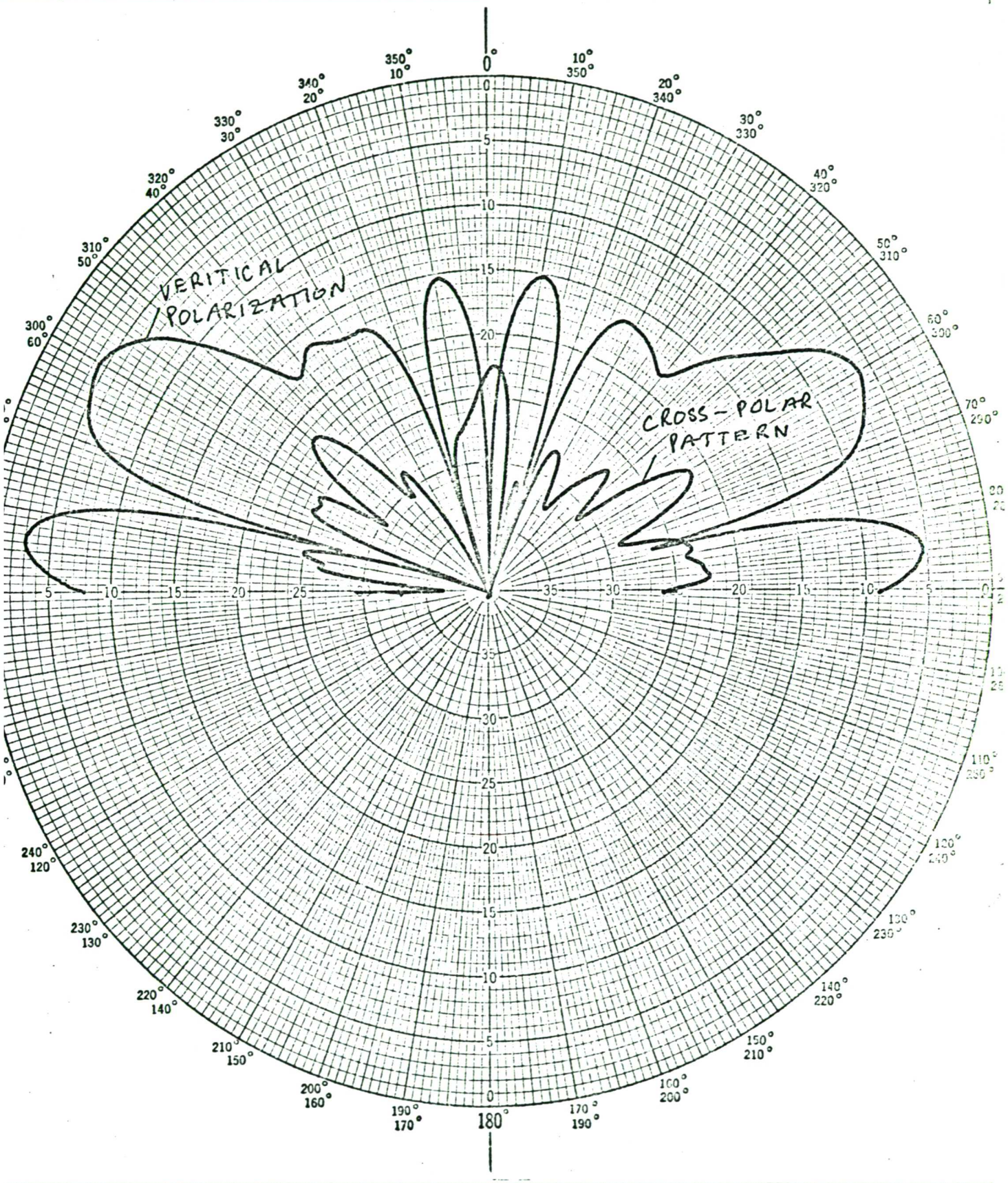

DATE:— 23-11-79	AERIAL:— CIRCULAR ARRAY	16 ELEMENTS

Figure 5.57 Measurement of the cross-polar pattern in the vertical plane for zeroth phase mode.

CALE:—	FREQUENCY:— 225 MHZ	POLARIZATION:-
ZIMUTH ANGLE:— 0°	DEFLECTION LAW:—LOG 40	PLANE:—VERTICAL E

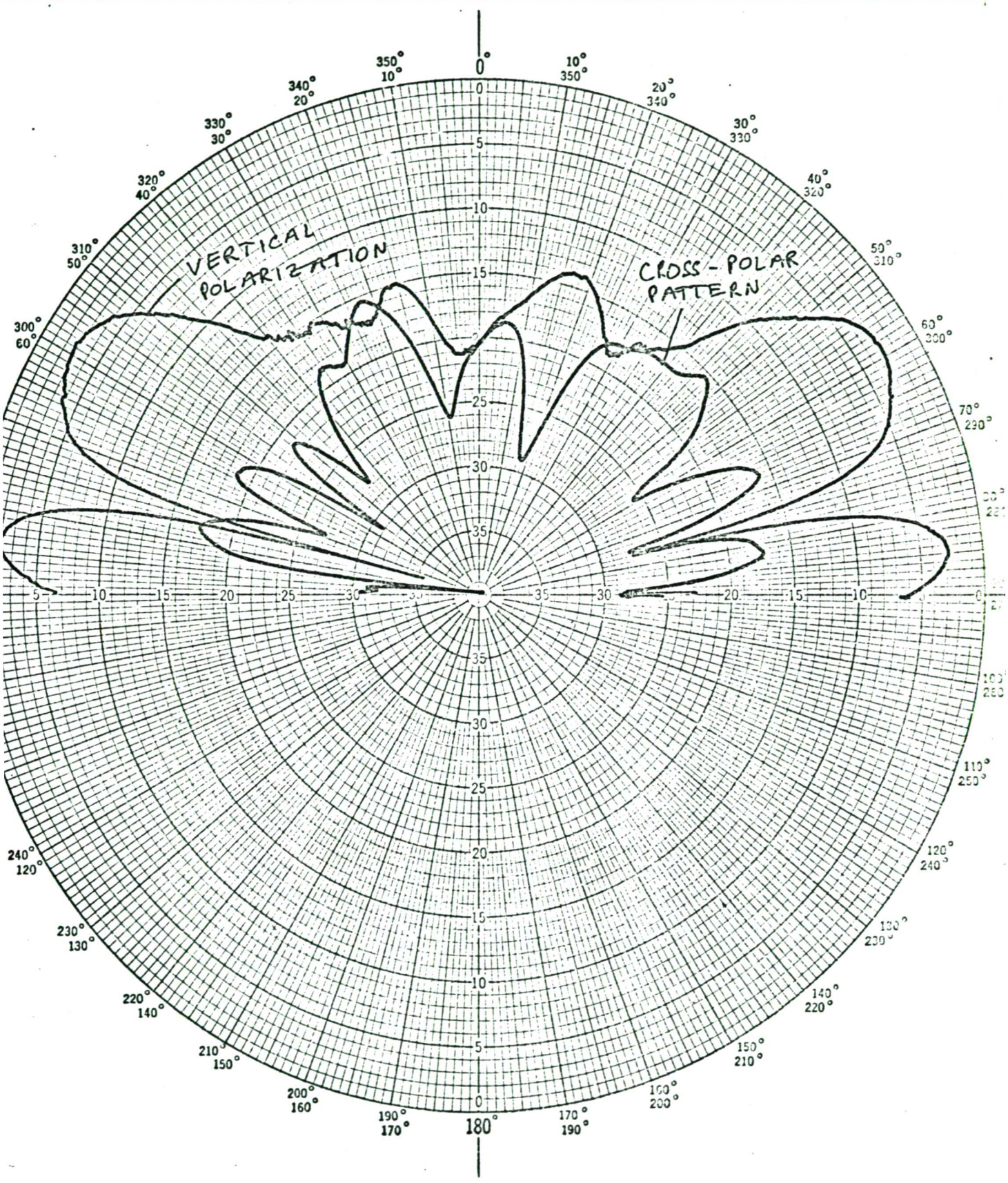

DATE:— 23-11-79		AERIAL:— CIRCULAR ARRAY	16 ELEMENTS

Figure 5.58 Measurement of the cross-polar pattern in the vertical plane for first phase mode.

CHAPTER VI

CONCLUSIONS AND IMPLICATIONS OF THE WORK

6.1 Conclusion

This thesis described a general mathematical analysis of circular arrays of directional antennas. The mode analysis technique for directional pattern synthesis in circular arrays of omnidirectional elements has been extended to circular arrays of directional elements. It is shown that the mode amplitude, when the array of directional elements is subjected to nth phase sequence excitation, is given by a complex Bessel function series, as opposed to the case of omnidirectional elements in which the amplitude is given by a single Bessel function. Consequently, the mode amplitude is stabilised with frequency changes for directive element array, hence improving the wideband performance.

Another feature of phase mode in circular arrays of directional elements is that it is shifted in space relative to the excitation on the array. This corresponds to temporal phase shift in the direction ϕ=0. The phase shift being dependent on mode order, radius in wavelengths and the type of directional element used. For directional pattern synthesis this phase shift will have to be compensated at the mode input of the network feeding the modes. The effect of using directional elements in circular arrays, on the vertical patterns, is to improve the omnidirectionality for lower order modes. And to cause variation of phase in the vertical plane as

opposed to the case of omnidirectional elements. It is shown that the effect of random amplitude and phase errors in the excitation of phase modes may be regarded as a distortion of the mode by the presence of higher order modes. These errors can be corrected to a certain extent at the higher order mode input. It is also shown that the effect of mutual coupling is to modify the mode amplitude and phase which can be compensated at the mode input.

A procedure is outlined for design of circular arrays of directional elements for producing specified far field directional patterns. It is shown that as the element pattern becomes more directive, the interelement spacing must be reduced to prevent degradation of the far field directional pattern.

New techniques are described for synthesis of single and 2n sharp nulls in an otherwise omnidirectional pattern of circular arrays, using spatial modes. Theoretical patterns show that with the use of five amplitude modes null width and gain ripple attainable are 15^{o} and $\pm$2dB respectively, for single null pattern. For the case of two nulls, using ten amplitude modes, the null width and gain ripple are 8^{o} and $\pm$1·5dB respectively, whereas the minimum allowable null separation is 15^{o}. Using fewer amplitude modes will result in wider nulls, larger gain ripple and larger minimum allowable null separation. It was also shown that the disadvantage with the Schelkunoff

synthesis technique for multiple nulls is that the null-widths are fairly broad and the gain between nulls is considerably reduced even when they are brought only 60^{o} apart. However, the advantage with the previous technique is that it utilises a small number of phase modes, hence it can be used for small radius circular arrays of a few elements. For larger arrays (n-1) nulls can be synthesised from arrays containing n elements.

For synthesis of single sharp null in an otherwise omni-directional pattern a new technique is described using the concept of imaginary nulls. It is shown that improved null pattern may be obtained when the imaginary nulls are placed on the 0.25 circle in the complex Z plane.

Appendix III describes some techniques for synthesis of beam patterns. It is shown that sidelobe levels can be reduced by the use of amplitude tapers on mode excitation by analogy with linear arrays.

Finally, the thesis describes experimental measurements on the 16 element circular array. The experimental results were in good agreement with theoretically studied properties of circular arrays of directional antennas. Various single null patterns were measured and properties were in agreement with the theoretical results. It was found that null depth was sensitive to amplitude and phase errors in the modes and in the excitation network.

6.2 Some Design Implications of the use of Directional Elements in Circular Arrays

The previous discussion has already made it clear that since the use of directional elements stabilises the mode amplitude of a circular array this will represent a significant advantage in the design of wide bandwidth patterns. If omnidirectional elements are used this is likely to result in significant variations in directional pattern over a broad band of operation. In principle, we could excite a circular array via a Butler matrix and impose a range of equalising networks at the input to each mode port of the matrix. These equalising networks could be designed so as to compensate for the variation of mode amplitude with frequency. This technique may, in principle, be used with omnidirectional elements in order to try to achieve some degree of mode stability. A fundamental problem here is that mode sensitivities can go to zero (corresponding to the zero of a Bessel function) and clearly no amount of equalisation can compensate for this. Nevertheless, the concept of such equalising networks may be a useful extension to the capability of circular arrays for either directional or non-directional elements. For example, there may well be applications in which the desired form of directional pattern would be different in different parts of the band and this would be achievable by means of such networks. It is important to add that these networks must not only take account of the required

amplitude excitation of each mode (which must in turn be compensated for mutual coupling) but must also give the correct phase excitation to take account of the spatial shift of phase modes with directional elements and any phase shift due to mutual coupling.

There is one rather interesting and unique feature of circular array patterns when excited by phase mode excitation: such patterns are theoretically broad band in the sense that their beamwidth and sidelobe structure do not change at all with frequency. We note that this result is quite different from that of linear arrays or for that of circular arrays when excited with beam cophasal type excitations. Clearly if a desired pattern can be broken down into a limited number of spatial harmonics and a circular array has sufficient elements such that these can be excited over a broad band without distortion, then the resultant far field pattern will remain identical over this band. This rather interesting situation offers a possible technique of producing precisely controlled patterns over large bandwidths. Obviously in practice there will be limitations. At the high frequency end of the band the inter-element spacing will ultimately become too large and higher order distortion modes will be excited resulting in a distorted pattern. The limitation at the low frequency end will arise when higher order modes correspond to phase variations around the array circumference faster than

2π per free space wavelength. This will correspond to setting up super-directive excitations on circular arrays. Clearly there is no theoretical reason to prevent such super-directive excitation but it is certainly likely to give rise to practical problems.

Returning to the question of the value of directional elements it is important to appreciate that in the case of a circular array the design of the directional pattern in the horizontal plane will automatically fix the pattern at all other angles (neglecting, for the moment, the additional parameter of the vertical directional pattern of each antenna element). In the case of omnidirectional elements this can be a severe constraint. Even for narrow band operation we find that the synthesis of a desired pattern in the plane of the circle is likely to lead to quite unsatisfactory patterns outside this plane. This is because the relative amplitudes of the different modes will be different for the different angles of elevation. Thus low sidelobes in the horizontal plane give no guarantee of low sidelobe patterns at other angles. This problem is almost entirely overcome by the use of directional elements. The improved stability of the modes with wavelength also provides an improved stability of the modes in terms of the vertical angle which in turn means that the variation of directional pattern as one goes away from the plane of the circle is substantially reduced. However, the problem with using directional elements is that it causes a

variation of phase in the vertical plane which will have an adverse effect on the vertical directional pattern.

The previous theoretical work has been upon the assumption of a directional element having the form $1+\cos\theta$. The experimental results are based upon an element whose general directional pattern is similar to this function. It is relevant to ask whether there is an optimum form of directional element and perhaps to justify the previous choice. The initial argument behind the above choice of elements relates to the fact that typical dipoles in front of a conducting screen are likely to exhibit patterns of this general shape. This is therefore a simple pattern which is easily, but not exactly achievable. The use of a more complex pattern would only be justifiable if it produced significant improvements. The previous analysis has suggested that the use of more directive elements will in fact introduce problems in the sense that the inter-element spacing must then be reduced. This fact alone is likely to be conflicting in practice since more directive elements are likely to be physically broader than $\lambda/2$. A more important conclusion is that the use of the $1+\cos\theta$ element appears to be a near optimum in terms of stabilising mode performance.

APPENDIX I

Spatial Harmonic Response of Circular Arrays of Directional Elements

Consider a circular array of directional elements with a current distribution

$$i = I^m \cos m\phi \qquad \text{A1.1}$$

A1.1 can also be written as

$$i = \frac{I^m}{2}(e^{jm\phi} + e^{-jm\phi}) \qquad \text{A1.2}$$

i.e. a spatial haromic is obtained by adding to equal and opposite phase modes.

We know from the expression developed in section 2.5 that the far field response of a circular array of directional elements subjected to mth sequence excitation is given by

$$F_m(\phi) = I_m |A_m| e^{J(m\phi + \psi m) + D_m(\phi)} \qquad \text{A1.3}$$

where

$$|A_m| e^{J\psi m} = \sum_{-L}^{L} C_\ell J^{m-\ell} J_{m-\ell}(\varepsilon) \qquad \text{A1.4}$$

and

$$D_m(\phi) = \sum_{-L}^{L} C_\ell \{ \sum_{q=1}^{\infty} J^{Nq+(m-\ell)} J_{Nq+(m-\ell)}^{(\varepsilon)} e^{j(Nq+m)\phi}$$

$$+ \sum_{q=1}^{\infty} J^{Nq-(m-\ell)} J_{Nq-(m-\ell)}^{(\varepsilon)} e^{-j(Nq-m)\phi} \qquad \text{A1.5}$$

The far field response of an array subjected to negative mth sequence excitation '$e^{-Jm\phi}$' will be given by

$$F_{-m}(\phi) = I^m |A_{-m}| e^{J(-m\phi+\psi-m)} + D_{-m}(\phi) \qquad \text{A1.6}$$

where

$$|A_{-m}| e^{j\psi-m} = \sum_{-L}^{L} C_\ell J^{-(m+\ell)} J_{-(m+\ell)}^{(\varepsilon)} \qquad \text{A1.7}$$

and

$$D_{-m}(\phi) = \sum_{-L}^{+L} C_\ell \{ \sum_{q=1}^{\infty} J^{Nq-(m+\ell)} J_{Nq-(m+\ell)}^{(\varepsilon)} e^{J(Nq-m)\phi}$$

$$+ \sum_{q=1}^{\infty} J^{Nq+(m+\ell)} J_{Nq+(m+\ell)}^{(\varepsilon)} e^{-J(Nq+m)\phi} \qquad \text{A1.8}$$

we know that

$$J^{-m} J_{-m}(\varepsilon) = J^m J_m(\varepsilon) \qquad \text{A1.9}$$

Using A1.9, equation A1.7 becomes

$$|A_{-m}|e^{J\psi-m} = |A_m|e^{j\psi m} . \qquad \text{A1.11}$$

provided, $C_{-\ell} = C_{\ell}$. This implies that the element directional pattern is symmetric about the radius vector - a reasonable assumption.

Similarly, it can be shown that

$$D_{-m}(\phi) = \sum_{-L}^{L} C_{\ell} \sum_{q=1}^{\infty} J^{Nq+(m-\ell)} J_{Nq+(m-\ell)}^{(\varepsilon)} e^{-j(Nq+m)\phi}$$

$$+ \sum_{q=1}^{\infty} j^{Nq-(m-\ell)} J_{Nq-1m-\ell)}^{(\varepsilon)} e^{J(Nq-m)\phi} \qquad \text{A1.12}$$

From eqaution A1.12 it is clear that the far field response for a circular array of directional elements subjected to mth harmonic excitation is given by

$$C_m(\phi) = F_m(\phi) + F_{-m}(\phi) \qquad \text{A1.13}$$

Using A1.3 and A1.6, we have

$$C_m(\phi) = |A_m|e^{J\psi m\{\cos(m\phi)\}} + C_{md}(\phi) \qquad \text{A1.14}$$

where the distortion term $C_{md}(\phi)$ is given by

$$C_{md}(\phi) = \sum_{-L}^{+L} C_{\ell}\{ \sum_{q=1}^{\infty} j^{Nq+(m-\ell)} J^{(\varepsilon)}_{Nq+(m-\ell)} \cos(Nq+m)\phi$$

$$+ \sum_{q=1}^{\infty} j^{Nq-(m-\ell)} J^{(\varepsilon)}_{Nq-(m-\ell)} \cos(Nq-m)\phi \qquad \text{A1.15}$$

Similarly by subtracting the two equal and opposite phase modes, we find that the array with excitation

$$i = I^{m} \sin m\phi \qquad \text{A1.16}$$

has a normalised far field response given by

$$S_{m}(\phi) = |A_{m}| e^{j\psi_{m}} \sin m\phi + S_{md}(\phi)$$

where

$$S_{md}(\phi) = \sum_{-L}^{+L} C_{\ell}\{ \sum_{q=1}^{\infty} j^{Nq+(m-\ell)} J^{(\varepsilon)}_{Nq+(m-\ell)} \sin(Nq+m)\phi$$

$$+ \sum_{q=1}^{\infty} j^{Nq-(m-\ell)} J^{(\varepsilon)}_{Nq-(m-\ell)} \sin(Nq-m)\phi \qquad \text{A1.17}$$

APPENDIX II

Computation of G_{om}

For a circular array of omnidirectional elements of size (2.44λ) diameter and 16 elements operating at 300MHz, the absolute gain for the zeroth order mode is given by

$$G_{om} = \frac{4\pi\, J_o^2(7.68)}{\int\int_{\phi\theta} J_o^2(7.68)\sin^3\theta\, d\theta\, d\phi} \qquad \text{A2.1}$$

$$= \frac{J_o^2(7.68)}{\int_o^{\pi/2} J_o^2(7.68\sin\theta)\sin^3\theta\, d\theta} \qquad \text{A2.2}$$

From Ref. 18

$$\int_o^{\pi/2} J_o^2(7.68\sin\theta)\sin^3\theta\, d\theta = -\frac{J_o(15.36)}{8(7.68)^2} + \frac{J_1(15.36)}{4x7.68}$$

$$+ \left\{\frac{1}{4x7.68} - \frac{1}{16x(7.68)^2}\right\} I_1 \qquad \text{A2.3}$$

where

$$I_1 = 2\sum_{r=o}^{\infty} J_{2r+1}(15.36)$$

$$I_1=2\{J_1(15.36)+J_3(15.36)+J_5(15.36)\ +....\} \qquad \text{A2.4}$$

$$I_1 = 1.068$$

$\therefore$

$$\int^{\pi/2} J_o{}^2(7.68\sin\theta)\sin^3\theta d\theta = -0.03$$

$\therefore$

$$G_{om} = -\frac{0.0566}{0.03}$$

$$G_{om} = 2.76dB$$

APPENDIX III

Beam formation in circular arrays

In order to enhance the gain in a given direction it may be desirable to synthesise a beam pattern. In this section some methods are described for synthesis of beam patterns using circular antenna arrays.

In linear antenna arrays, a broadside beam is formed if the elements are excited uniformly. Since phase modes of a circular array correspond to element excitation of linear arrays, a beam may be formed by uniformly exciting all the phase modes. If the phase modes excited range from $-\frac{N}{2}$ to $+\frac{N}{2}$, the beam pattern is given by

$$F(\phi) = \frac{\sin(N+1)\phi/2}{\sin\phi/2} \qquad \text{A3.1}$$

The 3dB beamwidth is given by

$$\gamma_n = \frac{2\pi}{N+1} \qquad \text{A3.2}$$

or

$$\gamma_n = \frac{\lambda}{D} \qquad \text{A3.3}$$

where D = diameter of the array

From equation A3.2 we see that beamwidth may be reduced by using larger number of modes. Fig. A3.1 shows the beam pattern for N=16. The 3dB beamwidth is 10^{o} and the sidelobe level is 11.0dB.

Analogous to linear arrays, by applying amplitude tapers to the modes the sidelobe level can be reduced. Fig. A3.2 shows a beam pattern with cosine amplitude taper. The directional pattern is given by

$$F(\phi) = \sum_{-M}^{M} \cos\left(\frac{2\pi m}{M}\right) \cos m\phi \qquad \text{A3.4}$$

where M = 8

The 3dB beamwidth is 14^{o} and the sidelobe level is 14.5dB.

Fig. A3.3 shows the beam pattern with cosine square amplitude taper. The directional pattern is given by

$$F(\phi) = \sum_{-M}^{M} \cos^{2}\left(\frac{2\pi m}{M}\right) \cos m\phi \qquad \text{A3.5}$$

where M = 8

The 3dB beamwidth is 18^{o} and the sidelobe level is 15.5dB.

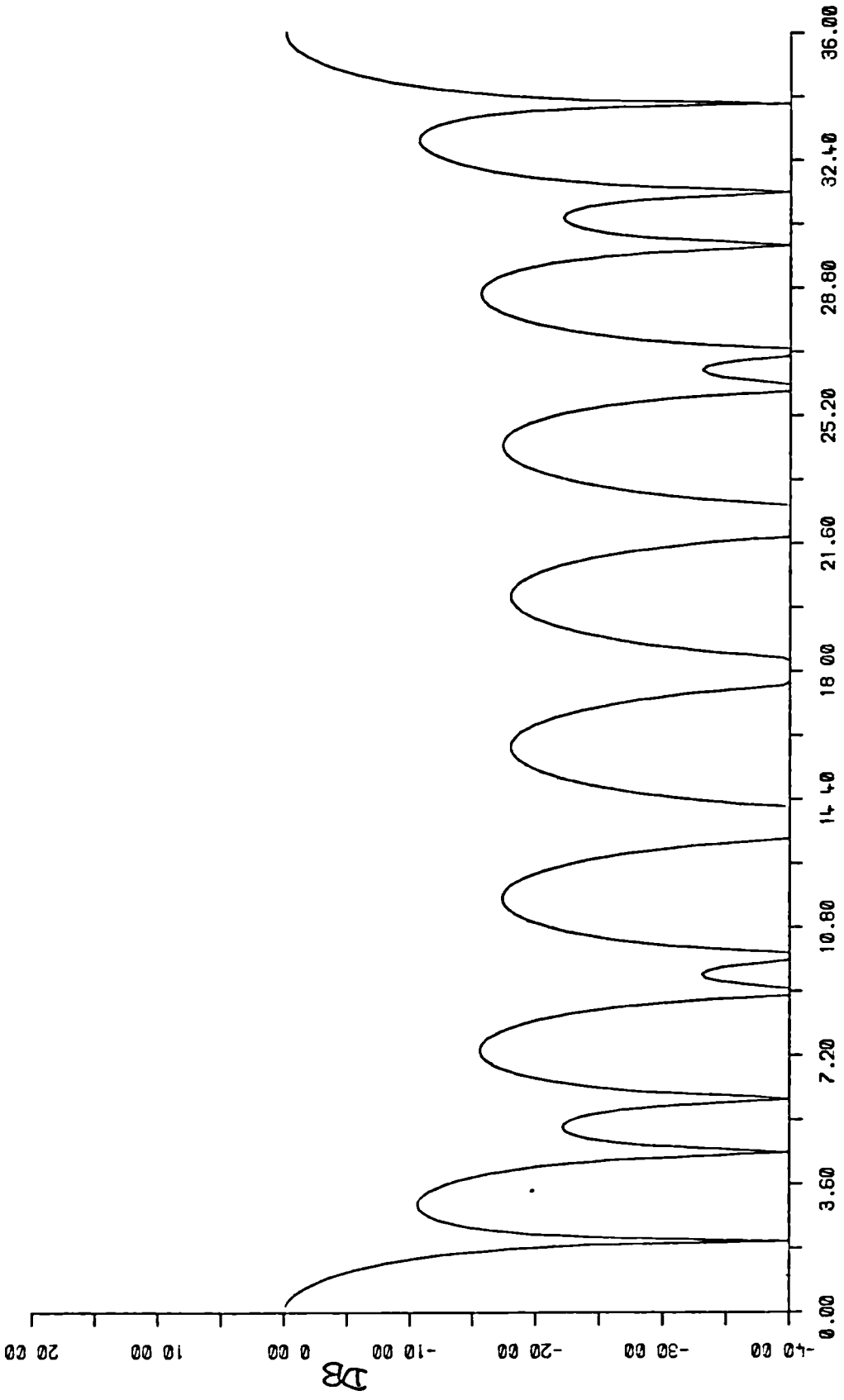
dB
20.00
10.00
0.00
-10.00
-20.00
-30.00
-40.00
0.00
3.60
7.20
10.80
14.40
18.00
21.60
25.20
28.80
32.40
36.00
ANGLE IN DEGREES *10⁻¹

FIGURE A3.1

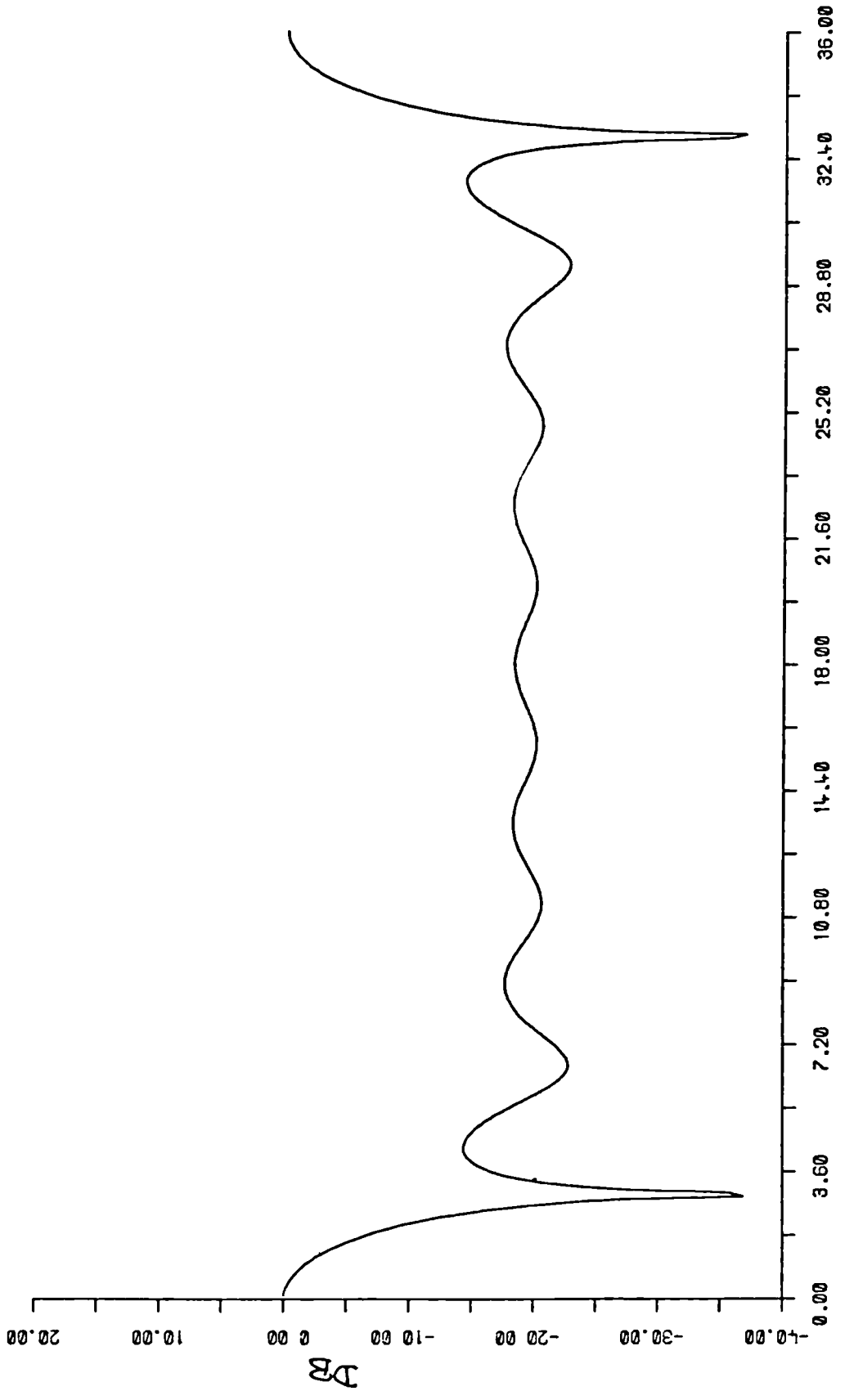
dB
20.00
10.00
0.00
-10.00
-20.00
-30.00
-40.00
0.00
3.60
7.20
10.80
14.40
18.00
21.60
25.20
28.80
32.40
36.00
ANGLE IN DEGREES *10⁻¹

FIGURE A3.2

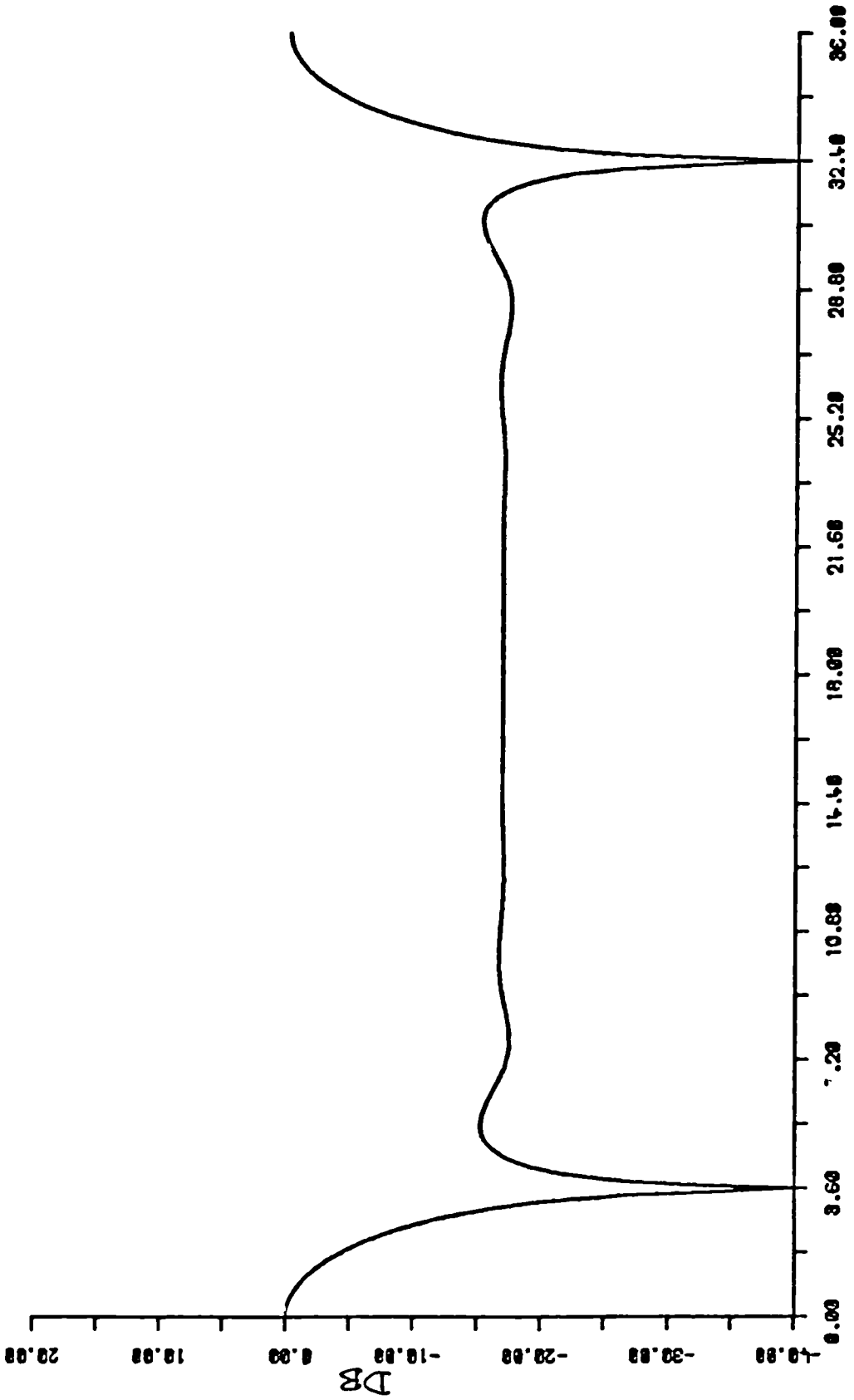
DB
20.00
10.00
0.00
-10.00
-20.00
-30.00
-40.00
0.00
3.60
7.20
10.80
14.40
18.00
21.60
25.20
28.80
32.40
36.00
ANGLE IN DEGREES x 10⁻¹

FIGURE A3.3

REFERENCES

(1) Longstaff, I.E., Chow, P.E.K. and Davies, D.E.N., 'Directional properties of circular arrays' Proc. IEE, Vol. 114, No. 6, June 1967

(2) Collins, R.E., Zucker, F.J., 'Antenna Theory' Part 1 pp. 163-172

(3) Tillman, J.D., Hickman, C.E., and Neff, H.P., 'The theory of a single-ring circular antenna array', Trans. Amer. Inst. Elec. Engrs., 1961 Part 1, p.110

(4) Le Page, W.R., Roys, C.S., and Seeley, S., 'Radiation from circular current sheets', Proc. Inst. Radio Engrs., 1950, 38, p.1069

(5) Davies, D.E.N., 'A transformation between the phasing techniques required for linear and circular aerial arrays', Proc. IEE, 1965, 112,(11), pp.2041-5

(6) Shelag, B., 'A matrix-fed circular array for continuous scanning' Proc. IEEE, Vol. 56, No. 11 Nov. 1968

(7) Fenby, R.G., 'Limitations on directional patterns of phase-compensated circular arrays', Radio Electronic Engr., 1965, 30, p.206

(8) Crampton, C., 'Naval radio direction-finding', J.IEE, 1947, 94, Part IIIA, p.132

(9) Fenby, R.G., and Davies, D.E.N., 'Circular array providing fast 360° electronic beam rotation' Proc. IEE, Vol. 115, No. 1, January 1968

(10) Davies, D.E.N., 'Independent angular steering of each zero of the directional pattern for a linear array', IEEE Trans., 1967, AP-15, pp.296-8

(11) Clarke, J., 'Steering of zeros in the directional pattern of a linear array', ibid., 1968, AP-16, pp.267-8

(12) Mellors, M., Davies, D.E.N. and Withers, M.J., 'Zero steering in the directional pattern of a linear array in the presence of mutual coupling', Proc. IEE, 1970, 117, (1), pp.35-40

(13) Lim, J.C., Davies, D.E.N., 'Synthesis of a single null response in an otherwise omnidirectional pattern using a circular array', Proc. IEE, Vol. 122, No. 4, April 1975

(14) Lim, J.C., 'Introduction of a sharp steerable null response in an otherwise omnidirectional pattern using a circular array', Journal IEE, Vol. 47, No. 1/2 pp. 30-32 January/February 1977

(15) Davies, D.E.N. and Rizk, M., 'Electronic steering of multiple nulls for circular arrays', Electronics Letters, Vol. 13, No. 22, 27 October 1977, pp.669

(16) Schelkunoff, S.A., 'A mathematical theory of linear arrays', Bell Systems Tech. J. Vol.22, p.80, January 1943

(17) Davies, D.E.N. and Rizk, M., 'Null steering antenna for mobile communication', Electron. Lett. 1976, 12, pp. 123-124

(18) Rizk, M., 'Null steering antennas for mobile communications', PhD thesis, University of London, February 1977

(19) Watson, G.N., 'Thoery of Bessel Functions' Cambridge University Press, Cambridge England 1944

(20) Mclachlan, N.W., 'Bessel Function for engineers', Oxford University Press, Oxford England 1934

(21) Ruse, J.(1952) 'The effect of aperture errors on antenna radiation patterns' Nuova Cimento, Supp. to Vol. IX, pp.364-380

(22) King, R.W.P., 'Theory of Linear Antennas', Harvard University Press, Cambridge, Mass., 1956